Rada Naukowa Dyscypliny
Inżynieria Materiałowa
Wydział Inżynierii Materiałowej
Politechnika Warszawska
ul. Wołoska 141
02-507 Warszawa

za pośrednictwem:

Rady Doskonałości Naukowej
pl. Defilad 1
00-901 Warszawa
(Pałac Kultury i Nauki, p. XXIV, pok. 2401)

Tomasz Suszko
Politechnika Koszalińska
Wydział Inżynierii Mechanicznej i Energetyki
ul. Śniadeckich 2
75-453 Koszalin

Wniosek
z dnia 6 listopada 2024

o przeprowadzenie postępowania w sprawie nadania stopnia doktora habilitowanego w dziedzinie **nauk inżynieryjno-technicznych** w dyscyplinie[1] **inżynieria materiałowa**

Określenie głównego osiągnięcia naukowego będącego podstawą ubiegania się o nadanie stopnia doktora habilitowanego:

Nowa klasa cienkich powłok o kompozytowej strukturze nanokolumnowej typu MeMC/a-C:H – wytwarzanie oraz właściwości fizykochemiczne

Wnioskuję – na podstawie art. 221 ust. 10 ustawy z dnia 20 lipca 2018 r. Prawo o szkolnictwie wyższym i nauce (Dz. U. z 2021 r. poz. 478 zm.) – aby komisja habilitacyjna podejmowała uchwałę w sprawie nadania stopnia doktora habilitowanego w głosowaniu ~~tajnym~~**/jawnym***[2]

Zostałem poinformowany, że:

Administratorem w odniesieniu do danych osobowych pozyskanych w ramach postępowania w sprawie nadania stopnia doktora habilitowanego jest Przewodniczący Rady Doskonałości Naukowej z siedzibą w Warszawie (pl. Defilad 1, XXIV piętro, 00-901 Warszawa). Kontakt za pośrednictwem e-mail: kancelaria@rdn.gov.pl , tel. 22 656 60 98 lub w siedzibie organu. Dane osobowe będą przetwarzane w oparciu o przesłankę wskazaną w art. 6 ust. 1 lit. c) Rozporządzenia UE 2016/679 z dnia z dnia 27 kwietnia 2016 r. w związku z art. 220 - 221 oraz art. 232 – 240 ustawy z dnia 20 lipca 2018 roku -

[1] Klasyfikacja dziedzin i dyscyplin wg. rozporządzenia Ministra Nauki i Szkolnictwa Wyższego z dnia 20 września 2018 r. w sprawie dziedzin nauki i dyscyplin naukowych oraz dyscyplin w zakresie sztuki (Dz. U. z 2018 r. poz. 1818).
[2] * Niepotrzebne skreślić.

Prawo o szkolnictwie wyższym i nauce, w celu przeprowadzenie postępowania o nadanie stopnia doktora habilitowanego oraz realizacji praw i obowiązków oraz środków odwoławczych przewidzianych w tym postępowaniu. Szczegółowa informacja na temat przetwarzania danych osobowych w postępowaniu dostępna jest na stronie www.rdn.gov.pl/klauzula-informacyjna-rodo.html

(podpis wnioskodawcy)

Załączniki:

1. Kopia dyplomu nadania stopnia doktora nauk technicznych.
2. Autoreferat przedstawiający opis dorobku i osiągnięć naukowych, w szczególności określonych w art. 16 ust. 2 ustawy w formie papierowej w języku polskim i angielskim.
3. Wykaz opublikowanych prac naukowych lub twórczych prac zawodowych oraz informacja o osiągnięciach dydaktycznych, współpracy naukowej i popularyzacji nauki w formie papierowej w języku polskim i angielskim.
4. Wykaz publikacji stanowiących osiągnięcie naukowe wraz z określeniem indywidualnego wkładu każdego ze współautorów i ich oświadczeniami potwierdzającymi prawdziwość podanych informacji.
5. Kopie wybranych publikacji autorstwa lub współautorstwa habilitanta stanowiących podstawę do wszczęcia postępowania oraz znajdujących się na tzw. liście filadelfijskiej JCR
6. Dane personalne i kontaktowe habilitanta.
7. Elektroniczna wersja składanego Wniosku habilitanta z dnia 18.03.2013 r. o przeprowadzenie postępowania habilitacyjnego w dziedzinie Nauki Techniczne w dyscyplinie Inżynieria Materiałowa wraz z załącznikami w dwóch egzemplarzach (płyta CD).

Autoreferat

Załącznik 2a do wniosku o przeprowadzenie
postępowania habilitacyjnego

Tomasz Suszko

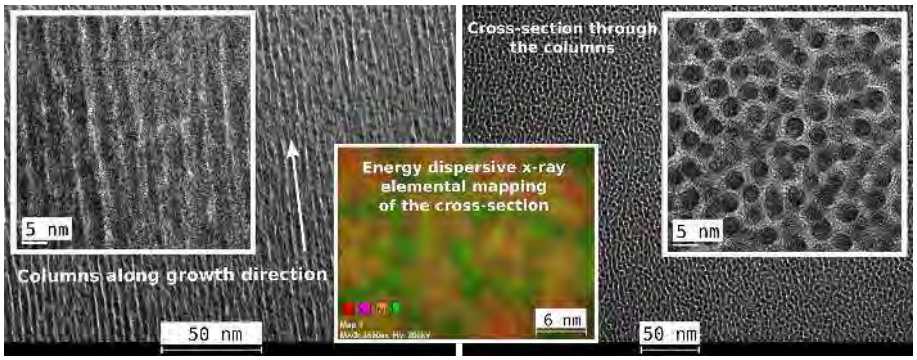

Streszczenie graficzne z: **T. Suszko** et al., „Amorphous FeCrNi/a-C:H coatings with self-organized nanotubular structure", *Scripta Materialia*, 136 (2017), 24–28

Koszalin, 6 listopada 2024

Spis treści

1 Podstawowe dane

1.1 Dane personalne

- Imię i nazwisko: Tomasz Suszko
- Data i miejsce urodzenia: —
- Miejsce pracy: Politechnika Koszalińska, Wydział Inżynierii Mechanicznej i Energetyki, Katedra Fizyki Technicznej i Nanotechnologii
- e-mail: tomasz.suszko@tu.koszalin.pl
- tel.: —
- Numer ORCID: 0000-0002-8355-891X
- Dane bibliometryczne (stan na 15.10.2024 r.):
  - Indeks Hirsha: Scopus – 14, Web of Science – 14, Google Scholar – 17.
  - Ogólna liczba cytowań (w nawiasie liczba bez autocytowań): Scopus – 928(905), Web of Science – 859(837), Google Scholar – 1137.
  - Liczba publikacji indeksowanych: Scopus – 23, Web of Science – 20, Google Scholar – 65, PBN – 80.
  - Sumaryczny *impact factor*: 92.3

1.2 Posiadane dyplomy, stopnie naukowe

- 1982 – Technik elektronik, Technikum Elektroniczne w Koszalinie
- 1990 – Magister fizyki, Uniwersytet Gdański w Gdańsku, Wydział Matematyki Fizyki i Chemii, kierunek: fizyka doświadczalna
- 2005 – Doktor nauk technicznych, Instytut Technologii Materiałów Elektronicznych w Warszawie, dyscyplina: inżynieria materiałowa, tytuł rozprawy doktorskiej: *Wysokotemperaturowe właściwości tribologiczne azotku molibdenu γ-Mo_2N domieszkowanego miedzią*

1.3 Informacja o dotychczasowym zatrudnieniu i aktywności naukowej

Po ukończeniu studiów przez kilka lat pracowałem w szkole jako nauczyciel fizyki, by w roku 1997 zostać zatrudnionym w Politechnice Koszalińskiej na stanowisku asystenta.

Na początku pracy na uczelni, oprócz pracy dydaktycznej, uczestniczyłem w pracach badawczych prowadzonych w Katedrze Fizyki, angażując się w prace doświadczalne i analizę danych w dwóch obszarach: azotowania gazowego i technologii PVD. W pracy dydaktycznej powierzono mi natomiast prowadzenie ćwiczeń rachunkowych z fizyki oraz laboratorium z tego przedmiotu.

W pracy badawczej skupiłem się najpierw na analizowaniu i rozwijaniu technologii azotowania gazowego, będąc aktywnym członkiem zespołu realizującego

grant badawczy wspólnie z **Instytutem Mechaniki Precyzyjnej w Warszawie**, który to grant obejmował nowoczesne podejście do modelowania procesów cieplno-chemicznych, jak i ich sterowaniem.

Nieco później zaczęły mnie także interesować zagadnienia z technologiami PVD, zwłaszcza że Politechnika Koszalińska była jednym z polskich prekursorów tej technologii, a w owym czasie funkcjonowały w Koszalinie dwie firmy z tego obszaru: **VTT Techniki i Technologie Próżniowe sp. z o.o.** oraz **Próżniowe Technologie Cienkowarstwowe Czesław Szypowski**.

Po zdobyciu pewnego doświadczenia, skupiłem się bardziej na technologii PVD i materiałach otrzymywanych tą metodą, a w końcówce 2001 r. otworzyłem w **Instytucie Technologii Materiałów Elektronicznych w Warszawie** przewód doktorski na temat syntezy i właściwości cienkich warstw azotku molibdenu. Równolegle do prac nad tym azotkiem angażowałem się w prace nad innymi powłokami nanoszonymi metodami PVD, a w szczególności nad ich właściwościami tribologicznymi. Prace te były prowadzone we współpracy z **Uniwersytetem Śródziemnomorskim w Marsylii** i z **Narodowym Instytutem Politechnicznym w Grenoble**, w ramach programu Polonium. Program ten umożliwił mi kilkukrotne stażowe wyjazdy do tych ośrodków badawczych i zdobycie cennego doświadczenia.

Równolegle do prac nad materiałami otrzymywanymi technikami PVD zajmowałem się azotowaniem gazowym w kontekście kontrolowania i sterowania procesem, w ramach współpracy Politechniki Koszalińskiej z **Instytutem Mechaniki Precyzyjnej w Warszawie**.

W roku 2005 obroniłem z wyróżnieniem pracę doktorską, a moje zainteresowania naukowe zwróciły się ku możliwościom rozwoju technologii PVD w kierunku wielośródłowego rozpylania magnetronowego i możliwości syntezy metalicznych powłok quasi-krystalicznych. Badania te prowadzone były we współpracy z przodującymi naukowymi instytucjami europejskimi skupionymi wokół finansowanego w latach 2005–2010 projektu **Complex Metallic Alloys – Network of Excellence** oraz we współpracy z **Instytutem Technologii Eksploatacji w Radomiu**.

Kolejne możliwości pracy nad rozwojem technologii PVD pojawiły się wraz z uzyskaniem przez uczelnię dużego grantu na opracowanie technologii modyfikacji powierzchni narzędzi do obróbki drewna (lata 2009–2012). Praca w projekcie dała możliwość skonfrontowania doświadczeń z pracy naukowej, laboratoryjnej z wymaganiami procesów przemysłowych. W ramach realizacji grantu odpowiedzialny byłem za opracowanie technologii syntezy pokryć przeciwzużciowych na narzędziach do obróbki drewna, na bazie azotku TiAlN.

W międzyczasie (2007–2008) zaangażowany byłem w prace nad uruchomieniem w uczelni kierunku studiów inżynieria materiałowa. Pracowałem nad opracowaniem programu tych studiów, sylabusów, materiałów dydaktycznych, promocją, a później także realizacją prac dyplomowych na tym kierunku.

Współpraca w tamtym czasie z **Instytutem Inżynierii Materiałowej Politechniki Szczecińskiej** skierowała moje zainteresowania naukowe na tak zwaną fazę S, inaczej rozszerzony austenit (ang. *expanded austenite*). Zagadnienie to leży na styku technologii azotowania i PVD, ponieważ rozszerzony austenit można otrzymać metodą azotowania (gazowego lub plazmowego) lub metodą rozpylania magnetronowego. To zainteresowanie zaowocowało wspólnym grantem badawczym, a w rezultacie też opracowaniem nowego rodzaju powłoki, FeCrNiC/ a-C:H omawianej dokładniej w p. 2.2. Zapoczątkowane

w projekcie prace kontynuowałem w ramach grantów uczelnianych.

W latach 2016–2020 zaangażowany byłem we współpracę z firmą **FANAR** z Ciechanowa, producentem narzędzi skrawających, która jako pierwsza w Polsce wprowadzała w produkcji narzędzi skrawających technologię HIPIMS (ang. *High Power Impulse Magnetron Sputtering*). Praca naszego zespołu z Politechniki Koszalińskiej polegała na dostosowaniu technologii do potrzeb firmy, optymalizacji parametrów, zapewnieniu powtarzalności procesów i ich monitorowaniu.

Obecnie kontynuuję wraz z zespołem, oraz we współpracy z **Centrum Nano BioMedycznym Uniwersytetu Adama Mickiewicza**, **Instytutem Fizyki Doświadczalnej Uniwersytetu Gdańskiego** oraz **Uniwersytetem w Linköping** badania nad właściwościami warstw MeMC/a-C:H, opisanych w p. 2, a głównie nad właściwościami elektrokatalitycznymi tego typu materiałów w katodowej reakcji HER elektrolizy wody (ang. *Hydrogen Evolution Reaction*).

2 Omówienie cyklu artykułów pn. „Nowa klasa cienkich powłok o kompozytowej strukturze nanokolumnowej typu MeMC/a-C:H – wytwarzanie oraz właściwości fizykochemiczne", stanowiącego podstawę wniosku o postępowanie habilitacyjne

Poniżej przedstawiam osiągnięcie, o których mowa w art. 219 ust. 1 pkt. 2 ustawy z dnia 20 lipca 2018 r. „Prawo o szkolnictwie wyższym i nauce" (Dz. U. z 2021 r. poz. 478 z późn. zm.) stanowiące podstawę wniosku o nadanie stopnia doktora habilitowanego. Jest nim **cykl pięciu artykułów** wymienionych poniżej i stanowiących załącznik do niniejszego wniosku. Dotyczą one **nowej klasy materiałów** syntetyzowanych w postaci cienkich warstw, posiadającej charakterystyczną kompozytową strukturę nanokolumnową. **Wytworzenie przeze mnie tych materiałów oraz zbadanie i opisanie ich wybranych właściwości jest w mojej opinii istotnym wkładem w rozwój inżynierii materiałowej**.

- (plik: Annex-5a.pdf) **T. Suszko**, W. Gulbiński, J. Morgiel, G. Greczynski, E. Dobruchowska, P. Dłużewski, J. Lu, & L. Hultman (2017). Amorphous FeCrNi/a-C:H coatings with self-organized nanotubular structure, *Scripta Materialia*, 136 (2017), 24–28. https://doi.org/10.1016/J.SCRIPTAMAT.2017.03.040.

- (plik: Annex-5b.pdf) **T. Suszko**, W. Gulbiński, E. Dobruchowska, G. Greczynski, L. Hultman, & J. Morgiel, Quasi-amorphous, nanostructural CoCrMoC/a-C:H coatings deposited by reactive magnetron sputtering, *Surface & Coatings Technology*, 378 (2019), 124910. https://doi.org/10.1016/J.SURFCOAT.2019.124910

- (plik: Annex-5c.pdf) E. Dobruchowska, **T. Suszko**, G. Greczynski, D. Adamczewska, W. Gulbiński, Amorphous/quasi-amorphous CoCrMo-C

coatings for improved electrochemical properties and tribocorrosion resistance of biomedical alloys, *Surface & Coatings Technology*, 460 (2023), 129398.
https://doi.org/10.1016/j.surfcoat.2023.129398.

- (plik: Annex-5d.pdf) **T. Suszko**, W. Gulbiński, K. Załęski, G. Greczynski, J. Morgiel, & V. Lapitskaya, Nano-columnar, self-organised NiCrC/a-C:H thin films deposited by magnetron sputtering, *Applied Surface Science*, 591 (2022), 153134.
https://doi.org/10.1016/j.apsusc.2022.153134

- (plik: Annex-5e.pdf) **T. Suszko**, E. Dobruchowska, W. Gulbiński, G. Greczynski, J. Morgiel, B. Kawczyński, K. Załęski, K. Dorywalski, & S. Pogorzelski, NiMo-C coatings synthesised by reactive magnetron sputtering for application as a catalyst for the hydrogen evolution reaction in an acidic environment, artykuł na etapie recenzji w *ACS Applied Materials & Interfaces* (2024).

2.1 Geneza i charakterystyka warstw typu MeMC/a-C:H na tle aktualnego stanu wiedzy

Węgliki metali przejściowych, szczególnie należących do czwartej, piątej i szóstej grupy układu okresowego, nanoszone w postaci cienkich warstw, dzięki swoim właściwościom takim jak wysoka twardość, przewodnictwo elektryczne czy też odporność na korozję, są przedmiotem licznych prac badawczych. W praktyce przemysłowej stosowane są one szeroko jako powłoki przeciwzużyciowe na narzędziach, powłoki antykorozyjne, a także materiały wysoko obciążonych kontaktów elektrycznych czy też elektrod w układach do elektrolitycznego wytwarzania wodoru. Niektóre z tych węglików są bio kompatybilne, co czyni je przydatnymi do zastosowań biomedycznych.

Wykorzystanie, w procesie ich wytwarzania, technik PVD, takich jak reaktywne rozpylanie magnetronowe czy też HiPIMS umożliwia modyfikację tych właściwości poprzez odpowiednie zmiany składu chemicznego i fazowego. Istnieje przy tym możliwość uzyskania powłok o specyficznej architekturze warstwowej, gradientowej, nanokompozytowej, której nie można uzyskać innymi metodami.

Węgliki metali, nanoszone w postaci powłok technikami PVD, badane są od ponad trzydziestu lat. W Politechnice Koszalińskiej pierwsze prace dotyczące tej tematyki pojawiły się pod koniec lat dziewięćdziesiątych [1–7]. Pośród publikacji były też artykuły, **których wnioskodawca jest współautorem** [5–8].

Badania nad wytwarzaniem cienkich warstw węglików metali dotyczyły początkowo materiałów o składzie stechiometrycznym. Dzięki specyfice technik PVD, umożliwiających prowadzenie procesu w atmosferze z nadmiarem gazu węglonośnego, uzyskano również powłoki o składzie niestechiometrycznym, zawierające pewien nadmiar węgla [9, 10]. Morfologię tych materiałów można opisać jako kompozyt złożony z nanokrystalitów węglików (TiC, TaC, MoC) rozmieszczonych losowo w matrycy amorficznego węgla.

Wiele z tych nanokompozytów ma znakomite właściwości przeciwzużyciowe. Mają one wysoką twardość, posiadają niski współczynnik tarcia w kontakcie z wieloma materiałami oraz charakteryzują się podwyższoną odpornością koro-

zyjną. Stąd też wynika zastosowanie tych materiałów na powłoki na narzędziach skrawających i na częściach maszyn.

Jednym z kierunków badań było poszukiwanie i wyjaśnienie korelacji pomiędzy właściwościami powłok, a morfologią tych materiałów. Badano relacje między wielkością wydzieleń węglików, gęstością ich rozmieszczenia, grubością osnowy węglowej), składem chemicznym węglików (TiC [11], VC, ZrC, MoC, WC) oraz rodzajem wiązań węglowych [12, 4]. Badano również powłoki o architekturze warstwowej, uzyskiwanej przez modulację parametrów procesu w trakcie ich nanoszenia (np. [13]).

Wymienione wyżej węgliki grup 4–6 układu okresowego charakteryzują się wysoką entalpią tworzenia, co pociąga za sobą wysoką ich stabilność chemiczną, a węgliki trójskładnikowe zawierające pierwiastki z tych grup, takie jak TiV-C, TiNb-C, VTa-C, mogą zawierać metale w dowolnych proporcjach [14].

Entalpia tworzenia węglików metali z grup kolejnych, a zwłaszcza grup 8–11, jest znacznie niższa, a nawet dodatnia, a w badaniach powłok wytwarzanych technikami PVD na bazie węglików metali silnie węglikotwórczych domieszkowanych metalami słabo węglikotwórczymi zaobserwowano, postępujące w wyniku tego domieszkowania, rozdrobnienie struktury, i następnie amorfizację depozytu. Im metal silnie węglikotwóczy ma mniejsze powinowactwo do węgla, tym depozyt łatwiej ulega amorfizacji pod wpływem domieszki [15].

Domieszkowaniu stabilnych węglików metalami słabo węglikotwórczymi towarzyszą procesy segregacji węgla, które to zjawiska badał między innymi zespół z Universytetu w Upsali [16].

Ten wątek połączyłem z moimi badaniami nad wytwarzaniem fazy S na drodze reaktywnego rozpylania magnetronowego stali austenitycznej w atmosferze zawierającej azot i węglowodór (metan lub acetylen).**W rezultacie uzyskałem przesycone węglem wieloskładnikowe powłoki oznaczone jako FeCrNi/a-C:H, o nieobserwowanej wcześniej strukturze nanokolumnowej, utworzonej z quasiamorficznych, metalicznych kolumn o średnicy kilku nanometrów, otoczonych warstwą amorficznego węgla**.

Zainspirowany odkryciem kontynuowałem badania w ramach kilku kolejnych przedsięwzięć, a specyficzna nanostruktura została otrzymana w jeszcze trzech układach, **tworząc nową klasa materiałów cienkowarstwowych**, oznaczanych dalej jako **MeMC/a-C:H**, gdzie Symbole Me i M oznaczają odpowiednio metale słabo i silnie węglikotwórcze. Symbol a-C:H oznacza natomiast amorficzny uwodorniony węgiel.

2.2 Powłoki FeCrNiC/a-C:H – struktura i podstawowe właściwości

Pierwsze wyniki moich prac nad należącymi do tej klasy materiałów zostały opublikowane w artykule **„Amorphous FeCrNi/a-C:H coatings with self-organized nanotubular structure"**, pierwszym należącym do cyklu przedstawianego we wniosku. W artykule przedstawiłem opis i wyniki badań nad pokryciami zawierającymi od 2 do 60% at. węgla uzyskanymi przez impulsowe rozpylanie magnetronowe stali austenitycznej w atmosferze Ar/C_2H_2.

Omówiłem ewolucję struktury powłok, zmieniającą się wraz ze zwiększającą się zawartością węgla – od krystalicznej (faza S), przez nanokrystaliczną, do amorficznej, następnie do kompozytowej nanokolumnowej.

W artykule tym przedyskutowałem potencjalne przyczyny formowania się tej specyficznej nanostruktury, wskazując na kluczowe znaczenie różnic w powinowactwie chemicznym do węgla poszczególnych składników metalicznych. Nierównowagowe termodynamicznie warunki nanoszenia metodą rozpylania magnetronowego, stosunkowo niska temperatura podłoża oraz obecność metali słabo węglikotwórczych, sprzyjają amorfizacji depozytu. Metale te, tworzą metastabilne dwu- i trójskładnikowe węgliki typu $Me_{1-x}M_xC$, które rozpadając się uwalniają atomy węgla tworzące później matrycę węglową.

Brak wydzieleń węglików węglików chromu i molibdenu, których pojawienia się można było oczekiwać jako termodynamicznie stabilnych w tym układzie, **wytłumaczyłem wysokim progiem energetycznym aktywacji dyfuzji atomów metali w porównaniu do progu aktywacji dyfuzji węgla**.

Opracowane powłoki FeCrNiC/a-C:H przebadałem pod kątem właściwości mechanicznych i tribologicznych. Zaobserwowałem skokową poprawę tych cech, gdy struktura powłoki przyjmowała formę omawianego nanokompozytu. **Powłoki zostały także przebadane pod kątem zjawisk korozyjnych** w 3% roztworze NaCl. Wykazane zostało przy tym znaczne spowolnienie utleniania metalicznych składników powłoki w stosunku do materiału wyjściowego, przy jednoczesnym wzroście odporności na korozję wżerową. **Na powłokę i sposób jej wytwarzania uzyskano patent** [17].

2.3 Powłoki CoCrMoC/a-C:H – struktura i właściwości mechaniczne

Interesujące rezultaty zainspirowały mnie do poszukiwania innych układów (stopów), które potencjalnie mogłyby syntetyzować w podobnej nanostrukturze. **Na obiekt badań został wybrany stop o składzie $Co_{64}Cr_{32}Mo_4$**, szeroko stosowany w implantologii. Zawiera on pierwiastki spełniające **określone przeze mnie kryteria doboru składników powłok do syntezy samoorganizujących się struktur amorficzno nanokolumnowych**, a ponadto ciągle prowadzone są badania nad poprawą właściwości użytkowych tego stopu, co dawało dodatkowy impuls do podjęcia badań.

Moje prace nad syntezą powłok na drodze reaktywnego rozpylania magnetronowego stopu $Co_{64}Cr_{32}Mo_4$ w atmosferze Ar/C_2H_2 zostały podsumowane w artykule **„Quasi-amorphous, nanostructural CoCrMoC/a-C:H coatings deposited by reactive magnetron sputtering"**, drugim z cyklu przedstawianego do oceny.

W pracy przedstawiłem w szczegółach ewolucję struktury powłoki wraz z rosnącą zawartością węgla. Ze względu na fakt, że stop wyjściowy jest dwufazowy, to początkowe zmiany struktury prowadzące do rozdrabniania krystalitów (do ok. 10% at.) są dość złożone. **W zaproponowanej interpretacji uwzględniłem różny skład fazowy w zależności od głębokości, obecność mikronaprężeń, a także możliwość wystąpienia przemiany martenzytycznej pod wpływem naprężeń.**

Powłoki zawierające powyżej 10% at. węgla stają się amorficzne, by dla jeszcze większej zawartości przejść w kompozytową strukturę nanokolumnową. **Dzięki analizie wyników z pomiarów XPS określiłem próg zawartości węgla powyżej którego następuje jego segregacja, tj. ok. 20% at**.

Obrazowanie TEM i HRTEM umożliwiło mi stwierdzić, że kompozytowa struktura nanokolumnowa powłoki występuje w szerokim zakresie zawartości węgla; od 30 do ponad 50% at., przy czym dla zawartości węgla 53% obserwuje się już pewne „załamywanie się" struktury.

Artykuł zawiera ponadto wyniki moich badań nad podstawowymi właściwościami mechanicznymi warstw, takimi jak adhezja do podłoża, twardość, odporność na odkształcenia plastyczne i współczynnik tarcia w kontakcie z ceramiką alundową. Podobnie jak w przypadku warstw FeCrNiC/a-C:H, powłoki CoCrMoC/a-C:H charakteryzują się bardzo dobrymi właściwościami mechanicznymi i tribologicznymi.

2.4 Powłoki CoCrMoC/a-C:H – odporność korozyjna i tribokorozyjna w sztucznym płynie ustrojowym

Kolejnym krokiem w badaniach nad powłokami CoCrMoC/a-C:H była ocena odporności korozyjnej tego materiału jako powłoki na stali AISI 316L, w środowisku symulatora płynów ustrojowych; HBSS (ang. *Hanks' Balanced Salt Solution*), który to elektrolit został wybrany ze względu na wspomniane zastosowanie stopu głównie w implantologii.

Raport z tych badań badań przedstawiony został w artykule **„Amorphous/ quasiamorphous CoCrMo-C coatings for improved electrochemical properties and tribocorrosion resistance of biomedical alloys"**, będącym trzecim z cyklu przedstawianego do oceny.

W artykule przedstawione zostały wyniki badań cienkich warstw zawierających od 0 do 65% atomowych węgla, mających strukturę zmieniającą się od nanokrystalicznej przez amorficzną do nanokolumnowej. Oprócz oceny odporności korozyjnej w oparciu o elektrochemiczne testy polaryzacyjne, przedstawione zostały wyniki badań metodą impedancyjnej spektroskopii elektrochemicznej (ang. *Elektrochemical Impedance Spectroscopy*, EIS) oraz rezultaty szeregu testów tribokorozyjnych.

Na podstawie rezultatów przeprowadzonych przeze mnie pomiarów impedancyjnych pokazałem, że wszystkie badane powłoki są bardziej stabilne niż masywny stop CoCrMo – szybciej ulegają one pasywacji, a powstająca warstwa tlenkowa ma większą zdolność blokowania penetracji przez jony niż to mam miejsce w przypadku stopu.

Testy polaryzacyjne wykazały natomiast wyraźny wzrost potencjału korozyjnego dla próbek amorficznych i kompozytowych o strukturze nanokolumnowej, a także wysoką odporność na korozję wżerową. Analiza wyników testów wykazała, że reakcje chemiczne zachodzą jedynie na powierzchni, bez penetracji jonów na wskroś powłoki.

Istotną częścią artykułu są wyniki testów tribokorozyjnych na **skonstruowanym i wykonanym przeze mnie tribotesterze**. Urządzenie umożliwia prowadzenie testów tarcia z jednoczesnym prowadzeniem pomiarów elektrochemicznych przy zadanym potencjale lub w warunkach obwodu otwartego.

Na podstawie uzyskanych wyników i analizy zjawisk zachodzących w obszarze kontaktu podczas testów tribokorozyjnych **opracowałem elektryczny model zastępczy układu powłoka-podłoże-elektrolit, który umożliwia powiązanie wielkości elektrycznych z rezultatami pomiarów tribologicznych**.

Wykazałem, że nanokopozytowe pokrycia CoCrMoC/a-C:H dzięki swojej odporności na utlenianie oraz obecności wolnego węgla charakteryzują się niskim współczynnikiem tarcia i zużycia. **Zaobserwowałem też bardzo silną korelację między natężeniem prądu anodowego i współczynnikiem zużycia próbek, co świadczy o utlenianiu i mechanicznym usuwaniu tlenków, jako o dominującym mechanizmie zużycia**.

2.5 Powłoki NiCrC/a-C:H – struktura i właściwości magnetyczne

Struktura nanokolumnowa badanych powłok, powstająca w wyniku opisanych wcześniej procesów samoorganizacji, ma z natury swojej charakter anizotropowy. Tak więc celem kolejnych kroków badawczych była weryfikacja tezy, że obserwowane uporządkowanie przekłada się na anizotropie wybranych właściwości powłok.

Celowi temu służyły badania powłok NiCrC/a-C:H, wytwarzanych na drodze reaktywnego rozpylania magnetronowego stopu $Ni_{80}Cr_{20}$. Skład stopu wypełnia sformułowane wcześniej kryteria doboru składników sprzyjających tworzeniu się badanych nanostruktur. Rezultaty przedstawiłem w artykule **„Nanocolumnar, self-organised NiCrC/a-C:H thin films deposited by magnetron sputtering"**, będącym czwartym z cyklu przedstawianego do oceny.

Zgodnie z oczekiwaniami uzyskałem powłoki nanokrystliczne, amorficzne, oraz kompozytowe o nanokolumnowej. W pracy określiłem próg zawartości węgla, powyżej którego występują jego wydzielenia ze struktury amorficznej, a do badań właściwości magnetycznych wybrałem próbki amorficzne (20% at. węgla) oraz próbki o zawartości 38 i 63% at. C, wykazujące charakterystyczną strukturę nanokolumnową.

Dzięki pomiarom metodą mikroskopii sił atomowych w modzie topograficznym oraz kontrastu magnetycznego (AFM/MPM) udało się wykazać, że nanokolumny rozciągają się do samej powierzchni próbki, a ich wierzchołki są widoczne na obrazie z kontrastem magnetycznym. **W artykule wykazałem też, że właściwości magnetyczne powłok zależą od zawartości węgla i w konsekwencji od nanostruktury materiału**.

Wyniki pomiarów magnetyzacji i koercji magnetycznej, wykonane w kierunku równoległym do powierzchni próbki (prostopadle do osi kolumn) i prostopadłym (równolegle do osi kolumn), umożliwiły sformułowanie kilku wniosków: **W większości pomiarów próbki wykazały słaby ferromagnetyzm**. Przy czym jednak próbka amorficzna w obrazie TEM była także anizotropowa magnetycznie. **Próbka o zawartości 38% węgla w kierunku prostopadłym do osi kolumn wykazała superparamagnetyzm, a tym samym największą anizotropię**. Dla próbki największej zawartości węgla efekt anizotropii zmniejszał się, co związane było zapewne z mniejszą średnicą metalicznych kolumn jak i być może z utratą ich ciągłości.

Jest interesującym, że magnetyzacja nasyceniowa rośnie wraz z zawartością węgla. **W artykule zaproponowałem wyjaśnienie tego zjawiska „wychwytywaniem" coraz większej liczby atomów chromu przez węgiel i zwiększającą się ilością nanowydzieleń ferromagnetycznego niklu**. Wynik modelowania krzywych M–H (namagnesowania w funkcji natężenia pola magnetycznego) dał rezultaty zgodne z danymi doświadczalnymi, a mediana rozkładu wielkości nanocząstek niklu, dająca najlepsze dopasowanie, miała wartość

około 8 nm, co okazuje się być bliskie obserwowanej średnicy nanokolumn.

2.6 Powłoki NiMoC/a-C:H – struktura i właściwości elektrokatalityczne w reakcji HER

Analizując potencjalne możliwości aplikacyjne pokryć o omawianej nanostrukturze, **zwróciłem uwagę na możliwość zastosowania niklu i stopów niklu jako katalizatora w elektrolizie wody**, a dokładniej w reakcji wytwarzania wodoru (ang. *hydrogen evolution reaction* – HER).

Pod kątem tego zastosowania na **obiekt badań wybrałem powłoki uzyskiwane przez reaktywne rozpylanie, z udziałem acetylenu, stopu $\mathbf{Ni_{80}Mo_{20}}$**. Materiał wyjściowy spełnia kryteria opisane wcześniej, wymagane do uzyskania obserwowanej na innych opisanych materiałach nanokompozytowej struktury amorficzno kolumnowej oraz jest paramagnetyczny, co umożliwia jego efektywne rozpylanie magnetronowe.

Nikiel jest znanym i używanym na skalę przemysłową katalizatorem reakcji HER zastępującym drogie katalizatory oparte na metalach grupy platyny. Jeszcze wyższą zdolność katalityczną wykazuje stop $Ni_{80}Mo_{20}$ będący też odrębną fazą. **Ważnym jest jednak, że mimo dobrej zdolności katalitycznej można je stosować tylko w środowisku zasadowym**, ponieważ nikiel, jak i $Ni_{80}Mo_{20}$ nie są odporne na działanie kwasów. W środowisku kwaśnym natomiast reakcja przebiega znacznie wydajniej niż w zasadowym.

Warstwy NiMo-C o odpowiedniej zawartości węgla dzięki amorficznej strukturze oraz wydzieleniom węgla powinny być znacząco odporniejsze na działanie kwasów niż czysty stop. Wyniki badań ukierunkowanych na te zagadnienia zamieściłem w artykule **„NiMo-C coatings synthesised by reactive magnetron sputtering for application as a catalyst for the hydrogen evolution reaction in an acidic environment"**, będącej piątą z cyklu przedstawianego do oceny.

Podobnie jak w przypadku pozostałych badanych do tej pory materiałów, **opisałem ewolucję struktury wraz ze zwiększającą się zawartością węgla**. W ogólnym zarysie zmiany struktury przebiegały jak w przypadku innych opisywanych materiałów; od nanokrystalicznej, przez amorficzną, do nanokolumnowej.

W pracy pokazałem, że i w tym układzie pierwiastków, przy udziale węgla większym niż około 40% at., powłoki syntetyzują w formie kompozytowej struktury nanokolumnowej, a ponadto warstwy o zawartości węgla ok. 23% at. i więcej wyróżniały się wysoką odpornością korozyjną w 0,1M $\mathbf{H_2SO_4}$.

Na potrzeby oceny zdolności elektrokatalitycznej **wykonałem szereg pomiarów potencjodynamicznych, a następnie przeanalizowałem wyniki pod kątem nachylenia Tafela krzywych polaryzacyjnych i charakterystycznych nadpotencjałów**. Próbki o najmniejszej zawartości węgla okazały się najaktywniejsze elektrokatalitycznie, ale nie były odporne na korozję. **W artykule wykazałem, że próbki kompozytowe nanokolumnowe o średniej zawartości węgla miały właściwości optymalne; dobrą odporność korozyjną, dobrą aktywność elektrokatalityczną, a także najlepszą stabilność w pomiarach cyklicznych**.

Istotnym także wynikiem badań jest stwierdzenie, że **próbki nawet o największej zawartości węgla wykazywały dobrą zdolność katalityczną**,

dużo lepszą niż grafit. Za przyczynę tego stanu rzeczy **uznałem fakt występowania metalicznych centrów katalitycznych („zwieńczeń" nanokolumn) na powierzchni próbek , a więc jednej z konsekwencji charakterystycznej budowy nanokompozytowej**. Obecność tych centrów została potwierdzona za pomocą mikroskopu AFM, pracującego w modzie przewodnościowym (C-AFM).

2.7 Posumowanie

W punktach 2.2–2.6 przedstawiłem opis szeregu właściwości nowej klasy powłok **typu MeMC/a-C:H**, o specyficznej **kompozytowej strukturze nanokolumnowej**.

Wytworzenie ich było rezultatem prowadzonych według mojej koncepcji badań nad wieloskładnikowymi powłokami węglikowymi. W wyniku tych początkowych badań zsyntetyzowałem opatentowaną później [17] powłokę FeCrNiC/a-C:H [18], a rezultatem kilku następnych przedsięwzięć była synteza innych nanokolumnowych powłok: CoCrMoC/a-C:H [19, 20], NiCr-C/a-C:H [21] i NiMoC/a-C:H [22]. Wszystkie opracowane pokrycia zostały przebadane pod kątem wybranych właściwości, a ich wybór wynikał z potencjalnych zastosowań.

Na etapie publikacji rezultatów prac badawczych, odpowiedzialny byłem za koncepcję badań, gromadzenie, analizę i prezentację danych, opisy stanu wiedzy, dyskusję wyników i konkluzje. We wszystkich przedstawionych do oceny pracach byłem autorem korespondencyjnym odpowiedzialnym także za poprawki i uzupełnienia związane z recenzjami manuskryptów.

Obecnie kontynuuję wraz z zespołem badania nad właściwościami warstw MeMC/a-C:H, a w szczególności nad właściwościami elektrokatalitycznymi. Obiektem bieżących badań są powłoki otrzymywane na bazie stopu NiW.

3 Informacja o osiągnięciach związanych z opracowaniem modeli wzrostu warstwy azotowanej, pod kątem sterowania procesem azotowania gazowego

Główna tematyka mojej pracy naukowej związana jest z badaniami i wytwarzaniem cienkich warstw metodami PVD, **znaczącą jednak część aktywności**, tak przed jak i po doktoracie **(do ok. 2009 r.), poświęciłem pracy nad analizą procesu azotowania gazowego**; jednej z powszechnie stosowanych obróbek cieplno-chemicznych na mocno obciążone elementy maszyn i narzędzi.

Od czasu wynalezienia azotowania w latach dziesiątych XX w. stopniowo pojawiała się potrzeba precyzyjnej kontroli procesu azotowania w celu uzyskania stosownej efektywnej grubości warstwy azotowanej i odpowiedniej grubości strefy azotków. Z tą tematyką wiązała się moja praca nad technologią azotowania. Oprócz głównego osiągnięcia opisanego w p. 2 **wyniki prac nad azotowaniem stanowią w mojej opinii pewien istotny wkład w rozwój inżynierii materiałowej**. Z tego powodu informację na ten temat zamieszczam w autoreferacie, choć osiągnięcia z tego zakresu badań nie można zaliczyć

do kategorii wymienionych w ustawie jak „monografia", „cykl artykułów" lub „osiągnięcie projektowe".

3.1 Opis prac i osiągniętych wyników

W badaniach procesu azotowania gazowego byłem aktywnym członkiem zespołu **zajmującego się zagadnieniami związanymi ze sterowaniem procesem, czujnikami służącymi temu celowi, oraz modelowaniem kinetyki wzrostu warstwy naazotowanej**. Prace te były realizowane między innymi w ramach następujących przedsięwzięć, w których uczestniczyłem jako jeden z głównych wykonawców:

1. Projekt badawczy KBN T08C 008 10 „Opracowanie podstaw projektowania automatycznie sterowanych procesów azotowania gazowego", 1996–1998.

2. Projekt badawczy KBN T08C 039 19 „Wpływ przypowierzchniowej warstwy azotków (węgloazotków) żelaza na kształtowanie się kinetyki wzrostu warstwy azotowanej", 2000–2003.

3. Projekt badawczy Nr PW 004/ITE/04/2006 „Opracowanie czujnika magnetycznego do pomiaru in situ wzrostu warstwy azotowanej w systemach monitorowania procesów azotowania gazowego", 2007–2008.

Jednym z efektów trzeciego z wymienionych przedsięwzięć **było stworzenie aplikacji komputerowej, służącej do symulacji kinetyki wzrostu warstwy azotowanej i projektowania procesu**. Moja rola w zespole obejmowała **opracowanie modeli matematycznych**, które stanowiły podstawę do przeprowadzania symulacji przebiegu procesu azotowania i przewidywania jego rezultatów.

Punktem wyjścia w moich pracach były fizyczne podstawy zjawisk i **modele analityczne** oparte głównie na równaniach dyfuzji Ficka. To podejście wraz z pracami doświadczalnymi umożliwia na przykład wyznaczenie współczynników dyfuzji w żelazie i stalach niskostopowych w warunkach stałego potencjału azotowego i temperatury. Umożliwia też, w pewnym zakresie, dobór parametrów procesu w celu uzyskania pożądanej grubości warstwy. Dodatkowo pewne wnioski wynikające z rozwiązań analitycznych równań, jak koncepcja tzw. stałej parabolicznego wzrostu, umożliwia obliczanie grubości poszczególnych monofazowych stref warstwy azotków tworzących się na powierzchni w trakcie procesu.

Na bazie modeli analitycznych **zbudowałem szereg bardziej złożonych modeli, obejmujących reakcje wiązania azotu z pierwiastkami stopowymi, dyfuzję i wzrost zewnętrznej warstwy azotków**. Takie układy równań stają się możliwe do rozwiązania jedynie metodami komputerowymi, i tworzą wraz z algorytmami obliczeniowymi oraz z ustrukturyzowanymi danymi **modele numeryczne**. W oparciu o dane doświadczalne została przeanalizowana ich wiarygodność, a potem **służyły one do symulacji kształtu profili stężeń azotu, zarówno tego związanego w azotki pierwiastków stopowych, jak i rozpuszczonego w sieci ferrytu**, Te profile stężeń azotu są kluczowe dla określenia rozkładu twardości w warstwie azotowanej.

Ponadto, dzięki dyskretyzacji czasu, podziałowi symulowanego procesu na etapy, możliwe stało się uwzględnienie zmienności czasie parametrów, takich jak

temperatura i skład atmosfery azotującej. **Opracowany przeze mnie model dość precyzyjnie odwzorowuje zarówno proces dyfuzji jak i reakcje wiązania azotu z pierwiastkami stopowymi**, realistyczne odwzorowując zachowanie materiału w trakcie procesu. Parametrami wejściowymi modelu są czasowe zależności temperatury i potencjału azotowego (lub składu atmosfery) oraz pewne umowne parametry zależne od rodzaju azotowanej stali. Rozwiązanie daje w wyniku czasowe zależności grubości warstw azotków, profile stężenia azotu w strefie dyfuzyjnej oraz profile azotu związanego z pierwiastkami stopowymi.

Analiza kinetyki wzrostu warstwy azotowanej na stalach stopowych za pomocą tego rodzaju modeli **umożliwiła również sformułowanie istotnych wniosków dotyczących projektowania procesów technologicznych, a ich użyteczność wykazano w kilku pracach**, jak na przykład [23, 24].

W stosowaniu modelu różniczkowego pojawiają się trudności związane ze wspomnianymi umownymi parametrami materiałowymi, które wymagają wyznaczenia eksperymentalnego, jak na przykład: i) współczynnik szybkości wiązania azotu z pierwiastkami stopowymi, który w sposób uśredniony opisuje wpływ pierwiastków o różnym powinowactwie do azotu, czy też ii) współczynnik przenikania azotu przez granicę gaz/powierzchnia azotowana.

Jednak, gdy fizyczny model zjawisk jest niepełny, lub gdy parametry takiego modelu są nieokreślone lub niepełne, to dysponując dostatecznie obszerną bazą danych parametrów procesów (rodzaj materiału, temperatura i skład atmosfery azotującej w poszczególnych etapach) oraz efektów azotowania (grubości warstw azotków, profile twardości, grubości efektywne), można szukać rozwiązania w modelach opartych na **sztucznych sieciach neuronowych**.

Korzystając z danych doświadczalnych zgromadzonych przez zespoły z Politechniki Koszalińskiej i Instytutu Mechaniki Precyzyjnej utworzyłem obszerną bazę danych, która posłużyła do trenowania opracowanych przez zespół sztucznych sieci neuronowych, wyznaczających zależności między parametrami procesu a właściwościami finalnej warstwy azotowanej. **Zastosowanie tego podejścia zaprezentowane zostało w pracach** [25, 26], a wspomniany wyżej model różniczkowy służył jako jeden z elementów weryfikacji otrzymanych rezultatów.

Uzupełniającą rolę w tym kontekście miał sposób poszukiwania optymalnych parametrów procesu azotowania oparty o **algorytmy genetyczne**. Algorytm taki umożliwia szybkie, efektywne przeszukanie obszaru zmienności parametrów procesu w celu uzyskania założonej budowy warstwy azotowanej (albo założonych właściwości). Model numeryczny (różniczkowy) lub wytrenowana sztuczna sieć neuronowa służyła za rodzaj „generatora" właściwości warstwy azotowanej. **Zastosowanie tego powstałego przy moim udziale, kompleksowego podejścia do symulacji i optymalizacji procesu azotowania przedstawiono w pracach** [27, 28].

3.2 Posumowanie

Moja praca nad modelowaniem procesu azotowania znalazła swoje praktyczne odzwierciedlenie w zespołowo zaprojektowanej w ramach programu PW 004/ITE/04/2006 aplikacji komputerowej **„Symulator procesu azotowania"**, będącej użytecznym narzędziem służącym w technologii azotowania gazowego do doboru zmiennych w czasie parametrów procesu, tj. temperatury i potencjału

azotowego w celu otrzymania założonych efektów tego procesu. Niestety należy w tym miejscu wspomnieć, że aplikacja w pewnym momencie przestała być rozwijana, głównie ze względu na śmierć twórcy kodu programu. Niektóre jednak jej elementy, jak **mój różniczkowy model wzrostu warstwy na stalach stopowych nadal jest stosowany**.

4 Informacja aktywności naukowej realizowanej w innych ośrodkach

Od początku mojej pracy na uczelni moja działalność naukowa była ściśle związana ze współpracą z innymi ośrodkami, tak w ramach staży, jak i współpracy bieżącej z zespołami innych ośrodków badawczych. **Chciałbym przy tym podkreślić, że praktycznie każda taka współpraca zaowocowała publikacjami będącymi potwierdzeniem efektywności współdziałania**. Poniżej zamieszczam zwięzły opis aktywności wraz z odnośnikami do publikacji.

2001–2007 Pierwszą instytucją, o której należy wspomnieć jest **Instytut Technologii Materiałów Elektronicznych w Warszawie** (obecnie Sieć Badawcza Łukasiewicz Instytut Mikroelektroniki i Fotoniki), w którym to instytucie prowadziłem część badań do doktoratu w latach 2001–2005, i gdzie stopień doktorski otrzymałem. Praca nad nim wiązała się także z realizacją grantu badawczego tzw. promotorskiego, realizowanego w tym instytucie. Oprócz samej rozprawy, efektem współpracy są trzy publikacje: dwie dotyczące syntezy i właściwości warstw azotku molibdenu (także domieszkowanego miedzią) [29, 30] oraz praca na temat tribologicznych właściwości implantowanej ceramiki alundowej testowanej w warunkach próżniowych [31].

2003 Ostatni wymieniony w poprzednim akapicie artykuł [31] powstał też dzięki pracy w innym ośrodku; **Austrian Research Center w Seibersdorf** (Austria). Będąc tam na miesięcznym stażu zdobywałem doświadczenie w badaniach tribologicznych prowadzonych w kontrolowanej atmosferze (także w próżni) oraz w technikach analizowania stanu powierzchni.

2000–2005 Kolejnym ośrodkiem, w którym zdobyłem dużo doświadczenia jest **Uniwersytet Śródziemnomorski w Marsylii** (obecnie Aix-Marseille University), gdzie kilkukrotnie wyjeżdżałem na kilkutygodniowe pobyty, najczęściej w ramach programu „Polonium". Efektem współpracy są między innymi publikacje dotyczące właściwości tribologicznych w nanoskali, określanych z wykorzystaniem mikroskopii sił atomowych (AFM) [32–34].

2003 Instytucją, gdzie miałem możliwość rozszerzyć swój warsztat o nowoczesne metody badań właściwości mechanicznych materiałów litych i w postaci powłok był **Leibniz Institute of New Materials, Saarbruecken**, gdzie także przebywałem na kilkutygodniowym stażu. Efektem pracy było oczywiście zdobyte doświadczenie ale i późniejsza publikacja dotycząca struktury i właściwości warstw nanokompozytu TiC/a-C:H [6].

1998–2009 Ważnym ośrodkiem w mojej pracy naukowej był **Instytut Mechaniki Precyzyjnej w Warszawie** (obecnie Warszawski Instytut Technologicz-

ny). Moja praca poświęcona procesowi azotowania gazowego była w większości wykonana we współpracy z IMP – począwszy od prac [35, 36] do [24, 26]. W tematyce azotowania istotną też była dodatkowa współpraca z **Instytutem Technologii Eksploatacji w Radomiu** (obecnie Sieć Badawcza Łukasiewicz – Instytut Technologii Eksploatacji). Rezultatem tej trójstronnej współpracy są publikacje [37, 38, 25, 39–42, 27, 26].

2008–2013 Istotnym także ośrodkiem z punktu mojej aktywności zawodowej jest **Zachodniopomorski Uniwersytet Technologiczny w Szczecinie**, a w szczególności Katedra Technologii Materiałowych. Współpracy z zespołem katedry zawdzięczam zainteresowanie fazą S [43–46], a wspólnemu projektowi badawczemu 2011/03/B/ ST8/06 wytworzenie pierwszego z materiałów opisywanej w p. 2 specyficznej nanostrukturze.

2005–2008 Cenne doświadczenia zebrałem także podczas realizacji projektu European Network of Excellence – Complex Metallic Alloys. Wizyty w laboratoriach renomowanych ośrodków europejskich jak: **University of Stuttgart w Stuttgarcie** (Niemcy), **University of Toulouse w Tuluzie** (Francja), **Fritz Haber Institute w Berlinie** (Niemcy), **Josef Stefan Institute w Lublianie** (Słowenia), **University of Greifswald w Greifswaldzie** (Niemcy) umożliwiły mi zapoznanie się z dostępnym sprzętem, metodyką badań i podobnymi aspektami, co wzbogaciło obraz aktualnych kierunków badań w interesującej mnie wtedy dziedzinie.

Praca w tym projekcie i dwóch kolejnych (PW-004/ITE/03/2006 oraz PW-004/ITE/ 04/2006) zaowocowała opracowaniem i zbudowaniem systemu kontroli i sterowania procesem wieloźródłowego rozpylania magnetronowego oraz zestawu źródeł magnetronowych wraz zasilaczami do nanoszenia powłok wieloskładnikowych i wielowarstwowych [47].

2012–2015 Należy tu też wspomnieć o współpracy z **Technical University of Liberec**, która z mojej strony polegała na pracy z doktorantką tamtej uczelni, prowadzącą badania w Koszalinie, w ramach projektu NCN 2011/03/B/ ST8/06130. Efektem tej współpracy była publikacja nt. zastosowania spektroskopii optycznej do sterowania procesem nanoszenia fazy S [48].

2016–2024 Prace opisane w p. 2, dotyczące warstw nanokompozytowych MeMC/a-C:H, nie byłby możliwe bez współpracy z innymi ośrodkami; **Linköping University** (Thin Film Physics Division) i **Instytutem Metalurgii i Inżynierii Materiałowej Polskiej Akademii Nauk** w Krakowie. Dzięki tej współpracy możliwe było określenie morfologii nanokompozytów , progów segregacji węgla jak i dokonanie analizy wiązań chemicznych.

Należy tu też wspomnieć o **Centrum NanoBioMedycznym Uniwersytetu Adama Mickiewicza z Poznania** a także z **Instytutem Fizyki Doświadczalnej Uniwersytetu Gdańskiego**. Dzięki współpracy z tym laboratorium możliwe stało się opisanie właściwości magnetycznych jednego z opracowanych nanokompozytów, map przewodnictwa powierzchniowego pokryć oraz zwilżalności powierzchni materiałów. Współpraca z wymienionymi w tym akapicie instytucjami trwa nadal i planowana jest publikacja wyników kolejnych wspólnych badań.

5 Informacja o osiągnięciach dydaktycznych, organizacyjnych oraz popularyzujących naukę

Od początku swojej pracy na uczelni prowadzę zajęcia dydaktyczne z fizyki, najpierw w formie ćwiczeń i laboratoriów, potem także w formie wykładów. Zajęcia te prowadzone są dla kierunków: mechanika i budowa maszyn, mechatronika, energetyka, budownictwo, sieci i instalacje budowlane, ochrona klimatu, i innych. Niektóre z wykładów mają charakter bardziej specjalistyczny jak na przykład wykłady z podstaw fizycznych nauk o żywności, fizyki atmosfery, czy podstaw fizyki kwantowej.

Na potrzeby zajęć dydaktycznych wydano trzy skrypty, których jestem współautorem [49–51], obejmujące materiały pomocnicze do laboratorium fizyki oraz do ćwiczeń rachunkowych z tego przedmiotu. Równolegle prowadzę stronę internetową w formie wiki do własnych zajęć, zawierającą także materiały multimedialne, symulacje i animacje.

Odpowiadam za merytoryczną stronę laboratorium fizyki, opracowując instrukcje do ćwiczeń, utrzymując jego witrynę internetową. Laboratorium to służy studentom Wydziału Inżynierii Mechanicznej i Energetyki oraz Wydziału Inżynierii Lądowej, Środowiska i Geodezji.

W ramach transgranicznego projektu Sieć BalticNet-PlasmaTec odpowiadałem za popularyzację zagadnień związanych z technologiami próżniowo plazmowymi w regionie koszalińskim. Opracowałem w celu realizacji tego zadania wykłady z demonstracjami oraz zajęcia praktyczne, które zostały przeprowadzone przeze mnie dla uczniów wielu szkół z Koszalina oraz bliższych i dalszych jego okolic. W ramach projektu zorganizowane zostało przedsięwzięcie International Student's Summer School „Nanotechnologies in Materials Engineering" 2006–2008, w którym uczestniczyłem z własnymi zajęciami.

Systematycznie prowadzę zajęcia dla szkół średnich z Koszalina i okolic. Najczęściej mają one formę wykładów typu „fizyka na scenie" i są bogato ilustrowane demonstracjami, takie jak: „Natura vacuum abhorret?", „Świat drga i faluje", „O!świecenie", „Plazma – czwarty stan skupienia" i inne. Oprócz tego dla młodzieży prowadzę także zajęcia laboratoryjne z fizyki, modyfikując ćwiczenia studenckie do potrzeb i poziomu szkolnego.

W roku 2009 współorganizowałem na uczelni wystawę Fusion Expo, która powstała dzięki funduszom europejskim i miała za zadanie szerzyć wiedzę na temat syntezy termojądrowej jako przyszłościowego źródła energii elektrycznej.

W latach 2010–2011 zaangażowany byłem w projekcie „Odkrywać nieznane, tworzyć nowe – program rozwijania zainteresowania fizyką" w ramach POKL. Przygotowałem i prowadziłem serię zajęć wykładowych i laboratoryjnych dla klasy akademickiej w I LO im. Księżnej Elżbiety, w Szczecinku.

W ramach projektu „Wirtualna fizyka, wiedza prawdziwa" (POKL.03.03.04-00-032/10), realizowanego w Politechnice Koszalińskiej w latach 2010–2013 opracowałem koncepcję i scenariusze do stu interaktywnych filmów-zadań, wydanych na płytach blue-ray. Jest to spójny zbiór materiałów dydaktycznych dla kursu fizyki w szkołach średnich. W tworzeniu tych materiałów korzystałem z własnego doświadczenia dydaktycznego nie tylko na uczelni, czy też w szkole (na początku kariery zawodowej), ale też doświadczenia zdobytego na zajęciach dla szkół prowadzonych w ramach współpracy placówek oświatowych z uczelnią. Do takich można zaliczyć wspomniane wykłady dla szkół, ale też zajęcia z fizyki

dla autorskiej klasy politechnicznej (2008–2010) w V LO w Koszalinie , czy też zajęcia z podstaw wiedzy technicznej uczniów I LO z Koszalina.

Od 2009 pracuję w komitecie konkursu „Bieg po indeks", który organizowany jest od prawie trzydziestu lat w Politechnice Koszalińskiej. Odpowiadam w nim za opracowanie zadań z fizyki w każdym z trzech etapów konkursu, a także za sprawdzanie rozwiązań. Na potrzeby konkursu został wydany skrypt mojego autorstwa pt. „«Bieg po Indeks» – zadania z fizyki z rozwiązaniami i komentarzem" [52]

Właściwym wydaje mi się też wspomnieć, że od wielu lat prowadzę na klub żeglarski po nazwą Yacht Club Politechniki Koszalińskiej zrzeszający studentów, absolwentów i pracowników uczelni. Oprócz pracy organizacyjnej prowadzę też szkolenia żeglarskie oraz zajęcia z budowy, obsługi i konserwacji sprzętu pływającego. Na przecięciu natomiast moich zainteresowań zawodowych i hobbystycznych było nauczanie fizyki i informatyki w miesięcznym rejsie "Niebieskiej Szkoły" na żaglowcu Fryderyk Chopin.

Tomasz Suszko

Literatura

[1] W. Precht, E. Lunarska, A. Czyzniewski, M. Pancielejko, W. Walkowiak, Corrosion resistance, structure and mechanical properties of PVD, $TiC_xN_{(1-x)}$ coatings, Vacuum 47 (6–8) (1996) 867–869. doi:10.1016/0042-207X(96)00084-X.

[2] W. Precht, M. Pancielejko, A. Czyzniewski, Structure and tribological properties of carbon and carbon nitride films, obtained by the ARC method, Vacuum 53 (1-2) (1999) 109–112. doi:10.1016/S0042-207X(98)00403-5.

[3] W. Precht, A. Czyzniewski, Deposition and some properties of carbide/amorphous carbon nanocomposites for tribological application, Surf. Coatings Technol. 174-175 (2003) 979–983. doi:10.1016/S0257-8972(03)00586-3.

[4] A. Czyzniewski, Deposition and some properties of nanocrystalline WC and nanocomposite WC/a-C:H coatings, Thin Solid Films 433 (1-2) (2003) 180–185. doi:10.1016/S0040-6090(03)00324-9.

[5] W. Gulbiński, T. Suszko, B. Warcholiński, Cienkie warstwy węglików molibdenu MoCx nanoszone metodą reaktywnego rozpylania magnetronowegoo Title, Inżynieria Mater. 6 (2003) 490–493.

[6] W. Gulbiński, S. Mathur, H. Shen, T. Suszko, A. Gilewicz, B. Warcholiński, Evaluation of phase, composition, microstructure and properties in TiC/a-C:H thin films deposited by magnetron sputtering, Appl. Surf. Sci. 239 (3-4) (2005) 302–310. doi:10.1016/j.apsusc.2004.05.278.

[7] W. Gulbiński, T. Suszko, A. Gilewicz, B. Warcholiński, Z. Kukliński, Structure and high-temperature tribological behavior of Ti–Si–C nanocomposite thin films, Surf. Coatings Technol. 200 (14-15) (2006) 4179–4184. doi:10.1016/J.SURFCOAT.2004.12.011.

[8] W. Gulbiński, B. Warcholiński, T. Suszko, A. Gilewicz, Z. Kukliński, Właściwości tribologiczne cienkich warstw TiC-aC:H implantowanych krzemem, Inżynieria Mater. 3 (2006) 395–398.

[9] O. Knotek, E. Lugscheider, F. Löffler, B. Bosserhoff, S. Schmitz, Superstoichiometric PVD carbide coatings, Mater. Sci. Eng. A 209 (1-2) (1996) 394–398. doi:10.1016/0921-5093(95)10122-5.

[10] S. Kacim, L. Binst, F. Reniers, F. Bouillon, Composition and structure of reactively sputter-deposited molybdenum-carbon films, Thin Solid Films 287 (1-2) (1996) 25–31. doi:10.1016/S0040-6090(95)08230-1.

[11] A. A. Voevodin, S. V. Prasad, J. S. Zabinski, Nanocrystalline carbide/amorphous carbon composites, J. Appl. Phys. 82 (July) (1997) 855–858.

[12] T. Zehnder, J. Patscheider, Nanocomposite TiC/a–C:H hard coatings deposited by reactive PVD, Surf. Coatings Technol. 133-134 (2000) 138–144. doi:10.1016/S0257-8972(00)00888-4.

[13] A. Voevodin, J. Zabinski, Superhard, functionally gradient, nanolayered and nanocomposite diamond-like carbon coatings for wear protection, Diam. Relat. Mater. 7 (2-5) (1998) 463–467. doi:10.1016/S0925-9635(97)00214-8.

[14] P. Vilars, A. Prince, H. Okamoto, Handbook of Ternary Alloy Phase Diagrams, ASM International, 1995.

[15] B. Trindade, M. T. Vieira, Modification of the structural order of transition metal–carbon systems by the addition of a Group VIII element, Mater. Sci. Eng. A 352 (1–2) (2003) 195–201. doi:http://dx.doi.org/10.1016/S0921-5093(02)00865-1.

[16] U. Jansson, E. Lewin, M. Råsander, O. Eriksson, B. André, U. Wiklund, Design of carbide-based nanocomposite thin films by selective alloying, Surf. Coatings Technol. 206 (4) (2011) 583–590. doi:http://dx.doi.org/10.1016/j.surfcoat.2010.06.017.

[17] T. Suszko, W. Gulbiński, Sposób wytwarzania cienkiej, amorficznej, odpornej na zużycie ścierne i korozję powłoki na bazie przesyconego węglem stopu FeCrNi oraz cienka, amorficzna, odporna na zużycie ścierne i korozję powłoka FeCrNi:C (2018).

[18] T. Suszko, W. Gulbiński, J. Morgiel, G. Greczynski, E. Dobruchowska, P. Dłużewski, J. Lu, L. Hultman, Amorphous FeCrNi/a-C:H coatings with self-organizednanotubular structure, Scr. Mater. 136 (2017) 24–28. doi:10.1016/j.scriptamat.2017.03.040.

[19] T. Suszko, W. Gulbiński, E. Dobruchowska, G. Greczynski, L. Hultman, J. Morgiel, Quasi-amorphous, nanostructural CoCrMoC/a-C:H coatings deposited by reactive magnetron sputtering, Surf. Coatings Technol. 378 (2019) 124910. doi:10.1016/j.surfcoat.2019.124910.

[20] E. Dobruchowska, T. Suszko, G. Greczynski, D. Adamczewska, W. Gulbiński, Amorphous/quasi-amorphous CoCrMo-C coatings for improved electrochemical properties and tribocorrosion resistance of biomedical alloys, Surf. Coatings Technol. 460 (2023) 129398. doi:10.1016/j.surfcoat.2023.129398.

[21] T. Suszko, W. Gulbiński, K. Załęski, G. Greczynski, J. Morgiel, V. Lapitskaya, Nano-columnar, self-organised NiCrC/a-C:H thin films deposited by magnetron sputtering, Appl. Surf. Sci. 591 (2022) 153134. doi:10.1016/j.apsusc.2022.153134.

[22] T. Suszko, E. Dobruchowska, W. Gulbiński, K. Załęski, K. Dorywalski, NiMo-C coatings synthesised by reactive magnetron sputtering as a catalyst for the hydrogen evolution reaction in an acidic environment, submitted to ACS Appl. Mater. Interfaces (2024).

[23] J. Ratajski, R. Olik, J. Tacikowski, T. Suszko, O. Łupicka, Intelligent control system for gaseous nitriding process, Metall. Ital. 98 (7-8) (2006) 21–27.

[24] J. Ratajski, T. Suszko, Modelling of the nitriding process, J. Mater. Process. Technol. 195 (1-3) (2008) 212–217. doi:10.1016/J.JMATPROTEC.2007.04.133.

[25] J. Ratajski, D. Lipiński, T. Suszko, J. Dobrodziej, J. Michalski, Zastosowanie sztucznej sieci neuronowej do prognozowania profili twardości w warstwie azotowanej, Inżynieria Mater. 3 (2006) 516–518.

[26] J. Ratajski, R. Olik, T. Suszko, J. Dobrodziej, J. Michalski, Design, Control and in Situ Visualization of Gas Nitriding Processes, Sensors 10 (1) (2009) 218–240. doi:10.3390/s100100218.

[27] J. Ratajski, R. Olik, T. Suszko, J. Dobrodziej, J. Michalski, A. Gilewicz, Precise formation the phase composition and the thickness of nitrided layers, J. Achiev. Mater. Manuf. Eng. 37 (2) (2009) 675–689.

[28] M. Kosikowski, Z. Suszyński, R. Olik, J. Ratajski, T. Suszko, The application of artificial neural networks and evolutionary algorithm the designing of gas nitriding process, in: Int. B. Ser. Inf. Sci. Comput., 2009, pp. 33–38.

[29] T. Suszko, W. Gulbiński, J. Jagielski, The role of surface oxidation in friction processes on molybdenum nitride thin films, Surf. Coatings Technol. 194 (2–3) (2005) 319–324. doi:10.1016/J.SURFCOAT.2004.07.119.

[30] T. Suszko, W. Gulbiński, J. Jagielski, Mo2N/Cu thin films — the structure, mechanical and tribological properties, Surf. Coatings Technol. 200 (22-23) (2006) 6288–6292. doi:10.1016/J.SURFCOAT.2005.11.041.

[31] J. Jagielski, A. Piatkowska, A. Merstallinger, Z. Librant, P. Aubert, R. Groetzschel, T. Suszko, Friction properties of implanted alumina for vacuum applications, Vacuum 81 (10) (2007) 1357–1362. doi:10.1016/J.VACUUM.2007.01.045.

[32] W. Gulbiński, T. Suszko, Tarcie w nanoskali – badania cienkich warstw tlenku molibdenu techniką AFM, Inżynieria Mater. 6 (2000) 294–297.

[33] W. Gulbinski, D. Pailharey, T. Suszko, Y. Mathey, Study of the influence of adsorbed water on AFM friction measurements on molybdenum trioxide thin films, Surf. Sci. 475 (1–3) (2001) 149–158. doi:10.1016/S0039-6028(00)01101-8.

[34] W. Gulbiński, T. Suszko, D. Pailharey, High load AFM friction and wear experiments on V2O5 thin films, Wear 254 (10) (2003) 988–993. doi:10.1016/S0043-1648(03)00304-1.

[35] J. Ratajski, J. Tacikowski, R. Olik, T. Suszko, Czujnik magnetyczny i model matematyczny – niezbędne narzędzia w kontroli procesu azotowania gazowego, Inżynieria Mater. 6 (2000) 418–422.

[36] J. Ratajski, J. Tacikowski, R. Olik, T. Suszko, Wpływ składu fazowego warstwy azotków żelaza na kinetykę wzrostu warstwy azotowanej, Inżynieria Mater. 6 (2000) 414–417.

[37] J. Ratajski, T. Suszko, J. Dobrodziej, J. Michalski, Chosen aspects of the modeling of kinetics of the (carbo) nitrided layer gowth, Probl. Eksploat. 2 (2006) 113–125.

[38] J. Ratajski, D. Lipiński, T. Suszko, J. Dobrodziej, J. Michalski, Artificial neural network predictions of the microhardness profile in the nitrided layers, Probl. Eksploat. 2 (2006) 139–148.

[39] J. Ratajski, T. Suszko, J. Dobrodziej, Development of the inteligent tools for designing of the nitriding processes, Inżynieria Mater. 3–4 (2007) 724–727.

[40] J. Dobrodziej, J. Ratajski, J. Michalski, T. Suszko, Komputerowe wspomaganie projektowania procesów azotowania gazowego z wykorzystaniem symulacji i metod sztucznej inteligencji, Inżynieria Powierzchni 3 (2007) 82–93.

[41] J. Michalski, J. Tacikowski, J. Dobrodziej, J. WojutProblemy Eksploatacjiyński, J. Ratajski, T. Suszko, Numeryczna symulacja potencjału azotowego i wymiany dwuskładnikowej atmosfery amoniak-amoniak dysocjowany w projektowaniu procesów azotowania gazowego, Probl. Eksploat. 2 (2007) 105–109.

[42] R. Olik, J. Ratajski, T. Suszko, J. Michalski, J. Dobrodziej, A. Gilewicz, Precyzyjne kształtowanie budowy fazowej oraz grubości warstwy azotowanej na przykładzie matryc do ciśnieniowego odlewania aluminium, Inżynieria Powierzchni 3 (2009) 15–20.

[43] J. Baranowska, S. Fryska, J. Przekop, T. Suszko, Charakterystyka powłok z fazy S otrzymywanych na drodze reaktywnego rozpylania magnetronowego, Elektron. – Konstr. Technol. Zastos. 9 (2009) 19–21.

[44] S. Fryska, J. Baranowska, J. Przekop, T. Suszko, The properties of hard coating composed of S-phase obtained by PVD method, Adv. Manuf. Sci. Technol. Vol. 33 (nr 4) (2009) 59–69.

[45] S. Fryska, J. Baranowska, T. Suszko, Wpływ parametrów procesu na formowanie powłok z fazy S otrzymanych metodą PVD, Elektron. – Konstr. Technol. Zastos. 52 (11) (2011) 14–16.

[46] J. Baranowska, S. Fryska, T. Suszko, The influence of temperature and nitrogen pressure on S-phase coatings deposition by reactive magnetron sputtering, Vacuum 90 (1) (2013) 160–164. doi:10.1016/j.vacuum.2012.03.054.

[47] W. Gulbiński, B. Warcholiński, T. Suszko, R. Kazimierowicz, Multisource, magnetron deposited Al-Cu-Fe thin film coatings - the structure and properties, Probl. Eksploat. 4 (2006) 69–79.

[48] T. Suszko, V. Jahodowa, W. Gulbiński, Plasma emission spectroscopy as a monitoring tool for deposition of S-phase layers by magnetron sputtering, Inżynieria Mater. (1) (2015) 2.

[49] J. Mazur, T. Suszko, Fizyka, materiały dydaktyczne dla studentów do laboratorium fizyki, Wydawnictwo Uczelniane Politechniki Koszalińskiej, Koszalin, 2010.

[50] J. Mazur, T. Suszko, Fizyka, materiały szkoleniowe dla studentów do laboratorium fizyki, Wydawnictwo Uczelniane Politechniki Koszalińskiej, Koszalin, 2011.

[51] J. Mazur, T. Suszko, Fizyka, materiały szkoleniowe dla studentów, Wydawnictwo Uczelniane Politechniki Koszalińskiej, Koszalin, 2012.

[52] T. Suszko, Bieg po Indeks – zadania z fizyki z rozwiązaniami i komentarzem, Wydawnictwo Uczelniane Politechniki Koszalińskiej, Koszalin, 2010.

Summary of Professional Accomplishments

Annex 2b to the application

Tomasz Suszko

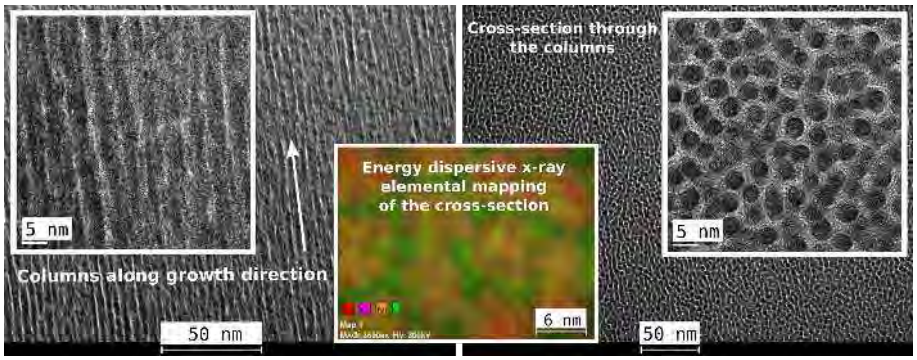

Graphical abstract from: **T. Suszko** et al., 'Amorphous FeCrNi/a-C:H coatings with self-organized nanotubular structure ', *Scripta Materialia*, 136 (2017), 24–28

Koszalin, November 6, 2024

Contents

1 Basic data

1.1 Personal data

- Name: Tomasz Suszko
- Birth date and place: —
- Workplace: Koszaln University of Technology, Faculty of Mechanical and Power Engineering
- E-mail: tomasz.suszko@tu.koszalin.pl
- Phone.: —
- ORCID No.: 0000-0002-8355-891X

- Bibliometric data (15th October 2024 r.):
  - H-index: Scopus – 14, Web of Science – 14, Google Scholar – 17.
  - Number of citations (in parenthesis the number without self-citations): Scopus – 928(905), Web of Science – 859(837), Google Scholar – 1137.
  - Number of indexed publications: Scopus – 23, Web of Science – 20, Google Scholar – 65, PBN – 80.
  - Total impact factor: **92.3**

1.2 Diplomas, degrees conferred in specific areas of science including the name of the institution which conferred the degree, year of degree conferment, title of the PhD dissertation

- 1982 – Electronics technician, Electronics Technical School in Koszalin
- 1990 – Master of Science in Physics, University of Gdańsk, Faculty of Mathematics, Physics and Chemistry
- 2005 – PhD in Technical Sciences. Discipline: Materials Engineering. Institution: Institute of Electronic Materials Technology in Warsaw. Title of the doctoral dissertation: 'High Temperature Tribological Properties of Copper-Doped γ-Mo_2N Molybdenum Nitride '

1.3 Information on employment in research institutes or faculties/departments or school of arts

After graduating, I worked at school as a physics teacher for several years, and in 1997 I was employed at the Koszalin University of Technology as an assistant.

At the beginning of my work at the university, in addition to teaching, I participated in research work conducted at the Department of Physics, engaging in experimental work and data analysis in two areas: gas nitriding and PVD technology. In my teaching work, I was entrusted with conducting exercises in physics and a laboratory in this subject.

In my research work, I focused initially on analysing and developing gas nitriding technology as an active member of the team implementing a research project together with the **Institute of Precision Mechanics in Warsaw**. The project covered a modern approach to modelling thermochemical processes and their control.

A little later I also became interested in issues related to PVD technologies, especially since the Koszalin University of Technology was one of the Polish forerunners of this technology. At that time, there were also two companies in Koszalin operating in this area: **VTT Techniki i Technologie Próżowe sp. z o.o.** and **Próżniowe Technologie Cienkowarstwowe Czesław Szypowski**.

After gaining some experience, I focused more on PVD technology and materials obtained by this method, and at the end of 2001 I started a doctoral dissertation at the **Institute of Electronic Materials Technology in Warsaw** on the synthesis and properties of thin films based on doped molybdenum nitrides. In parallel to the work on this nitride, I was involved in work on other coatings deposited using PVD methods, and in particular on their tribological properties. This work was carried out in cooperation with the **Mediterranean University in Marseille** and the **National Polytechnic Institute in Grenoble**, as part of the Polonium program. This program allowed me to travel to these research centers several times for internships and gain valuable experience.

In 2005, I defended my doctoral thesis, and my scientific interests turned to the possibilities of developing PVD technology towards multi-source magnetron sputtering and the possibility of synthesizing quasicrystalline metallic coatings. This research was conducted in cooperation with leading European scientific institutions gathered in the **Complex Metallic Alloys – Network of Excellence**, project financed in 2005–2010, and in cooperation with the **Institute of Exploitation Technology in Radom**.

Further opportunities for work on the development of PVD technology appeared when the Koszalin University of Technology received a large grant for the development of surface modification technology for woodworking tools (2009–2012). Working in the project gave the opportunity to confront the experience from scientific and laboratory work with the requirements of industrial processes. As part of the grant, I was responsible for developing the technology for the synthesis of anti-wear coatings on woodworking tools based on TiAlN nitride.

In the meantime (2007–2008) I was involved in the work on launching the materials engineering course at the university. I worked on developing the program of these studies, syllabuses, teaching materials, promotion, and later also on the implementation of diploma theses in this field.

Collaboration at that time with the **Institute of Materials Science and Engineering of the Szczecin University of Technology** directed my scientific interests to the so-called S-phase (expanded austenite). This issue lies at the interface of nitriding and PVD technology, because expanded austenite can be obtained by nitriding (gas or plasma) or by magnetron sputtering. This interest resulted in a joint research grant and, as a result, in the development of a new type of coating, FeCrNiC/ a-C:H, discussed in more detail in section 2.2.

In the years 2016–2020 I was involved in cooperation with the company **FANAR Ciechanów**, a manufacturer of cutting tools, which was the first

in Poland to introduce HIPIMS (High Power Impulse Magnetron Sputtering) technology in the production of cutting tools. The work of our team from the Koszalin University of Technology consisted in adapting the technology to the company's needs, optimizing parameters, ensuring the repeatability of processes and their monitoring.

Currently, together with my team and in cooperation with researchers from the **NanoBioMedical Centre of Adam Mickiewicz University**, the **Institute of Experimental Physics of the University of Gdańsk** and the **University of Linköping**, I am continuing research on the properties of MeMC/a-C:H layers, described in section 2, and mainly on the electrocatalytic properties of this type of materials in the cathodic hydrogen evolution reaction (HER) of water electrolysis.

2 Summary of the article series entitled 'A new class of thin coatings with a MeMC/a-C:H type nanocolumnar, composite structure. Synthesis and physicochemical properties '– presented as a basis for the habilitation procedure application

Below I present the achievement that is the basis for the habilitation degree application. It is a series of five articles listed below and attached to this application. They concern a new class of materials synthesized in the form of thin films, having a characteristic nanocolumnar, composite structure. **The synthesis of these materials by me and the study and description of their selected properties is, in my opinion, a significant contribution to the development of materials engineering**.

- (plik: Annex-5a.pdf) **T. Suszko**, W. Gulbiński, J. Morgiel, G. Greczynski, E. Dobruchowska, P. Dłużewski, J. Lu, & L. Hultman (2017). Amorphous FeCrNi/a-C:H coatings with self-organized nanotubular structure, *Scripta Materialia*, 136 (2017), 24–28.
  https://doi.org/10.1016/J.SCRIPTAMAT.2017.03.040.

- (plik: Annex-5b.pdf) **T. Suszko**, W. Gulbiński, E. Dobruchowska, G. Greczynski, L. Hultman, & J. Morgiel, Quasi-amorphous, nanostructural CoCrMoC/a-C:H coatings deposited by reactive magnetron sputtering, *Surface & Coatings Technology*, 378 (2019), 124910.
  https://doi.org/10.1016/J.SURFCOAT.2019.124910

- (plik: Annex-5c.pdf) E. Dobruchowska, **T. Suszko**, G. Greczynski, D. Adamczewska, W. Gulbiński, Amorphous/quasi-amorphous CoCrMo-C coatings for improved electrochemical properties and tribocorrosion resistance of biomedical alloys, *Surface & Coatings Technology*, 460 (2023), 129398.
  https://doi.org/10.1016/j.surfcoat.2023.129398.

- (plik: Annex-5d.pdf) **T. Suszko**, W. Gulbiński, K. Załęski, G. Greczynski, J. Morgiel, & V. Lapitskaya, Nano-columnar, self-organised NiCrC/a-C:H thin films deposited by magnetron sputtering, *Applied Surface Science*, 591 (2022), 153134.
https://doi.org/10.1016/j.apsusc.2022.153134

- (plik: Annex-5e.pdf) **T. Suszko**, E. Dobruchowska, W. Gulbiński, G. Greczynski, J. Morgiel, B. Kawczyński, K. Załęski, K. Dorywalski, & S. Pogorzelski, NiMo-C coatings synthesised by reactive magnetron sputtering for application as a catalyst for the hydrogen evolution reaction in an acidic environment, article at the review stage in *ACS Applied Materials & Interfaces* (2024).

2.1 Origin and characteristics of MeMC/a-C:H type films in the context of the current state of knowledge

Thin films of transition metal carbides, especially those belonging to the fourth, fifth and sixth groups of the periodic table, are the subject of numerous research activities due to their properties such as high hardness, electrical conductivity and corrosion resistance. In industrial practice, they are widely used as anti-wear coatings on tools, anti-corrosion coatings, as well as materials for highly loaded electrical contacts or electrodes in electrolytic hydrogen production systems. Some of the carbides are bio-compatible, making them useful for biomedical applications.

The application of advanced PVD techniques in their production process, such as reactive magnetron sputtering or HiPIMS, allows the modification of these properties through appropriate changes in chemical and phase composition. It is also possible to produce coatings with a specific layered, gradient, nanocomposite architecture, which cannot be synthesised by other methods.

Metal carbides, applied as coatings using PVD techniques, have been studied for over thirty years. The first works on this topic appeared at the Koszalin University of Technology in the late nineties [1–7]. Among the published works **there were also articles of which I am a co-author** [5–8].

Research on the production of metal carbides thin layers initially concerned materials with a stoichiometric composition. Thanks to the specificity of PVD techniques, which allow the process to be carried out in an atmosphere with an excess of carbon-bearing gas, coatings with a non-stoichiometric composition, containing a certain excess of carbon, were also obtained [9, 10]. The morphology of these materials can be described as a composite of carbide nanocrystallites (TiC, TaC, MoC) dispersed in an amorphous carbon matrix.

Many of these nanocomposites have excellent anti-wear properties. They have high hardness, a low coefficient of friction in contact with many materials, and are characterized by increased corrosion resistance. This is why these materials are used for coatings on cutting tools and machine parts.

One of the research directions was searching for and explaining the correlation between properties of coatings and the morphology of these materials. The relationships among properies as: i) the carbide precipitates sizes, ii) density of their distribution, iii) the carbon matrix thickness, iv) the chemical composition of carbides (TiC, VC, ZrC, MoC, WC) and v) the type of carbon bonds were

being studied [11, 12, 4]. Coatings with layered architecture obtained by modulating the process parameters during their deposition were also investigated (e.g. [13]).

The above-mentioned carbides of groups 4–6 of the periodic table are characterized by a high enthalpy of formation, which entails their high chemical stability, and ternary carbides containing elements from these groups, such as TiV-C, TiNb-C, VTa-C, can contain metals in any proportions [14].

The formation enthalpy of carbides from consecutive groups, especially groups 8-11, is significantly lower and even positive. These metals form a group of weakly carbide-forming elements. In studies on coatings produced by PVD techniques based on carbides of strongly carbide-forming metals doped with weakly carbide-forming metals, a progressive amorphisation of the deposit was observed as a result. The lower the affinity of the strongly carbide-forming metal for the carbon, the more readily the deposit amorphises under the influence of the doping [15].

Doping of stable carbides with weakly carbide-forming metals is accompanied by carbon segregation processes, which phenomena were studied, among others, by a team from the University of Uppsala [16].

I have linked this thread to my research on the fabrication of the S-phase by reactive magnetron sputtering of austenitic steel in atmosphere containing nitrogen and hydrocarbons (methane or acetylene). **As a result, I obtained carbon-saturated multicomponent FeCrNi/a-C:H coatings, with a previously unobserved nanocolumnar structure formed by quasiamorphous metallic columns with diameter of several nanometres, surrounded by a layer of amorphous carbon**.

Inspired by this discovery, I continued my research in several subsequent projects, and the specific nanostructure was obtained in three more systems **creating a new class of thin-film materials** hereinafter designated as **MeMC/a-C:H**, where the symbols Me and M denote weakly and strongly carbide-forming metals, respectively. The symbol a-C:H denotes amorphous hydrogenated carbon.

2.2 FeCrNiC/a-C:H coatings – structure and properties

The results of the research on the first of the coatings belonging to this class of materials are discussed in the publication **'Amorphous FeCrNi/a-C:H coatings with self-organized nanotubular structure'** – the first from the series reported in this application. In the article, I presented a description and results of the study of coatings containing 2 to 60 at.% carbon obtained by sputtering austenitic steel in an Ar/C_2H_2 atmosphere.

I discussed the evolution of the coatings' structure changing with increasing carbon content – from crystalline (S phase) through nanocrystalline to amorphous, and then to the nanocolumnar, composite structure.

In this paper, I have discussed the potential reasons for the formation of this specific nanostructure, pointing out the key importance of differences in the chemical affinity to carbon of the metallic components. The thermodynamically non-equilibrium conditions of magnetron sputtering, the relatively low substrate temperature and the presence of weak carbide-forming metals, favour the amorphisation of the deposit. These metals

form metastable bi- and tri-component carbides of the $Me_{1-x}M_xC$ type, which decompose releasing carbon atoms that later form the carbon matrix.

I explained the absence of chromium and molybdenum carbides, the appearance of which could be expected in this system, by the high activation threshold energy of metal atoms diffusion, compared to the activation threshold of carbon diffusion.

I tested the FeCrNiC/a-C:H coatings for their mechanical and tribological properties. I observed a stepwise improvement in these features when the coating structure took the form of the discussed nanocomposite. **The coatings were also tested for corrosion phenomena** in a 3% NaCl solution. It was demonstrated that the oxidation of the metallic components of the coating was significantly slower than in the starting material, while the resistance to pitting corrosion increased at the same time. A patent was obtained for the coating and the method of its production [17].

2.3 CoCrMoC/a-C:H coatings – structure and properties

The interesting results inspired me to search for other systems (alloys) that could potentially synthesise in a similar nanostructure. **A medical alloy of the $Co_{64}Cr_{32}Mo_4$ composition, widely used in implantology, was chosen as the object of studies**. The alloy contains **elements that meet the criteria I identified as necessary for synthesis in an amorphous-nanocolumnar form**. Moreover there are ongoing researches into improving the functional properties of this alloy, which gave additional impetus to the study.

My work on the synthesis of coatings by reactive sputtering the CoCrMo alloy in an argon and acetylene atmosphere has been summarized in the article **'Quasi-amorphous, nanostructural CoCrMoC/a-C:H coatings deposited by reactive magnetron sputtering'**, which is the second in the series submitted for evaluation.

In this paper, I have detailed the evolution of the coating structure with increasing carbon content. As the starting alloy is biphasic, the structural changes in terms of crystallite refinement (up to about 10 at.%) are quite complex. **In the proposed interpretation, I have taken into account the depth-depending phase composition, the presence of micro-stresses, as well as the possibility of martensitic transformation under stress.**

Coatings containing more than 10 at.% carbon become amorphous, and for even higher contents they transform into a nanocolumnar, composite structure. **By analyzing the results of XPS measurements I determined the carbon content threshold above which its segregation occurs, i.e. about 20 at.%**.

TEM and HRTEM imaging allowed me to determine that the composite nanocolumnar structure of the coating occurs over a wide range of carbon contents; from 30 to over 50 at.%, with some "collapse" of the structure observed for a carbon content of 53%.

The work contains the results of my research on basic mechanical properties of the coatings, such as hardness, resistance to plastic deformation, coefficient of friction in contact with alundum ceramics. Similarly to the FeCrNiC/a-C:H films, CoCrMoC/a-C:H coatings are characterized by very good mechanical properties.

2.4 CoCrMoC/a-C:H coatings – corrosion and tribocorrosion resistance in artificial body fluid

The next step in the research on CoCrMoC/a-C:H coatings was to assess the corrosion resistance of this material as a coating on AISI 316L steel in the environment of Hanks' balanced salt solution – one of body fluid simulators.

The report of these studies is presented in the paper **'Amorphous/quasi-amor-phous CoCrMo-C coatings for improved electrochemical properties and tribocorrosion resistance of biomedical alloys'**, being the third in the series submitted for evaluation.

The article presents the results of tests on samples containing from 0 to 65 at.% of carbon, with a structure varying from nanocrystalline through amorphous to nanocolumnar. In addition to the assessment of corrosion resistance based on polarisation tests, the results of electrochemical impedance spectroscopy measurements and a series of tribocorrosion tests are presented.

Based on the results of the impedance measurements I carried out, I showed that all the tested coatings are more stable than the massive CoCrMo alloy – they passivate faster, and the oxide layer that is formed has a greater ability to block ion penetration than is the case with the alloy.

Polarization tests showed a significant increase in corrosion potential for amorphous and nanocolumnar, composite samples, as well as high resistance to pitting corrosion. Analysis of the test results showed that chemical reactions occur only on the surface, without ion penetration through the coating.

An important part of the article are the results of **tribocorrosion tests on a tribotester designed and manufactured by me.** The device allows for friction tests to be conducted with simultaneous electrochemical measurements at a given potential or in open circuit conditions.

Based on the obtained results and analysis of phenomena occurring in the contact area during tribocorrosion tests, **I developed an electrical equivalent model of the coating-substrate-electrolyte system, which enables the connection of electrical quantities with the results of tribological measurements**.

I have shown that CoCrMoC/a-C:H nanocomposite coatings, due to their resistance to oxidation and the presence of free carbon, are characterized by low friction and wear coefficients. **I have also observed a very strong correlation between the anodic current intensity and the wear coefficient of the samples, which indicates oxidation and oxide removal as the dominant wear mechanism**.

2.5 NiCrC/a-C:H coatings – structure and magnetic properties

The nanocolumnar structure of the studied coatings, resulting from the self-assembly processes described earlier, is anisotropic by nature. Therefore, the aim of the next research steps was to verify the thesis that the observed ordering translates into anisotropy of selected coating properties.

This purpose was served by studies of NiCrC/a-C:H coatings produced by reactive magnetron sputtering of the $Ni_{80}Cr_{20}$ alloy. The alloy composition meets the criteria formulated earlier for the selection of components that promote the

formation of the tested nanostructures. I presented the results in the article **'Nano-columnar, self-organised NiCrC/a-C:H thin films deposited by magnetron sputtering'**, which is the fourth in the series presented for evaluation.

As expected, I obtained nanocrystalline, amorphous, and composite coatings with the nanocolumnar structure. In my work, I determined the carbon content threshold above which its precipitation from the amorphous structure occurs, and for the study of magnetic properties I selected amorphous samples (20 at.% carbon) and samples with 38 and 63 at.% C, showing a characteristic nanocolumnar structure.

Thanks to measurements using atomic force microscopy in topographic mode and magnetic contrast (AFM/MPM), it was possible to show that the nanopillars extend to the sample surface, and their finials are visible in the image with magnetic contrast. In the article, **I also showed that the magnetic properties of the coatings depend on the carbon content and, consequently, on the nanostructure of the material.**

The results of the magnetization and magnetic coercivity measurements, performed in the direction perpendicular to the column axis and parallel to the axis, allowed for the formulation of several conclusions: **In most measurements, the samples showed weak ferromagnetism.** However, the amorphous sample in the TEM image was also magnetically anisotropic. **The sample with a 38% carbon content showed superparamagnetism in the direction perpendicular to the column axis, and thus the greatest anisotropy.** For the sample with the highest carbon content, the anisotropy effect somehow decreased, which was probably related to the smaller diameter of the metallic columns and perhaps to the loss of their continuity.

It is interesting that the saturation magnetization increases with carbon content. **In the article I proposed to explain this phenomenon by capturing of more and more chromium atoms by carbon and the increasing number of ferromagnetic nickel nanoprecipitates**. The modeling of M–H curves (magnetization as a function of magnetic field strength) gave results consistent with the experimental data, and the median size distribution of nickel nanoparticles, giving the best fit, was about 8 nm, which turns out to be close to the observed diameter of the nanopillars.

2.6 NiMoC/a-C:H coatings – structure and properties

While analysing the potential application possibilities of coatings with the discussed nanostructure, **I drew attention to the possibility of using nickel and nickel alloys as a catalyst in water electrolysis**, or more precisely in the hydrogen evolution reaction (HER).

For this application, **I selected coatings obtained by reactive sputtering, using acetylene, of the $\mathbf{Ni_{80}Mo_{20}}$ alloy as the object of research**. The starting material meets the criteria described earlier, required to obtain the nanocolumnar composite structure observed on other described materials, and is paramagnetic, which enables its effective magnetron sputtering.

Nickel is a well-known and industrially used catalyst for the HER reaction replacing expensive catalysts based on platinum group metals. Even higher catalytic capacity is demonstrated by the $Ni_{80}Mo_{20}$ alloy, which is also a separate phase. **It is important, however, that despite their good catalytic ac-**

tivity, they can only be used in an alkaline environment, because nickel and $Ni_{80}Mo_{20}$ are not resistant to acids. In an acidic environment, however, the reaction is much more efficient than in an alkaline environment.

NiMo-C layers with the appropriate carbon content, due to their amorphous structure and carbon precipitates, should be significantly more resistant to acids than the pure alloy. I have included the results of research focused on these issues in the article **'NiMo-C coatings synthesised by reactive magnetron sputtering for application as a catalyst for the hydrogen evolution reaction in an acidic environment'**, which is the fifth in the series presented for evaluation.

As in the case of other materials studied so far, **I described the evolution of the structure with increasing carbon content**. In general, the changes in structure were as in the case of other described materials; from nanocrystalline, through amorphous, to nanocolumnar.

In my work **I showed that also in this system of elements, with a carbon content greater than about 40 at.%, the coatings synthesized in the form of a nanocolumnar composite structure**, and also that the layers with a carbon content of about 23 at.% and more were distinguished by high corrosion resistance in 0.1M H_2SO_4.

For the purpose of assessing the electrocatalytic activity, **I performed a series of potentiodynamic measurements and then analysed the results in terms of the Tafel slope of the polarization curves and characteristic overpotentials**. Samples with the lowest carbon content were the most active electrocatalytically, but they were not resistant to corrosion. **In the article, I showed that composite nanocolumnar samples with an medium carbon content had optimal properties; good corrosion resistance, good electrocatalytic activity, and the best stability in cyclic measurements**.

Another important result of the research is the finding that even **the highest carbon content samples showed good catalytic activity**, much better than graphite. **I considered the presence of metallic catalytic centers ('nanocolumn finials') on the samples surfaces as the reason for this effect, which is one of the consequences of the characteristic nanocomposite structure**. The presence of these centers was confirmed using an AFM microscope operating in the conductivity mode (C-AFM).

2.7 Summary

In Sections 2.2–2.6, I briefly discuss the main research themes developed in the five articles that make up the series I have submitted for evaluation. **All articles concern a new class of coatings with a specific nanocolumnar composite structure, designated as MeMC/a-C:H**.

Their production was the result of my research on multicomponent carbide based coatings. As a result of these initial studies, I synthesized the FeCrNiC/a-C:H coating [18], patented later [17], and the result of several subsequent projects was the synthesis of other nanocolumnar coatings: CoCrMoC/a-C:H [19, 20], NiCr-C/a-C:H [21] and NiMoC/a-C:H [22]. All developed coatings were tested for selected properties, and their selection was based on potential applications.

At the stage of publication of the research results, I was responsible for the research concepts, gathering, analysis and presentation of data, state of the art descriptions, results discussion and conclusions. In all the works submitted for evaluation, I was the corresponding author responsible also for corrections and additions related to the manuscript reviews.

Currently, I continue my research on the properties of MeMC/a-C:H coatings, and in particular on their electrocatalytic activity in the hydrogen evolution reaction. The object of the research are coatings obtained by reactive magnetron sputtering of NiW alloys.

3 Information on achievements in the development of nitrided layer growth models in the context of gas nitriding process control

The main subject of my scientific work is related to research on thin films synthesised by PVD methods. However, **a significant part of my activity, both before and after my doctorate (until approx. 2009), was devoted to work on the analysis of the gas nitriding process**; one of the commonly used thermo-chemical treatments for heavily loaded machine and tool parts.

Since the invention of nitriding in the 1910s, the need for precise control of the nitriding process has gradually emerged in order to obtain the appropriate effective thickness of the nitrided layer. My work on nitriding technology was related to this topic, and the results of this work, in addition to the achievement described in Section 2, in my opinion constitute a significant contribution to the development of materials engineering. For this reason, I am placing a short description of the achievement here, although they cannot be included in the categories listed in the Act as "monograph", "series of articles" or "design achievement".

3.1 Description of works and results achieved

In the research on the gas nitriding process, I was an active member of the team dealing with issues related to process control, sensors for this purpose, and modeling the kinetics of nitrided layer growth. This work was carried out, among others, within the following projects, in which I participated as one of the main contractors:

1. Project KBN T08C 008 10 'Development of the design basis for automatically controlled gas nitriding processes', 1996–1998.
2. Project KBN T08C 039 19 'The influence of the surface iron nitrides (carbonitrides) on the formation and the growth kinetics of the nitrided layer', 2000–2003.
3. Project PW 004/ITE/04/2006 'Development of a magnetic sensor for in situ measurement of nitrided layer growth in gas nitriding process monitoring systems', 2007–2008.

One of the effects of the third project was **a computer application used to simulate the kinetics of nitrided layer growth and to design the**

process. My role in the team was **to develop mathematical models** that were the basis for simulating the nitriding process and predicting its results.

The starting point of my work was the physical basis of phenomena and **analytical models** based mainly on Fick's diffusion equations. This approach, together with experimental work, allows, for example, determining the diffusion coefficients in iron and low-alloy steels under constant nitrogen potential and temperature. It also allows, to some extent, the selection of process parameters in order to obtain the desired layer thickness. Additionally, certain conclusions resulting from the analytical solutions of the equations, such as the concept of the so-called parabolic growth constant, allow the calculation of monophase zones thicknesses formed on the surface during the process.

Based on analytical models, **I built a series of more complex models. The models included nitrogen binding reactions with alloying elements, diffusion and growth of the outer compound layer**. Such systems of equations become solvable only by computer methods, and together with computational algorithms, they create **the numerical models**. Their reliability was analyzed based on experimental data, and then **they were used to simulate the shape of nitrogen concentration profiles, both the one bound in the nitrides of alloying elements and the one dissolved in the ferrite**. These nitrogen concentration profiles are crucial for determining the hardness distribution in the nitrided layer.

Moreover, thanks to time discretization, division of the simulated process into stages, it became possible to take into account the time variability of parameters such as temperature, composition of the nitriding atmosphere. **The model I developed quite precisely maps both the diffusion process and the reactions of nitrogen bonding with alloying elements, realistically mapping the behaviour of the material during the process.** The input parameters of the model are the time dependencies of temperature and nitrogen potential (or atmosphere composition) and some conventional parameters depending on the type of nitrided steel. The solution results in the time dependencies of the thickness of the nitride layers, profiles of nitrogen concentration in the diffusion zone and profiles of nitrogen bonded to alloying elements. **The analysis of nitrided layer growth using such models also made it possible to formulate important conclusions regarding the design of technological processes, and their usefulness was demonstrated in several works**, such as [23, 24].

When using the differential model, there are difficulties related to the aforementioned conventional material parameters that require experimental determination. However, when the physical model of the phenomena is incomplete, or when the parameters of such a model are undefined, then having a sufficiently extensive database of process parameters (type of material, temperature and composition of the nitriding atmosphere in the individual stages) and nitriding effects (thicknesses of nitride layers, hardness profiles, effective thicknesses), one can seek a solution in models based on **artificial neural networks**.

Using the experimental data collected by the teams from the Koszalin University of Technology and the Institute of Precision Mechanics, I created a database, which was used to train the artificial neural networks developed by the team, determining the relationships between the process parameters and the properties of the final nitrided layer. **The application of this approach was presented in the works** [25, 26], and the above-mentioned

differential model was used as one of the methods of verification the obtained results.

A complementary role in this context was played by the method of searching for optimal parameters of the nitriding process based on **genetic algorithms**. Such an algorithm enables fast, effective searching through the range of process parameter variability in order to obtain the assumed structure of the nitrided layer (or assumed properties). The numerical (differential) model or trained artificial neural network served as a kind of 'generator' of the nitrided layer's properties. **The application of this comprehensive approach to simulation and optimization of the nitriding process, developed with my participation, was presented in the works [27, 28]**.

3.2 Summary

My work on modeling the nitriding process found its practical reflection in the computer application **"Nitriding process simulator"**, designed as part of the PW 004/ITE/04/2006 project. The application was a useful tool used in gas nitriding technology to select time-varying process parameters, i.e. temperature and nitrogen potential, in order to obtain the intended effects of this process. Unfortunately, it should be mentioned here that the application was discontinued at some point, mainly due to the death of the program code creator. However, some of its elements, such as **my differential model of layer growth on alloy steels, is still used**.

4 Information on research activities carried out in other centres

Since the beginning of my work at the university, my scientific activities have been closely linked to cooperation with other centres. **I would like to emphasise that practically every such cooperation has resulted in publications confirming the effectiveness of the cooperation**. Below is a concise description of the activity with links to publications.

2001–2007 The first institution to be mentioned is the **Institute of Electronic Materials Technology** in Warsaw (now Łukasiewicz Research Network Institute of Microelectronics and Photonics), where I did some of my research for my PhD between 2001 and 2005, and where I received my doctoral degree.

In addition to the thesis itself, the collaboration has resulted in three publications: two on the synthesis and properties of molybdenum nitride layers (also doped with copper) [29, 30] and a paper on the tribological properties of implanted alumina ceramics under vacuum conditions.

2003 This last article was also written thanks to my work at another centre; the **Austrian Research Center** in Seibersdorf (Austria). While there for a month-long internship, I gained experience in tribological research conducted in a controlled atmosphere (including vacuum) and surface condition analysis techniques.

2000–2005 Another centre where I have gained a lot of experience is the **Mediterranean University of Marseille** (now Aix-Marseille University), where I have gone on several occasions for stays of several weeks, usually as part of the 'Polonium' programme. This collaboration has resulted, among other things, in publications on tribological properties at the nanoscale, determined using atomic force microscopy (AFM) [31–33].

2003 An institution where I had the opportunity to expand my workshop with modern methods of investigating the properties of solid and coated materials was the **Leibniz Institute of New Materials** in Saarbruecken (Germany), where I also spent several weeks as an internship. The work resulted in the experience gained, but also in a subsequent publication on the structure and properties of TiC/a-C:H nanocomposite films [6].

1998–2009 An important centre in my scientific work was the **Institute of Precision Mechanics** in Warsaw (now the Warsaw Institute of Technology). Most of my work related to the gas nitriding process was carried out in collaboration with IMP - starting from papers [34, 35] to [24, 26].

In the field of nitriding, additional cooperation with the **Institute of Sustainable Technologies** in Radom (now Łukasiewicz Research Network Institute of Sustainable Technologies) was also significant. The results of this trilateral cooperation are publications [36, 37, 25, 38–41, 27, 26].

2008–2015 An important centre from the point of view of my professional activity is also the **West Pomeranian University of Technology** in Szczecin, and in particular the Department of Materials Technology. I owe my interest in the S-phase to the cooperation with the department [42–45], and the synthesis of the first material from the group with the specific nanostructure, described in Section 2, to the joint research project.

2005–2008 I also gained valuable experience during the European Network of Excellence - Complex Metallic Alloys project. Visits to the laboratories of renowned European centres such as the **University of Stuttgart**, Stuttgart (Germany), the **University of Toulouse**, Toulouse (France), **Fritz Haber Institute**, Berlin (Germany), **Josef Stefan Institute**, Ljubljana (Slovenia), the **University of Greifswald**, Greifswald (Germany) enabled me to familiarise myself with available equipment, research methodology and similar aspects, which enriched the picture of current research directions in the field I was then interested in.

The work in this project resulted in the development and construction, under my leadership, of a multi-source magnetron sputtering process control and control system and a set of magnetron sources with power supplies for the application of multicomponent and multilayer coatings [46].

2012–2015 It is also important to mention the cooperation with the **Technical University of Liberec**, Liberec (Czechia), which, on my part, consisted of working with a doctoral student from that university, conducting research in Koszalin. This cooperation resulted in a publication on the use of optical spectroscopy to control the S-phase deposition process [47].

2012–2015 The achievements described in Section 2, concerning MeMC/a-C:H nanocomposite films, would not have been possible without cooperation with

other centres such as **Linköping University** (Thin Film Physics Division) and the **Institute of Metallurgy and Materials Science of the Polish Academy of Sciences** in Krakow. Thanks to this collaboration, it was possible to determine the morphology of the nanocomposites, the carbon segregation thresholds as well as to analyse the chemical bonds. In the context of MeMC/a-C:H nanocomposites, the **NanoBioMedical Centre of the Adam Mickiewicz University** in Poznan should also be mentioned. Cooperation with this laboratory has made it possible to describe the magnetic properties of one of the developed nanocomposites. Colleagues from the **University of Gdańsk** (Faculty of Mathematics, Physic and Informatics) have recently joined the group of collaborating scientists, working on wettability of the NiMoC/a-C:H coatings.

Cooperation with the institutions mentioned in this paragraph continues and publication of the results of joint research is planned.

5 Information about teaching, organizational and science popularization achievements

Since the beginning of my work at the university, I have been teaching physics. First in the form of exercises and laboratories, then also in the form of lectures. These classes are conducted for the following fields of study: mechanics and machine construction, mechatronics, energy, construction, building networks and installations, climate protection, and others. Some of the lectures are more specialized, such as lectures on the physics foundations of food science, atmospheric physics, or the fundamentals of quantum physics.

For the needs of the classes, three scripts were published, of which I am a co-author [48–50], including auxiliary materials for physics and physics laboratory. In parallel, I run a website (in the form of a wiki) for my own classes, also containing multimedia materials, simulations and animations.

I am responsible for the content side of the physics laboratory, developing instructions for exercises and maintaining the laboratory website.

As part of the cross-border project 'BalticNet-PlasmaTec Network' I was responsible for popularizing issues related to vacuum plasma technologies in the Koszalin region. In order to carry out this task, I developed lectures with demonstrations and practical classes, which I conducted for students of many schools in our region. As part of the 'BalticNet-PlasmaTec' project, the International Student's Summer School 'Nanotechnologies in Materials Engineering' 2006–2008 was organized, in which I participated with my own classes.

In 2009, I co-organized the Fusion Expo exhibition at our university, which was created thanks to European funds and aimed to disseminate knowledge about thermonuclear fusion as a future source of electrical energy.

In 2010–2011 I was involved in the project 'Discovering the Unknown, Creating the New – a program for developing interest in physics' within the framework of POKL programme. I prepared and conducted a series of lectures and laboratory classes for the academic class in the STO High School in Szczecinek.

As part of the project 'Virtual Physics, True Knowledge' (POKL.03.03.04-00-032/10), carried out at the Koszalin University of Technology (2010–2013), I developed the concept and scenarios for one hundred interactive film-tasks,

released on blue-ray discs.

This was a coherent collection of teaching materials for a physics course in secondary schools (high schools). In creating these materials, I used my own teaching experience not only at the university or at school (at the beginning of my professional career), but also the experience gained in classes for schools conducted as part of cooperation between educational institutions and my university. The cooperation include the aforementioned lectures for schools, but also physics exercises for a polytechnic class (2008-2010) at the V LO (5th High School) in Koszalin, or lectures on the Fundamentals of Technical Knowledge for students of the I LO (1st High School) in Koszalin.

I regularly conduct classes for secondary schools in Koszalin and the surrounding area. Most often in the form of lectures of the 'physics on stage'-type, richly illustrated with demonstrations, such as: 'Natura vacuum abhorret?', 'The world vibrations and waves', 'En!light!enment', 'Plasma - the fourth state of matter' and others. In addition, I also conduct laboratory exercises in physics for young people, modifying student exercises to the needs of school level.

Since 2009 I have been working in the committee of the 'Run for the Student Index' competition, which has been organized for almost thirty years at the Koszalin University of Technology. I am responsible for formulating physics problems in each of the three stages of the competition, as well as for checking the solutions. For the needs of the competition, a script of my authorship was published entitled '‹Run for the Student Index› – physics problems with solutions and commentary' [51]

It seems appropriate to mention that for many years I have been running the Yacht Club Politechniki Koszalińskiej (Koszalin University of Technology Yacht Club), which brings together students, graduates and employees of the university. In addition to organizational work, I also run sailing training and classes on the construction, operation and maintenance of boats. At the intersection of my profession and hobby was teaching physics and computer science during a month-long cruise of the "Blue School" on the sailing ship Fryderyk Chopin.

Tomasz Suszko

References

[1] W. Precht, E. Lunarska, A. Czyzniewski, M. Pancielejko, W. Walkowiak, Corrosion resistance, structure and mechanical properties of PVD, $TiC_xN_{(1-x)}$ coatings, Vacuum 47 (6–8) (1996) 867–869. doi:10.1016/0042-207X(96)00084-X.

[2] W. Precht, M. Pancielejko, A. Czyzniewski, Structure and tribological properties of carbon and carbon nitride films, obtained by the ARC method, Vacuum 53 (1-2) (1999) 109–112. doi:10.1016/S0042-207X(98)00403-5.

[3] W. Precht, A. Czyzniewski, Deposition and some properties of carbide/amorphous carbon nanocomposites for tribological application, Surf. Coatings Technol. 174-175 (2003) 979–983. doi:10.1016/S0257-8972(03)00586-3.

[4] A. Czyzniewski, Deposition and some properties of nanocrystalline WC and nanocomposite WC/a-C:H coatings, Thin Solid Films 433 (1-2) (2003) 180–185. doi:10.1016/S0040-6090(03)00324-9.

[5] W. Gulbiński, T. Suszko, B. Warcholiński, Cienkie warstwy węglików molibdenu MoCx nanoszone metodą reaktywnego rozpylania magnetronowegoo Title, Inżynieria Mater. 6 (2003) 490–493.

[6] W. Gulbiński, S. Mathur, H. Shen, T. Suszko, A. Gilewicz, B. Warcholiński, Evaluation of phase, composition, microstructure and properties in TiC/a-C:H thin films deposited by magnetron sputtering, Appl. Surf. Sci. 239 (3-4) (2005) 302–310. doi:10.1016/j.apsusc.2004.05.278.

[7] W. Gulbiński, T. Suszko, A. Gilewicz, B. Warcholiński, Z. Kukliński, Structure and high-temperature tribological behavior of Ti–Si–C nanocomposite thin films, Surf. Coatings Technol. 200 (14-15) (2006) 4179–4184. doi:10.1016/J.SURFCOAT.2004.12.011.

[8] W. Gulbiński, B. Warcholiński, T. Suszko, A. Gilewicz, Z. Kukliński, Właściwości tribologiczne cienkich warstw TiC-aC:H implantowanych krzemem, Inżynieria Mater. 3 (2006) 395–398.

[9] O. Knotek, E. Lugscheider, F. Löffler, B. Bosserhoff, S. Schmitz, Superstoichiometric PVD carbide coatings, Mater. Sci. Eng. A 209 (1-2) (1996) 394–398. doi:10.1016/0921-5093(95)10122-5.

[10] S. Kacim, L. Binst, F. Reniers, F. Bouillon, Composition and structure of reactively sputter-deposited molybdenum-carbon films, Thin Solid Films 287 (1-2) (1996) 25–31. doi:10.1016/S0040-6090(95)08230-1.

[11] A. A. Voevodin, S. V. Prasad, J. S. Zabinski, Nanocrystalline carbide/amorphous carbon composites, J. Appl. Phys. 82 (July) (1997) 855–858.

[12] T. Zehnder, J. Patscheider, Nanocomposite TiC/a–C:H hard coatings deposited by reactive PVD, Surf. Coatings Technol. 133-134 (2000) 138–144. doi:10.1016/S0257-8972(00)00888-4.

[13] A. Voevodin, J. Zabinski, Superhard, functionally gradient, nanolayered and nanocomposite diamond-like carbon coatings for wear protection, Diam. Relat. Mater. 7 (2-5) (1998) 463–467. doi:10.1016/S0925-9635(97)00214-8.

[14] P. Vilars, A. Prince, H. Okamoto, Handbook of Ternary Alloy Phase Diagrams, ASM International, 1995.

[15] B. Trindade, M. T. Vieira, Modification of the structural order of transition metal–carbon systems by the addition of a Group VIII element, Mater. Sci. Eng. A 352 (1–2) (2003) 195–201. doi:http://dx.doi.org/10.1016/S0921-5093(02)00865-1.

[16] U. Jansson, E. Lewin, M. Råsander, O. Eriksson, B. André, U. Wiklund, Design of carbide-based nanocomposite thin films by selective alloying, Surf. Coatings Technol. 206 (4) (2011) 583–590. doi:http://dx.doi.org/10.1016/j.surfcoat.2010.06.017.

[17] T. Suszko, W. Gulbiński, Sposób wytwarzania cienkiej, amorficznej, odpornej na zużycie ścierne i korozję powłoki na bazie przesyconego węglem stopu FeCrNi oraz cienka, amorficzna, odporna na zużycie ścierne i korozję powłoka FeCrNi:C (2018).

[18] T. Suszko, W. Gulbiński, J. Morgiel, G. Greczynski, E. Dobruchowska, P. Dłużewski, J. Lu, L. Hultman, Amorphous FeCrNi/a-C:H coatings with self-organizednanotubular structure, Scr. Mater. 136 (2017) 24–28. doi:10.1016/j.scriptamat.2017.03.040.

[19] T. Suszko, W. Gulbiński, E. Dobruchowska, G. Greczynski, L. Hultman, J. Morgiel, Quasi-amorphous, nanostructural CoCrMoC/a-C:H coatings deposited by reactive magnetron sputtering, Surf. Coatings Technol. 378 (2019) 124910. doi:10.1016/j.surfcoat.2019.124910.

[20] E. Dobruchowska, T. Suszko, G. Greczynski, D. Adamczewska, W. Gulbiński, Amorphous/quasi-amorphous CoCrMo-C coatings for improved electrochemical properties and tribocorrosion resistance of biomedical alloys, Surf. Coatings Technol. 460 (2023) 129398. doi:10.1016/j.surfcoat.2023.129398.

[21] T. Suszko, W. Gulbiński, K. Załęski, G. Greczynski, J. Morgiel, V. Lapitskaya, Nano-columnar, self-organised NiCrC/a-C:H thin films deposited by magnetron sputtering, Appl. Surf. Sci. 591 (2022) 153134. doi:10.1016/j.apsusc.2022.153134.

[22] T. Suszko, E. Dobruchowska, W. Gulbiński, K. Załęski, K. Dorywalski, NiMo-C coatings synthesised by reactive magnetron sputtering as a catalyst for the hydrogen evolution reaction in an acidic environment, submitted to ACS Appl. Mater. Interfaces (2024).

[23] J. Ratajski, R. Olik, J. Tacikowski, T. Suszko, O. Łupicka, Intelligent control system for gaseous nitriding process, Metall. Ital. 98 (7-8) (2006) 21–27.

[24] J. Ratajski, T. Suszko, Modelling of the nitriding process, J. Mater. Process. Technol. 195 (1-3) (2008) 212–217. doi:10.1016/J.JMATPROTEC.2007.04.133.

[25] J. Ratajski, D. Lipiński, T. Suszko, J. Dobrodziej, J. Michalski, Zastosowanie sztucznej sieci neuronowej do prognozowania profili twardości w warstwie azotowanej, Inżynieria Mater. 3 (2006) 516–518.

[26] J. Ratajski, R. Olik, T. Suszko, J. Dobrodziej, J. Michalski, Design, Control and in Situ Visualization of Gas Nitriding Processes, Sensors 10 (1) (2009) 218–240. doi:10.3390/s100100218.

[27] J. Ratajski, R. Olik, T. Suszko, J. Dobrodziej, J. Michalski, A. Gilewicz, Precise formation the phase composition and the thickness of nitrided layers, J. Achiev. Mater. Manuf. Eng. 37 (2) (2009) 675–689.

[28] M. Kosikowski, Z. Suszyński, R. Olik, J. Ratajski, T. Suszko, The application of artificial neural networks and evolutionary algorithm the designing of gas nitriding process, in: Int. B. Ser. Inf. Sci. Comput., 2009, pp. 33–38.

[29] T. Suszko, W. Gulbiński, J. Jagielski, The role of surface oxidation in friction processes on molybdenum nitride thin films, Surf. Coatings Technol. 194 (2–3) (2005) 319–324. doi:10.1016/J.SURFCOAT.2004.07.119.

[30] T. Suszko, W. Gulbiński, J. Jagielski, Mo2N/Cu thin films — the structure, mechanical and tribological properties, Surf. Coatings Technol. 200 (22-23) (2006) 6288–6292. doi:10.1016/J.SURFCOAT.2005.11.041.

[31] W. Gulbiński, T. Suszko, Tarcie w nanoskali – badania cienkich warstw tlenku molibdenu techniką AFM, Inżynieria Mater. 6 (2000) 294–297.

[32] W. Gulbinski, D. Pailharey, T. Suszko, Y. Mathey, Study of the influence of adsorbed water on AFM friction measurements on molybdenum trioxide thin films, Surf. Sci. 475 (1–3) (2001) 149–158. doi:10.1016/S0039-6028(00)01101-8.

[33] W. Gulbiński, T. Suszko, D. Pailharey, High load AFM friction and wear experiments on V2O5 thin films, Wear 254 (10) (2003) 988–993. doi:10.1016/S0043-1648(03)00304-1.

[34] J. Ratajski, J. Tacikowski, R. Olik, T. Suszko, Czujnik magnetyczny i model matematyczny – niezbędne narzędzia w kontroli procesu azotowania gazowego, Inżynieria Mater. 6 (2000) 418–422.

[35] J. Ratajski, J. Tacikowski, R. Olik, T. Suszko, Wpływ składu fazowego warstwy azotków żelaza na kinetykę wzrostu warstwy azotowanej, Inżynieria Mater. 6 (2000) 414–417.

[36] J. Ratajski, T. Suszko, J. Dobrodziej, J. Michalski, Chosen aspects of the modeling of kinetics of the (carbo) nitrided layer gowth, Probl. Eksploat. 2 (2006) 113–125.

[37] J. Ratajski, D. Lipiński, T. Suszko, J. Dobrodziej, J. Michalski, Artificial neural network predictions of the microhardness profile in the nitrided layers, Probl. Eksploat. 2 (2006) 139–148.

[38] J. Ratajski, T. Suszko, J. Dobrodziej, Development of the inteligent tools for designing of the nitriding processes, Inżynieria Mater. 3–4 (2007) 724–727.

[39] J. Dobrodziej, J. Ratajski, J. Michalski, T. Suszko, Komputerowe wspomaganie projektowania procesów azotowania gazowego z wykorzystaniem symulacji i metod sztucznej inteligencji, Inżynieria Powierzchni 3 (2007) 82–93.

[40] J. Michalski, J. Tacikowski, J. Dobrodziej, J. WojutProblemy Eksploatacjiyński, J. Ratajski, T. Suszko, Numeryczna symulacja potencjału azotowego i wymiany dwuskładnikowej atmosfery amoniak-amoniak dysocjowany w projektowaniu procesów azotowania gazowego, Probl. Eksploat. 2 (2007) 105–109.

[41] R. Olik, J. Ratajski, T. Suszko, J. Michalski, J. Dobrodziej, A. Gilewicz, Precyzyjne kształtowanie budowy fazowej oraz grubości warstwy azotowanej na przykładzie matryc do ciśnieniowego odlewania aluminium, Inżynieria Powierzchni 3 (2009) 15–20.

[42] J. Baranowska, S. Fryska, J. Przekop, T. Suszko, Charakterystyka powłok z fazy S otrzymywanych na drodze reaktywnego rozpylania magnetronowego, Elektron. – Konstr. Technol. Zastos. 9 (2009) 19–21.

[43] S. Fryska, J. Baranowska, J. Przekop, T. Suszko, The properties of hard coating composed of S-phase obtained by PVD method, Adv. Manuf. Sci. Technol. Vol. 33 (nr 4) (2009) 59–69.

[44] S. Fryska, J. Baranowska, T. Suszko, Wpływ parametrów procesu na formowanie powłok z fazy S otrzymanych metodą PVD, Elektron. – Konstr. Technol. Zastos. 52 (11) (2011) 14–16.

[45] J. Baranowska, S. Fryska, T. Suszko, The influence of temperature and nitrogen pressure on S-phase coatings deposition by reactive magnetron sputtering, Vacuum 90 (1) (2013) 160–164. doi:10.1016/j.vacuum.2012.03.054.

[46] W. Gulbiński, B. Warcholiński, T. Suszko, R. Kazimierowicz, Multisource, magnetron deposited Al-Cu-Fe thin film coatings - the structure and properties, Probl. Eksploat. 4 (2006) 69–79.

[47] T. Suszko, V. Jahodowa, W. Gulbiński, Plasma emission spectroscopy as a monitoring tool for deposition of S-phase layers by magnetron sputtering, Inżynieria Mater. (1) (2015) 2.

[48] J. Mazur, T. Suszko, Fizyka, materiały dydaktyczne dla studentów do laboratorium fizyki, Wydawnictwo Uczelniane Politechniki Koszalińskiej, Koszalin, 2010.

[49] J. Mazur, T. Suszko, Fizyka, materiały szkoleniowe dla studentów do laboratorium fizyki, Wydawnictwo Uczelniane Politechniki Koszalińskiej, Koszalin, 2011.

[50] J. Mazur, T. Suszko, Fizyka, materiały szkoleniowe dla studentów, Wydawnictwo Uczelniane Politechniki Koszalińskiej, Koszalin, 2012.

[51] T. Suszko, Bieg po Indeks – zadania z fizyki z rozwiązaniami i komentarzem, Wydawnictwo Uczelniane Politechniki Koszalińskiej, Koszalin, 2010.

Wykaz osiągnięć naukowych lub artystycznych stanowiących znaczny wkład w rozwój określonej dyscypliny

Załącznik 3a do wniosku o przeprowadzenie postępowania habilitacyjnego

Tomasz Suszko

6 listopada 2024

1 Wykaz osiągnięć naukowych albo artystycznych, o których mowa w art. 219 ust. 1. pkt 2 ustawy

1.1 Monografia naukowa, zgodnie z art. 219 ust. 1. pkt 2a ustawy; lub

—

1.2 Cykl powiązanych tematycznie artykułów naukowych, zgodnie z art. 219 ust. 1. pkt 2b ustawy

Cykl artykułów pod nazwą „Nowa klasa cienkich powłok o nanokompozytowej strukturze amorficzno kolumnowej typu MeMC/a-C:H – wytwarzanie oraz właściwości fizykochemiczne". Osiągnięcie jest opisane bliżej w autoreferacie, a prace tworzące cykl zamieszczone są w załącznikach od Annex-5a.pdf do Annex-5e.pdf.

1.3 Wykaz zrealizowanych oryginalnych osiągnięć projektowych, konstrukcyjnych, technologicznych lub artystycznych, zgodnie z art. 219 ust. 1. pkt 2c ustawy

—

2 Wykaz aktywności naukowej albo artystycznej

2.1 Wykaz opublikowanych monografii naukowych (z zaznaczeniem pozycji niewymienionych w pkt 1.1)

—

2.2 Wykaz opublikowanych rozdziałów w monografiach naukowych

—

2.3 Wykaz członkostwa w redakcjach naukowych monografii

—

2.4 Wykaz opublikowanych artykułów w czasopismach naukowych niewymienionych w pkt 1.2

Poniżej zamieszczam listę moich publikacji naukowych **niewymienionych w pkt 1.2**, z podziałem na te przed i po doktoracie.

Przed doktoratem:

1. J. Ratajski, J. Tacikowski, R. Olik, T. Suszko, Czujnik magnetyczny i model matematyczny - niezbędne narzędzia w kontroli procesu azotowania gazowego, Inżynieria Mater. 6 (2000) 418–422.

2. J. Ratajski, J. Tacikowski, R. Olik, T. Suszko, Wpływ składu fazowego warstwy azotków żelaza na kinetykę wzrostu warstwy azotowanej, Inżynieria Mater. 6 (2000) 414–417.

3. W. Gulbiński, T. Suszko, Tarcie w nanoskali - badania cienkich warstw tlenku molibdenu techniką AFM, Inżynieria Mater. 6 (2000) 294–297.

4. W. Gulbinski, D. Pailharey, T. Suszko, Y. Mathey, Study of the influence of adsorbed water on AFM friction measurements on molybdenum trioxide thin films, Surf. Sci. 475 (2001) 149–158. https://doi.org/10.1016/S0039-6028(00)01101-8.

5. J. Ratajski, J. Tacikowski, R. Olik, T. Suszko, The Effect of the Phase Composition of Compound Layer on the Growth Kinetics of the Nitrided Layer., Inżynieria Mater. 5 (2001) 757–761.

6. J. Ratajski, J. Tacikowski, T. Suszko, Role of the layer of iron (carbo) nitrides in the kinetics of diffusion layer growth on alloys steels, in: 9th Int. Semin. IFHTSE, Nitriding Technol. Warsaw, 2003: pp. 77–87.

7. W. Gulbiński, T. Suszko, B. Warcholiński, Cienkie warstwy węglików molibdenu MoCx nanoszone metodą reaktywnego rozpylania magnetronowegoo, Inżynieria Mater. 6 (2003) 490–493.

8. W. Gulbiński, T. Suszko, D. Pailharey, High load AFM friction and wear experiments on V_2O_5 thin films, Wear 254 (2003) 988–993. https://doi.org/10.1016/S0043-1648(03)00304-1.

9. W. Gulbiński, T. Suszko, W. Sienicki, B. Warcholiński, Tribological properties of silver- and copper-doped transition metal oxide coatings, Wear 254 (2003) 129–135. https://doi.org/10.1016/S0043-1648(02)00292-2.

10. J. Ratajski, J. Tacikowski, T. Suszko, O. Łupicka, Modelowanie struktury i własności materiałów w procesie azotowania gazowego, Inżynieria Powierzchni 4 (2004) 12–15.

11. W. Gulbiński, A. Gilewicz, T. Suszko, B. Warcholiński, Z. Kukliński, Ti–Si–C sputter deposited thin film coatings, Surf. Coatings Technol. 180–181 (2004) 341–346. https://doi.org/10.1016/J.SURFCOAT.2003.10.084.

12. W. Gulbiński, A. Gilewicz, T. Suszko, Z. Kukliński, B. Warcholiński, Właściwości tribologiczne cienkich warstw węglika tytanu nanoszonych metodą reaktywnego rozpylania magnetronowego, Inżynieria Mater. 4 (2004) 51–56.

13. W. Gulbiński, S. Mathur, H. Shen, T. Suszko, A. Gilewicz, B. Warcholiński, Evaluation of phase, composition, microstructure and properties in TiC/a-C:H thin films deposited by magnetron sputtering, Appl. Surf. Sci. 239 (2005) 302–310. https://doi.org/10.1016/j.apsusc.2004.05.278.

14. J. Ratajski, J. Tacikowski, T. Suszko, Modelowanie struktury i własności materiałów w procesie azotowania gazowego., Inżynieria Powierzchni 1 (2005) 49–58.

15. J. Ratajski, R. Olik, J. Tacikowski, T. Suszko, O. Łupicka, Układ sterowania procesem azotowania gazowego nowej generacji, Inżynieria Mater. 5 (2005) 549–561.

Po doktoracie:

16. T. Suszko, W. Gulbiński, J. Jagielski, The role of surface oxidation in friction processes on molybdenum nitride thin films, Surf. Coatings Technol. 194 (2005) 319–324.
https://doi.org/10.1016/J.SURFCOAT.2004.07.119.

17. J. Ratajski, D. Lipiński, T. Suszko, J. Dobrodziej, J. Michalski, Application of relational data base concerning processes and effects of surface layers deposition, Probl. Eksploat. 2 (2006) 139–147.

18. J. Ratajski, D. Lipiński, T. Suszko, J. Dobrodziej, J. Michalski, Artificial neural network predictions of the microhardness profile in the nitrided layers, Probl. Eksploat. 2 (2006) 139–148.

19. J. Ratajski, T. Suszko, J. Dobrodziej, J. Michalski, Chosen aspects of the modeling of kinetics of the (carbo) nitrided layer gowth, Probl. Eksploat. 2 (2006) 113–125.

20. J. Ratajski, R. Olik, J. Tacikowski, T. Suszko, O. Łupicka, Intelligent control system for gaseous nitriding process, Metall. Ital. 98 (2006) 21–27.

21. J. Ratajski, D. Lipiński, T. Suszko, J. Dobrodziej, J. Michalski, Zastosowanie sztucznej sieci neuronowej do prognozowania profili twardości w warstwie azotowanej, Inżynieria Mater. 3 (2006) 516–518.

22. T. Suszko, W. Gulbiński, J. Jagielski, Mo2N/Cu thin films — the structure, mechanical and tribological properties, Surf. Coatings Technol. 200 (2006) 6288–6292.
https://doi.org/10.1016/J.SURFCOAT.2005.11.041.

23. W. Gulbiński, B. Warcholiński, T. Suszko, R. Kazimierowicz, Multisource, magnetron deposited Al-Cu-Fe thin film coatings - the structure and properties, Probl. Eksploat. 4 (2006) 69–79.

24. W. Gulbiński, T. Suszko, A. Gilewicz, B. Warcholiński, Z. Kukliński, Structure and high-temperature tribological behavior of Ti–Si–C nanocomposite thin films, Surf. Coatings Technol. 200 (2006) 4179–4184. https://doi.org/10.1016/J.SURFCOAT.2004.12.011.

25. W. Gulbiński, T. Suszko, Thin films of Mo2N/Ag nanocomposite—the structure, mechanical and tribological properties, Surf. Coatings Technol. 201 (2006) 1469–1476. https://doi.org/10.1016/J.SURFCOAT.2006.02.017.

26. W. Gulbiński, T. Suszko, Thin films of MoO3–Ag2 O binary oxides – the high temperature lubricants, Wear 261 (2006) 867–873. https://doi.org/10.1016/J.WEAR.2006.01.008.

27. W. Gulbiński, B. Warcholiński, T. Suszko, A. Gilewicz, Z. Kukliński, Właściwości tribologiczne cienkich warstw TiC-aC:H implantowanych krzemem, Inżynieria Mater. 3 (2006) 395–398.

28. J. Ratajski, T. Suszko, J. Dobrodziej, Development of the inteligent tools for designing of the nitriding processes, Inżynieria Mater. 3–4 (2007) 724–727.

29. J. Jagielski, A. Piatkowska, A. Merstallinger, Z. Librant, P. Aubert, R. Groetzschel, T. Suszko, Friction properties of implanted alumina for vacuum applications, Vacuum 81 (2007) 1357–1362. https://doi.org/10.1016/J.VACUUM.2007.01.045.

30. J. Dobrodziej, J. Ratajski, J. Michalski, T. Suszko, Komputerowe wspomaganie projektowania procesów azotowania gazowego z wykorzystaniem symulacji i metod sztucznej inteligencji, Inżynieria Powierzchni 3 (2007) 82–93.

31. J. Dobrodziej, A. Mazurkiewicz, J. Ratajski, T. Suszko, J. Michalski, The methodology of fuzzy logic application in the modelling of thermo-diffusive and PVD processes, in: 16th Int. Fed. Heat Treat. Surf. Eng. Congr., 2007.

32. J. Michalski, J. Tacikowski, J. Dobrodziej, J. WojutProblemy Eksploatacjiyński, J. Ratajski, T. Suszko, Numeryczna symulacja potencjału azotowego i wymiany dwuskładnikowej atmosfery amoniak-amoniak dysocjowany w projektowaniu procesów azotowania gazowego, Probl. Eksploat. 2 (2007) 105–109.

33. J. Ratajski, T. Suszko, Modelling of the nitriding process, J. Mater. Process. Technol. 195 (2008) 212–217. https://doi.org/10.1016/J.JMATPROTEC.2007.04.133.

34. R. Olik, J. Ratajski, J. Dobrodziej, T. Suszko, J. Michalski, D. Lipiński, Projektowanie, kontrola i wizualizacja in-situ procesu azotowania., Inżynieria Mater. 1–3 (2008) 839–843.

35. J. Baranowska, S. Fryska, J. Przekop, T. Suszko, Charakterystyka powłok z fazy S otrzymywanych na drodze reaktywnego rozpylania magnetronowego, Elektron. – Konstr. Technol. Zastos. 9 (2009) 19–21.

36. J. Ratajski, R. Olik, T. Suszko, J. Dobrodziej, J. Michalski, Design, Control and in Situ Visualization of Gas Nitriding Processes, Sensors 10 (2009) 218–240.
https://doi.org/10.3390/s100100218.

37. J. Ratajski, W. Gulbiński, J. Staśkiewicz, J. Walkowicz, P. Myśliński, A. Czyżniewski, T. Suszko, A. Gilewicz, B. Warcholiński, Hard coatings for woodworking tools–a review, Manuf. Eng. 37 (2009) 668–674.

38. J. Ratajski, R. Olik, T. Suszko, J. Dobrodziej, J. Michalski, A. Gilewicz, Precise formation the phase composition and the thickness of nitrided layers, J. Achiev. Mater. Manuf. Eng. 37 (2009) 675–689.

39. R. Olik, J. Ratajski, T. Suszko, J. Michalski, J. Dobrodziej, A. Gilewicz, Precyzyjne kształtowanie budowy fazowej oraz grubości warstwy azotowanej na przykładzie matryc do ciśnieniowego odlewania aluminium, Inżynieria Powierzchni 3 (2009) 15–20.

40. R. Olik, J. Ratajski, J. Dobrodziej, T. Suszko, D. Lipiński, J. Michalski, Projektowanie i monitorowanie procesu azotowania gazowego, Probl. Eksploat. 1 (2009) 145–156.

41. M. Kosikowski, Z. Suszyński, R. Olik, J. Ratajski, T. Suszko, The application of artificial neural networks and evolutionary algorithm the designing of gas nitriding process, in: Int. B. Ser. Inf. Sci. Comput., 2009: pp. 33–38.

42. S. Fryska, J. Baranowska, J. Przekop, T. Suszko, The properties of hard coating composed of S-phase obtained by PVD method, Adv. Manuf. Sci. Technol. Vol. 33 (2009) 59–69.

43. R. Olik, B. Warcholiński, T. Suszko, A. Gilewicz, J. Ratajski, Modelowanie procesów azotowania i PVD podwyższających trwałość narzędzi ze stali WCL, Pomiary Autom. Kontrola 7 (2010) 819–823.

44. T. Suszko, W. Gulbiński, A. Urbanowicz, W. Gulbiński, Preferentially oriented vanadium nitride films deposited by magnetron sputtering, Mater. Lett. 65 (2011) 2146–2148.
https://doi.org/10.1016/j.matlet.2011.04.038.

45. S. Fryska, J. Baranowska, T. Suszko, Wpływ parametrów procesu na formowanie powłok z fazy S otrzymanych metodą PVD, Elektron. – Konstr. Technol. Zastos. 52 (2011) 14–16.

46. J. Baranowska, S. Fryska, T. Suszko, The influence of temperature and nitrogen pressure on S-phase coatings deposition by reactive magnetron sputtering, Vacuum 90 (2013) 160–164.
https://doi.org/10.1016/j.vacuum.2012.03.054.

47. V. Jahodowa, T. Suszko, Nitrogen doped steel coatings, Fine Mech. Opt. 58 (2013) 326–327.

48. T. Suszko, V. Jahodowa, W. Gulbiński, Plasma emission spectroscopy as a monitoring tool for deposition of S-phase layers by magnetron sputtering, Inżynieria Mater. (2015) 2.

49. Ł. Tomaszewski, A. Urbanowicz, T. Suszko, W. Gulbiński, Przeciwzużyciowe powłoki TiAlN modyfikowane wanadem, Inżynieria Mater. 36 (2015) 310–313.

50. Ł. Tomaszewski, W. Gulbiński, A. Urbanowicz, T. Suszko, A. Lewandowski, W. Gulbiński, TiAlN based wear resistant coatings modified by molybdenum addition, Vacuum 121 (2015) 223–229. https://doi.org/10.1016/j.vacuum.2015.08.027.

2.5 Wykaz osiągnięć projektowych, konstrukcyjnych, technologicznych niewymienione w pkt 1.3

Przed doktoratem:

1. Opracowanie oraz budowa skomputeryzowanego układu do sterowania i akwizycji danych z fotograficznego spektrometru optycznego PGS 2 przeznaczonego do badań widma emisyjnego plazmy – w ramach statutowych prac badawczych Katedry Fizyki PK (1998).

2. Opracowanie układu do synchronicznego pomiaru parametrów sondy Langmuira do badania plazmy wyładowania magnetronowego wzbudzanej impulsowo – w ramach badań własnych Katedry Fizyki (1999).

3. Opracowanie konstrukcji wysokotemperaturowego testera tarcia oraz budowa programu (w oparciu o pakiet DASYLab i komputerową kartę pomiarową) do sterowania jego pracą i akwizycji danych – w ramach grantu badawczego KBN nr 7T08C 00816 (2000).

4. Opracowanie metody oceny naprężeń ścinających opartej o zmodyfikowane urządzenie Revetest i opracowany model matematyczny zjawiska – w ramach grantu badawczego KBN nr 7T08C00816 (2000).

5. Napisanie programu do odczytu, eksportu i analizy danych z mikroskopu sił atomowych NANOSCOPE III firmy Digital Instruments – w ramach programu Polonium (2001).

6. Zbudowanie programu (z wykorzystaniem pakietu DASYLab) do sterowania procesem reaktywnego rozpylania magnetronowego za pomocą kontroli widma emisyjnego plazmy oraz do zbierania parametrów pracy próżniowego stanowiska technologicznego – w ramach przewodu doktorskiego (2002).

7. Technologia nanoszenia azotków molibdenu Mo_2N i MoN (także domieszkowanych miedzią i srebrem) za pomocą reaktywnego rozpylania magnetronowego — w ramach grantu badawczego KBN nr 7T08C00816 i przewodu doktorskiego (2004)

Po doktoracie:

8. „Opracowanie modeli matematycznych wzrostu warstwy azotowanej na stali w procesie azotowania gazowego". Osiągnięcie jest **opisane bliżej w autoreferacie** wraz z odnośnikami do prac, w których modele zostały wykorzystane.

9. Projekt i budowa zestawu źródeł magnetronowych oraz opracowanie założeń konstrukcyjnych zasilaczy do pracy z tymi źródłami do nanoszenia powłok wieloskładnikowych i wielowarstwowych — ramach projektu PW-004/ITE/03/2006.

10. Technologia nanoszenia azotku wanadu za pomocą reaktywnego rozpylania magnetronowego — w ramach projektu POIG.01.03.01-32-052/08.

11. Modernizacja i adaptacja urządzenia typu Bułat na potrzeby technologii wytwarzania powłok na wybrane narzędzia do obróbki drewna — w ramach projektu POIG.01.03.01-32-052/08.

12. Opracowanie systemu sterowania magnetronowym nanoszeniem warstw azotowej i węglowej fazy S, w oparciu o emisyjne widmo plazmy rejestrowane spektrometrem optycznym, i regulację natężenia przepływu gazów roboczych — ramach projektu NCN nr 2011/03/B/ST8/06.

13. Technologia nanoszenia nanokolumnowych quasiamorficznych warstw typu MeMC/a-C:H metodą reaktywnego rozpylania magnetronowego — ramach projektu NCN nr 2011/03/B/ST8/06 oraz badań własnych katedry.

14. Projekt i budowa tribotestera do elektrochemicznych badań tribokorozyjnych w cieczy, z synchronicznym pomiarem siły i wielkości elektrycznych mierzonych potencjostatem. W ramach projektu wewnętrznego PK.

2.6 Wykaz publicznych realizacji dzieł artystycznych (z zaznaczeniem pozycji niewymienionych w pkt 1.3)

—

2.7 Wykaz wystąpień na krajowych lub międzynarodowych konferencjach naukowych lub artystycznych, z wyszczególnieniem przedstawionych wykładów na zaproszenie i wykładów plenarnych

1. W. Gulbiński, **T. Suszko**. Badania składu chemicznego cienkich warstw tlenku molibdenu MoO3-x metodą XPS. IV Ogólnopolska Konferencja Naukowa Obróbka powierzchniowa' 99, Częstochowa-Kule , 5–8 października 1999 r.

2. W. Gulbinski, **T. Suszko**, W. Sienicki, B. Warcholinski. Tribological properties of ag and cu doped transition metal oxide coatings. 2nd World Tribology Congress, Wiedeń, Austria, 3–7 września 2001 r.

3. W. Gulbiński, **T. Suszko**. Wytwarzanie i właściości tribologiczne cienkich warstw molibdenianów srebra. V Ogólnopolska Konferencja Naukowa Óbróbka powierzchniowa"2002, Częstochowa-Kule, 18–20 września 2002 r.

4. W. Gulbiński, **T. Suszko**, D. Pailharey. High Load AFM Friction and Wear Experiments on V2O5 Thin Films. 3rd International Colloquim Micro-tribology 2001 , Jastarnia, 28-30 października 2001 r.

5. W. Gulbiński, **T. Suszko**, B. Warcholiński. „Cienkie warstwy węglików molibdenu MoCx nanoszone metodą reaktywnego rozpylania magnetronowego". II Krajowa Konferencja „Nowe materiały – nowe technologie w przemyśle okrętowym i maszynowym", Szczecin-Międzyzdroje, 7–10 września 2003 r.

6. **T. Suszko**, W. Gulbiński, J. Jagielski. „Mo2N/Cu Films – Structure, Mechanical and Tribological Properties". E-MRS 2005 Spring Meeting, Strasbourg (Francja), 31 maja – 3 czerwca 2005 r.

7. **T. Suszko**, W. Gulbiński, J. Morgiel, G. Greczynski, E. Dobruchowska, P. Dłużewski, J. Lu. Ćarbon Supersaturated Fe-Cr-Ni-C Thin Films with a Unique Nanocolumnar Structure - a Tough, Low Friction and Corrosion Resistant Coating". 44th International Conference on Metallurgical Coatings and Thin Films ICMCTF 2017, San Diego (CA, USA), 24–28 kwietnia 2017 r.

8. **T. Suszko**, W. Gulbiński, J. Morgiel, G. Greczynski, E Dobruchowska, P. Dłużewski, J Lu. „Amorphous FeCrNi/a-C:H coatings with self-organized nanotubular structure". 10-th Symposium on Vacuum based Science and Technology, Kołobrzeg, 28–30 listopada 2017 r.

9. **T. Suszko**, W. Gulbiński, E Dobruchowska, G. Greczynski, J. Morgiel. „Mechanical and tribological properties of CoCrMo/a-C:H coatings deposited by magnetron sputtering of ISO 5832-12 medical alloy", 10-th Symposium on Vacuum based Science and Technology, Kołobrzeg, 28–30 listopada 2017 r.

10. **T. Suszko**, E. Dobruchowska, W. Gulbiński, G. Greczynski, L. Hultman, J. Morgiel. Ńanostructural CoCrMoC/a-C:H coatings deposited by reactive magnetron sputtering", European Materials Research Society Spring Meeting 2019, Nicea, Francja, 27-31 maja 2019 r.

2.8 Wykaz udziału w komitetach organizacyjnych i naukowych konferencji krajowych lub międzynarodowych, z podaniem pełnionej funkcji

—

2.9 Wykaz uczestnictwa w pracach zespołów badawczych realizujących projekty finansowane w drodze konkursów krajowych lub zagranicznych, z podziałem na projekty zrealizowane i będące w toku realizacji, oraz z uwzględnieniem informacji o pełnionej funkcji w ramach prac zespołów

Projekty naukowe zrealizowane przed doktoratem:

1. Projekt badawczy KBN nr T08C 008 10 „Opracowanie podstaw projektowania automatycznie sterowanych procesów azotowania gazowego" (1996–1998), wykonawca.

2. Projekt badawczy KBN nr T08C 039 19 „Wpływ przypowierzchniowej warstwy azotków (węgloazotków) żelaza na kształtowanie się kinetyki wzrostu warstwy azotowanej" (2000–2003), wykonawca.

3. Projekt badawczy KBN nr 4 T08C02924 – „Nanokompozytowe powłoki cienkowarstwowe do zastosowań w warunkach tarcia suchego w podwyższonych temperaturach" (2003-2005), wykonawca.

4. Projekt „Polonium" nr 4978.I.2003 z Narodowym Instytutem Politechnicznym w Grenoble (2003–2004), wykonawca.

5. Projekt typu NATO Collaborative Linkage Grant „Nano-Structured Functional Coatings for Optical and Lubrication Applications"; we współpracy z Institute of New Materials w Saarbruecken (2004–2005), wykonawca.

Projekty naukowe i wdrożeniowe zrealizowane doktoracie:

6. Projekt „Polonium" nr 5578.I/2004 z Uniwersytetem Śródziemnomorskim w Marsylii (2004–2005), wykonawca.

7. European Network of Excellence „Complex Matallic Alloys- CMA", nr projetu: NOE 500140 (2005–2009), wykonawca.

8. Projekt badawczo-rozwojowy nr PW-004/ITE/04/2004 zamawiany w ramach Programu Wieloletniego PW004 „Nanokompozytowe pokrycia antyścierne na bazie quasikrystalicznych stopów metali" (2005–2006), wykonawca.

9. Projekt badawczo-rozwojowy nr PW 004/ITE/04/2006 „Opracowanie czujnika magnetycznego do pomiaru in situ wzrostu warstwy azotowanej w systemach monitorowania procesów azotowania gazowego" (2007–2008), wykonawca.

10. Projekt badawczo-rozwojowy nr PW-004/ITE/04/2006 „Prototyp systemu kontroli i sterowania procesem wielоźródłowego rozpylania magnetronowego oparty o emisyjną spektroskopię plazmy"(2007–2008), wykonawca.

11. Projekt badawczo-rozwojowy nr PW-004/ITE/03/2006 „Zestaw źródeł magnetronowych wraz z systemami zasilania i sterowania do nanoszenia powłok wieloskładnikowych i wielowarstwowych"(2007–2008), kierownik.

12. Projekt nr POIG.01.03.01-32-052/08 „Hybrydowe technologie modyfikacji powierzchni narzędzi do obróbki drewna", zadanie nr 2: „Opracowanie technologii przeciwzużyciowych warstw na bazie TiAlN, Politechnika Koszalińska (2009–2012), kierownik zadania.

13. Projekt NCN nr 2011/03/B/ST8/06, „Nowe, zaawansowane kompozytowe powłoki przeciwzużyciowe na stali austenitycznej", Politechnika Koszalińska (2012-2015), główny wykonawca.

14. Projekt typu B+R NCBiR , POIR.01.01.01-00-0531/15-00, „Opracowanie narzędzi i mikronarzędzi trzpieniowych ze szczególnym uwzględnieniem pokryć PVD nanostrukturalnych", przedsiębiorstwo FANAR, Ciechanów (2016–2018), wykonawca.

15. Projekt typu B+R NCBiR, POIR.01.01.01-00-0274/17 pt. „Opracowanie typoszeregu gwintowników i wierteł pokrywanych powłokami nanostrukturalnymi do pracy z materiałami trudno obrabialnymi". Przedsiębiorstwo FANAR, Ciechanów (2016–2018), wykonawca.

Projekty będące obecnie na etapie oceny:

- Projekt „Self-organised coatings on 3D substrates for Hydrogen Evolution Reaction – synthesis, nanostructure and properties" , złożony do NCN w konkursie OPUS 2024.

2.10 Wykaz członkostwa w międzynarodowych lub krajowych organizacjach i towarzystwach naukowych wraz z informacją o pełnionych funkcjach

—

2.11 Wykaz staży w instytucjach naukowych lub artystycznych, w tym zagranicznych, z podaniem miejsca, terminu, czasu trwania stażu i jego charakteru

Lista zagranicznych staży i pobytów naukowych:

2000 Mediterranean University of Marseille (obecnie Aix-Marseille University), Marsylia (Francja), 3 tygodnie, pobyt badawczy w ramach współpracy naukowej finansowanej przez stronę francuską.

2001 Mediterranean University of Marseille (obecnie Aix-Marseille University), Marsylia (Francja), 3 tygodnie, pobyt badawczy w ramach programu "Polonium".

2002 Mediterranean University of Marseille (obecnie Aix-Marseille University), Marsylia (Francja), 3 tygodnie, pobyt badawczy w ramach programu "Polonium".

2003 National Polytechnic Institute of Grenoble CNRS-LEMD (obecnie French National Centre for Scientific Research CNRS), Grenoble (Francja), 1 tydzień, pobyt badawczy w ramach programu "Polonium".

2003 Mediterranean University of Marseille (obecnie Aix-Marseille University), Marsylia (Francja), 2 tygodnie, pobyt badawczy w ramach programu "Polonium".

2004 Leibniz Institute of New Materials, Saarbruecken (Niemcy), 2 tygodnie, pobyt badawczy w ramach grantu NATO-CLG.

2004 Aerospace & Space Materials Technology Testhouse, Austrian Research Center, Seibersdorf (Austria), 4 tygodnie, pobyt badawczy w ramach europejskiego programu AMTT, (aplikacja II-83).

2005 Mediterranean University of Marseille (obecnie Aix-Marseille University), 2 tygodnie, pobyt badawczy w ramach programu "Polonium".

2006 University of Stuttgart, Stuttgard (Niemcy), 1 tydzień, wyjazd roboczy w ramach projektu European Network of Excellence – Complex Metallic Alloys.

2006 University of Toulouse, Tuluza (Francja), 1 tydzień, wyjazd roboczy w ramach projektu European Network of Excellence – Complex Metallic Alloys.

2006 Fritz Haber Institute, Berlin (Niemcy), 1 tydzień, wyjazd roboczy w ramach projektu European Network of Excellence – Complex Metallic Alloys.

2006 Josef Stefan Institute, Lublana (Słowenia), 1 tydzień, wyjazd roboczy (EuroSchool 2006) w ramach projektu European Network of Excellence – Complex Metallic Alloys.

2007 University of Greifswald, Greifswald (Niemcy), wyjazd roboczy w ramach projektu BalticNet-PlasmaTec.

2007 University of Toulouse (organizator), Fira (Grecja), wyjazd roboczy w ramach projektu European Network of Excellence – Complex Metallic Alloys.

2007 National Polytechnic Institute of Grenoble CNRS-LEMD (obecnie French National Centre for Scientific Research CNRS), Grenoble (Francja), 1 tydzień, wyjazd badawczy na zaproszenie strony francuskiej w ramach projektu ECONET.

2008 University of Aix-Marseilles, Marsylia (Francja), wyjazd roboczy w ramach projektu European Network of Excellence – Complex Metallic Alloys.

2008 Josef Stefan Institute, Lublana (Słowenia), 1 tydzień, wyjazd roboczy (EuroSchool 2008) w ramach projektu European Network of Excellence – Complex Metallic Alloys.

2008 University of Nancy, Nancy (Francja), wyjazd roboczy w ramach projektu European Network of Excellence – Complex Metallic Alloys.

2009 Josef Stefan Institute, Lublana (Słowenia), wyjazd organizacyjny wystawy Fusion Expo.

2013 Technical University of Liberec, Liberec (Czechy), 1 tydzień, praca badawcza w ramach projektu Erasmus – Staff Training Mobility.

2.12 Wykaz członkostwa w komitetach redakcyjnych i radach naukowych czasopism wraz z informacją o pełnionych funkcjach (np. redaktora naczelnego, przewodniczącego rady naukowej, itp.)

—

2.13 Wykaz recenzowanych prac naukowych, w szczególności publikowanych w czasopismach międzynarodowych

Blisko połowa moich prac (p. 2.4) została opublikowana w recenzowanych, uznanych czasopismach międzynarodowych z listy JCR.

Od 2007 r. systematycznie recenzuję artykuły w czasopiśmie Surface & Coatings Technology.

2.14 Wykaz uczestnictwa w programach europejskich lub innych programach międzynarodowych

1. Projekt „Polonium" nr 4978.I.2003 z Narodowym Instytutem Politechnicznym w Grenoble (2003–2004), wykonawca.
2. Projekt typu NATO Collaborative Linkage Grant „Nano-Structured Functional Coatings for Optical and Lubrication Applications"; we współpracy z Institute of New Materials w Saarbruecken (2004–2005), wykonawca.
3. Projekt „Polonium" nr 5578.I/2004 z Uniwersytetem Śródziemnomorskim w Marsylii (2004–2005), wykonawca.
4. European Network of Excellence „Complex Matallic Alloys- CMA", nr projektu: NOE 500140, realizacja 2005-2009, wykonawca.

2.15 Wykaz udziału w zespołach badawczych, realizujących projekty inne niż określone w pkt. 2.9

—

2.16 Wykaz uczestnictwa w zespołach oceniających wnioski o finansowanie badań, wnioski o przyznanie nagród naukowych, wnioski w innych konkursach mających charakter naukowy lub dydaktyczny

—

3 Współpra z otoczeniem społecznym i gospodarczym

3.1 Wykaz dorobku technologicznego

Patrz p. 2.5

3.2 Współpraca z sektorem gospodarczym.

Z przedsięwzięć badawczych wymienionych w p. 2.9 trzy niżej wymienione dotyczyły bezpośrednio współpracy z otoczeniem gospodarczym.

- Projekt nr POIG.01.03.01-32-052/08 „Hybrydowe technologie modyfikacji powierzchni narzędzi do obróbki drewna", zadanie nr 2: „Opracowanie technologii przeciwzużyciowych warstw na bazie TiAlN, Politechnika Koszalińska (2009–2012), kierownik zadania.

- Projekt typu B+R NCBiR , POIR.01.01.01-00-0531/15-00, „Opracowanie narzędzi i mikronarzędzi trzpieniowych ze szczególnym uwzględnieniem pokryć PVD nanostrukturalnych", przedsiębiorstwo FANAR, Ciechanów (2016–2018), wykonawca.

- Projekt typu B+R NCBiR, POIR.01.01.01-00-0274/17 pt. „Opracowanie typoszeregu gwintowników i wierteł pokrywanych powłokami nanostrukturalnymi do pracy z materiałami trudno obrabialnymi". Przedsiębiorstwo FANAR, Ciechanów (2016–2018), wykonawca.

Najważniejszymi partnerami były firmy: FANAR S.A. Ciechanów, FABA S.A. Baboszewo, AB Wood Sławno, VTT Koszalin. Oprócz tego do współpracy z otoczeniem gospodaczym zaliczyć można wykonywanie ekspertyz i innych tego typu opracowań dla firm. Ekspertyzy z ostatnich lat wymieniłem w p. 3.5.

3.3 Wykaz uzyskanych praw własności przemysłowej, w tym uzyskanych patentów krajowych lub międzynarodowych.

- **Tomasz Suszko**, Witold Gulbiński, Sposób wytwarzania cienkiej, amorficznej, odpornej na zużycie ścierne i korozję powłoki na bazie przesyconego węglem stopu FeCrNi oraz cienka, amorficzna, odporna na zużycie ścierne i korozję powłoka FeCrNi:C, Pat.230506, Urząd Patentowy RP, 2018.

- **Tomasz Suszko**, Ewa Dobruchowska, Witold Gulbiński, Sposób wytwarzania cienkiej, amorficznej, odpornej na korozję w środowisku kwaśnym, powłoki na bazie nanokompozytu typu NiMoC/a-C:H, przeznaczonej na elektrody do elektrokatalitycznego wytwarzania wodoru oraz cienka, amorficzna, odporna na korozję w środowisku kwaśnym powłoka NiMoC/a-C:H. Zgłoszenie patentowe, Urząd Patentowy RP, 2024

3.4 Wykaz wdrożonych technologii.

Uczestniczyłem w pracach wdrożeniowych technologii pokrywania narzędzi powłokami PVD (w tym technologii HPIMS) przez przedsiębiorstwo FANAR S.A. z Ciechanowa w ramach dwóch wymienionych wyżej (p. 2.9) projektów.

3.5 Wykaz wykonanych ekspertyz lub innych opracowań wykonanych na zamówienie instytucji publicznych lub przedsiębiorców.

1. Analiza właściwości powłok TiAlN nanoszonych techniką magnetronową na narzędzia ze stali szybkotnących (HSS) i opracowanie rekomendacji w zakresie optymalizacji adhezji powłok. Przedsiębiorstwo FANAR S.A., Ciechanów, w ramach projektu POIR.01.01.01-00-0531/15-00, 2016 r.

2. Dobór parametrów procesu nanoszenia magnetronowego powłok TiAlN, TiAlCN oraz TiAlSiN z wykorzystaniem metody Taguchi, w celu uzyskania optymalych właściwości powłok. Przedsiębiorstwo FANAR S.A., Ciechanów, w ramach projektu POIR.01.01.01-00-0531/15-00, 2017–18 r.

3. Badania przestrzennych rozkładów parametrów plazmy w procesach magnetronowego osadzania powłok TiAlN+TiN z wykorzystaniem emisyjnej

spektroskopii optycznej w celu określenia użytecznej przestrzeni komory technologicznej. Przedsiębiorstwo FANAR S.A., Ciechanów, w ramach projektu POIR.01.01.01-00-0531/15-00, 2017 r.

4. Analiza bazowych procedur wytwarzania powłok FerroCon, FerroCon Gold , Ferrocon WCC, InoxaCon w urządzeniu CC800/9 HiPIMS oraz optymalizacja parametrów procesów dla poprawy właściwości powłok. Przedsiębiorstwo FANAR S.A., Ciechanów, w ramach projektu POIR.01.01.01-00-0274/17, 2018 r.

5. Analiza porównawcza wyników analizy emisyjnego widma plazmy optycznej z procesów na urządzeniu CC800/9 HiPIMS z właściwościami strukturalnymi i mechanicznymi otrzymanych warstw opartych na TiAlN. Przedsiębiorstwo FANAR S.A., Ciechanów, w ramach projektu POIR.01.01.01-00-0274/17, 2019 r.

6. Badanie mikrostruktury próbek wykonanych ze stali narzędziowej M42. Fabryka Narzędzi FANAR S.A., (współautorstwo ekspertyzy), 2023 r.

7. Badanie mikrostruktury próbek blachy Al (stop 3005) z powłoką polimerową. PRO-WAM Sp. z o.o., (współautorstwo ekspertyzy), 2023 r.

8. Badanie mikrostruktury taśmy 76 mm oraz rurki Ø25 mm wykonanych ze stali LDX2101. HEXONIC Sp. z o.o., (współautorstwo ekspertyzy), 2023 r.

9. Badanie mikrostruktury powłok PVD wytwarzanych na narzędziach trzpieniowych. Fabryka Narzędzi FANAR S.A., (współautorstwo ekspertyzy), 2023 r.

10. Badanie mikrostruktury rowka wiórowego narzędzi trzpieniowych na różnych etapach obróbki powierzchniowej. Fabryka Narzędzi FANAR S.A., (współautorstwo ekspertyzy), 2023 r.

11. Badanie mikrostruktury wkładek węglikowych stosowanych w narzędziach chirurgicznych. Aesculap Chifa sp. z o.o., (współautorstwo ekspertyzy), 2023 r.

12. Badanie mikrostruktury wygniataka M12 z powłoką PVD. Fabryka Narzędzi FANAR S.A., (współautorstwo ekspertyzy), 2024 r.

13. Badanie mikrostruktury próbek wykonanych ze stali S600. P.P.U. ESPA Paweł Szumski, (współautorstwo ekspertyzy), 2024 r.

3.6 Wykaz udziału w zespołach eksperckich lub konkursowych.

—

3.7 Wykaz projektów artystycznych realizowanych ze środowiskami pozaartystycznymi.

—

4 Dane naukometryczne

Poniżej zamieszczone dane dotyczą stanu na 15.10.2024 r.

4.1 Impact factor

W bazach Scopus i Web of Science indeksowanych jest 20 moich publikacji, w bazie Google Scholar 65, a w PBN 79. W czasopismach naukowych indeksowanych w Journal Citation Reports zarejestrowanych jest 21 artykułów. Do obliczenia wskaźnika wzięto pięcioletni średni impact factor czasopism indeksowanych w JCR oraz liczbę artykułów opublikowanych w danym czasopiśmie.

- Surface & Coatings Technology, IF 4.9, 7 art.
- Vacuum, IF 3.5, 3 art.
- Wear, IF 5.2, 3 art
- Applied Surface Science, IF 5.9, 2 art.
- Journal of Materials Processing Technology, IF 6.1, 1 art.
- Materials Letters, IF 2.7, 1 art.
- Metallurgia Italiana, IF 0.2, 1 art.
- Sensors, IF 3.7, 1 art.
- Scipta Materialia, IF 5.7, 1 art.
- Surface Science, IF 1.7, 1 art.

Sumaryczny *impact factor* **92.3**

4.2 Liczba cytowań publikacji wnioskodawcy, z oddzielnym uwzględnieniem autocytowań

Poniższe dane odnoszą się do ogólnej liczby cytowań w danej bazie. W nawiasie podano tę liczbę z pominięciem autocytowań:

- Scopus – 918 (894), Web of Science – 848 (826), Google Scholar – 1287 (b.d.).

4.3 Indeks Hirscha

Mój indeks Hirscha ma wysokość:

- Scopus – 14, Web of Science – 14, Google Scholar – 17.

Tomasz Suszko

List of scientific or artistic achievements which present a major contribution to the development of a specific discipline

Annex 3b to the application

Tomasz Suszko

November 6, 2024

1 Information on scientific or artistic achievements set out in art. 219 para 1. point 2 of the Act

1.1 Scientific monograph, pursuant to art. 219 para 1. point 2a of the Act; or

—

1.2 Cycle of scientific articles related thematically, pursuant to art. 219 para 1. point 2b of the Act

A series of articles called 'A new class of thin nanocomposite films of the MeMC/a-C:H type – synthesis and physicochemical properties'. The achievement is described in details in the Summary of Professional Accomplishments, and the works constituting the series are included in the appendices (Annex-5a.pdf – Annex-5e.pdf).

1.3 List of completed original project, engineering and design, technological or artistic achievements, pursuant to art. 219 para 1. point 2c of the Act

—

2 Information on scientific or artistic activity

2.1 List of published scientific monographs (including the monographs not mentioned in section 1.1)

—

2.2 List of published chapters in scientific monographs

—

2.3 Information about membership in editorial boards preparing scientific monographs for publication

—

2.4 List of articles published in scientific journals (including the articles not mentioned in section 1.2

Below, I put a list of my scientific publications not mentioned in point 1.2, divided into those before and after awarding the PhD degree.

Before awarding the PhD degree:

1. J. Ratajski, J. Tacikowski, R. Olik, T. Suszko, Czujnik magnetyczny i model matematyczny - niezbędne narzędzia w kontroli procesu azotowania gazowego, Inżynieria Mater. 6 (2000) 418–422.

2. J. Ratajski, J. Tacikowski, R. Olik, T. Suszko, Wpływ składu fazowego warstwy azotków żelaza na kinetykę wzrostu warstwy azotowanej, Inżynieria Mater. 6 (2000) 414–417.

3. W. Gulbiński, T. Suszko, Tarcie w nanoskali - badania cienkich warstw tlenku molibdenu techniką AFM, Inżynieria Mater. 6 (2000) 294–297.

4. W. Gulbinski, D. Pailharey, T. Suszko, Y. Mathey, Study of the influence of adsorbed water on AFM friction measurements on molybdenum trioxide thin films, Surf. Sci. 475 (2001) 149–158. https://doi.org/10.1016/S0039-6028(00)01101-8.

5. J. Ratajski, J. Tacikowski, R. Olik, T. Suszko, The Effect of the Phase Composition of Compound Layer on the Growth Kinetics of the Nitrided Layer., Inżynieria Mater. 5 (2001) 757–761.

6. J. Ratajski, J. Tacikowski, T. Suszko, Role of the layer of iron (carbo) nitrides in the kinetics of diffusion layer growth on alloys steels, in: 9th Int. Semin. IFHTSE, Nitriding Technol. Warsaw, 2003: pp. 77–87.

7. W. Gulbiński, T. Suszko, B. Warcholiński, Cienkie warstwy węglików molibdenu MoCx nanoszone metodą reaktywnego rozpylania magnetronowegoo, Inżynieria Mater. 6 (2003) 490–493.

8. W. Gulbiński, T. Suszko, D. Pailharey, High load AFM friction and wear experiments on V_2O_5 thin films, Wear 254 (2003) 988–993. https://doi.org/10.1016/S0043-1648(03)00304-1.

9. W. Gulbiński, T. Suszko, W. Sienicki, B. Warcholiński, Tribological properties of silver- and copper-doped transition metal oxide coatings, Wear 254 (2003) 129–135. https://doi.org/10.1016/S0043-1648(02)00292-2.

10. J. Ratajski, J. Tacikowski, T. Suszko, O. Łupicka, Modelowanie struktury i własności materiałów w procesie azotowania gazowego, Inżynieria Powierzchni 4 (2004) 12–15.

11. W. Gulbiński, A. Gilewicz, T. Suszko, B. Warcholiński, Z. Kukliński, Ti–Si–C sputter deposited thin film coatings, Surf. Coatings Technol. 180–181 (2004) 341–346. https://doi.org/10.1016/J.SURFCOAT.2003.10.084.

12. W. Gulbiński, A. Gilewicz, T. Suszko, Z. Kukliński, B. Warcholiński, Właściwości tribologiczne cienkich warstw węglika tytanu nanoszonych metodą reaktywnego rozpylania magnetronowego, Inżynieria Mater. 4 (2004) 51–56.

13. W. Gulbiński, S. Mathur, H. Shen, T. Suszko, A. Gilewicz, B. Warcholiński, Evaluation of phase, composition, microstructure and properties in TiC/a-C:H thin films deposited by magnetron sputtering, Appl. Surf. Sci. 239 (2005) 302–310. https://doi.org/10.1016/j.apsusc.2004.05.278.

14. J. Ratajski, J. Tacikowski, T. Suszko, Modelowanie struktury i własności materiałów w procesie azotowania gazowego., Inżynieria Powierzchni 1 (2005) 49–58.

15. J. Ratajski, R. Olik, J. Tacikowski, T. Suszko, O. Łupicka, Układ sterowania procesem azotowania gazowego nowej generacji, Inżynieria Mater. 5 (2005) 549–561.

After awarding the PhD degree::

16. T. Suszko, W. Gulbiński, J. Jagielski, The role of surface oxidation in friction processes on molybdenum nitride thin films, Surf. Coatings Technol. 194 (2005) 319–324. https://doi.org/10.1016/J.SURFCOAT.2004.07.119.

17. J. Ratajski, D. Lipiński, T. Suszko, J. Dobrodziej, J. Michalski, Application of relational data base concerning processes and effects of surface layers deposition, Probl. Eksploat. 2 (2006) 139–147.

18. J. Ratajski, D. Lipiński, T. Suszko, J. Dobrodziej, J. Michalski, Artificial neural network predictions of the microhardness profile in the nitrided layers, Probl. Eksploat. 2 (2006) 139–148.

19. J. Ratajski, T. Suszko, J. Dobrodziej, J. Michalski, Chosen aspects of the modeling of kinetics of the (carbo) nitrided layer gowth, Probl. Eksploat. 2 (2006) 113–125.

20. J. Ratajski, R. Olik, J. Tacikowski, T. Suszko, O. Łupicka, Intelligent control system for gaseous nitriding process, Metall. Ital. 98 (2006) 21–27.

21. J. Ratajski, D. Lipiński, T. Suszko, J. Dobrodziej, J. Michalski, Zastosowanie sztucznej sieci neuronowej do prognozowania profili twardości w warstwie azotowanej, Inżynieria Mater. 3 (2006) 516–518.

22. T. Suszko, W. Gulbiński, J. Jagielski, Mo2N/Cu thin films — the structure, mechanical and tribological properties, Surf. Coatings Technol. 200 (2006) 6288–6292. https://doi.org/10.1016/J.SURFCOAT.2005.11.041.

23. W. Gulbiński, B. Warcholiński, T. Suszko, R. Kazimierowicz, Multisource, magnetron deposited Al-Cu-Fe thin film coatings - the structure and properties, Probl. Eksploat. 4 (2006) 69–79.

24. W. Gulbiński, T. Suszko, A. Gilewicz, B. Warcholiński, Z. Kukliński, Structure and high-temperature tribological behavior of Ti–Si–C nanocomposite thin films, Surf. Coatings Technol. 200 (2006) 4179–4184. https://doi.org/10.1016/J.SURFCOAT.2004.12.011.

25. W. Gulbiński, T. Suszko, Thin films of Mo2N/Ag nanocomposite—the structure, mechanical and tribological properties, Surf. Coatings Technol. 201 (2006) 1469–1476. https://doi.org/10.1016/J.SURFCOAT.2006.02.017.

26. W. Gulbiński, T. Suszko, Thin films of MoO3–Ag2 O binary oxides – the high temperature lubricants, Wear 261 (2006) 867–873. https://doi.org/10.1016/J.WEAR.2006.01.008.

27. W. Gulbiński, B. Warcholiński, T. Suszko, A. Gilewicz, Z. Kukliński, Właściwości tribologiczne cienkich warstw TiC-aC:H implantowanych krzemem, Inżynieria Mater. 3 (2006) 395–398.

28. J. Ratajski, T. Suszko, J. Dobrodziej, Development of the inteligent tools for designing of the nitriding processes, Inżynieria Mater. 3–4 (2007) 724–727.

29. J. Jagielski, A. Piatkowska, A. Merstallinger, Z. Librant, P. Aubert, R. Groetzschel, T. Suszko, Friction properties of implanted alumina for vacuum applications, Vacuum 81 (2007) 1357–1362. https://doi.org/10.1016/J.VACUUM.2007.01.045.

30. J. Dobrodziej, J. Ratajski, J. Michalski, T. Suszko, Komputerowe wspomaganie projektowania procesów azotowania gazowego z wykorzystaniem symulacji i metod sztucznej inteligencji, Inżynieria Powierzchni 3 (2007) 82–93.

31. J. Dobrodziej, A. Mazurkiewicz, J. Ratajski, T. Suszko, J. Michalski, The methodology of fuzzy logic application in the modelling of thermo-diffusive and PVD processes, in: 16th Int. Fed. Heat Treat. Surf. Eng. Congr., 2007.

32. J. Michalski, J. Tacikowski, J. Dobrodziej, J. WojutProblemy Eksploatacjiyński, J. Ratajski, T. Suszko, Numeryczna symulacja potencjału azotowego i wymiany dwuskładnikowej atmosfery amoniak-amoniak dysocjowany w projektowaniu procesów azotowania gazowego, Probl. Eksploat. 2 (2007) 105–109.

33. J. Ratajski, T. Suszko, Modelling of the nitriding process, J. Mater. Process. Technol. 195 (2008) 212–217. https://doi.org/10.1016/J.JMATPROTEC.2007.04.133.

34. R. Olik, J. Ratajski, J. Dobrodziej, T. Suszko, J. Michalski, D. Lipiński, Projektowanie, kontrola i wizualizacja in-situ procesu azotowania., Inżynieria Mater. 1–3 (2008) 839–843.

35. J. Baranowska, S. Fryska, J. Przekop, T. Suszko, Charakterystyka powłok z fazy S otrzymywanych na drodze reaktywnego rozpylania magnetronowego, Elektron. – Konstr. Technol. Zastos. 9 (2009) 19–21.

36. J. Ratajski, R. Olik, T. Suszko, J. Dobrodziej, J. Michalski, Design, Control and in Situ Visualization of Gas Nitriding Processes, Sensors 10 (2009) 218–240.
https://doi.org/10.3390/s100100218.

37. J. Ratajski, W. Gulbiński, J. Staśkiewicz, J. Walkowicz, P. Myśliński, A. Czyżniewski, T. Suszko, A. Gilewicz, B. Warcholiński, Hard coatings for woodworking tools–a review, Manuf. Eng. 37 (2009) 668–674.

38. J. Ratajski, R. Olik, T. Suszko, J. Dobrodziej, J. Michalski, A. Gilewicz, Precise formation the phase composition and the thickness of nitrided layers, J. Achiev. Mater. Manuf. Eng. 37 (2009) 675–689.

39. R. Olik, J. Ratajski, T. Suszko, J. Michalski, J. Dobrodziej, A. Gilewicz, Precyzyjne kształtowanie budowy fazowej oraz grubości warstwy azotowanej na przykładzie matryc do ciśnieniowego odlewania aluminium, Inżynieria Powierzchni 3 (2009) 15–20.

40. R. Olik, J. Ratajski, J. Dobrodziej, T. Suszko, D. Lipiński, J. Michalski, Projektowanie i monitorowanie procesu azotowania gazowego, Probl. Eksploat. 1 (2009) 145–156.

41. M. Kosikowski, Z. Suszyński, R. Olik, J. Ratajski, T. Suszko, The application of artificial neural networks and evolutionary algorithm the designing of gas nitriding process, in: Int. B. Ser. Inf. Sci. Comput., 2009: pp. 33–38.

42. S. Fryska, J. Baranowska, J. Przekop, T. Suszko, The properties of hard coating composed of S-phase obtained by PVD method, Adv. Manuf. Sci. Technol. Vol. 33 (2009) 59–69.

43. R. Olik, B. Warcholiński, T. Suszko, A. Gilewicz, J. Ratajski, Modelowanie procesów azotowania i PVD podwyższających trwałość narzędzi ze stali WCL, Pomiary Autom. Kontrola 7 (2010) 819–823.

44. T. Suszko, W. Gulbiński, A. Urbanowicz, W. Gulbiński, Preferentially oriented vanadium nitride films deposited by magnetron sputtering, Mater. Lett. 65 (2011) 2146–2148.
https://doi.org/10.1016/j.matlet.2011.04.038.

45. S. Fryska, J. Baranowska, T. Suszko, Wpływ parametrów procesu na formowanie powłok z fazy S otrzymanych metodą PVD, Elektron. – Konstr. Technol. Zastos. 52 (2011) 14–16.

46. J. Baranowska, S. Fryska, T. Suszko, The influence of temperature and nitrogen pressure on S-phase coatings deposition by reactive magnetron sputtering, Vacuum 90 (2013) 160–164.
https://doi.org/10.1016/j.vacuum.2012.03.054.

47. V. Jahodowa, T. Suszko, Nitrogen doped steel coatings, Fine Mech. Opt. 58 (2013) 326–327.

48. T. Suszko, V. Jahodowa, W. Gulbiński, Plasma emission spectroscopy as a monitoring tool for deposition of S-phase layers by magnetron sputtering, Inżynieria Mater. (2015) 2.

49. Ł. Tomaszewski, A. Urbanowicz, T. Suszko, W. Gulbiński, Przeciwzużyciowe powłoki TiAlN modyfikowane wanadem, Inżynieria Mater. 36 (2015) 310–313.

50. Ł. Tomaszewski, W.W. Gulbiński, A. Urbanowicz, T. Suszko, A. Lewandowski, W.W. Gulbiński, TiAlN based wear resistant coatings modified by molybdenum addition, Vacuum 121 (2015) 223–229. https://doi.org/10.1016/j.vacuum.2015.08.027.

2.5 List of project, engineering and design as well as technological achievements (including the achievements not mentioned in section 1.3

Before awarding the PhD degree:

1. Development and construction of a computerized system for control and data acquisition from the PGS 2 photographic optical spectrometer intended for the measurements of the emission spectrum of plasma" – as part of the statutory research of the Department of Physics, KUT (1998).

2. Development of a system for synchronous measurement of Langmuir probe parameters for studying pulse-excited magnetron discharge plasma. – as part of the statutory research of the Department of Physics, KUT (1999).

3. Development of the design of a high-temperature tribotester and a program (based on the DASYLab package and a computer measurement card) to control its operation and for data acquisition – as part of the project No. KBN nr 7T08C 00816 (2000).

4. Development of a method for assessing shear stresses based on a modified Revetest device and a developed mathematical model of the phenomenon – as part of the project No. KBN 7T08C00816 (2000).

5. Writing software for reading, exporting and analysing data from the NANOSCOPE III atomic force microscope from Digital Instruments – as a part of 'Polonium' programme (2001).

6. Building a program (using the DASYLab package) to control the reactive magnetron sputtering process using the plasma emission spectrum control and to collect the operating parameters of the vacuum technological device – as part of works on my PhD thesis – 2002.

7. Deposition technology of of molybdenum nitrides Mo_2N and MoN (also doped with copper and silver) with reactive magnetron sputtering – as part of the project No. KBN 7T08C00816, and works on my PhD thesis – 2002.

After awarding the PhD degree:

8. 'Development of mathematical models of nitrided layer growth on steel in the gas nitriding process'. The achievement is **described in detail in the Summary of Professional Accomplishments** along with links to the works in which the models were used.

9. Design and construction of a set of magnetron sources and development of design assumptions for power supplies to work with these sources for deposition multi-component and multi-layer coatings – as part of the project No. PW-004/ITE/03/2006.

10. Vanadium nitride and carbo-nitride deposition technology by reactive magnetron sputtering – as part of the project No. POIG.01.03.01-32-052/08.

11. Modernization and adaptation of the Bułat-type device for the needs of coatings production technology on selected woodworking tools – as part of the project No. POIG.01.03.01-32-052/08.

12. Development of a control system for a magnetron deposition system of nitrogen and carbon stabilised S-phase coatings, based on the monitoring of plasma emission spectrum and working gases flow rate regulation – as part of the project No. NCN 2011/03/B/ST8/06.

13. Technology of depositing nanocolumnar quasiamorphic of the MeMC/a-C:H type films by reactive magnetron sputtering – as part of the project No. NCN 2011/03/B/ST8/06 and the University internal projects (2015–2024).

14. Design and construction of a tribotester for tribocorrosion tests in liquids, with synchronous measurement of force and electrical quantities measured by a connected potentiostat – as part of the University internal project (2021).

2.6 List of public realizations of works of art (including the works not mentioned in section 1.3)

—

2.7 Information on presentations given at national or international scientific or arts conferences, including a list of lectures delivered upon invitation and plenary lectures

1. W. Gulbiński, T. Suszko. 'Badania składu chemicznego cienkich warstw tlenku molibdenu MoO_{3-x} metodą XPS (Studies of the chemical composition of thin layers of molybdenum oxide MoO_{3-x} using the XPS method)'. IV Ogólnopolska Konferencja Naukowa Obróbka powierzchniowa' 99, Częstochowa-Kule , Oct 5–8 1999 r.

2. W. Gulbinski, T. Suszko, W. Sienicki, B. Warcholinski. 'Tribological properties of Ag and Cu doped transition metal oxide coatings'. 2nd World Tribology Congress, Wiedeń, Austria, Sept 3–7 2001 r.

3. W. Gulbiński, Tomasz Suszko. 'Wytwarzanie i właściości tribologiczne cienkich warstw molibdenianów srebra (Synthesis and tribological properties of silver molybdate thin films)'. V Ogólnopolska Konferencja Naukowa "Obróbka powierzchniowa" '2002, Częstochowa-Kule, Sept 18–20 2002 r.

4. W. Gulbiński, T. Suszko, D. Pailharey. 'High Load AFM Friction and Wear Experiments on V_2O_5 Thin Films'. 3rd International Colloquim Micro-tribology 2001 , Jastarnia, Oct 28-30 2001 r.

5. W. Gulbiński, T. Suszko, B. Warcholiński. 'Cienkie warstwy węglików molibdenu MoC_x nanoszone metodą reaktywnego rozpylania magnetronowego (Molybdenum carbide MoC_x thin films deposited by reactive magnetron sputtering)'. II Krajowa Konferencja „Nowe materiały – nowe technologie w przemyśle okrętowym i maszynowym", Szczecin-Międzyzdroje, Sept 7–10 2003 r.

6. T. Suszko, W. Gulbiński, J. Jagielski. 'Mo_2N/Cu Films – Structure, Mechanical and Tribological Properties'. E-MRS 2005 Spring Meeting, Strasbourg (Francja), May 31 – Jun 3 2005 r.

7. T. Suszko, W. Gulbiński, J. Morgiel, G. Greczynski, E. Dobruchowska, P. Dłużewski, J. Lu. 'Carbon Supersaturated Fe-Cr-Ni-C Thin Films with a Unique Nanocolumnar Structure - a Tough, Low Friction and Corrosion Resistant Coating'. 44th International Conference on Metallurgical Coatings and Thin Films ICMCTF 2017, San Diego (CA, USA), Apr 24–28 2017 r.

8. T. Suszko, W. Gulbiński, J. Morgiel, G. Greczynski, E Dobruchowska, P. Dłużewski, J Lu. 'Amorphous FeCrNi/a-C:H coatings with self-organized nanotubular structure'. 10-th Symposium on Vacuum based Science and Technology, Kołobrzeg, Nov 28–30 2017 r.

9. T. Suszko, W. Gulbiński, E Dobruchowska, G. Greczynski, J. Morgiel. 'Mechanical and tribological properties of CoCrMo/a-C:H coatings deposited by magnetron sputtering of ISO 5832-12 medical alloy', 10-th Symposium on Vacuum based Science and Technology, Kołobrzeg, Nov 28–30 2017 r.

10. T. Suszko, E. Dobruchowska, W. Gulbiński, G. Greczynski, L. Hultman, J. Morgiel. 'Nanostructural CoCrMoC/a-C:H coatings deposited by reactive magnetron sputtering', European Materials Research Society Spring Meeting 2019, Nice, May 27-31 2019 r.

2.8 Information on participation in organizational and scientific committees at national or international conferences, including the applicant's function

—

2.9 Information on participation in the works of research teams realizing projects financed through national and international competitions, including the projects which have been completed and projects in progress, and information on the function performed in the team

Research projects completed before awarding the PhD degree:

1. Research project No. KBN T08C 008 10 'Development of the Design Basis for Automatically Controlled Gas Nitriding Processes', 1996–1998, contractor.

2. Project 'Polonium' in cooperation with Mediterranean University of Marseille (2000–2002), contractor.

3. Research project No. KBN T08C 039 19 'The influence of the surface layer of iron nitrides (carbonitrides) on the formation of the growth kinetics of the nitrided layer', 2000–2003, contractor.

4. Research project No. KBN T08C02924 – 'Nanocomposite Thin Film Coatings for Dry Friction Applications at Elevated Temperatures' (2003-2005), contractor.

5. Project 'Polonium' No. 4978.I.2003 with National Polytechnic Institute in Grenoble (2003–2004), contractor.

6. Project NATO Collaborative Linkage Grant 'Nano-Structured Functional Coatings for Optical and Lubrication Applications'; in cooperation with Institute of New Materials w Saarbruecken (2004–2005), contractor.

Research projects completed after awarding the PhD degree:

7. Project 'Polonium' No. 5578.I/2004 in cooperation with Mediterranean University of Marseille (2004–2005), contractor.

8. European Network of Excellence 'Complex Matallic Alloys- CMA', Project No. NOE 500140, 2005–2009, contractor.

9. R&D project No. PW-004/ITE/04/2004, 'Nanocomposite anti-abrasive coatings based on quasicrystalline alloys' (2005–2006), contractor.

10. R&D project No. PW 004/ITE/04/2006 'Development of a magnetic sensor for in situ measurement of nitrided layer growth in gas nitriding process monitoring systems', 2007–2008, contractor.

11. R&D project No. PW-004/ITE/04/2006 'Prototype of a multi-source magnetron sputtering process control and monitoring system based on emission plasma spectroscopy', 2007–2008, contractor.

12. R&D project No. PW-004/ITE/03/2006 'Magnetron source assembly with power and control systems for multicomponent and multilayer coating application', 2007–2008, leader.

13. R&D project No. POIG.01.03.01-32-052/08 'Hybrid technologies for woodworking tools surface modification', leader of the task 'Development of technology for antiwear coatings based on TiAlN', 2009-2012, task leader.

14. Research project No. NCN 2011/03/B/ST8/06, 'New advanced composite anti-wear coatings on austenitic steel', 2012-2015, main contractor.

15. R&D project No. POIR.01.01.01-00-0531/15-00, 'Development of shank tools and micro-tools with special emphasis on nanostructured PVD coatings", FANAR S.A., Ciechanów, 2016–2018, researcher.

16. R&D project No. POIR.01.01.01-00-0274/17 pt. 'Development of a range of nanostructured coated taps and drills for difficult-to-machine materials', FANAR S.A., Ciechanów, 2018–2020, researcher.

Projects currently under evaluation:

- Project 'Self-organised coatings on 3D substrates for Hydrogen Evolution Reaction – synthesis, nanostructure and properties', submitted to National Science Center, OPUS 2024 competition.

2.10 Membership in international or national organizations and scientific societies, including the functions performed by the applicant

—

2.11 Information on internships completed in scientific or artistic institutions, also abroad, including the place, time and duration of the internship and its character

List of foreign internships and research stays:

- Mediterranean University of Marseille (now Aix-Marseille University), Marseille (France), 3 weeks, 2000 r., research stay as part of scientific cooperation financed by the French side.
- Mediterranean University of Marseille (now Aix-Marseille University), Marseille (France), 3 weeks, 2001 r., research stay within the 'Polonium' programme.
- Mediterranean University of Marseille (now Aix-Marseille University), Marseille (France), 3 weeks, 2002 r., research stay within the 'Polonium' programme.
- National Polytechnic Institute of Grenoble CNRS-LEMD (now French National Centre for Scientific Research CNRS), Grenoble (France), 1 week, 2003 r., research stay within the 'Polonium' programme.
- Mediterranean University of Marseille (now Aix-Marseille University), Marseille (France), 2 weeks, 2003 r., research stay within the 'Polonium' programme.
- Leibniz Institute of New Materials, Saarbruecken (Germany), 2 tweeks, 2003 r., research stay within the NATO-CLG programme.
- Aerospace & Space Materials Technology Testhouse, Austrian Research Center, Seibersdorf (Austria), 4 weeks, 2003 r., research stay within the AMTT programme (application II-83).
- Mediterranean University of Marseille (now Aix-Marseille University), Marseille (France),2 weeks, Jun 2005 r., research stay within the 'Polonium' programme.
- University of Stuttgart, Stuttgard (Germany), 1 week, Feb 2006, work trip within the project European Network of Excellence – Complex Metallic Alloys.

- University of Toulouse, Toulouse (France), 1 week, Mar 2006, work trip within the project European Network of Excellence – Complex Metallic Alloys.
- Fritz Haber Institute, Berlin (Germany), 1 week, May 2006, work trip within the project European Network of Excellence – Complex Metallic Alloys.
- Josef Stefan Institute, Lublana (Slovenia), 1 week, Jun 2006, symposium EuroSchool 2006 within the project European Network of Excellence – Complex Metallic Alloys.
- University of Greifswald, Greifswald (Germany), 1 week, Feb 2007, work trip within the project BalticNet-PlasmaTec.
- University of Toulouse (organiser), Fira (Greece), 1 week, Jun 2007, work trip within the project European Network of Excellence – Complex Metallic Alloys.
- National Polytechnic Institute of Grenoble CNRS-LEMD (now French National Centre for Scientific Research CNRS), Grenoble (France), 1 week, Nov 2007, research trip at the invitation of the French side within the framework of the ECONET project.
- University of Aix-Marseille, Marseille (France), Apr 2008, work trip within the project European Network of Excellence – Complex Metallic Alloys.
- Josef Stefan Institute, Lublana (Slovenia), 1 week, Jun 2008, symposium EuroSchool 2008 within the project European Network of Excellence – Complex Metallic Alloys.
- University of Nancy, Nancy (France), 1 week, Dec 2008, work trip within the project European Network of Excellence – Complex Metallic Alloys.
- Josef Stefan Institute, Lublana (Slovenia), Mar 2009, organisation trip of the Fusion Expo exhibition.
- Technical University of Liberec, Liberec (Czechia), 1 week, Sep 2013, research stay within the program Erasmus – Staff Training Mobility.

2.12 Membership in editorial committees and scientific boards of journals, including the functions performed by the applicant (e.g. editor-in-chief, chairman of scientific board etc.)

—

2.13 Information on scientific or artistic works reviewed, in particular those published in international journals

Almost half of my works (p. 2.4) have been published in peer-reviewed, recognized international journals from the JCR list.

Since 2007, I have been systematically reviewing articles in the journal Surface & Coatings Technology.

2.14 Information on participation in European or other international programmes

1. Project 'Polonium' in cooperation with Mediterranean University of Marseille (2000–2002), contractor.
2. Project 'Polonium' No. 4978.I.2003 with National Polytechnic Institute in Grenoble (2003–2004), contractor.
3. Project NATO Collaborative Linkage Grant 'Nano-Structured Functional Coatings for Optical and Lubrication Applications'; in cooperation with Institute of New Materials w Saarbruecken (2004–2005), contractor.
4. Project 'Polonium' No. 5578.I/2004 in cooperation with Mediterranean University of Marseille (2004–2005), contractor.
5. European Network of Excellence 'Complex Matallic Alloys- CMA', Project No. NOE 500140, 2005–2009, contractor.

2.15 Information on participation in research teams realizing projects other than those defined in section 2.9.

—

2.16 Information on membership in the teams assessing applications for financing of research projects, applications for scientific awards, applications in other competitions of scientific or didactic character

—

3 Information on cooperation with social and economic environment

3.1 List of technological works

See Section 2.5

3.2 Information on cooperation with economic sector

Of the research projects listed in p. 2.9, the following three were directly concerned with cooperation with the economic environment.

- R&D project No. POIG.01.03.01-32-052/08 'Hybrid technologies for woodworking tools surface modification', 2009-2012.
- R&D project No. POIR.01.01.01-00-0531/15-00, 'Development of shank tools and micro-tools with special emphasis on nanostructured PVD coatings", FANAR S.A., Ciechanów, 2016–2018.
- R&D project No. POIR.01.01.01-00-0274/17 pt. 'Development of a range of nanostructured coated taps and drills for difficult-to-machine materials', FANAR S.A., Ciechanów, 2018–2020.

The most important partners were the companies: FANAR S.A. Ciechanów, FABA S.A. Baboszewo, AB Wood Sławno, VTT Koszalin. In addition to this, cooperation with the business environment includes the production of expert opinions and other such studies for companies. Expert reports from recent years are listed in p. 3.5.

3.3 Obtaining the right of industrial property, including the national or international patents granted

- Tomasz Suszko, Witold Gulbiński, 'Method for producing thin, amorphous coating, resistant to abrasive wear and corrosion, based on carbon saturated FeCrNi alloy and the thin, amorphous FeCrNi:C coating, resistant to abrasive wear and corrosion', Pat.230506, Patent Office of the Republic of Poland , 2018.

- Tomasz Suszko, Ewa Dobruchowska, Witold Gulbiński, 'Method for producing a thin, amorphous, corrosion-resistant, acidic NiMoC/a-C:H nanocomposite-based coating for electrodes for electrocatalytic hydrogen generation and a thin, amorphous, corrosion-resistant, acidic NiMoC/a-C:H coating'. Parent notification, Patent Office of the Republic of Poland, 2024

3.4 Information on implemented technologies

I have participated in the implementation of PVD coating technology (including HPIMS) by FANAR S.A., Ciechanów, as part of the two projects mentioned above (Section. 2.9).

3.5 Information on performed expert analyses or other studies prepared on request of public institutions or entrepreneurs

1. Analysis of the TiAlN coatings properties, deposited by magnetron sputtering on high-speed steel (HSS) tools, and development of recommendations for the optimisation of coating adhesion. FANAR S.A., Ciechanów, in the frame of the project POIR.01.01.01-00-0531/15-00, 2016 r.

2. Determining the parameter of the magnetron deposition process of TiAlN, TiAlCN and TiAlSiN coatings using the Taguchi method, in order to obtain optimal coating properties. FANAR S.A., Ciechanów, in the frame of the project POIR.01.01.01-00-0531/15-00, 2017–18 r.

3. Investigation of spatial distributions of plasma parameters in magnetron deposition processes of TiAlN+TiN coatings using emission optical spectroscopy to determine the usable space of the process chamber. FANAR S.A., Ciechanów, in the frame of the project POIR.01.01.01-00-0531/15-00, 2017 r.

4. Analysis of the baseline manufacturing procedures for FerroCon, FerroCon Gold , Ferrocon WCC, InoxaCon coatings on the CC800/9 HiPIMS device and optimisation of process parameters for improved coating properties. FANAR S.A., Ciechanów, in the frame of the project POIR.01.01.01-00-0274/17, 2018 r.

5. Comparative analysis of the optical plasma emission spectra from processes on the CC800/9 HiPIMS device with the structural and mechanical properties of the obtained TiAlN-based films. FANAR S.A., Ciechanów, in the frame of the project POIR.01.01.01-00-0274/17, 2019 r.
6. Microstructure survey of M42 tool steel specimens. FANAR S.A., (co-authorship of the expert study), 2023 r.
7. Microstructural study of Al (Alloy 3005) sheet samples with polymer coating. PRO-WAM Sp. z o.o., (co-authorship of the expert study), 2023 r.
8. Microstructure investigation of strip and tube samples made of LDX2101 steel. HEXONIC Sp. z o.o., (co-authorship of the expert study), 2023 r.
9. Microstructural investigation of PVD coatings produced on shank tools. FANAR S.A., (co-authorship of the expert study), 2023 r.
10. Examination of the microstructure of the chip groove of shank tools at different stages of surface treatment. FANAR S.A., (co-authorship of the expert study), 2023 r.
11. Microstructural study of carbide inserts used in surgical instruments. Aesculap Chifa sp. z o.o., (co-authorship of the expert study), 2023 r.
12. Study of the microstructure of a PVD-coated M12 blank. FANAR S.A., (co-authorship of the expert study), 2024 r.
13. Microstructural study of S600 steel samples. P.P.U. ESPA Paweł Szumski, (co-authorship of the expert study), 2024 r.

3.6 Information on participation in expert and competition teams

—

3.7 Information on artistic projects realized in non-artistic environment.

—

4 Scientometric information

The data below are as of October 15, 2024.

4.1 Information on the Impact Factor (in the fields and disciplines in which this parameter is commonly used as a scientometric index)

There are 22 of my publications indexed in the Scopus and the Web of Science databases, in the Google Scholar 65, and the PBN 79. There are 21 articles registered in scientific journals indexed in Journal Citation Reports. The five-year average impact factor of JCR-indexed journals and the number of articles published in a given journal were taken to calculate the IF-factor.

- Surface & Coatings Technology, IF 4.9, 7 papers
- Vacuum, IF 3.5, 3 papers
- Wear, IF 5.2, 3 papers
- Applied Surface Science, IF 5.9, 2 papers
- Journal of Materials Processing Technology, IF 6.1, 1 paper
- Materials Letters, IF 2.7, 1 paper
- Metallurgia Italiana, IF 0.2, 1 paper
- Sensors, IF 3.7, 1 paper
- Scipta Materialia, IF 5.7, 1 paper
- Surface Science, IF 1.7, 1 paper

Total impact factor **92.3**

4.2 Information on the number of citations of the applicant's publications, including a separate list of self-citations.

The figures below refer to the total number of citations in a given database. In parentheses, this number is given excluding self-citations.

- Scopus – 918 (894), Web of Science – 848 (826), Google Scholar – 1287 (n.a.).

4.3 Information on h-index held

- Scopus – 14, Web of Science – 13, Google Scholar – 17.

Tomasz Suszko

Wykaz publikacji stanowiących osiągnięcie naukowe wraz z określeniem indywidualnego wkładu każdego ze współautorów

stanowiący załącznik nr 4 do wniosku o przeprowadzenie postępowania w sprawie nadania stopnia doktora habilitowanego

Poniżej zamieszczono listę publikacji, oraz opis wkładu merytorycznego współautorów zgodnie z *Contributor Roles Taxonomy* (CrediT) wraz podpisami głównych współautorów potwierdzającymi ich rolę w powstaniu artykułów.

1. T. Suszko, W. Gulbiński, J. Morgiel, G. Greczynski, E. Dobruchowska, P. Dłużewski, J. Lu, L. Hultman, Amorphous FeCrNi/a-C:H coatings with self-organized nanotubular structure, Scr. Mater. 136 (2017) 24–28. https://doi.org/10.1016/j.scriptamat.2017.03.040.

   1. **Tomasz Suszko:**
   Koncepcja badań i opracowanie metodologii. Gromadzenie danych i metadanych. Synteza PVD próbek i preparatyka. Przeprowadzenie pomiarów i analiza danych XRD. Analiza danych XPS. Badania właściwości mechanicznych i tribologicznych. Przygotowanie rysunków i wykresów do artykułu. Przygotowanie wstępnej i końcowej wersji artykułu. Poprawki i uzupełnienia związane z recenzjami manuskryptów. Złożenie do wydawnictwa, autor korespondencyjny.

   2. Witold Gulbiński:
   Recenzja i korekta wstępnej wersji artykułu. Mentoring.

   3. Jerzy Morgiel:
   Obrazowanie TEM próbek. Recenzja końcowej wersji artykułu.

   4. Grzegorz Greczynski:
   Badania XPS próbek. Recenzja i korekta końcowej wersji artykułu.

   5. Ewa Dobruchowska:
   Badania odporności korozyjnej próbek – pomiary, gromadzenie danych i metadanych, analiza wyników, przygotowanie wykresów. Przygotowanie wstępnej wersji artykułu.

   6. Piotr Dłużewski:
   Mapowanie TEM/EDS.

   7. Jun Lu:
   Mapowanie TEM/EDS.

   8. Lars Hultman:
   Recenzja i korekta końcowej wersji artykułu.

2. T. Suszko, W. Gulbiński, E. Dobruchowska, G. Greczynski, L. Hultman, J. Morgiel, Quasi-amorphous, nanostructural CoCrMoC/a-C:H coatings deposited by reactive magnetron sputtering, Surf. Coatings Technol. 378 (2019) 124910. https://doi.org/10.1016/j.surfcoat.2019.124910.

   1. **Tomasz Suszko:**
   Koncepcja badań i opracowanie metodologii. Gromadzenie danych i metadanych. Synteza PVD próbek i preparatyka. Przeprowadzenie pomiarów i analiza danych XRD. Analiza danych XPS. Badania właściwości mechanicznych i tribologicznych. Przygotowanie rysunków i wykresów do artykułu. Przygotowanie wstępnej i końcowej wersji artykułu. Poprawki i uzupełnienia związane z recenzjami manuskryptów. Złożenie do wydawnictwa, autor korespondencyjny.

   2. Witold Gulbiński:
   Recenzja i korekta wstępnej wersji artykułu. Mentoring.

   3. Ewa Dobruchowska: Badania odporności korozyjnej próbek – pomiary, gromadzenie danych i metadanych analiza wyników, przygotowanie wstępnej wersji wykresów. Przygotowanie wstępnej wersji artykułu.

   4. Grzegorz Greczynski:
   Badania XPS próbek. Recenzja i korekta końcowej wersji artykułu.

   5. Jerzy Morgiel:
   Obrazowanie TEM próbek. Recenzja końcowej wersji artykułu.

   6. Lars Hulpman:
   Recenzja i korekta końcowej wersji artykułu.

3. E. Dobruchowska, T. Suszko, G. Greczynski, D. Adamczewska, W. Gulbiński, Amorphous/quasi-amorphous CoCrMo-C coatings for improved electrochemical properties and tribocorrosion resistance of biomedical alloys, Surf. Coatings Technol. 460 (2023) 129398. https://doi.org/10.1016/j.surfcoat.2023.129398.

   1. Ewa Dobruchowska: Koncepcja badań i opracowanie metodologii. Badania odporności korozyjnej próbek. Analiza danych XPS. Pomiary, gromadzenie z potencjodynamiczych pomiarów polaryzacyjnych i tribokorozyjne. Gromadzenie danych i metadanych. **Pisanie** - Przygotowanie wstępnej i końcowej wersji artykułu, opis stanu wiedzy i genezy pracy, dyskusja wyników i konkluzje. Poprawki i uzupełnienia związane z recenzjami manuskryptów.

   2. **Tomasz Suszko:**
   Koncepcja badań i opracowanie metodologii. Synteza PVD i preparatyka próbek. Przeprowadzenie pomiarów i analiza danych XRD. Analiza danych XPS. Pomiary

i analiza danych z pomiarów EIS. Pomiary tribokorozyjne i analiza danych. Prezentacja danych. Przygotowanie rysunków i wykresów do artykułu. Przygotowanie wstępnej i końcowej wersji artykułu. Poprawki i uzupełnienia związane z recenzjami manuskryptów. Złożenie do wydawnictwa, autor korespondencyjny.

3. GRZEGORZ GRECZYNSKI:
Badania XPS próbek. Recenzja i korekta końcowej wersji artykułu.

4. DOROTA ADAMCZEWSKA:
Pomiary potencjodynamiczne. Zgromadzenie danych i metadanych.
Nie można uzyskać podpisu ze względu na brak kontaktu

5. WITOLD GULBIŃSKI:
Recenzja i korekta końcowej wersji artykułu.

4. T. Suszko, W. Gulbiński, K. Załęski, G. Greczynski, J. Morgiel, V. Lapitskaya, Nanocolumnar, self-organised NiCrC/a-C:H thin films deposited by magnetron sputtering, Appl. Surf. Sci. 591 (2022) 153134. https://doi.org/10.1016/j.apsusc.2022.153134.

1. **TOMASZ SUSZKO:** Koncepcja i metodologia badań. Synteza PVD i preparatyka próbek. Przeprowadzenie pomiarów i analiza danych XRD. Analiza struktury krystalicznej i składu fazowego. Analiza danych XPS i danych z pomiarów magnetycznych. Analiza i prezentacja danych. Przygotowanie rysunków i wykresów do artykułu. Przygotowanie wstępnej i końcowej wersji artykułu. Poprawki i uzupełnienia związane z recenzjami manuskryptów. Złożenie do wydawnictwa, autor korespondencyjny.

2. WITOLD GULBIŃSKI:
Przygotowanie wstępnej wersji artykułu.

3. KAROL ZAŁĘSKI: Pomiary magnetyczne próbek i analiza danych z pomiarów. Przygotowanie roboczej wersji wykresów. Przygotowanie wstępnej wersji artykułu.

4. GRZEGORZ GRECZYNSKI:
Badania XPS próbek. Recenzja i korekta końcowej wersji artykułu.

5. JERZY MORGIEL:
Obrazowanie TEM próbek. Recenzja końcowej wersji artykułu.

6. VASILINA LAPITSKAYA:
   Obrazowanie AFM, M-AFM.

5. T. Suszko, E. Dobruchowska, W. Gulbiński, G.~Greczynski, J. Morgiel, B. Kawczyński, K. Załęski, K. Dorywalski, S. Pogorzelski, NiMo-C coatings synthesised by reactive magnetron sputtering for application as a catalyst for the hydrogen evolution reaction in an acidic environment, artykuł złożony do ACS Applied Materials & Interfaces (2024)

   1. **TOMASZ SUSZKO:** Koncepcja i metodologia badań. Synteza PVD i preparatyka próbek. Przeprowadzenie pomiarów i analiza danych XRD. Analiza struktury krystalicznej i składu fazowego. Analiza danych XPS i danych z pomiarów magnetycznych. Pomiary i analiza danych z pomiarów EIS. Pomiary tribokorozyjne i analiza danych. Przygotowanie rysunków i wykresów do artykułu. Przygotowanie wstępnej i końcowej wersji artykułu. Poprawki i uzupełnienia związane z recenzjami manuskryptów.
      Złożenie do wydawnictwa, autor korespondencyjny.

   2. EWA DOBRUCHOWSKA:
      Koncepcja badań i opracowanie metodologii. Badania odporności korozyjnej próbek. Analiza danych XPS. Pomiary, gromadzenie z potencjodynamiczych pomiarów polaryzacyjnych i tribokorozyjne. Gromadzenie danych i metadanych. Przygotowanie wykresów do artykułu. Przygotowanie wstępnej i końcowej wersji artykułu. Poprawki i uzupełnienia związane z recenzjami manuskryptów.

   3. WITOLD GULBIŃSKI:
      Przygotowanie wstępnej wersji artykułu.

   4. GRZEGORZ GRECZYŃSKI:
      Badania XPS próbek. Recenzja i korekta końcowej wersji artykułu.

   5. JERZY MORGIEL:
      Obrazowanie TEM próbek. Recenzja końcowej wersji artykułu.

   6. BARTOSZ KAWCZYŃSKI, KAROL ZAŁĘSKI:
      Obrazowanie AFM i C-AFM. Uzupełnienia do końcowej wersji artykułu.

   7. KRZYSZTOF DORYWALSKI, STANISŁAW POGORZELSKI:
      Pomiary zwilżalności powierzchni.

Scripta Materialia 136 (2017) 24–28

Contents lists available at ScienceDirect

Scripta Materialia

journal homepage: www.elsevier.com/locate/scriptamat

Regular Article

Amorphous FeCrNi/a-C:H coatings with self-organized nanotubular structure

Tomasz Suszko[a,*], Witold Gulbiński[a], Jerzy Morgiel[c], Grzesgorz Greczynski[b], Ewa Dobruchowska[a], Piotr Dłużewski[d], Jun Lu[b], Lars Hultman[b]

[a] Koszalin University of Technology, Ul. Śniadeckich 2, Koszalin 75-453, Poland
[b] Thin Film Physics Division, Department of Physics (IFM), Linköping 581 83, Sweden
[c] Institute of Metallurgy and Materials Sciences, Polish Academy of Science, Ul. Reymonta 25, Kraków 30-059, Poland
[d] Institute of Physics, Polish Academy of Sciences, Al. Lotników 32-46, Warszawa 02-668, Poland

ARTICLE INFO

Article history:
Received 21 February 2017
Received in revised form 30 March 2017
Accepted 30 March 2017
Available online 12 April 2017

Keywords:
Austenitic stainless steel
Magnetron sputtering
Thin films
Nanocomposities
Carbon self-organized structure

ABSTRACT

Amorphous FeCrNi/a-C:H coatings are deposited by pulsed magnetron sputtering of austenitic stainless steel in argon/acetylene atmosphere. High-resolution transmission electron microscopy, electron energy loss spectroscopy and energy dispersive X-ray mapping reveal a pronounced nanotubular structure consisting of metallic cores that thread along the film growth direction and are encapsulated by amorphous carbon shells in a cream-roll fashion. The coatings exhibit excellent mechanical, tribological, and anti-corrosion properties.

Research on magnetron sputtering of austenitic, stainless steel targets in a reactive atmosphere containing hydrocarbons yields so called carbon-stabilized expanded austenite γ^C coatings. Earlier, layers of that type were traditionally formed on austenitic stainless steels by gas carburization [1,2]. These crystalline layers have been shown to improve the surface properties of inherently soft austenitic steels commonly used in food industry and for medical instrumentation. The γ^C layers show enhanced hardness and wear resistance [3].

Low temperature physical vapor deposition (PVD) technique, is considered as an alternative for the well-established high temperature carburization of austenitic steels. Early studies on sputtering of Fe-Cr-Ni-based austenitic steel targets in a methane containing atmosphere report X-ray amorphous coatings containing 5 to 12 at.% of carbon [4–8] In general, structures of these amorphous Fe-Cr-Ni/a-C:H films were featureless in electron microscopy, whereas carbon segregation which can be expected for these graphitization-inducing metals was not investigated in detail.

Here, we report systematic studies on the structure, chemical and phase composition as well as on the mechanical and tribological properties of FeCrNi/a-C:H coatings obtained by reactive magnetron sputtering of the AISI 316L alloy ($Fe_{69}Cr_{18}Ni_{11}Mo_2$) in acetylene-containing atmosphere. We observe a unique amorphous self-organized metal/amorphous hydrogenated carbon nano-columnar structure. This original nano-material offers excellent mechanical, tribological and anti-corrosion properties.

FeCrNi/a-C:H coatings were deposited in a small (25 × 25 cm) cylindrical vacuum chamber by pulsed, reactive magnetron sputtering of the 316L steel target in Ar/C_2H_2 atmosphere. The argon flow was kept constant at 6 sccm in every process, while the acetylene flow was varied from 0 to 4 sccm. The magnetron source with target diameter 100 mm was working in unbalanced mode at the frequency of 100 kHz with 1 kHz modulation. The discharge average current was controlled and set at 1 A. The atomic emission line Cr^I (521 nm) from magnetron plasma was used for the process stability monitoring. The coatings were deposited on Si (100) wafers heated to 300 °C and kept at the DC bias potential of −50 V. The total pressure during the deposition was ca. 6×10^{-3} mbar (0.6 Pa).

The structure of the coatings was examined by the X-ray diffraction of Co Kα radiation in ϑ-2ϑ geometry. The chemical composition

* Corresponding author.
E-mail address: tomasz.suszko@tu.koszalin.pl (T. Suszko).

http://dx.doi.org/10.1016/j.scriptamat.2017.03.040
1359-6462/

of the coatings was determined by X-ray photoelectron spectroscopy (XPS). The XPS analysis was performed in an Axis Ultra DLD instrument (Kratos Analytical, UK) with monochromatic Al Kα radiation ($h\nu = 1486.6$ eV). The base pressure during spectra acquisition was 1.1×10^{-9} Torr (1.5×10^{-7} Pa). The binding energy scale was calibrated by examining the sputter-cleaned Au, Ag, and Cu samples according to the recommended ISO standards for monochromatic Al Kα sources that place Au $4f_{7/2}$, Ag $3d_{5/2}$, and Cu $2p_{3/2}$ peaks at 83.96, 368.21 and 932.62 eV, respectively [9]. Casa XPS software (version 2.3.16) was used for quantification of XPS spectra, based upon peak areas from narrow energy range scans and elemental sensitivity factors supplied by Kratos Analytical Ltd. The confidence level is typically around ±5%.

The FIB-Quanta 3D dual beam instrument was used for preparation of lamellas for transmission electron microscopy investigations. High resolution observations of the coatings microstructure were preformed using Tecnai G2 F20 operating at 200 kV accelerating voltage and applying Titan Cubed 80-300 microscope operating at 300 kV acceleration voltage equipped with GIF Quantum 966 electron energy losses spectrometer for Fe and C elements mapping.

Evaluation of electrochemical corrosion resistance was made by carrying out potentiodynamic polarization tests with use of Atlas 0531 potentiostat (Atlas Sollich, Poland). The measurements were performed in a three-electrode cell where the sample acted as a working electrode. The active surface area of each sample was equal to 0.29 cm^2. Saturated standard calomel electrode (SCE) and platinum plate were used as reference and counter electrodes, respectively. All measurements were conducted at room temperature ($25 \pm 1\ ^\circ$C) in unstirred 3 wt % NaCl aqueous solution at pH = 6.5. Prior to the beginning of the measurements, the samples had been kept in contact with the electrolyte for 1 h at open circuit conditions (OCP).

Tribological properties were tested in T-01 M ball-on-disc tester (ITE, Poland). Alumina ball of 10 mm in diameter under normal load of 10 N in laboratory air of 50% relative humidity was used for measurement of friction coefficient. Wear rate of the coating was calculated from the wear track cross section area measured by a stylus profile-meter. High load tribological tests were performed with 5 mm alumina ball and normal load of 80 N.

Coatings with carbon content χ_C up to 65 at.%, as determined by wave dispersive spectroscopy (WDS) and XPS, were deposited by means of reactive pulsed magnetron sputtering. The X-ray diffraction studies (XRD), cf. Fig. 1a, revealed that structure of these coatings change from (i) crystalline ferrite-containing ($\chi_C < 3$ at. %), (ii) ferrite and expanded austenite ($3 < \chi_C < 11$ at.%), through (iii) nanocrystalline ($12 < \chi_C < 15$ at.%) with crystalline size estimated from ferrite (110) peak broadening of about 7 nm, to (iv) amorphous one ($15 > \chi_C$ at. %). It is necessary to mention that the coatings most likely contain significant amounts of hydrogen however it was not directly measured.

Coatings containing more than 15 at.% C showed amorphous-like XRD patterns. For even higher carbon concentrations, $\chi_C > 30$ at.%, segregation of free sp^2 bonded carbon was revealed by the XPS studies as shown below. Fig. 1b shows a set of the C1s core level spectra as a function of increasing C content. Initially, for $\chi_C \leq 27.7$ at.% the spectra is dominated by a single peak at 283.2 eV due to carbide formation [10]. With further increasing χ_C to 38.4 at.% a second peak appears at 284.4 eV, indicative of sp^2-bonded carbon [11,12]. The intensity of the sp^2 C1s peak increases with further increasing carbon content and eventually, for $\chi_C > 64.9$ at.% dominates the XPS spectrum (cf. Fig. 1c). Cr 2p core-level spectra recorded from amorphous films with $\chi_C \geq 38.4$ at.% (not presented here) give a signature of carbide formation, in accordance with the corresponding C1s spectra, and in agreement with the strong affinity of Cr to carbon.

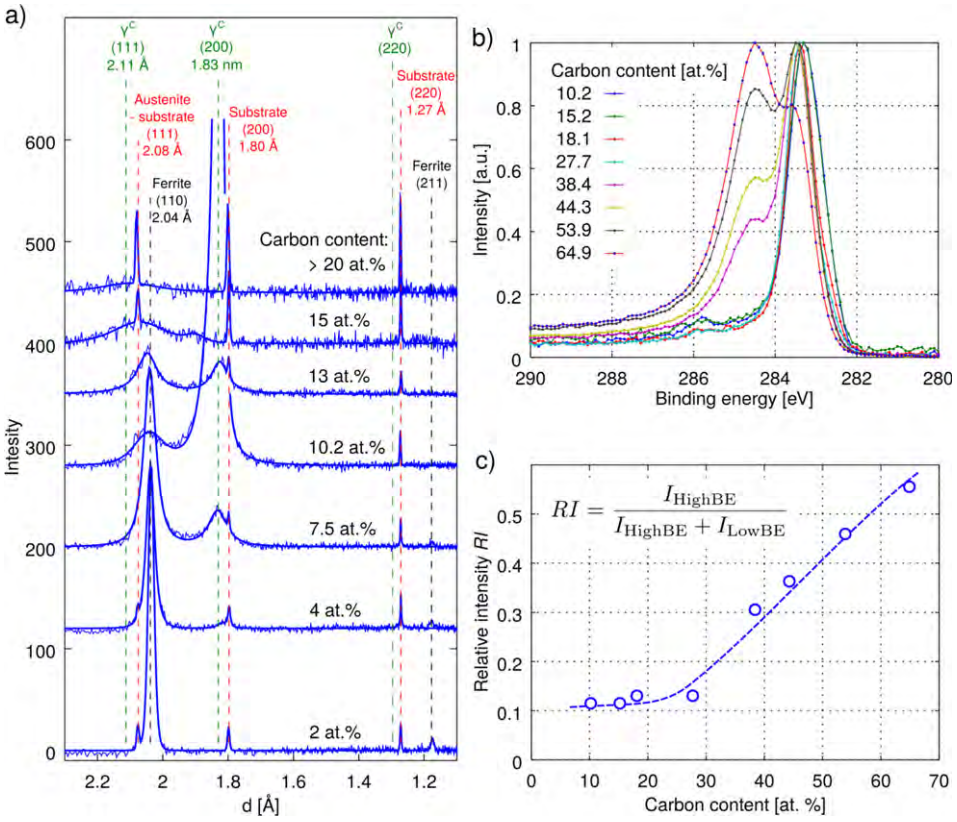

Fig. 1. XRD patterns for a series of FeCrNi/a-C:H coatings with increasing C content (a), C1s core level spectra for coatings containing up to 65 at.% of carbon (b) and the relative intensity of C1s core level line component corresponding to sp^2 bonded carbon vs carbon content in the deposit (c).

Due to significant changes in properties observed for samples with carbon concentration higher than 35 at.% and to gain more insight into the nanostructure of amorphous films, coatings containing 44 at.% C were selected for detailed transmission electron microscopy (TEM) studies. Bright field (BF) TEM and high-resolution TEM (HR-TEM) observations revealed formation of a unique nanocolumnar structure. Fig. 2a and b, are cross-sectional TEM and HR-TEM images showing the film composed of oriented nano-columns, with axes parallel to the growth direction. The presence of nanocolumns with an average diameter of 4 nm was additionally confirmed by the plan-view TEM and HR-TEM images in Fig. 2c and d, also exposing hexagonal shape in this view. Electron energy loss spectroscopy (EELS) revealed that the cores of the nano-columns are metal (iron)-rich (cf. Fig. 3a), whereas the column shells were predominantly composed of amorphous carbon (cf. Fig. 3b). The same conclusions can be drawn from results of electron dispersive X-ray (EDX) analysis (cf. Fig. 3d, e) where concentration map for major elements of the coating is shown. It should be recognized that the columns cores are amorphous although diffuse selected area electron diffraction (SAED) pattern (cf. Fig. 3c) indicates a short range ordering corresponding to the ferrite bcc structure with significantly larger lattice constant (about 2.98 Å) or to the tetragonal structure of martensite also with expanded lattice.

The chemistry and crystalline structure of sputter-deposited binary transition metal carbides was recently reviewed by U. Jansson et al., who proposed a general classification of binary carbides which are formed by metals with strong (groups 4–6) or weak and very weak (groups 7–10) affinity to carbon [13]. The enthalpies of carbide formation for weak carbide formers are slightly negative or even positive, as it is the case for Fe_3C, Co_2C or Ni_3C [14]. It has also been shown that the enrichment of binary systems made of 3d, 4d and 5d (Ti, V, Cr; Zr, Nb, Mo, Hf, Ta, W) metals with carbon results in the formation of a crystalline nanocomposite structures showing attractive properties like high hardness, wear resistance and low friction accompanied by high toughness. The design concept for that type of nanocomposite materials was also proposed [15]. For ternary carbides, containing two metals with high affinity to carbon, as for TiC-VC, TiC-NbC, VC-TaC or HfC-TaC systems, a complete miscibility is observed, whereas sputter deposited films are crystalline [16]. Structure and properties of those composite coatings have been the subject of many previous works such as, for example: M.P. Delplancke-Ogletree et al. [17], M. Stüber et al. [18], T. Zehnder et al. [19] and W. Gulbiński et al. [20].

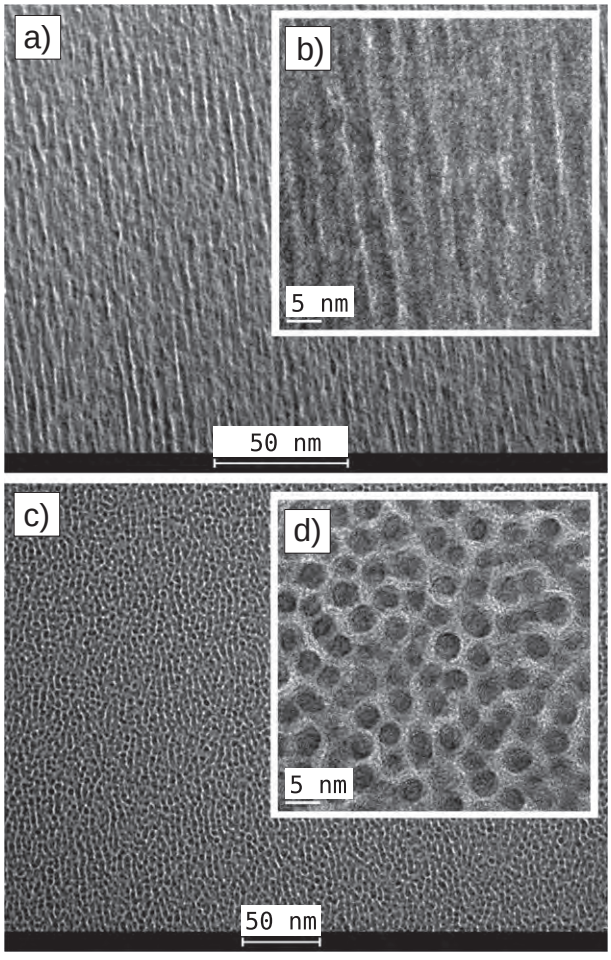

Fig. 2. HRTEM images of the coating in (a) (b) cross-section and (c) (d) plan-view with respect to the substrate surface.

The situation becomes more complex in the case of ternary compounds when the second metal to be dissolved in the group 4–6 transition metal carbide is a week carbide former like iron, cobalt or nickel. Sputter deposition of such coatings frequently leads to amorphous deposits as discussed by B. Trindade et al. [21]. Increasing the amount of the weak carbide former promotes the amorphisation process. Those authors have also shown that in the case of iron added to group 4–6 metal carbides, the Fe content required for amorphisation of the deposit depends on the affinity of carbide forming metal to carbon. Simultaneously, deposition conditions can also strongly influence the concentration threshold of weak carbide formers above which amorphisation sets in.

Beside the amorphisation effect discussed above, alloying with a weak carbide former can lead to the segregation of carbon. U. Jansson et al. discussed the case of titanium carbide alloyed during sputtering with a weak carbide former (like Ni or Fe) denoted as Me [13,22]. They have shown that the segregation of carbon is, in such a case, more energetically favourable than the formation of substitutional, ternary phase $(Ti_{1-y}Me_y)C$. Furthermore, they stressed that substitutional diffusion of Me atoms requires more energy and will generally be slower than the interstitial diffusion of carbon.

Carbon segregation in the present coatings could also be promoted by the well-known catalytic properties of iron and nickel. That type of the process was discussed by S. Esconjauregui et al. in the context of carbon nanotubes growth catalyzed by 3d metals (Fe, Ni) nanoparticles, in the atmosphere containing hydrocarbons [23]. On the basis of thermodynamic considerations, these authors pointed out the role of acetylene which is one of the most reactive carbon sources. This high reactivity of C_2H_2 promotes the formation of metastable carbides (Ni_3C, Fe_3C) which than easily release C atoms at the temperature as low as 350 °C. Carbon segregation/precipitation during co-deposition of iron and carbon resulting in formation of bcc-Fe nanoparticles in graphitic matrix was discussed by Babonneau et al. [24]. R. Lamber et al. studied interactions between bulk amorphous carbon and highly dispersed nickel leading to aggregation of Ni in nanoclusters and graphitization of carbon [25]. A *dissolution-diffusion-precipitation* mechanism was proposed to explain formation of graphite shells around nickel nanoparticles.

The considerations presented above help to understand the sputter deposition process in the case of even more complex multicomponent metal-carbon systems, such as FeCrNi-based austenitic steel targets operated in a reactive carbon containing atmosphere, as it is the case in our work. Since the 316L steel target is composed of a weak (Fe, Ni) and a relatively strong (Cr, Mo) carbide formers, amorphisation of grown films followed by carbon segregation could be expected and was indeed observed. More importantly, however, the results presented in Figs. 2 –3 show that the diffusion-driven segregation of carbon resulted in a new, self-organized amorphous nano-columnar structure.

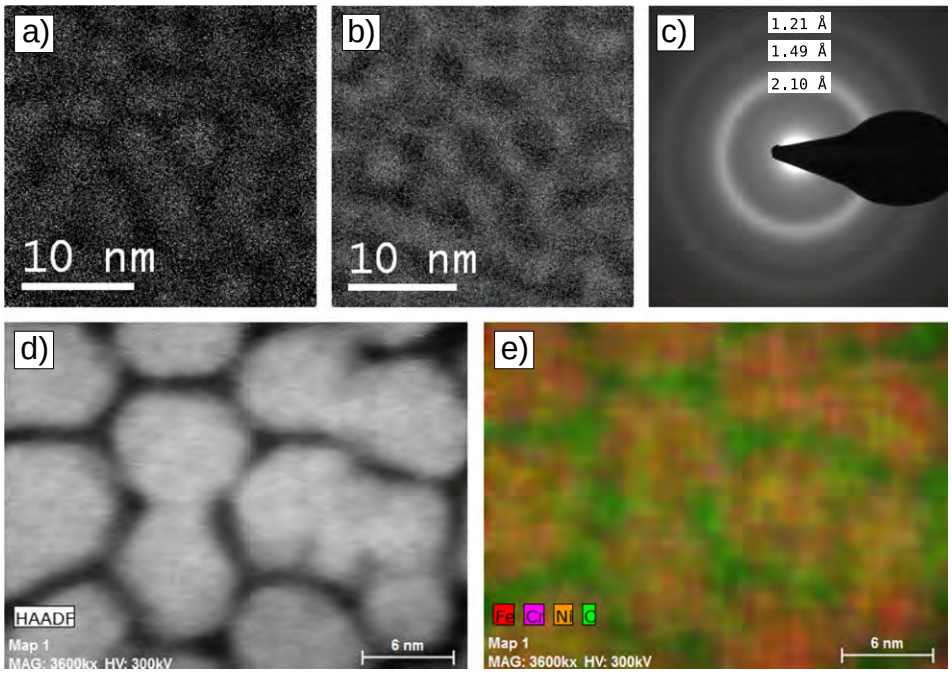

Fig. 3. High resolution analysis of the coating in plan-view: energy filtered transmission electron microscopy (EFTEM) elemental imaging for (a) Fe-L and (b) C-K maps (bright tone indicates higher concentration of the element), selected area electron diffraction pattern (SAED) of a column core (c), high-angle annular dark-field (HAADF) image (d) and corresponding electron dispersive X-ray (EDX) map of major elements in the coating.

The change in coating structure from crystalline through nanocrystalline to amorphous with segregated carbon resulted in significant changes of mechanical, tribological and anti-corrosion properties (cf. Fig. 4). Release of free, sp^2 bonded hydrogenated carbon proved to be very beneficial for mechanical properties. Although coating hardness, for carbon content between 20 and

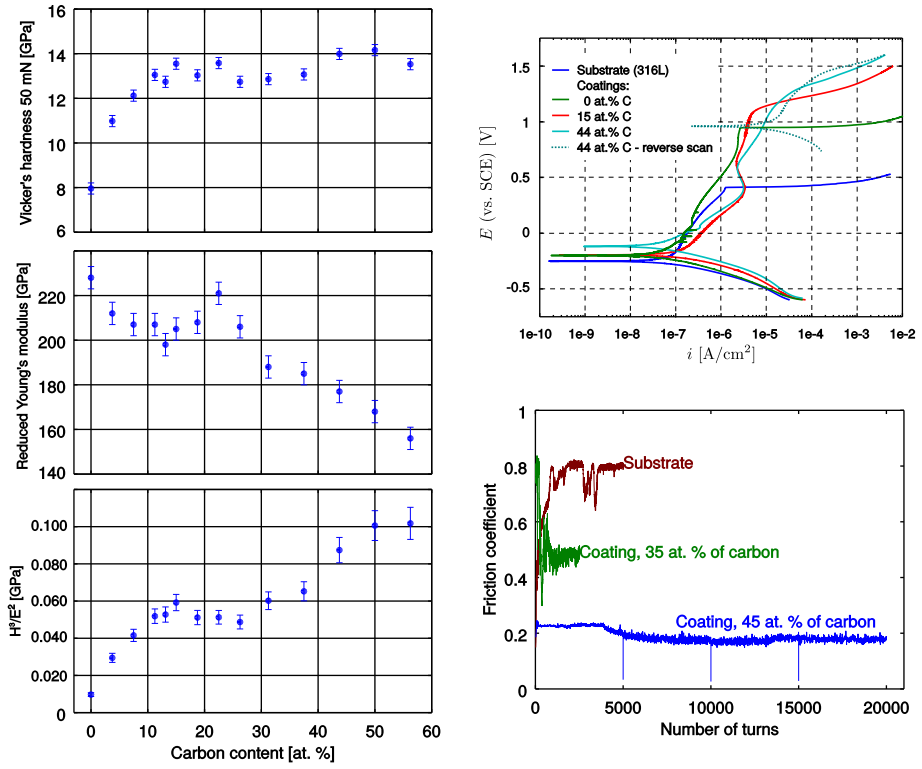

Fig. 4. Vickers microhardness H, reduced Young's modulus E, and toughness H^3/E^2 for studied coatings vs carbon content (a). Polarization curves recorded for the studied substrate-coating system in 3 wt% NaCl solution (b). Friction coefficient vs alumina ball 10 mm in diameter and 10 N normal force, for FeCrNi/a-C:H based coatings with increasing carbon content (c).

55 at.% remained almost unchanged at the level of 13 ± 1 GPa, the H^3/E^2 ratio, the parameter understood as an indirect measure of coating toughness, increased more than 10 times up to 0.12 GPa (cf. Fig. 4a).

Potentiodynamic polarization tests in 3 wt % NaCl aqueous solution (cf. Fig. 4b) revealed an active-passive behavior of the bare 316L steel substrate, the substrate covered with crystalline ferrite-containing coating and amorphous film with χ_c equal to 15 at.%. Further increase of the carbon content to 44 at.% caused the change in the shape of the polarization curve; no clear passive range was visible in the anodic range. It leads to the conclusion that in the composite coating consisting of carbon saturated Fe-Cr-Ni matrix and excessive sp^2-bonded hydrogenated carbon, oxidation of metallic alloy components is significantly suppressed. Cyclic potentiodynamic polarization test performed for this sample demonstrated that the reverse scan runs nearly the same path as the forward one. Such behavior indicates that the studied system is highly resistant to localized attack (pitting) of the corrosive medium utilized [26]. Low susceptibility of the sample to the formation of the stable pits, together with higher corrosion potential ($E_{corr} = -0.117$ V), as compared to the substrate ($E_{corr} = -0.250$ V), makes the composite coating effective protection for 316L steel in an environment containing chloride ions.

Our amorphous coatings containing free amorphous sp^2 bonded hydrogenated carbon have shown excellent tribological behavior in unlubricated friction test vs alumina ball. High carbon content films (ca. 45 at.%) demonstrated low friction ($\mu = 0.2$) and the wear rate of $0.6 \times 10^{-15} m^3 N^{-1} m^{-1}$, which is at least three orders of magnitude lower than that registered for uncoated 316L steel (cf. Fig. 4c). Carbon-rich coatings also withstand heavy plastic deformation without any delamination as was confirmed by additional friction tests with a 5 mm alumina ball and the normal load of 80 N.

In summary, we have deposited a new type of amorphous FeCrNi/a-C:H coatings by means of the reactive pulsed magnetron sputtering of 316L austenitic steel targets in an argon/acetylene atmosphere. The unique self-organized cream-roll-like nano-tubular structure of these coatings was revealed by high resolution electron microscopy and elemental mapping. The nano-columns are composed of metallic cores surrounded by amorphous carbon shells, whereas their axes are parallel to the growth direction. The self-organization observed in these amorphous coatings is interpreted as related to a thermodynamically beneficial segregation of carbon from the metastable 3d metal (Fe, Ni) carbides and probably from substitutional, ternary phases $(Cr_{1-y}Me_y)C$ where Me = Fe, Ni, formed during sputter deposition. This new nano-material exhibits superior mechanical, tribological and anti-corrosion properties.

Acknowledgments

The project was funded by the Polish National Centre for Science based on the following decision: UMO-2011/03/B/ST8/06130.

References

[1] Modified Low Temperature Case Hardening Processes, 2003, http://www.google.com/patents/US6547888.
[2] T.S. Hummelshøj, T.L. Christiansen, M.A.J. Somers, Scr. Mater. 63 (7) (2010) 761–763. http://dx.doi.org/10.1016/j.scriptamat.2010.05.031.
[3] L. Ceschini, C. Chiavari, E. Lanzoni, C. Martini, Mater. Des. 38 (2012) 154–160. http://dx.doi.org/10.1016/j.matdes.2012.02.019.
[4] T.W. Barbee, B.E. Jacobson, D.L. Keith, Thin Solid Films 63 (1979) 143–150.
[5] S. Malavasi, A. Oueldennaoua, M. Foos, C. Frantz, Couches minces nanocristallines d'alliages inoxydables Fe-Ni-Cr et Fe-Ni-Cr-C obtenues par pulverization cathodique, Memoires et Etudes Scientifiques Revue de Metallurgie, 1986, 553–560.
[6] S. Malavasi, A. Oueldennaoua, M. Foos, C. Frantz, J. Vac. Sci. Technol. A 5 (1987) 1888–1891.
[7] A. Billard, M. Foos, C. Frantz, M. Gantois, Surf. Coat. Technol. 4344 (1990) 521–532.
[8] S. Cusenza, P. Schaaf, Appl. Phys. A 94 (2009) 139–154.
[9] M.P. Seah, Surf. Interface Anal. 31 (8) (2001) 721–723. http://dx.doi.org/10.1002/sia.1076.
[10] NIST X-ray Photoelectron Spectroscopy Database, Version 4.1, 2012, http://srdata.nist.gov/xps/.
[11] S.T. Jackson, R.G. Nuzzo, Appl. Surf. Sci. 90 (2) (1995) 195–203. http://dx.doi.org/10.1016/0169-4332(95)00079-8.
[12] V. Zavaleyev, J. Walkowicz, G. Greczynski, L. Hultman, Surf. Coat. Technol. 236 (2013) 444–449. http://dx.doi.org/10.1016/j.surfcoat.2013.10.023.
[13] U. Jansson, E. Lewin, Thin Solid Films 536 (2013) 1–24. http://dx.doi.org/10.1016/j.tsf.2013.02.019.
[14] S.V. Meschel, O.J. Kleppa, J. Alloys Compd. 257 (1-2) (1997) 227–233.
[15] A.A. Voevodin, S.V. Prasad, J.S. Zabinski, J. Appl. Phys. 82 (1997) 855–858.
[16] P. Vilars, A. Prince, H. Okamoto, Handbook of Ternary Alloy Phase Diagrams, ASM International. 1995.
[17] M.-P. Delplancke-Ogletree, O.R. Monteiro, J. Vac. Sci. Technol. A 15 (4) (1997) 1943–1950. http://dx.doi.org/10.1116/1.580663.
[18] M. Stüber, H. Leiste, S. Ulrich, H. Holleck, D. Schild, Surf. Coat. Technol. 150 (2-3) (2002) 218–226. http://dx.doi.org/10.1016/S0257-8972(01)01493-1.
[19] T. Zehnder, J. Patscheider, Surf. Coat. Technol. 133-134 (2000) 138–144. http://dx.doi.org/10.1016/S0257-8972(00)00888-4.
[20] W. Gulbiński, S. Mathur, H. Shen, T. Suszko, A. Gilewicz, B. Warcholiński, Appl. Surf. Sci. 239 (3-4) (2005) 302–310. http://dx.doi.org/10.1016/j.apsusc.2004.05.278.
[21] B. Trindade, M.T. Vieira, Mater. Sci. Eng. A 352 (1-2) (2003) 195–201. http://dx.doi.org/10.1016/S0921-5093(02)00865-1.
[22] U. Jansson, E. Lewin, M. Rsander, O. Eriksson, B. Andr, U. Wiklund, Surf. Coat. Technol. 206 (4) (2011) 583–590. http://dx.doi.org/10.1016/j.surfcoat.2010.06.017.
[23] S. Esconjauregui, C.M. Whelan, K. Maex, Carbon 47 (2009) 659–669.
[24] D. Babonneau, J. Briatico, F. Petroff, T. Cabioch, A. Naudon, J. Appl. Phys. 87 (7) (2000) 3432–3443. http://dx.doi.org/10.1063/1.372363.
[25] R. Lamber, N. Jaeger, G. Schulz-Ekloff, Surf. Sci. 197 (3) (1988) 402–414. http://dx.doi.org/10.1016/0039-6028(88)90636-X.
[26] Z. Bou-Saleh, A. Shahryari, S. Omanovic, Thin Solid Films 515 (11) (2007) 4727–4737. http://dx.doi.org/10.1016/j.tsf.2006.11.054.

Surface & Coatings Technology 378 (2019) 124910

Contents lists available at ScienceDirect

Surface & Coatings Technology

journal homepage: www.elsevier.com/locate/surfcoat

Quasi-amorphous, nanostructural CoCrMoC/a-C:H coatings deposited by reactive magnetron sputtering

Tomasz Suszko[a,*], Witold Gulbiński[a], Ewa Dobruchowska[a], Grzegorz Greczynski[b], Lars Hultman[b], Jerzy Morgiel[c]

[a] Koszalin University of Technology, Ul. Śniadeckich 2, Koszalin 75-453, Poland
[b] Thin Film Physics Division, Department of Physics (IFM), Linköping 581 83, Sweden
[c] Institute of Metallurgy and Materials Sciences, Polish Academy of Science, Ul. Reymonta 25, Kraków 30-059, Poland

ARTICLE INFO

Keywords:
CoCrMo alloys
Magnetron sputtering
Thin films
Nanocomposites
Carbon self-organized structure

ABSTRACT

CoCrMo-C coatings have been deposited on CoCrMo ISO 5832-12 alloy substrates by reactive magnetron sputtering from targets of the same alloy in the C_2H_2/Ar atmosphere. Their structure evolution with increasing carbon content as well as chemical and phase composition were investigated by X-ray diffraction, X-ray photoelectron spectroscopy and transmission electron microscopy. Hardness, Young's modulus, and tribological properties in ambient air were studied. Results show that microstructure of deposits evolves from biphasic, containing γ (fcc) and ε (hcp) metallic phases for low carbon content, through nanocrystalline and amorphous for carbon content between 10 and 20 at.%, to quasi-amorphous nanostructural for even higher content of carbon. Segregation of amorphous carbon leads to the formation of self-organized tubular nanostructure for coatings containing more than 30 at.% of carbon. Introduction of carbon into CoCrMo alloy results in a significant increase of hardness up to 14 GPa and improvement of load-bearing capacity which reached 120 MPa. Compared to uncoated CoCrMo substrate, deposited coatings with high carbon content exhibited superior tribological properties with low friction coefficient around 0.2 and wear rate about 2×10^{-15} m^3/N/m.

1. Introduction

Nanostructural thin films, due to their attractive and unique features, are scientifically intriguing and technologically important. Properties of such layers predominantly depend on their composition, crystalline structure, and morphology. Under certain synthesis conditions it is possible to produce nanostructural films with desired morphology that can be shaped or modified to obtain improved characteristics.

Our recent research on magnetron sputter deposition and properties of thin films based on FeCrNiMo-C system [1] resulted in developing quasi-amorphous coatings showing a specific self-organized nanocolumnar structure and superior anti-corrosion and mechanical properties. Peculiar properties of the coatings encouraged us to investigate also the CoCrMo-C system. We turned our attention to CoCrMo alloys belong to the group of materials offering properties desirable in biomedical applications, in particular for artificial joints and other implants [2-4].

While the alloys meet many requirements, a lot of research was done for further improving their performance by increasing wear and corrosion resistance which are crucial for implant service life. Among surface treatments used for this purpose gas and plasma nitriding [5-10] or carburizing [10,11] have been tested resulting in improving the properties by the generation of so-called expanded austenite (S-phase) [12,13]. An increase in performance was also achieved by duplex treatment. Luo and Li carried out plasma carburizing of CoCrMo alloy and subsequent magnetron deposition of commercial Cr-doped carbon-based Graphit-iC (GiC) coating [13]. These authors reported a significant lowering of friction coefficient due to the application of the C-based top coating. Simultaneously, the load-bearing capacity of the duplex treated alloy was found to be about four times higher than that of untreated samples.

An alternative approach was deposition of hard, wear-resistant coatings like DLC [14-16], TiN [17,18], TiAlN [19] as well as more complex systems like TiAlVCN/CN_x [20] or TiSiON [21]. Recently, C. Liu and co-workers proposed a surface modification of CoCrMo alloy by carbon implantation, leading to amorphization of the near-surface zone [22,23]. The thickness of the modified surface layer was up to 150 nm, depending on the implantation dose that varied from 1 to 9×10^{17} ions/cm^2, whereas carbon concentration reached 47 at.%.

* Corresponding author.
E-mail address: tomasz.suszko@tu.koszalin.pl (T. Suszko).

https://doi.org/10.1016/j.surfcoat.2019.124910
Received 3 October 2018; Received in revised form 6 August 2019; Accepted 15 August 2019
Available online 29 August 2019

Tests conducted in a simulated body fluid revealed that carbon implantation resulted in spectacular improvement of pitting corrosion resistance. Authors pointed at the superior self-passivation ability of the amorphous layer. However, what can be some drawback of this interesting treatment is a very small thickness of the modified layer, not sufficient to improve the mechanical properties of CoCrMo.

Analysis of surface modifications of CoCrMo alloy conducted till now and leading to improvement of mechanical or corrosion properties has shown that in each case obtained results only partly met application needs. Simultaneously, usage of carbon deposited in the form of DLC coatings or introduced by diffusion-driven carburizing or implantation, was found as the most profitable in terms of wear and corrosion resistance. Thus, the research challenge is to propose the CoCrMo alloy surface modification method which allows forming a few micrometres thick, well adherent CoCrMo based layer, properties and microstructure of which can be tuned in the wide range by carbon concentration.

In the current work, we present a surface modification of CoCrMo alloy by deposition of quasi-amorphous CoCrMoC/a-C:H coatings obtained by reactive magnetron sputtering of CoCrMo ISO 5832-12 alloy target in Ar/C_2H_2 atmosphere. Structure evolution of the coatings with increasing carbon content is discussed together with their chemical and phase composition investigated by X-ray diffraction (XRD), X-ray photoelectron spectroscopy (XPS) and transmission electron microscopy (TEM). The basic mechanical and tribological properties over a wide range of carbon content are also presented.

2. Experimental

The 4.5–5 μm thick CoCrMo-C coatings were deposited in a small laboratory chamber by pulsed, reactive magnetron sputtering of the CoCrMo ISO 5832-12 alloy target (with a diameter of 100 mm and the chemical composition given in Table 1) in Ar/C_2H_2 atmosphere. The argon flow was kept constant at 6 sccm for each deposition, while the acetylene flow was varied from 0 to 5 sccm. The total gas pressure during the deposition process was about 0.4–0.5 Pa depending on the acetylene flow. The magnetron source was working in an unbalanced mode at the frequency of 100 kHz with 1 kHz modulation. The average discharge current was set at 1 A and the resulting power was 1.1–1.2 kW. The coatings were deposited on mirror polished, disc-shaped substrates cut from CoCrMo ISO 5832-12 alloy rod as well as on Si (100) wafers. Substrates were heated to 300 °C and kept at DC bias potential of −50 V. The distance between substrates and the target surface was 8 cm with no movement during deposition. The processes started with target cleaning by sputtering in pure argon, then acetylene was stepwise added to the atmosphere and finally, when the magnetron discharge was stable, substrates were exposed to sputtered particles. The constant intensity of the Cr^I 521 nm optical emission line from the magnetron plasma was treated as an indicator of discharge stability. No kind of interlayer was applied.

Thanks to the high pumping speed of the vacuum system with a turbopump, the deposition system worked in so-called overpumping mode; the flow of the reacting gas was much higher than its consumption. No hysteresis in pressure–flow dependence was observed, and the sputtering process was stable in this respect.

The thickness of coatings was measured by Hommel Waveline T8000 stylus profilograph as an offset between the coating surface and a part of the substrate surface intentionally covered against deposition.

The structure and phase composition were examined by the XRD using Panalytical Empyrean 3 diffractometer employing Cu-Kα radiation. Two diffraction geometries were used: Bragg-Brentano (ϑ-2ϑ) and the geometry with constant incidence angle ω. In the first case the tilt angle ψ was 0 and the interference reflections from planes parallel to the sample surface were recorded. In the second geometry several values of the ω angle were used what entails varying tilt angles and X-ray penetration depths d_p. For low-carbon samples values of d_p and ω are listed below. The diffraction angle $2\vartheta = 50°$. is there assumed. Well known Scherrer's and Willson's equations and also Williamson-Hall's approach were used for estimating the crystallite size and the level of microstrains [24].

ω [deg.]	3	5	10	15	20	25
d_p [μm]	0.5	0.8	1.6	2.4	3.2	4.0
ψ [deg.]	22	20	15	10	5	0

Lamellas for TEM investigations were prepared by using FIB-Quanta 3D dual beam instrument. High-resolution observations of the coatings microstructure were performed using Tecnai G2 F20 TEM operating at 200 kV accelerating voltage. The chemical composition of the coatings was determined by XPS. The XPS analysis was performed in an Axis Ultra DLD instrument (Kratos Analytical, UK) with monochromatic Al-Kα radiation ($h\nu$ = 1486.6 eV). The base pressure during spectra acquisition was 1.5×10^{-7} Pa. The binding energy scale was calibrated by examining the sputter-cleaned Au, Ag, and Cu samples according to the recommended ISO standards for monochromatic Al Kα sources that place Au $4f_{7/2}$, Ag $3d_{5/2}$, and Cu $2p_{3/2}$ peaks at 83.96; 368.21, and 932.62 eV, respectively [25]. Prior to analyses all samples were sputter-cleaned to remove adsorbed contaminants, first with 4 keV Ar^+ ions for 120 s followed by 0.5 keV Ar^+ for 600 s, both at the take-off angle of 20°. The intention of the second sputter-cleaning step was to minimize the damage caused by the Ar+ bombardment [26]. All spectra were collected from the area of 0.3×0.7 mm^2 and at normal emission angle. The analyzer pass energy was set to 20 eV which results in the full width at half maximum of 0.55 eV for the Ag $3d_{5/2}$ peak. Casa XPS software (version 2.3.16) was used for quantification of XPS spectra, based upon peak areas from narrow energy range scans and elemental sensitivity factors supplied by Kratos Analytical Ltd. The confidence level is typically around ± 5%.

Vicker's microhardness and Young's modulus of the coatings were measured using Fisherscope 2000 instrument equipped with diamond Berkovich indenter (tip radius 0.15 μm) with the maximal applied load of 50 mN. Calculations were made by software included with the device, from load-displacement data. Maximal indentation depth was smaller than 0.17 μm. For every presented value two samples of given composition were measured and ten indentations on each one were done.

Adhesion of coatings was evaluated by using the Rockwell adhesion test also referred as the Daimler-Benz test [27]. It uses a Rockwell C-type diamond cone indenter with an applied load of 1470 N (150 kg). Tribological properties were tested on the ITE T-01 M ball-on-disc

Table 1
Chemical composition of the ISO 5832-12 alloy declared by the producer (L. Klein S.A.) and the composition of the target material and the coatings measured with XPS – mean values from all measurements and the standard deviation is given. The analysis is limited to described elements. Atomic proportions between the main metallic components are marked in bold.

	Producer declaration		XPS
Element	wt%	at.%	at.%
Co	65.140	63.4 (**65.3**)	**65.0 ± 3.0**
Cr	27.600	30.4 (**31.3**)	**31.0 ± 1.5**
Mo	5.5200	3.30 (**3.4**)	**4.0 ± 0.4**
Si	0.6200	1.3	–
Mn	0.8200	0.86	–
N	0.1820	0.74	–
Ni	0.0900	0.57	–
C	0.0450	0.21	–
Fe	0.1800	0.18	–
Cu	0.0100	0.009	–
W	0.020	0.006	–
P	0.0030	0.0056	–
S	0.0005	0.0009	–

tester. As a counterpart, an alumina ball with a diameter of 10 mm was used. Friction tests were done under normal load of 5 and 10 N (mean Hertzian stress 0.58 and 0.73 GPa respectively) in laboratory air of 40% relative humidity without any lubricants. A rotational speed of 60 rpm and a track radius of 10 and 12 mm was applied what corresponded to the linear speed of about 7 cm/s. Wear rate of the coating was calculated from the wear track cross-section area measured several times with the stylus profilometer. Two samples for each composition were prepared and two tests on each sample were carried out.

3. Results and discussion

Deposition rate in the above-described conditions varied from 0.22 to 0.13 μm/min depending on the acetylene flow rate. Thus the time needed for synthesizing 4.5 μm coatings varied from 20 to 35 min – longer for carbon-rich layers. A parabolic relationship between the acetylene flow and the content of carbon was observed: 1.5 at.% at the lowest acetylene flow (0.3 sccm) and 65 at.% at the highest (5 sccm). It should be mentioned here that for obtaining carbon-free coatings a long target cleaning (and the chamber conditioning) is required otherwise even at zero flow of acetylene the sample may contain some amount of carbon. This is mainly caused by the carbon dissolved in the target during earlier processes.

The coatings contain a certain amount of oxygen; at most 2 at.% in carbon-free samples and at least 0.4 at.% for carbon rich-ones – the more acetylene in the atmosphere the less oxygen in the coatings. The use of the acetylene flow greater than 5 sccm lead to powder like deposits with no adhesion to the substrates.

3.1. Structure of the coatings

CoCrMo alloy from which the cathode and substrates were made is biphasic containing γ (fcc) and ε (hcp) phases (cf. Fig. 1a). Positions of the peaks in the XRD pattern are in good agreement with those in ICDD (International Centre for Diffraction Data) cards No. 04-016-6869 and 04-016-6870. The observed contraction of *d*-spacings is at most 0.5% for ε(100), 0.3% for γ(111), ε(100), γ(200), and 0.1% for other planes. Using the Williamson-Hall's plot for the data gained from the pattern it was possible to calculate a value of microstrains and the crystallite size. The values are about 2.5% and 90 nm respectively. It is worth to mention here that direct applying the Scherrer's formula gives the value of mean crystallite size about 20 nm, so much less. The contraction of *d*-spacings and microstrains can be related to stress generated by the manufacturing process of the substrates. Surface grinding and polishing does not introduce additional strains – the Williamson-Hall analysis made for an XRD pattern recorded with constant small incidence angle $\omega = 5^{\circ}$ gives even lower difference between measured *d*-spacings and those from ICDD cards – 0.05–0.3%.

The deposition in pure argon leads to strained and textured films. (cf. Fig. 1b). There are several differences between XRD patterns of the bulk CoCrMo alloy (substrate) and the film. Some peaks disappear and the ones that remain are common for both phases except the ε(101) peak. All the peaks are significantly shifted to higher diffraction angles which means tensile stress along the surface plane. The *d*-spacings are smaller by about 1.2% for ε(002)/γ(111) and ε(101) peaks. Calculated from the ε(002)/γ(111) peak crystallite size is about 250 nm and from the ε(101) only 4 nm. Williamson-Hall approach was not possible for the coatings since only singular peaks are visible in the XRD patterns and because of the coating's texture.

The patterns recorded with constant incidence angles (not presented here) are similar with increasing *d*-spacing shift for decreasing ω which is most probably caused by the different angular position of crystallographic planes with respect to the surface and the stress direction. The calculation of crystallite size from ε(002)/γ(111) peaks parameters

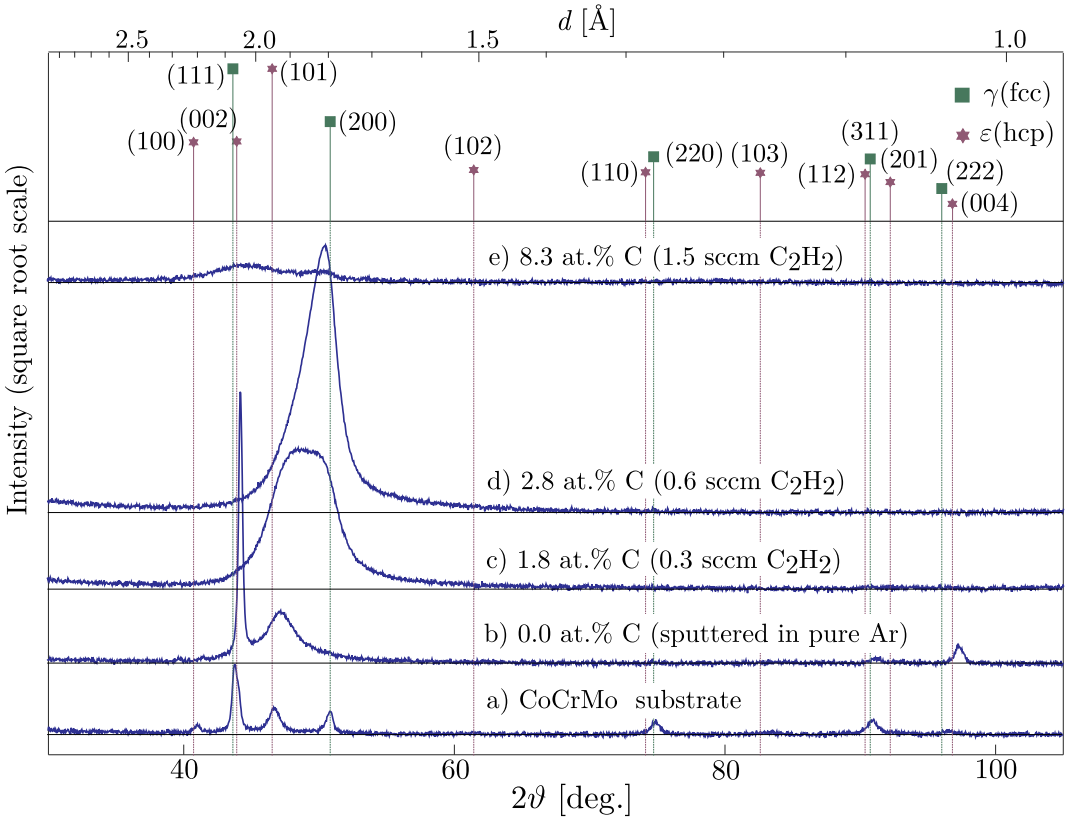

Fig. 1. XRD patterns of the CoCrMo substrate, CoCrMo, and CoCrMoC coatings with increasing carbon content. All the patterns were recorded in the same ϑ-2ϑ geometry and the same diffractometer parameters. The square root scale of intensity is applied to make weak peaks visible.

gives the value of about 80 nm for the lowest ω-angles and ≈170 nm for $\omega \geq 10^{\circ}$. The crystallite size calculated from $\varepsilon(101)$ peaks is about 3.5 nm independently on ω angle. Given that $\gamma(111)$ and $\varepsilon(002)$ planes are coherent [28] and both fcc and hcp structures differ only with stacking order one can assume that the coating consists mainly of ε phase preferentially oriented with $\varepsilon(002)$ planes parallel do the substrate surface. High density of stacking faults can be also expected.

When acetylene is added to the process atmosphere, the microstructure of CoCrMo-C coatings undergoes the following gradual transitions with increasing carbon content:

- grain refinement,
- amorphization,
- carbon segregation (CoCrMoC/a-C:H nanostructure development),
- self-organized quasi-amorphous nanocomposite formation,
- degradation of the coating.

3.1.1. Grain refinement

A small addition of acetylene to the process atmosphere leads to fuzzy diffraction pattern (cf. Fig. 1c, d). The sole broad peak is located just between $\varepsilon(101)$ and $\gamma(200)$ and is difficult for interpretation.

Supplemental data provided by XRD patterns recorded at constant ω angles can clarify the situation (cf. Fig. 2a). The pattern recorded with $\omega = 15^{\circ}$ can be deconvoluted into broad $\varepsilon(101)$ peak with a tiny share off $\gamma(200)$ peak. For higher ω (greater penetration depth) the γ component increases, and for lower ω it decreases. This proves that phase composition changes with depth. The unambiguous asymmetry of the $\gamma(200)$ peak can be caused by occurrence areas with different carbon content – it is known that introduction of carbon into CoCrMo alloys yields to so-called S-phase (expanded austenite) [10]. It is also visible that deviations in *d*-spacings for both phases have opposite signs and high value (even 2.5%) what indicates contrary and strong microstrains.

These observations and the fact that the deposition process was stable and there was no reason to expect a composition gradient, lead to the conclusion that the coating under the influence of the stress undergoes a strain-induced partial martensitic transformation of metastable γ phase to ε. Such transformation for bulk CoCrMo alloys is commonly observed [2,28,29]. In our case the transformation most probably begins at the top of the coating after the deposition process, moves toward the substrate and leads to the gradual relaxation of the microstrains.

The same behavior is even more clearly observed for the sample with higher carbon content (cf. Figs. 1d and 2b). For highest penetration depths (ω = 20 and 25°) the XRD patterns consist almost only the $\gamma(200)$ asymmetric peak. Presence of carbon seems to promote growing γ crystallites what is in agreement with results reported for carburizing CoCrMo alloys [30]. For ω = 10 and 15° peaks from both phases are visible and for ω = 3 and 5° almost only the common $\gamma(111)/\varepsilon(002)$ peak is present. Crystallite size for both compositions (1.8 and 2.8 at.% of carbon) calculated from parameters of the $\varepsilon(101)$ peaks is about 3 nm and for the $\gamma(200)$ peaks is about 4 nm. These values should be treated with caution because the peak broadening can be also originated from microstrains undoubtedly present in the films. The microstrains calculated from Wilson's formula are of about 2.5%, and again should be treated with caution. Observed grain refinement can be interpreted as a consequence of carbon presence which disturbs the growth of grains and leads to re-nucleation of new ones.

3.1.2. Amorphization

Further increasing carbon content leads at first to homogenizing of the coating; independently on the ω-angle the XRD patterns look very similar and can be deconvoluted onto three broad peaks: $\gamma(200)/\varepsilon(002)$, $\varepsilon(101)$ and $\gamma(200)$ as it is shown in Fig. 2c. Positions of the ε peaks are closer to those reported in the ICDD cards but still the opposite microstrains are observed for the largest penetration depths. The

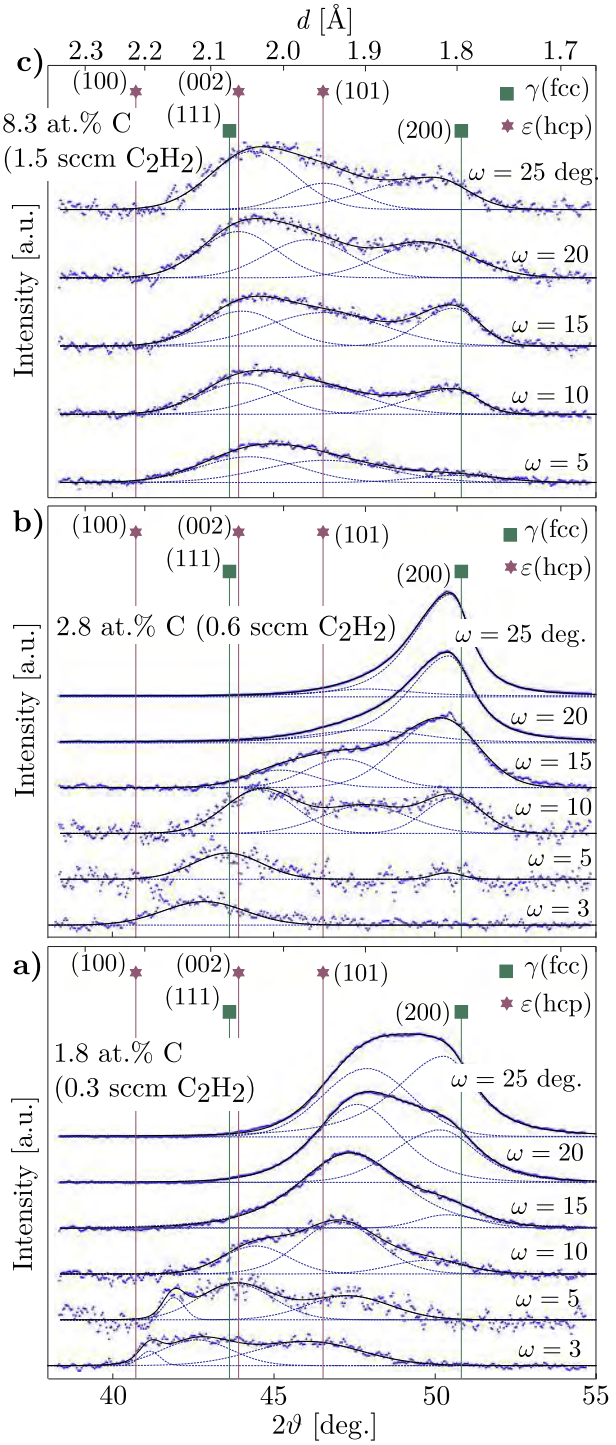

Fig. 2. XRD patterns of CoCrMo-C coating with various carbon content recorded at constant values of the incidence ω-angle. The intensity scale is linear but different for every pattern in order to make visible also weak signals recorded at small incidence angles.

average value of *d*-spacing calculated from all $\gamma(200)$ in the figure is larger by about 1% than that in the ICDD card and as stated above can be attributed to dissolved carbon in the fcc lattice or to the microstrains.

Even greater carbon content results in amorphization of deposits and flat XRD patterns with gradually appearing peaks from substrates – not presented here. The amorphization at relatively small carbon content is characteristic for sputter deposition of ternary carbide coatings containing transition metals with both low and high chemical affinity to

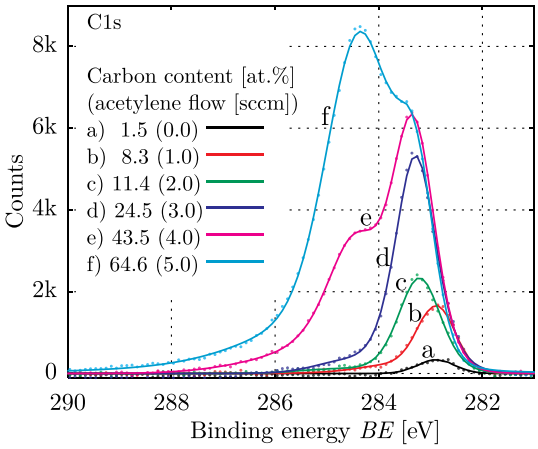

Fig. 3. XPS C 1s core-level spectra obtained from the coatings with different carbon content.

carbon – so-called weak and strong carbide formers. Trindade and Vieira [31] for example reported that in case of chromium and molybdenum carbides, alloying with small amount of a weak carbide former (iron in that instance) leads to amorphous deposits.

In the case of CoCrMo-C coatings, crystallization of thermodynamically stable carbides like Cr_7C_3 ($\Delta H_0 = -14.1 \pm 0.8$ kJ/mol [32]), $Cr_{23}C_6$ ($\Delta H_0 = -22.5$ kJ/mol [33]) or Mo_2C ($\Delta H_0 = -27 \pm 3$ kJ/mol [34]) is hindered by high content of cobalt, known to be weak carbide former. Its carbides are thermodynamically unstable: for Co_2C $\Delta H_0 = 2.8 \pm 1.3$ and for Co_3C $\Delta H_0 = 2.4 \pm 1.4$ kJ/mol [32].

3.1.3. Carbon segregation

Aside from amorphization, the next phenomenon is observed for coatings with greater carbon content. As shown in Fig. 3, C 1s core level spectra evolve with increasing carbon content. For $\chi_C > 10$ at.%, the C 1s peak characteristic for carbides and for interstitially bonded carbon in alloys (283.2 eV) shifts to slightly higher binding energy (cf. Fig. 3, line c) and then for carbon content 24.5 at.% and more, a second higher energy peak appears at 284.4 eV (cf. Fig. 3, lines d,e,f). This indicates the presence of sp^2-bonded carbon and so carbon segregation occurs [35,36]. The relative intensity of the high binding energy component of the C1s spectra increases linearly with increasing carbon content above a threshold (cf. Fig. 4). From the plot it can be seen that the carbon segregation begins when carbon content $\chi_C > 20$ at.%.

Segregation of carbon is well known in binary metal-carbon thin films. For 3d, 4d, and 5d early transition metals from groups 4–6 that

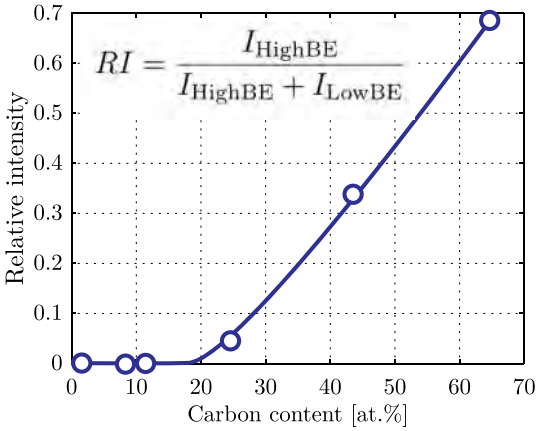

Fig. 4. The relative intensity (RI) of the high binding energy (BE) component in the C1s spectra for the coatings with increasing carbon content.

form stable carbides, this segregation leads to the formation of nanocomposite structures, where nanocrystalline metal carbides are embedded in an amorphous carbon matrix. The matrix is formed when carbon content exceeds Me/C ratio for corresponding carbide [37-39]. In case of transition 3d metals from groups 8–10, forming much less stable carbides, chemical nature and geometrical form of precipitates depend on deposition conditions. Deposits synthesized at low substrate temperature, as it was in our study, contain metastable carbide precipitates like Ni_3C and in higher temperature metallic precipitates are observed [40,41].

Segregation of carbon in the studied CoCrMo-C coatings occurs if the carbon content exceeds 20 at.% which is also a level ensuing from $Me_{23}C_6$-type carbides stoichiometry (21 at.% C). Carbon release is induced by alloying of the carbide-forming Cr-Mo-C system with cobalt. The mechanism of carbon segregation in sputter-deposited ternary metal-carbon coatings containing both, weak and strong carbide formers, was discussed by M. Råsander et al. [42] and Jansson and Lewin [43]. Even if the decomposition of metastable ternary phases $(Me^s_{(1-x)}Me^w_{(x)})C_y$, where Me^s and Me^w denote strong and weak carbide former respectively, into stable phases; Me^sC carbide plus Me^w could be thermodynamically expected, during deposition another route can be also observed i.e. carbon is released from the metastable ternary compound. The explanation of this phenomenon is that the second route requires smaller activation energy (for initiation of carbon interstitial diffusion) [42]. The first route needs higher activation energy associated with substitutional diffusion of metal atoms and thus it can be expected when the deposition process is conducted at higher temperature.

In our recent paper, we have shown that described above mechanism of carbon segregation is valid also for more complex, quaternary system like FeNiCrMoC/a-C:H [1] where the similar phenomenon was observed. It is also necessary to mention that due to hydrocarbon gas (acetylene) usage during sputter deposition of CoCrMoC/a-C:H coatings, they most likely contain sp^2 bonded carbon in hydrogenated form [44]. For this reason, they are denoted using C:H suffix.

3.1.4. Self-organized quasi-amorphous nanocomposite formation

TEM studies of deposits confirmed that their structure, for $\chi_C \approx 11$ at.% is quasi-amorphous (cf. Fig. 5a). For carbon content above the segregation threshold, HRTEM analysis revealed a self-organized nanostructure in the form of columns oriented along the film growth direction (cf. Fig. 5b). This nanostructure becomes more diffuse when the carbon content further increases (cf. Fig. 5c).

Selected area electron diffraction patterns contain one fuzzy ring corresponding to the *d*-spacing of 2.05–2.15 Å – exactly the same in every TEM-studied samples. This value can be attributed to the distance between close-packed planes, and it is in good agreement with the $\gamma(111)$ and $\varepsilon(002)$ *d*-spacing. However, it is must be a short-range order; it was impossible to find any areas of visible crystallographic arrangement there.

The columnar structure of the coating was additionally confirmed by the plan view TEM image (cf. Fig. 6), where the nanorods are clearly visible. The similar nanocolumnar structure was observed in our FeNiCrMoC/a-C:H coatings deposited by magnetron sputtering [1]. Such structures were also observed earlier in binary coatings (Ni-C and Co-C) obtained by plasma sputtering of nickel and cobalt targets in a methane atmosphere by F.L. Wang et al. [45] and A.A. El Mel et al. [46,47]. However, in both systems we have studied thus far, FeCrNiMoC/a-C:H and CoCrMoC/a-C:H, and in contrast to the cited works, the formed nanorods are quasi-amorphous.

3.2. Mechanical and tribological properties

Introduction of carbon into CoCrMo alloy results in a pronounced change of the microstructure as well as mechanical and tribological

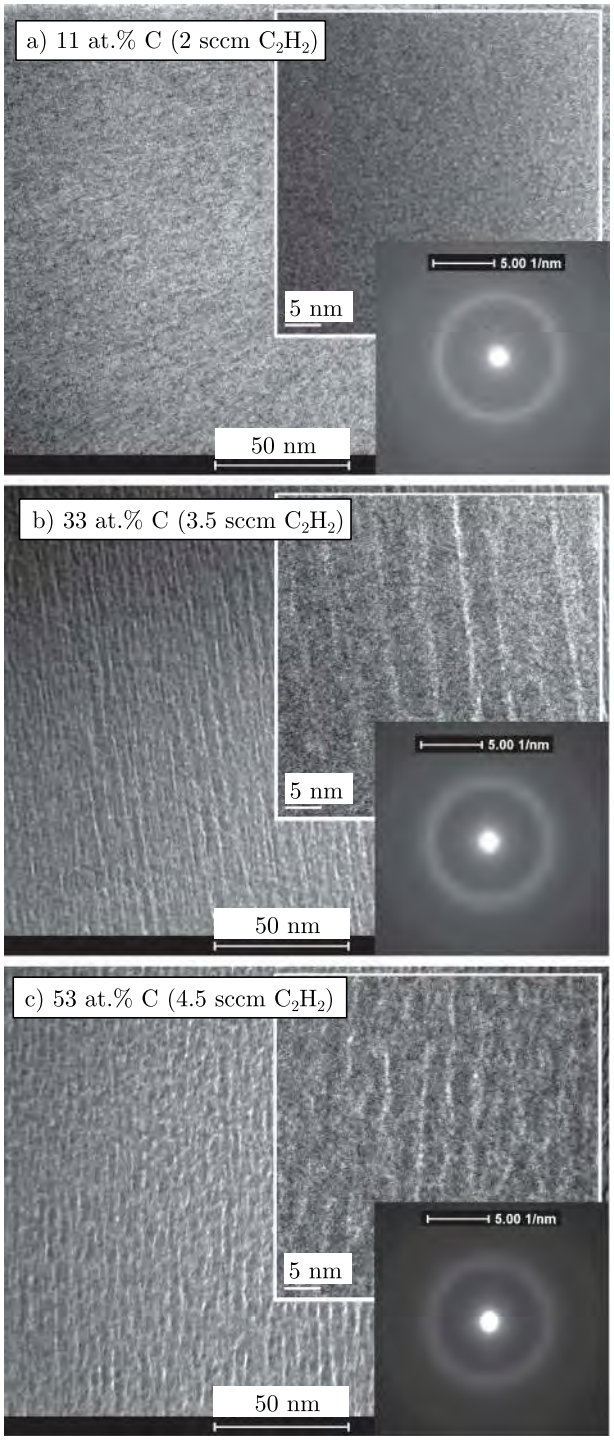

Fig. 5. HRTEM cross-section pictures, and SAED patterns of CoCrMo-C coatings with different content of carbon.

properties of studied coatings. As shown in Fig. 7a, initial grain size refinement leads to hardness increase from 11 GPa for CoCrMo up to 13 GPa obtained with $\chi_C \approx 20$ at.% reaching almost 14 GPa for higher carbon contents. Simultaneously, segregation of amorphous carbon phase for $\chi_C > 20$ at.%, modifies elastic properties of deposits. The elastic modulus decreases gradually with carbon content. The H^3/E^2 ratio, the parameter understood as an indirect measure of coating toughness or load bearing-capacity, [48] increases from 25 MPa up to 120 MPa (cf. Fig. 7b). It means that coatings became more resistant to plastic deformation and better accommodate elastic strain.

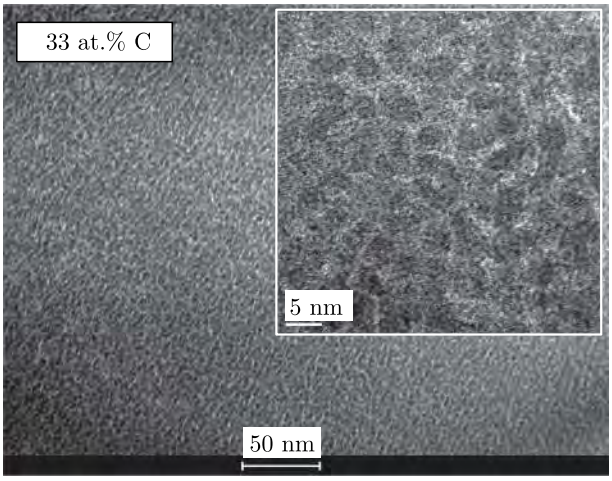

Fig. 6. HRTEM plan view of the CoCrMoC/a-C:H coating with carbon content 33 at.%.

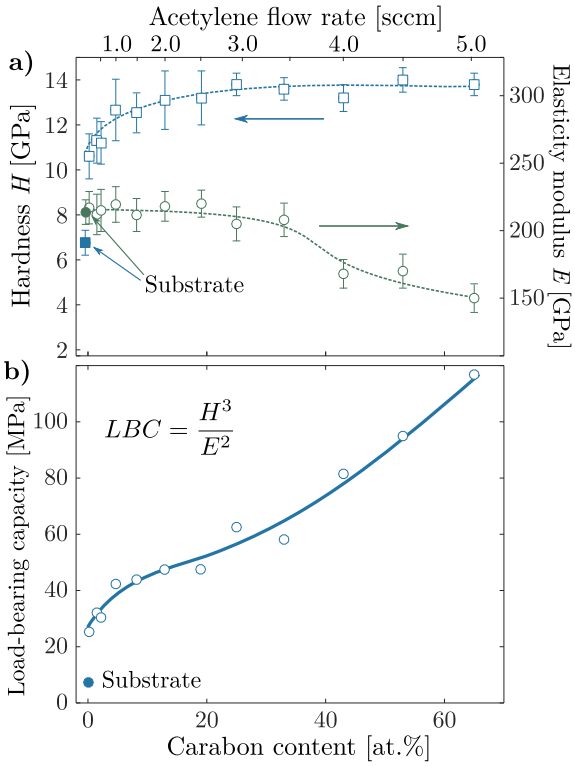

Fig. 7. Microhardness and elasticity modulus (a) and load-bearing capacity as the H^3/E^2 ratio (b) for CoCrMo-C coatings with increasing carbon content.

Adhesion of coatings changes remarkably with carbon content and follows the same trend as the H^3/E^2 ratio. Brittle cracking and delamination typical for low adhesion classified as HF4 in the Daimler-Benz test scale [27] were observed for hard but brittle, nanocrystalline low carbon coatings (cf. Fig. 8a). Enrichment of deposits with carbon results in much better tolerance to elastic deformation. Stresses generated by the Rockwell indenter were not high enough to induce coating delamination. Radial cracking without delamination of the coating in the indentation circumferential zone confirmed very good adhesion, classified as HF1 (cf. Fig. 8b and c). The coatings lose their adhesion when carbon content exceeds 70 at.%. Undoubtedly the adhesion of low-carbon film can be improved by a suitable sublayer although it was not the subject of the studies.

The best tribological behavior of studied coatings was observed for

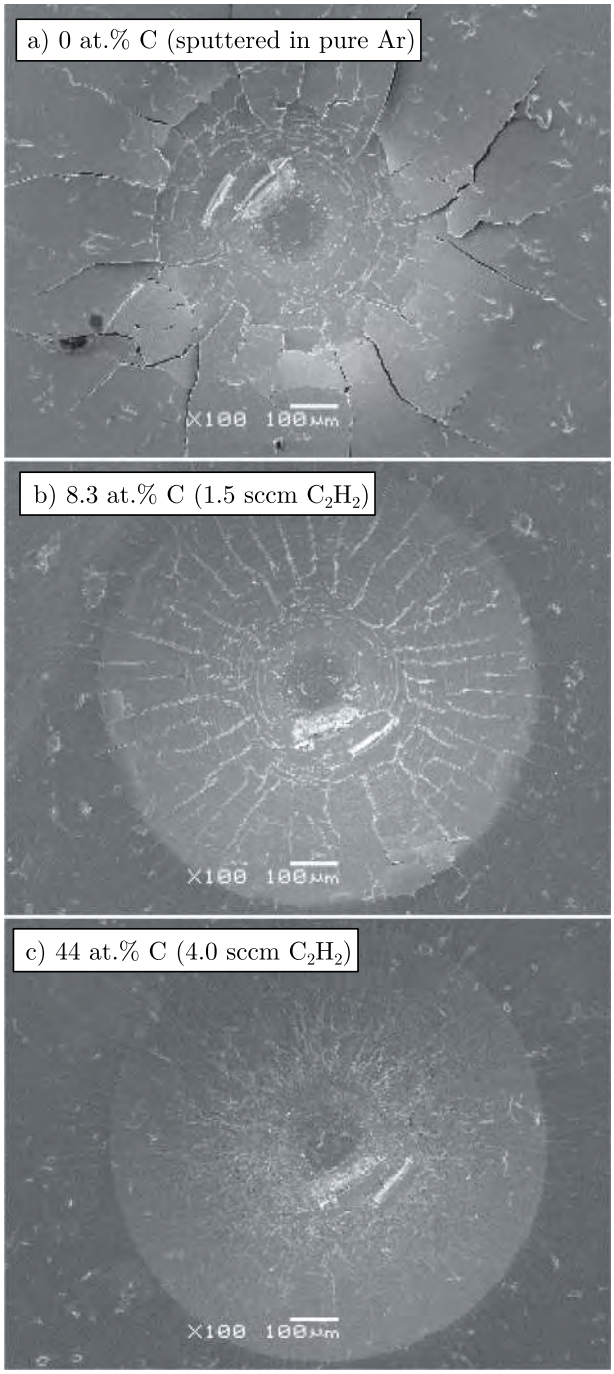

Fig. 8. Indentation pictures after Daimler-Benz test for 4.5 μm thick CoCrMo-C coatings deposited on CoCrMo alloy.

$35 < \chi_C < 65$ at.% (acetylene flow rates 3.5–5 sccm). For films containing less than 30 at.% carbon, high hardness and brittleness were the reason for catastrophic wear and high friction. Low friction coefficient, below 0.2, and wear rate for carbon-rich coatings ($\chi_C > 60$ at.%) reaching 2×10^{-15} m^3/N/m (cf. Fig. 9b) are interpreted as a consequence of (a) self-lubricating properties of graphitic sp^2 bonded carbon present in the coating, and (b) an enhanced load-bearing capacity improving the resistance of carbon-rich coatings to dynamic loads during tribological tests.

4. Conclusions

In the present paper, we report on thin film coatings deposited by magnetron sputtering of the CoCrMo alloy target in Ar/C_2H_2 atmosphere. Their structure evolves:

- from nanocrystalline for carbon content χ_C between 1.5 and 10 at. %, through
- amorphous for $10 < \chi_C < 20$ at.% C, to
- amorphous self-ordered nanotubular structure for carbon-rich coatings – $30 < \chi_C < 65$ at.% C denoted as CoCrMoC/a-C:H.

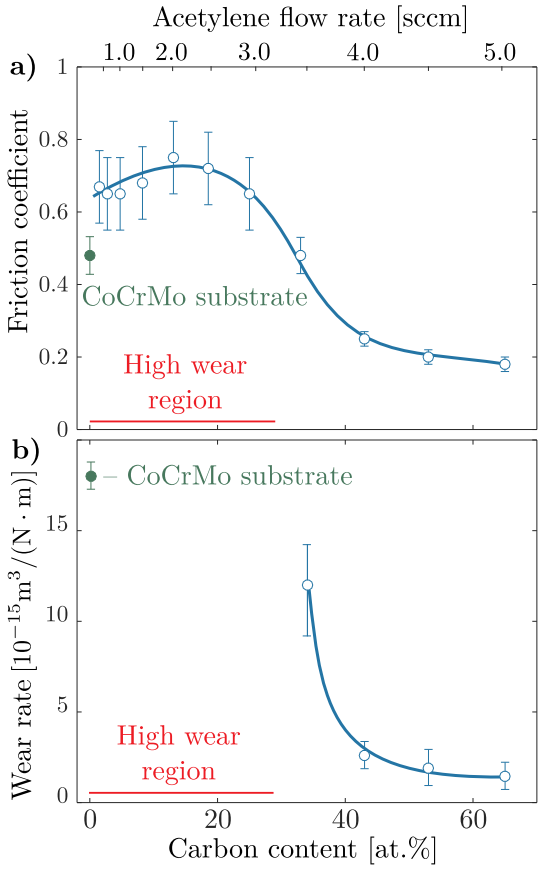

Fig. 9. Friction coefficient vs alumina ball (a) and wear rate (b) for CoCrMo-C coatings with increasing carbon content.

Segregation of carbon at relatively small its content is interpreted as a result of decomposition of metastable ternary phases ($Me^s_{(1-x)}Co^w_x)C_y$), formed during deposition. Introducing a larger amount of carbon into the deposits yields quasi-amorphous self-ordered coating providing good mechanical protection of the core material. Mechanical and tribological properties of the coatings substantially improve with increasing carbon content beyond 30 at.%, due to phase separation. The hardness of the deposits reaches 14 GPa. The load-bearing capacity (H^3/E^2) ratio, understood as an indirect measure of coating toughness) increases from 0.03 up to 0.12 GPa. Friction coefficient measured vs alumina ball decreased to 0.2 and the wear rate drops to 2×10^{-15} m^3/N/m.

References

[1] T. Suszko, W. Gulbiński, J. Morgiel, G. Greczynski, E. Dobruchowska, P. Dłużewski, J. Lu, L. Hultman, Amorphous FeCrNi/a-C:H coatings with self-organized nanotubular structure, Scr. Mater. 136 (2017) 24–28, https://doi.org/10.1016/J.SCRIPTAMAT.2017.03.040.

[2] Y. Dong, P. Svoboda, M. Vrbka, D. Kostal, F. Urban, J. Cizek, P. Roupcova, H. Dong, I. Krupka, M. Hartl, Towards near-permanent CoCrMo prosthesis surface by combining micro-texturing and low temperature plasma carburising, J. Mech. Behav. Biomed. Mater. 55 (2016) 215–227, https://doi.org/10.1016/J.JMBBM.2015.10.023.

[3] Z. Guo, X. Pang, Y. Yan, K. Gao, A.A. Volinsky, T.-Y. Zhang, CoCrMo alloy for orthopedic implant application enhanced corrosion and tribocorrosion properties by nitrogen ion implantation, Appl. Surf. Sci. 347 (2015) 23–34, https://doi.org/10.1016/J.APSUSC.2015.04.054.

[4] Y. Liao, E. Hoffman, M. Wimmer, A. Fischer, J. Jacobs, L. Marks, CoCrMo metal-on-metal hip replacements, Phys. Chem. Chem. Phys. 15 (3) (2013) 746–756, https://doi.org/10.1039/c2cp42968c.

[5] A. Bazzoni, S. Mischler, N. Espallargas, Tribocorrosion of pulsed plasma-nitrided CoCrMo implant alloy, Tribol. Lett. 49 (1) (2013) 157–167, https://doi.org/10.1007/s11249-012-0047-0.

[6] D. Ba, L. Xu, Q. Wang, Effects of plasma nitriding ion beam flux density and time on the properties of CoCrMo alloy, Vacuum 119 (2015) 214–222, https://doi.org/10.1016/J.VACUUM.2015.05.032.

[7] A. Çelik, Ö. Bayrak, A. Alsaran, İ. Kaymaz, A.F. Yetim, Effects of plasma nitriding on mechanical and tribological properties of CoCrMo alloy, Surf. Coat. Technol. 202 (11) (2008) 2433–2438, https://doi.org/10.1016/J.SURFCOAT.2007.08.030.

[8] Q. Wang, C. Huang, L. Zhang, Microstructure and tribological properties of plasma nitriding cast CoCrMo alloy, J. Mater. Sci. Technol. 28 (1) (2012) 60–66, https://doi.org/10.1016/S1005-0302(12)60024-3.

[9] R. Wei, T. Booker, C. Rincon, J. Arps, High-intensity plasma ion nitriding of orthopedic materials: part I. Tribological study, Surf. Coat. Technol. 186 (1–2) (2004) 305–313, https://doi.org/10.1016/J.SURFCOAT.2004.02.052.

[10] R. Liu, X. Li, X. Hu, H. Dong, Surface modification of a medical grade CoCrMo alloy by low-temperature plasma surface alloying with nitrogen and carbon, Surf. Coat. Technol. 232 (2013) 906–911, https://doi.org/10.1016/j.surfcoat.2013.06.122.

[11] X.Y. Li, N. Habibi, T. Bell, H. Dong, Microstructural characterisation of a plasma carburised low carbon Co-Cr alloy, Surf. Eng. 23 (1) (2007) 45–51, https://doi.org/10.1179/174329407X161564.

[12] H. Dong, S-phase surface engineering of Fe-Cr, Co-Cr and Ni-Cr alloys, Int. Mater. Rev. 55 (2) (2010) 65–98, https://doi.org/10.1179/095066009X12572530170589.

[13] X. Luo, X. Li, Design and characterisation of a new duplex surface system based on S-phase hardening and carbon-based coating for ASTM F1537 CoCrMo alloy, Appl. Surf. Sci. 292 (2014) 336–344, https://doi.org/10.1016/j.apsusc.2013.11.141.

[14] T. Di, D. Mingjiang, F. Wenbin, L. Songsheng, W. Chunbei, Z. Mingchun, Performance of CoCrMo alloy with Me-doped DLC coatings prepared by a magnetron sputtering method, Rare Metal Mater. Eng. 44 (12) (2015) 2982–2986, https://doi.org/10.1016/S1875-5372(16)60034-6.

[15] T.F. Zhang, Q.Y. Deng, B. Liu, B.J. Wu, F.J. Jing, Y.X. Leng, N. Huang, Wear and corrosion properties of diamond like carbon (DLC) coating on stainless steel, CoCrMo and Ti6Al4V substrates, Surf. Coat. Technol. 273 (1) (2015) 12–19, https://doi.org/10.1016/j.surfcoat.2015.03.031.

[16] H. Holeczek, C.B. Santos, L. Haubold, M. Metzner, DLC-coated CoCrMo steel for use in medical implants - wear and corrosion resistance influence of different surface finishing techniques, in: O. Dössel, W.C. Schlegel (Eds.), World Congress on Medical Physics and Biomedical Engineering, September 7–12, 2009, Munich, Germany, Springer Berlin Heidelberg, Berlin, Heidelberg, 2010, pp. 1800–1803.

[17] U. Türkan, O. Öztürk, A.E. Eroğlu, Metal ion release from TiN coated CoCrMo orthopedic implant material, Surf. Coat. Technol. 200 (16–17) (2006) 5020–5027, https://doi.org/10.1016/J.SURFCOAT.2005.05.005.

[18] R.P. Van Hove, I.N. Sierevelt, B.J. Van Royen, P.A. Nolte, Titanium-nitride coating of orthopaedic implants: a review of the literature, Biomed. Res. Int. 2015 (2015) 1–9, https://doi.org/10.1155/2015/485975.

[19] C. Canto, E. Andrade, M. Rocha, B. Alemón, M. Flores, Adhesive and tribocorrosive behavior of TiAlPtN/TiAlN/TiAl multilayers sputtered coatings over CoCrMo, Nucl. Instrum. Methods Phys. Res., Sect. B: Beam Interact. Mater. At. 406 (2017) 32–37, https://doi.org/10.1016/J.NIMB.2017.02.054.

[20] B. Alemón, M. Flores, W. Ramírez, J. Huegel, E. Broitman, Tribocorrosion behavior and ions release of CoCrMo alloy coated with a TiAlVCN/CNx multilayer in simulated body fluid plus bovine serum albumin, Tribol. Int. 81 (2015) 159–168, https://doi.org/10.1016/J.TRIBOINT.2014.08.011.

[21] M. Dinu, M. Cojocaru, V. Braic, M. Tarcolea, M. Braic, F. Miculescu, A. Vladescu, C. Cotrut, Improvement of the tribological performance in corrosive environment of CoCr alloy by TiSiON coatings, Appl. Surf. Sci. 332 (2015) 295–299, https://doi.org/10.1016/J.APSUSC.2015.01.221.

[22] C. Liu, Z. Zhou, K.-Y. Li, Improved corrosion resistance of CoCrMo alloy with self-passivation ability facilitated by carbon ion implantation, Electrochim. Acta 241 (2017) 331–340, https://doi.org/10.1016/j.electacta.2017.04.127.

[23] C. Liu, Z. Zhou, P. Shum, K.-Y. Li, Surface gradient CoCrMo alloy generated by carbon ion implantation with enhanced tribocorrosion resistance, Surf. Coat. Technol. 320 (2017) 590–594, https://doi.org/10.1016/j.surfcoat.2016.10.085.

[24] V. Uvarov, I. Popov, Metrological characterization of X-ray diffraction methods at different acquisition geometries for determination of crystallite size in nano-scale materials, Mater. Charact. 85 (2013) 111–123, https://doi.org/10.1016/J.MATCHAR.2013.09.002.

[25] M. Seah, Summary of ISO/TC 201 standard: VII ISO 15472:2001 - surface chemical analysis - X-ray photoelectron spectrometers - calibration of energy scales, Surf. Interface Anal. 31 (8) (2001) 721–723, https://doi.org/10.1002/sia.1076.

[26] G. Greczynski, D. Primetzhofer, J. Lu, L. Hultman, Core-level spectra and binding energies of transition metal nitrides by non-destructive X-ray photoelectron spectroscopy through capping layers, Appl. Surf. Sci. 396 (2017) 347–358, https://doi.org/10.1016/J.APSUSC.2016.10.152.

[27] N. Vidakis, A. Antoniadis, N. Bilalis, The VDI 3198 indentation test evaluation of a reliable qualitative control for layered compounds, J. Mater. Process. Technol. 143–144 (1) (2003) 481–485, https://doi.org/10.1016/S0924-0136(03)00300-5.

[28] A. Ramirez-Ledesma, E. Lopez-Molina, H. Lopez, J. Juarez-Islas, Athermal ϵ-martensite transformation in a Co-20Cr alloy: effect of rapid solidification on plate nucleation, Acta Mater. 111 (2016) 138–147, https://doi.org/10.1016/J.ACTAMAT.2016.03.047.

[29] B.-S. Lee, Y. Koizumi, H. Matsumoto, A. Chiba, Collective behavior of strain-induced martensitic transformation (SIMT) in biomedical CoCrMoN alloy polycrystal: an ex-situ electron backscattering diffraction study, Mater. Sci. Eng.: A 611 (2014) 263–273, https://doi.org/10.1016/J.MSEA.2014.05.071.

[30] J. Cassar, B. Mallia, A. Karl, J. Buhagiar, EIS of carburised CoCrMo: evolution of parameters characterising the metal-electrolyte interface, Surf. Coat. Technol. 292 (2016) 90–98, https://doi.org/10.1016/j.surfcoat.2016.03.033.

[31] B. Trindade, M.T. Vieira, Modification of the structural order of transition metal-carbon systems by the addition of a Group VIII element, Mater. Sci. Eng.: A 352 (1–2) (2003) 195–201, https://doi.org/10.1016/S0921-5093(02)00865-1.

[32] S.V. Meschel, O.J. Kleppa, Standard enthalpies of formation of some 3d transition metal carbides by high temperature reaction calorimetry, J. Alloys Compd. 257 (1–2) (1997) 227–233, https://doi.org/10.1016/S0925-8388(97)00023-6.

[33] L. Pankratz, Thermodynamic properties of carbides, nitrides, and other selected substances, 696 United States Bureau of Mines Bulletin, 1994, pp. 1–957.

[34] G.K. Johnson, W.N. Hubbard, E.K. Storms, The enthalpies of formation of Mo_2C(c) and Mo_3C_2(c) by fluorine bomb calorimetry, J. Chem. Thermodyn. 9 (11) (1977) 1021–1026, https://doi.org/10.1016/0021-9614(77)90178-1.

[35] S.T. Jackson, R.G. Nuzzo, Determining hybridization differences for amorphous carbon from the XPS C 1s envelope, Appl. Surf. Sci. 90 (2) (1995) 195–203, https://doi.org/10.1016/0169-4332(95)00079-8.

[36] V. Zavaleyev, J. Walkowicz, G. Greczynski, L. Hultman, Effect of substrate temperature on properties of diamond-like films deposited by combined DC impulse vacuum-arc method, Surf. Coat. Technol. 236 (2013) 444–449, https://doi.org/10.1016/J.SURFCOAT.2013.10.023.

[37] A.A. Voevodin, S.V. Prasad, J.S. Zabinski, Nanocrystalline carbide/amorphous carbon composites, J. Appl. Phys. 82 (1997) 855–858 July.

[38] W. Gulbiński, S. Mathur, H. Shen, T. Suszko, A. Gilewicz, B. Warcholiński, Evaluation of phase, composition, microstructure and properties in TiC/a-C:H thin films deposited by magnetron sputtering, Appl. Surf. Sci. 239 (3–4) (2005) 302–310, https://doi.org/10.1016/j.apsusc.2004.05.278.

[39] T. Zehnder, J. Patscheider, Nanocomposite TiC/a-C:H hard coatings deposited by reactive PVD, Surf. Coat. Technol. 133–134 (2000) 138–144, https://doi.org/10.1016/S0257-8972(00)00888-4.

[40] S. Kukiełka, W. Gulbiński, Y. Pauleau, S.N. Dub, J.J. Grob, Composition, mechanical properties and friction behavior of nickel/hydrogenated amorphous carbon composite films, Surf. Coat. Technol. 200 (22–23 SPEC. ISS.) (2006) 6258–6262, https://doi.org/10.1016/j.surfcoat.2005.11.045.

[41] K. Sedláčková, R. Grasin, T. Ujvári, I. Bertóti, G. Radnóczi, Carbon-metal (Ni or Ti) nanocomposite thin films for functional applications, Solid State Sci. 11 (10) (2009) 1815–1818, https://doi.org/10.1016/J.SOLIDSTATESCIENCES.2009.05.018.

[42] M. Råsander, E. Lewin, O. Wilhelmsson, B. Sanyal, M. Klintenberg, O. Eriksson, U. Jansson, Carbon release by selective alloying of transition metal carbides, J. Phys. Condens. Matter 23 (35) (2011) 355401, https://doi.org/10.1088/0953-8984/23/35/355401.

[43] U. Jansson, E. Lewin, Sputter deposition of transition-metal carbide films – a critical review from a chemical perspective, Thin Solid Films 536 (2013) 1–24, https://doi.org/10.1016/j.tsf.2013.02.019.

[44] C. Casiraghi, J. Robertson, A.C. Ferrari, Diamond-like carbon for data and beer storage, Mater. Today 10 (1–2) (2007) 44–53, https://doi.org/10.1016/S1369-7021(06)71791-6.

[45] F.L. Wang, J.C. Jiang, E.I. Meletis, Microstructural evolution of Co nanostructures in diamond-like carbon by plasma-assisted processing, J. Appl. Phys. 95 (9) (2004) 5069–5074, https://doi.org/10.1063/1.1691181.

[46] A. El Mel, E. Gautron, B. Angleraud, A. Granier, P. Tessier, Synthesis of nickel-filled carbon nanotubes at 350 °C, Carbon 49 (2011) 4595–4607, https://doi.org/10.1016/j.carbon.2011.06.001.

[47] A.A. El Mel, N. Bouts, E. Grigore, E. Gautron, A. Granier, B. Angleraud, P.Y. Tessier, Shape control of nickel nanostructures incorporated in amorphous carbon films: from globular nanoparticles toward aligned nanowires, J. Appl. Phys. 111 (11) (2012) 114309, https://doi.org/10.1063/1.4728164.

[48] J. Musil, F. Kunc, H. Zeman, H. Poláková, Relationships between hardness, Young's modulus and elastic recovery in hard nanocomposite coatings, Surf. Coat. Technol. 154 (2–3) (2002) 304–313, https://doi.org/10.1016/S0257-8972(01)01714-5.

Surface & Coatings Technology 460 (2023) 129398

Contents lists available at ScienceDirect

Surface & Coatings Technology

journal homepage: www.elsevier.com/locate/surfcoat

Full Length Article

Amorphous/quasi-amorphous CoCrMo-C coatings for improved electrochemical properties and tribocorrosion resistance of biomedical alloys

Ewa Dobruchowska [a], Tomasz Suszko [a,*], Grzegorz Greczynski [b], Dorota Adamczewska [a], Witold Gulbiński [a]

[a] Koszalin University of Technology, Ul. Śniadeckich 2, Koszalin, 75-453, Poland
[b] Thin Film Physics Division, Department of Physics (IFM), Linköping University, 581 83 Linköping, Sweden

ARTICLE INFO

Keywords:
316L austenitic steel
CoCrMo medical alloy
CoCrMo-C coatings
Electrochemical impedance spectroscopy
Potentiodynamic polarization tests
Tribocorrosion

ABSTRACT

Coatings based on CoCrMo cobalt alloy have been designed to increase corrosion resistance of AISI 316L austenitic steel in body fluids. The CoCrMo-C coatings, with different carbon content (from 0 to 65 at.%), were synthesised by reactive magnetron sputtering of the medical CoCrMo (ISO 5832-12) alloy in the argon-acetylene atmosphere. Evolution of their structure, crystalline phase and chemical composition with increasing carbon fraction were investigated by X-ray diffractometry and X-ray photoelectron spectroscopy. Evaluation of corrosion resistance of CoCrMo-C films on 316L steel substrates was performed in Hanks' Balanced Salt Solution (HBSS) by means of electrochemical impedance spectroscopy and potentiodynamic polarisation tests. The studies have revealed high chemical inertness of all coatings. Passive/blocking layers formed on their surfaces exhibit a capacitive character, while their resistivity is nearly two orders of magnitude higher compared to the corresponding values obtained for the CoCrMo and 316L alloys tested under similar conditions. The CoCrMo-C coatings provide pitting corrosion protection for 316L austenitic steel. This is expected to extend the residence time of stainless steel in the tissue environment. The 316L/CoCrMo-C systems were also subjected to tribocorrosion tests in HBSS at three electrochemical potentials, i.e. at open circuit, cathodic, and anodic potential. A model was developed to relate the electrical values recorded during tribocorrosion experiments with the phenomena that characterize the coating wear process. It was found that the friction coefficient systematically decreased from 0.7 to 0.1 with increasing the carbon content under all potentials applied. The wear rate observed for majority of the coatings was lower than that for CoCrMo and 316L alloys. For the samples with the highest carbon content, the wear rate under oxidative conditions became even lower than for the cathodic potential.

1. Introduction

The requirements imposed on metallic biomaterials, applied for example in orthopaedic implantology and maxillofacial surgery, motivate studies for developing new materials, distinguished by a set of appropriately chosen parameters, as well as to gain a complete characterisation of the existing ones. Currently, FeCrNiMo stainless steels and CoCrMo alloys, next to titanium and Ti alloys, are the most common metallic biomaterials used for the production of temporary (e.g. intramedullary needles, bone plates, nails, screws) and long-term (e.g. joint prostheses) implants [1,2]. These materials exhibit high biotolerance and good physico-chemical properties due to their ability to passivation i.e. formation of a seal layer on the surface protecting the alloy interior against body fluids, when implanted [3–6].

A non-porous, defect-free oxide layer limits the transport of charge carriers (ions and electrons) through the metal-solution interface. However, under dynamic conditions, the implants are exposed to fatigue and friction wear leading to disruption of the passive layer, corrosion (tribocorrosion, corrosion-wear) and penetration of metal ions into a tissue environment. The measured concentration level of ions released by me-

* Corresponding author.
E-mail address: tomasz.suszko@tu.koszalin.pl (T. Suszko).

https://doi.org/10.1016/j.surfcoat.2023.129398
Received 8 December 2022; Received in revised form 24 February 2023; Accepted 1 March 2023
Available online 11 March 2023

chanically accelerated corrosion depends on the type of endoprosthesis, the type of body fluid or tissue, and the methods used to perform the tests. [7,8]

From a material (alloy) point of view, the rate of metal ions release and thus the rate of corrosion, depends strongly on time required for the surface regeneration understood as the oxide layer reconstruction. It has been found that the repassivation time for CoCrMo alloys is shorter compared to FeCrNiMo steels, and a number of ions leached correspondingly lower [2]. On the other hand, there are well documented reports on systemic cobaltism as a complication after total hip and knee arthroplasty [9–12]. The syndrome, resulting from tribocorrosion processes, has been diagnosed for both metal-on-metal [9–11] and metal-on-polyethylene [12] joint replacements. In the latter case, full-thickness polyethylene wear even enabled the contact of two metal surfaces. A correlation has been found between the increase of blood cobalt concentration level and the intensifying neurological, cardiac, thyroid and periprosthetic joint dysfunctions [10,13]. Therefore, CoCrMo alloys, although naturally passive, still require modification to improve their surface properties and thus their usability. The currently used solutions, include surface texturing [14], enhancement of the oxide layer [15], ion beam treatment [16,17] and coatings deposition [2]. It has been found that the use of carbon, introduced into alloys by ion implantation or deposited in the form of diamond-like coatings, is advantageous with respect to the corrosion-wear resistance [16,18,19]. Further, carbon based coatings and materials demonstrate high bio- and hemocompatibility, effectively limit the migration of metal ions and are able to integrate with adjoining tissues [19].

Recently, we have reported on CoCrMo-C coatings obtained by reactive magnetron sputtering of a medical cobalt alloy (ISO 5832-12) in the acetylene/argon atmosphere [20]. The research performed showed that depending on the carbon content, the films structure changes from crystalline to quasi-amorphous. The introduction of carbon in an amount higher than 30 at.% into the coatings resulted in: the segregation of amorphous carbon, the formation of self-organized cylindrical nanostructures and a significant improvement in tribological properties compared to the CoCrMo alloy. The friction coefficient value of ca. 0.2 versus alumina balls and the wear rate of ca. 2×10^{-15} $m^3/N/m$ [20] have been achieved.

These promising preliminary results encouraged us to carry out further research, the purpose of which was to determine the relationship between the carbon content, and thus the structural properties of the coatings, and their corrosion resistance tested in the environment of the simulated body fluid. For this purpose Hanks' Balanced Salt Solution (HBSS) has been selected as accurately imitating the chemical composition of the fluid in muscles and joints [21]. Further, the protective properties of CoCrMo-C coatings have been verified in relation to CoCrMo alloy and AISI 316L stainless steel, both in a bulk form. The latter of these biomaterials still attracts a lot of interest due to its low cost, ease of manufacture and appropriate mechanical strength [22]. However, 316L stainless steel is sensitive to local corrosion that caused damage to 24% of implanted endoprostheses [23]. It is expected that eliminating the phenomenon of pitting corrosion by applying CoCrMo-C coatings will extend the residence time of stainless steel temporary or long-term implants in the tissue environment and open new possibilities for its biomedical applications. Studies of the resistance of 316L/CoCrMo-C systems to local corrosion are supplemented by tribocorrosion tests performed in HBSS at three different electrochemical potentials (open circuit potential and the chosen cathodic and anodic potentials).

2. Experimental

2.1. Samples preparation

CoCrMo-C coatings were obtained in a laboratory chamber by pulsed reactive magnetron sputtering of the CoCrMo alloy (ISO 5832-12) with the following chemical composition (wt.%): Co – 65.14, Cr – 27.6, Mo – 5.52, Si – 0.62, Mn – 0.82, N – 0.18, Ni – 0.09, C – 0.045, Fe – 0.18, Cu – 0.01, W – 0.02, P – 0.003, S – 0.0005. The CoCrMo target with a diameter of 100 mm was sputtered with the constant average discharge current of 1 A resulting in power of 1.1–1.2 kW. The magnetron power supply worked at the frequency of 100 kHz with 1 kHz pulse modulation. The sputtering atmosphere consisted of argon and acetylene. The Ar flow was constant at 6 sccm, while the C_2H_2 flow was varied from 0 to 5 sccm to obtain coatings with different carbon content. Consequently, the total gas pressure varied from 0.4 to 0.5 Pa during the deposition processes. Si (100) wafers and discs made from AISI 316L austenitic steel (ISO 4404-316) were used as the substrates. The chemical composition (wt.%) of the steel under investigation was: C – 0.021, Cr – 17.6, Ni – 12.45, Mo – 2.29, Mn – 1.05, S – 0.002, P – 0.031, Fe – balance. The substrates were heated to the temperature of 250 °C and electrically biased with a voltage of −70 V. The deposition time was 25–35 min. in order to obtain coatings with the thickness of 4.5–5 μm. The coating thickness was measured by Hommel Waveline T8000 stylus profilograph. For this purpose, a part of the substrate was left uncoated and served as a reference level. No kind of adhesion interlayer was applied.

2.2. Samples characterisation

XPS experiments were performed in an Axis Ultra DLD spectrometer (Kratos Analytical) with the background pressure of 1.5×10^{-7} Pa, using monochromatised Al-Kα X-rays with the photon energy of 1486.6 eV. Prior to the spectra acquisition, the samples were subjected to a two-step sputter-cleaning procedure, with 4 keV Ar^+ ions for 120 s in the first approach and with 0.5 keV Ar^+ for 600 s in the second one. The intention of the first step was to remove surface contaminants while the second step was used to minimise the extent of Ar^+ sputter damage [24]. Both steps were performed at the take-off angle of 20°. The binding energy scale was calibrated using sputter-etched Au, Ag and Cu standard samples, according to [25], that exhibit Au $4f_{7/2}$, Ag $3d_{5/2}$ and Cu $2p_{3/2}$ peak positions at 83.96 eV, 368.21 eV and 932.62 eV, respectively. All spectra are charge-referenced to the Fermi edge [26]. The pass energy was set at 20 eV for all measurements. That provided the full width at half maximum (FWHM) of 0.56 eV for the silver (Ag $3d_{5/2}$) line. The XPS spectra were gathered from the sample areas of 0.3 × 0.7 mm^2. Quantification of the spectra obtained was performed by Casa XPS software (version 2.3.16) with accuracy of around 5%.

The phase composition of the coatings was analysed by X-ray diffractometry using Panalytical Empyrean 3 diffractometer working with Cu-Kα radiation. The experiments were performed employing Bragg-Brentano (θ–2θ) diffraction geometry. Detailed information on the measurement procedure is given elsewhere [20].

Electrochemical studies were carried out using ATLAS 0531 Electrochemical Unit (Atlas-Solich) equipped with a frequency response analyser module. All measurements were conducted: (1) in a standard electrochemical cell with a sample (active area of 0.3 cm^2) and a platinum plate operating as the working electrode and the counter electrode, respectively, (2) with reference to the saturated calomel electrode (SCE, $Hg/Hg_2Cl_2/KCl$), (3) in the environment of unstirred simulated body fluid (volume of 0.05 dm^3) – HBSS (H8264, Sigma-Aldrich) with the chemical composition and concentrations (in g/dm^3) as follows: $CaCl_2 \times 2H_2O$ – 0.185, $MgSO_4$ – 0.098, KCl – 0.4, KH_2PO_4 – 0.06, $NaHCO_3$ – 0.35, NaCl – 8, NaH_2PO_4 – 0.048, D-glucose – 1, (4) at ambient temperature (25 ± 1 °C) and solution pH close to neutral (pH = 7.2). Before electrochemical tests, all specimens were washed in the same manner (in ethyl alcohol by using an ultrasonic bath) to ensure similar surface conditions.

Electrochemical impedance spectroscopy (EIS) experiments were performed for CoCrMo alloy and CoCrMo-C coatings deposited on silicon substrates. In the latter case, the coatings themselves served as the working electrodes. Thus, an influence of the substrate on the results

obtained was considered negligible. EIS tests were performed in the frequency range from 10^{-2} Hz to 105 kHz with five points per decade. The amplitude of AC excitation signal was 10 mV, and the constant component was equal to the open circuit potential (OCP). The first frequency response of impedance was recorded after one-hour immersion of the samples in HBSS and has been regarded as the starting point of the measurement series. The successive impedance spectra were acquired at one- and two-hour intervals over a period of 22 hours. Equivalent electrical circuits (EEC) were matched with help of Z-View® software from Scribner Associates.

To evaluate corrosion resistance of 316L steel, bare and coated with CoCrMo-C, potentiodynamic polarisation tests were carried out. Prior to polarisation, the samples were maintained in contact with HBSS at open circuit conditions for 1 h. Next, the potentiodynamic measurements were performed at the scan rate of 1 mV/s over the potential range from −0.5 V/SCE to 1 V/SCE and repeated at least three times.

The resulting polarisation curves were subsequently used to estimate corrosion parameters by the Tafel's extrapolation method. Note that, the anodic curves were strongly influenced by passivation processes, therefore slopes of the cathodic branches ($-b_c$) were used to calculate the corrosion current density values [27].

Cyclic potentiodynamic tests were conducted by scanning upward until the potential value of 0.6 V/SCE or the anodic current density of 5×10^{-3} A/cm^2 were reached. Then, the scanning direction was reversed and the measurements proceeded towards lower potential values. Cyclic potentiodynamic measurements were preceded by 12-hour immersion of the samples in HBSS, throughout changes in OCP were monitored.

The results of electrochemical experiments (EIS, potentiodynamic measurements) were analysed using AtlasLab (ver. 2.10-Base) software dedicated to the ATLAS 0531 Electrochemical Unit. In addition, the corroded parts of the samples were observed with a scanning electron microscope (SEM, LV 5500, JEOL), and compared to those not treated with HBSS. The SEM observations were carried out at the pressure of 2×10^{-5} Pa and the accelerating voltage of 20 kV.

Tribocorrosion tests were carried out in a three-electrode system (similarly to other electrochemical studies) coupled with a ball-on-disc tribometer working in reciprocating mode. Polished alumina rods with a diameter of 5 mm were used as the counterparts. Tips of the rods being in contact with the samples were rounded to imitate balls with a diameter of 10 mm. Alumina was selected as a counterface material due to its high chemical inertness to both the coating material and HBSS used as an electrolyte. The drive mechanism provided a constant speed of 10 mm/s, which is close to that of adult's gait (given the size and geometry of the femoral head). Sliding occurred between turning points 10 mm apart. The normal force of 2 N was applied by a dead load. The initial Hertzian mean pressure under measurement conditions was estimated to be about 0.4 GPa. The value of the initial pressure was selected so as to remove during friction the natural oxide film from the surface of both the reference alloys (316L, CoCrMo) and the CoCrMo-C coatings. Though, it is low enough to avoid plastic deformations of the coating and substrate.

The friction force, and thus the coefficient of friction (COF), was measured using strain gauges connected to the counter-sample arm. The specific wear rate k (wear volume V divided by the product of the normal load F and the sliding distance d), was calculated from the equation derived from a transformation of the definition formula:

$$k = \frac{V}{Fd} = \frac{Al}{Fln} = \frac{A}{Fn}, \quad (1)$$

where: A is wear track cross-sectional area, l is the wear track length, and n is the number of the pin passes. Cross-sectional areas were estimated from at least three surface profiles across the tracks obtained with the HOMMEL-ETAMIC T8000 profilometer.

The tribocorrosion tests were carried out at three potentials versus SCE: OCP, −0.6 V (cathodic potential) and 0.2 V (anodic potential). The sample surface area exposed to the electrolyte was 1.3 cm^2. The temperature was maintained at 25 ± 1 °C, similar to potentiodynamic polarisation tests, EIS experiments and our previous studies [20,28]. A 10-minute stabilisation of the sample in the electrolyte was applied, before and after the 1-hour friction test at 0.5 Hz sliding frequency. The friction time was selected to obtain measurable wear profiles, and at the same time to prevent complete abrasion of the coatings. During the tests, potential or the cathodic/anodic current density, and the friction coefficient were recorded simultaneously. The tests, at each of the selected potentials, were carried out three times using separate samples. For every test a new counter-sample was taken.

3. Results and discussion

3.1. Chemical and phase composition of CoCrMo-C

Evolution of the CoCrMo-C coatings chemical and phase composition with increasing carbon content were investigated by X-ray photoelectron spectroscopy and X-ray diffractometry. Based on the XPS measurements it was found that the mutual proportion between the major target elements i.e. Co/Cr/Mo was about 16/6/1 and remained constant regardless the carbon content. Carbon concentrations in subsequent coatings have been estimated at 1.5, 5, 13, 25, 43 and 65 at.% depending on the acetylene flow (0, 0.8, 2.2, 3, 4 and 5 sccm, respectively). Based on that the studied films are named as follows: 0C (to emphasize that the coating was deposited without acetylene), 5C, 13C, 25C, 43C, 65C. Note that, carbon may appear in small amounts in the coating composition due to contamination with carbon compounds desorbed from the chamber surface, even when the coating is deposited in an atmosphere of pure Ar.

As it was shown in our previous work [20], the main component of the alloy (cobalt) is an element belonging to the group of so called weak carbide formers, and its carbides are thermodynamically unstable with positive enthalpy of formation. Co 2p, Cr 2p, and Mo 3d core level spectra presented in the Fig. 1, and especially the chemical shift observed for the elements (Fig. 1d), indicate that the charge transfer between metals and carbon atoms takes place.

For Cr 2p and Mo 3d the chemical shift increases systematically with increasing carbon content. In the case of Co 2p, the shift is absent up to about 20 at.%. C, leading to the conclusion that carbon is mainly bound to chromium and molybdenum, i.e. the strong carbide formers. Considering the release of free carbon and the formation of nanocomposite structures, once the carbon content in the CoCrMo-C films exceeds 20 at.% [20], the small Co 2p chemical shift observed in this range does not necessarily imply the presence of Co-C bonds. Instead it can be caused by the screening effect of carbon shells, leading to lower kinetic energy of escaping photoelectrons, and thus, higher binding energy [29].

X-ray diffraction patterns recorded for the CoCrMo (ISO 5832-12) and CoCrMo-C coatings are presented in Fig. 2. The pattern for CoCrMo alloy indicating the presence of γ(fcc) and ϵ(hcp) phases is compliant with ICDD (International Centre for Diffraction Data) cards No. 04-016-6869 and 04-016-6870. As a result of sputtering in pure argon (0C), strained and textured films are obtained. One can notice that some of the peaks characteristic of CoCrMo fade away, while others are common to both the γ(fcc) and ϵ(hcp) phases. The exception is the ϵ(101) peak not belonging to the γ phase. However, since γ(111) and ϵ(002) planes are coherent [30] and the fcc and hcp structures differ only with stacking order, it can be assumed that the 0C coating consists mainly of the hcp phase with (002) planes preferentially oriented parallel to the substrate. All peaks are significantly shifted towards higher 2θ angles due to smaller interplanar spacings, which implies that the coating can be strained in the substrate plane. The corresponding ϵ(002)/γ(111) and ϵ(101) d-spacings are smaller by about 1.2% compared to ICDD data.

The addition of acetylene to the process atmosphere causes the XRD patterns of the coatings to become fuzzy. The pattern obtained for the 5C coating is distinguished by the presence of two broad peaks, difficult to interpret, located between ϵ(100) and γ(200) reflections.

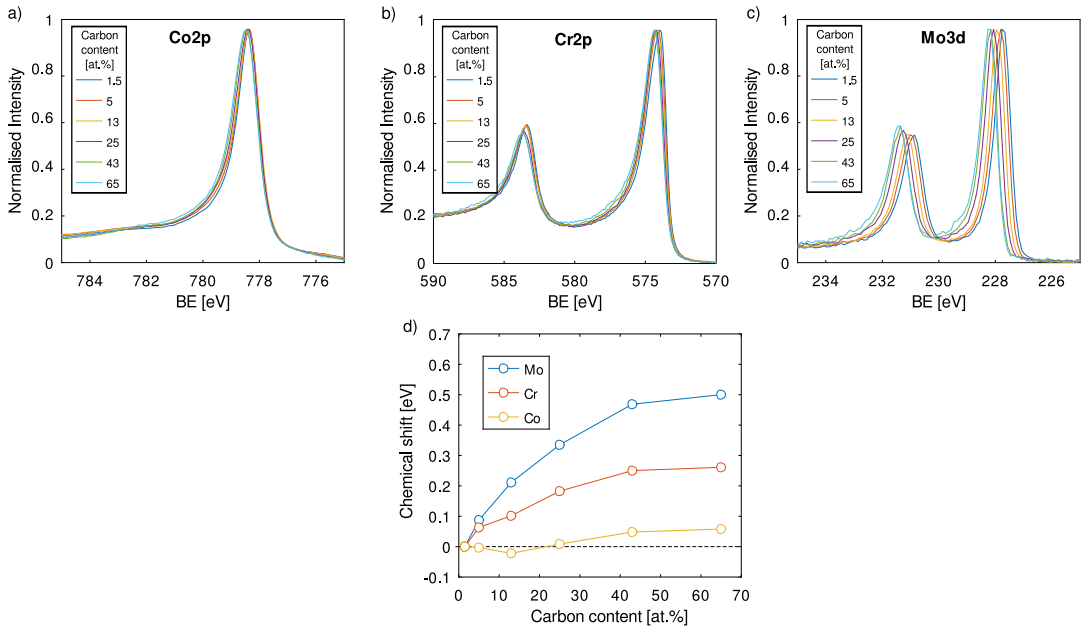

Fig. 1. Co $2p_{3/2}$, Cr $2p_{3/2,1/2}$, Mo $3d_{5/2,3/2}$ core level spectra for coatings with various carbon content (a, b, c). Intensity of the lines has been normalised to the maximum value for each spectrum. The chemical shift of Co $2p_{3/2}$, Cr $2p_{3/2}$, Mo $3d_{5/2}$ lines as a function of the carbon content (d).

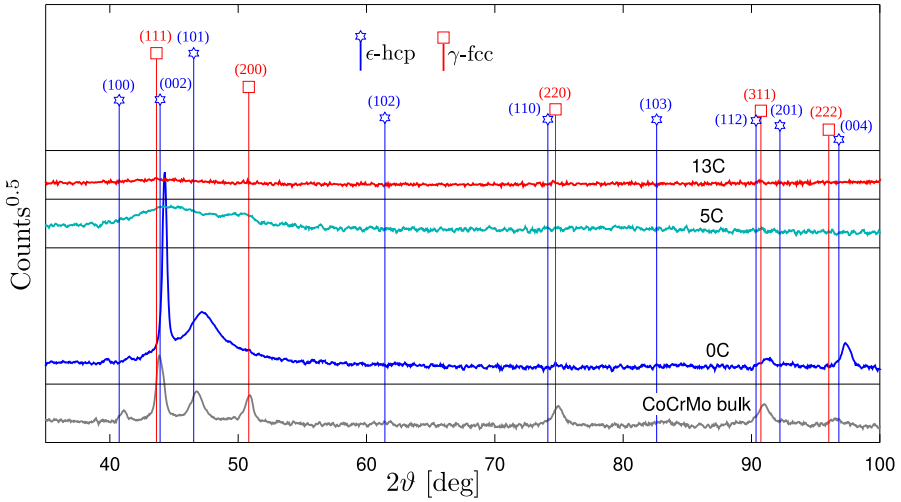

Fig. 2. X-ray diffraction patterns of the CoCrMo alloy and the CoCrMo-C coatings.

Detailed XRD analysis presented in [20] led to the conclusion that coatings containing less than 10 at.% of carbon include both phases in a nanocrystalline form, wherein the contribution of a given phase varies with depth.

A further increase in carbon content leads to amorphisation of the coatings which results in a flattened XRD pattern as for the 13C sample. A similar pattern shape is also observed for samples containing a larger amount of carbon, i.e. 43 and 65 at.% (XRD patterns not shown here). Additionally, our previous studies with high-resolution transmission electron microscopy showed that carbon segregation, observed in samples containing more than 20 at.% C, lead to the formation of specific self-organised nanostructures. Such quasi-amorphous coatings possess pronounced nanotubular (nanocolumnar) structure consisting of metallic/carbide cores that thread along the film growth direction and are encapsulated by amorphous carbon shells [20].

To sum up, the magnetron sputtering of the CoCrMo alloy leads to the synthesis of layers exhibiting the following structures, in the order corresponding to the increasing carbon content: 0C – fine-crystalline, 5C – nanocrystalline, 13C – amorphous, 25C – amorphous with signs of carbon segregation, 43C – quasi-amorphous/nanotubular.

3.2. Electrochemical properties

3.2.1. Results of electrochemical impedance spectroscopy

Basic information about properties of the interface between the samples and the electrolyte (HBSS) are provided by the EIS test results. Selected CoCrMo-C coatings, differing in carbon content and structural properties (nanocrystalline, amorphous/quasi-amorphous), deposited on silicon substrates were tested. CoCrMo alloy was used as the reference sample.

The 22-hour tests provided a good insight into the changes in the electrical properties of coatings surface over time. The results of the tests – complex impedance as a function of frequency, were used to model the EECs.

An exemplary set of data, in the form of the Bode plot, collected from the EIS measurements after 6 hours of immersion in the electrolyte is shown in Fig. 3. A clear difference can be seen in the shape of the curves

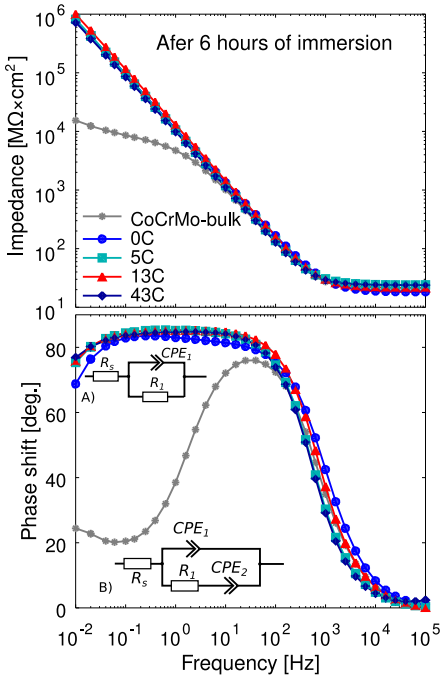

Fig. 3. Bode plots for CoCrMo-C coatings and CoCrMo alloy from EIS measurements performed after six hours of immersion in HBSS. Solid lines are the result of fitting with EEC depicted in: inset (A) – for coatings, inset (B) – for CoCrMo bulk sample.

obtained for CoCrMo-C coatings compared to those received for the bulk sample made of CoCrMo alloy. It results in two types of equivalent circuits used for fitting the experimental data.

For all coatings, the use of the simplest EEC with only one time constant (cf. Fig. 3, inset A) yielded very good agreement with the experimental data. The circuit consists of the electrolyte resistance R_s, and the resistance R_1 parallel to the constant-phase element CPE_1, characterised by constants Y and N, or σ and N. The impedance Z (in ohms) of a CPE is equal to:

$$Z_{\mathrm{CPE}} = \frac{1}{Y(j\omega)^N} \quad \text{or} \quad Z_{\mathrm{CPE}} = \frac{\sigma}{(j\omega)^N}\,, \tag{2}$$

where Y is expressed in $\mathrm{S\,s}^N$ (siemens seconds to the power N), and σ in $\Omega\,\mathrm{s}^{-N}$. When N is close to 1, Z_{CPE} has a capacitive character, and Y is interpreted as a capacitance expressed in farads [31]. Note that if the impedance Z is expressed in $\Omega\,\mathrm{cm}^2$ units, then Y is expressed in $\mathrm{S\,s}^N/\mathrm{cm}^2$, and σ in $\Omega\,\mathrm{s}^N\mathrm{cm}^2$.

Modelling the equivalent circuit for the CoCrMo bulk sample required the use of a second constant phase element CEP_2 (Fig. 3, inset B). Values of parameters of the main components of the equivalent circuit as a function of time are presented in Fig. 4.

The graphs do not show the resistance R_s value, which was approximately 22 Ω, and the values of the CPE_2 parameters. The phase shift of the CPE_2 increases monotonically with time from 36° (N_2 = 0.40) to 39° (N_2 = 0.43), and the σ_2 parameter changes from 2.5 $\mathrm{k\Omega\,s}^{-0.40}\mathrm{cm}^2$ to 6.7 $\mathrm{k\Omega\,s}^{-0.43}\mathrm{cm}^2$. The value of the phase shift close to 45° (Warburg impedance) suggests a diffusive nature of CPE_2 [31]. This may be related to the polycrystalline character of bulk CoCrMo sample compared to the nanocrystalline or amorphous/quasi-amorphous structure of the studied films, and possible diffusion of reagents along the grain boundaries. An additional argument in favour of this interpretation is provided by relatively small values of the resistance R_1 (cf. Fig. 4), which are below the resolution of the graph and range from 5 to 23 $\mathrm{k\Omega\,cm}^2$ (linearly increasing with time).

The resistance R_1 for all coatings is much higher (several $\mathrm{M\Omega\,cm}^2$). High values of the resistance and the capacitive nature of CPE1 (phase shift close to 90°, N_1 close to 1), are considered to characterise a non-porous passive layer forming quickly under experimental conditions.

In general, it is difficult to establish any systematic relationship between the EEC parameters and the carbon content in the films. However, it can be seen that the surface of nanocrystalline (0C and 5C) and nanocolumnar (43C) coatings show similar electrical properties. For instance, R_1 values, despite some irregular deviations, exhibit an analogous trend over the course of the experiment; they initially increase and then stabilise for several hours. Contrary, R_1 gained for the 13C sample increases monotonically, reaching the highest value of 14 $\mathrm{M\Omega\,cm}^2$. This coating is amorphous and does not yet show the presence of the nanotubular/nanocolumnar structure. It appears that the oxide layer formed on such a featureless surface effectively blocks the flow of charge at the electrolyte-coating interface. This is confirmed by the fact that the 13C coating also has the most capacitive character.

3.2.2. *Results of potentiodynamic polarisation tests*

In order to verify the anti-corrosion properties of CoCrMo-C coatings, particularly pitting corrosion resistance, the films were deposited onto 316L stainless steel and subjected to potentiodynamic polarisation tests. The coatings tested were those for which the electrical properties had been previously verified by EIS. In addition, the measurements were carried out for the 316L steel and CoCrMo alloy as reference materials.

The exemplary results of electrochemical studies, performed for 316L and CoCrMo reference samples at the open circuit conditions and by the potentiodynamic polarisation method, are presented in Fig. 5 and Table 1. The curve representing OCP changes (Fig. 5a), recorded for the steel substrate, reveals strong fluctuations of the potential value, related to the alternating processes of formation and dissolution of corrosion products. This effect confirms the susceptibility of 316L steel to local corrosion in HBSS. The CoCrMo alloy exhibits a different behaviour. The systematic potential increase indicates the formation/growth of a stable oxide layer composed primarily of chromium (III) oxide (similarly to 316L) with a small share of cobalt (II) oxide, wherein a part of Cr_2O_3 and CoO is converted into $Cr(OH)_3$ and $Co(OH)_2$, respectively [32,15,33]. OCP stabilises after 6 hours of immersion at the final value of 0.078 V, higher by 0.172 V compared to the 316L sample (cf. Table 1).

The polarisation curves recorded for both reference samples (Fig. 5b) show the presence of an unstable passive range, following directly the Tafel region. The characteristic inflection of the curves within the passive range, located at 0.1 V, can be attributed, according to the literature [33], to the solid state conversion of Cr_2O_3 (p-type) into CrO_2 (n-type). In the case of 316L stainless steel, the passive current density varies between 10^{-6} and 10^{-5} A/cm² until the breakdown potential value of 0.358 V is reached. With the breakdown potential, the passivity is interrupted and the anodic current density increases rapidly, which is related to the formation/development of stable pits [34]. In the contrary, the anodic current density recorded for the CoCrMo alloy, after exceeding the value of 0.1 V, increases only slightly with potential. This feature is attributed to slow release of cobalt ions into the surrounding environment that pass through the oxide layer without breakdown [33].

Applying the 0C and 5C coatings on steel results in a shift of the corrosion potential (E_{corr}) towards more noble values, up to −0.127 V and −0.104 V respectively (Table 1), proving higher corrosion resistance of the 316L/0C and 316L/5C systems in HBSS as compared to the uncoated steel substrate. Both, the E_{corr} values and the shape of the potentiodynamic characteristics (Fig. 6) become similar to the results obtained for the CoCrMo alloy (Fig. 5b). In the anodic range of the curves (i.e. after exceeding E_{corr}), two specific current peaks located at 0.1 V and 0.7 V appear. The latter (observed also for CoCrMo, and not shown here) begins the region of transpassive oxidation leading to the formation of Cr (VI) species and the dissolution of cobalt compounds present in the oxide layer. However, the contribution of

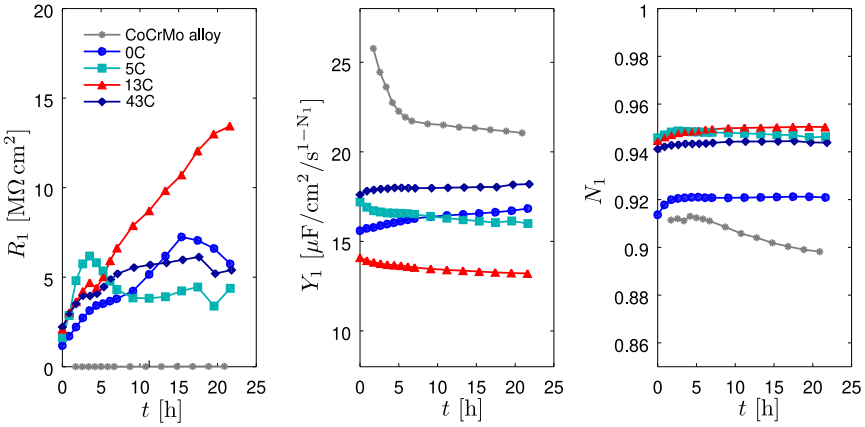

Fig. 4. Time dependence for the main EEC parameters (cf. Fig. 3) for CoCrMo-C coatings, and for CoCrMo alloy.

Table 1
Electrochemical parameters determined for 316L austenitic steel, CoCrMo alloy and 316L/CoCrMo-C systems.

Sample	E_{corr} [V]	i_{corr} [10^{-8} A/cm^2]	$-b_c$ [V/dec]	OCP (12h) [V]
316L	−0.245 ± 0.014	14 ± 6	0.14 ± 0.05	−0.094
CoCrMo	−0.121 ± 0.054	7.6 ± 1.6	0.15 ± 0.03	0.078
316L/0C	−0.127 ± 0.012	1.4 ± 0.4	0.08 ± 0.02	0.060
316L/5C	−0.104 ± 0.013	2.9 ± 0.6	0.12 ± 0.03	0.060
316L/13C	0.042 ± 0.007	5.1 ± 0.6	0.24 ± 0.03	0.062
316L/43C	0.046 ± 0.006	8.5 ± 1.2	0.21 ± 0.03	0.068

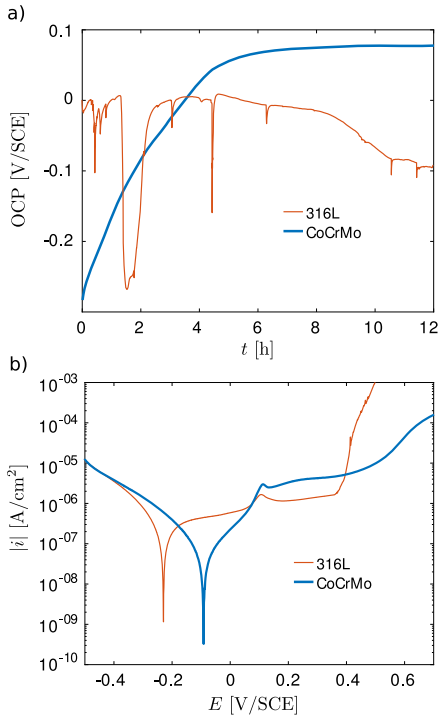

Fig. 5. Comparison of open circuit potentials (a) and polarisation curves (b) recorded for 316L austenitic steel and CoCrMo alloy in Hanks' Balanced Salt Solution.

oxygen evolution cannot be excluded here [35,4]. The breakdown potential characteristic for 316L stainless steel has not been observed.

For comparative purposes, potentiodynamic tests were performed for the 0C and 5C coatings deposited on the silicon substrates. The results of these measurements are presented as an inset in Fig. 6. Silicon

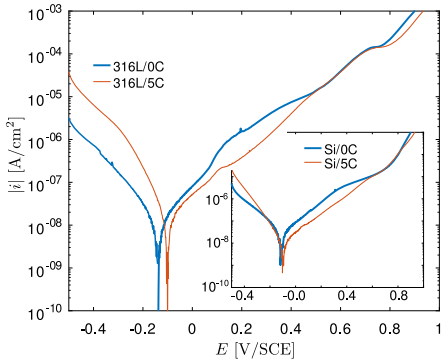

Fig. 6. Polarisation curves recorded in HBSS, for CoCrMo-C coatings with low carbon content deposited on 316L steel substrates (316L/0C, 316L/5C). Inset: polarisation curves recorded for the same coatings deposited on silicon substrates.

as a chemically inert material is expected to remain unaffected by the body fluid simulator applied. Therefore, one can assume that the signal observed will entirely derive from electrochemical reactions occurring at the film surface. The convergence of polarisation curves recorded for 0C(5C) and the 316L/0C(5C) systems indicates that corrosion processes taking place in 316L/0C(5C) proceed without the steel substrate contribution.

These conclusions are supported by the observations of 316L/0C and 316L/5C samples in areas corroded by HBSS and in untreated areas (Fig. 7). The SEM micrographs shown in Fig. 7b and Fig. 7d reveal only shallow surface changes. This particularly applies to the 316L/5C sample, where characteristic defects and reliefs (remaining after electrolytic polishing of steel) are visible in the etching area, and observed also at the coating surface not exposed to the electrolyte.

The increase of E_{corr}, resulting from application of the 0C and 5C coatings on 316L steel, is accompanied by a decrease of the corrosion current density (i_{corr}), as shown in Table 1. Low values of i_{corr}, interpreted according to Faraday's law as the rate of electrochemical processes, indicate a slower kinetics of the oxidation reaction of the 0C and 5C films compared to both reference samples. This behaviour is very likely related to the small grain size in the films, which notably refers to the coating containing 5 at.% of carbon.

As indicated by the XRD pattern (cf. Fig. 2) and our previous research [20], a small addition of carbon interferes the grain growth while leading to the formation of new nucleation centres. According to Ralston et al. [36,37], the fine-grained structure of metals and metal alloys favours the development of stable passive layers. High grain boundary density in such structures facilitates the conduction/diffusion of metal (e.g. Cr) ions and hence the oxides formation within the passive layer.

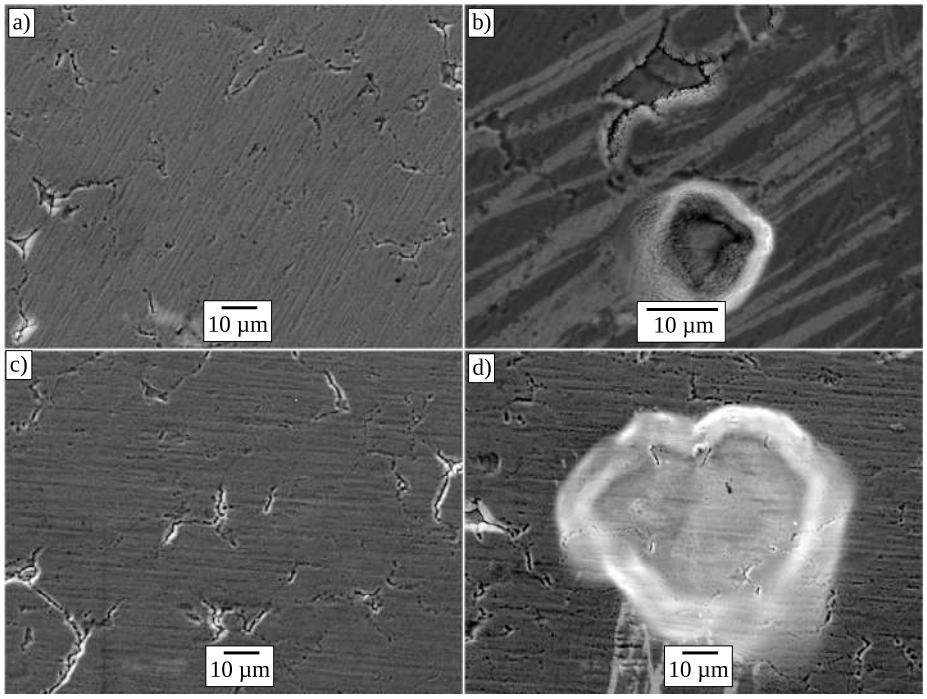

Fig. 7. SEM micrographs of 316L/0C (a, b) and 316L/5C (c, d) samples, before (a, c) and after (b, d) corrosion tests in Hanks' Balanced Salt Solution.

In polarisation electrochemical tests, these features are manifested by a stabilisation and/or a shift of the corrosion potential towards higher values, and by a reduction of the corrosion rate expressed as a decrease of the corrosion current density demonstrated for the 316L/0C and 316L/5C samples. These observations are consistent with the results of the EIS study. The polarisation resistance (R_1, cf. Fig. 4) determined for the 0C and 5C coatings is three orders of magnitude higher compared to the CoCrMo alloy.

The polarisation curves obtained for the 316L/13C and 316L/43C systems, presented in Fig. 8, indicate that the corrosion behaviour of the coatings changes significantly with further increase of the carbon content. Carbon addition in the amount of 13 at.% or more, contributes to the coating amorphisation, which is illustrated by the flattening of the XRD pattern shown in Fig. 2. It is known that structure-less coatings with a limited number of voids, micropores and microcolumns hinder the diffusion of electrolyte towards the substrate, and thus constitute a tight protective barrier [38,39]. In the case of 13C and 43C films, the structure amorphisation contributes to a considerable increase in the corrosion potential, compared to the other specimens under investigation (cf. Table 1).

It should be noted that E_{corr} takes similar, positive values for both the 316L/13C and 316L/43C systems. This suggests that after crossing the amorphisation threshold, located according to Suszko et al., at about 10 at.% of C [20], a further increase in carbon content does not significantly change susceptibility of the deposits to electrochemical corrosion in HBSS.

Along with the E_{corr} ennoblement, the shape of the anodic polarisation curves changes, which is particularly noticeable in the case of the 316L/43C system. After exceeding the active maximum, located at the potential value of 0.1 V, a rapid decrease in the current density is observed, reaching the minimum at $E = 0.17$ V. One can explain this transition by a different nature of the passive/blocking layer present on the surface of 43C film compared to the CoCrMo alloy and the low carbon coatings.

Milosev [33] reports that the thickness of passive layer formed on CoCrMo alloy surface in HBSS increases linearly at the rate of 1.5 nm/V until reaching the potential value of 0.3 V. Since Cr^3+ constitutes the main fraction of cations present in the oxide layer, the thickness increase is related to the amount of $Cr_2O_3/Cr(OH)_3$. In the contrary, for the 43C coating, the majority of chromium cations are bonded to carbon as confirmed by the results of XPS studies (cf. Fig. 1).

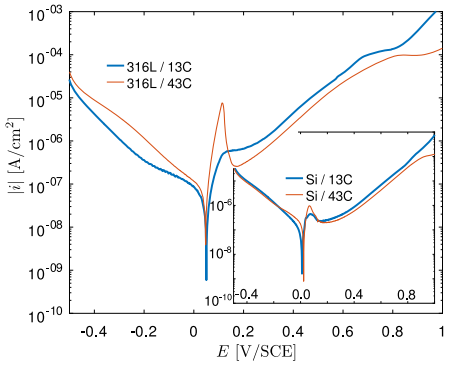

Fig. 8. Polarisation curves recorded in Hanks' Balanced Salt Solution for 316L steel substrate covered with amorphous/quasi-amorphous coatings (316L/13C, 316L/43C). Inset: polarisation curves recorded for the same coatings on silicon substrates.

Deficiency of unbound chromium causes rapid oxidation of cobalt (a weak carbide-forming element). The Co oxidation reaction, proceeding at a high rate is the cause of the corrosion current density determined for the 316L/43C system (cf. Table 1). The formation and incorporation of $CoO/Co(OH)_2$ into the oxide layer results in a decrease in the anodic current density, which, after exceeding the potential value of 0.17 V increases monotonically due to slow release of cobalt ions into solution.

The participation of molybdenum in the observed phenomena can be excluded due to its strong affinity to carbon, similarly to Cr. The results of the previous studies show that the inclusion of molybdenum oxides into the passive layer occurs only at E > 0.3 V [4,33]. In turn, the lack of a current maximum in the course of the polarisation curve recorded for the 316L/13C system can be most likely attributed to the presence of free chromium, oxidizing of which contributes to the formation of an unstable passive state, visible in the potential range from 0.12 V to 0.18 V.

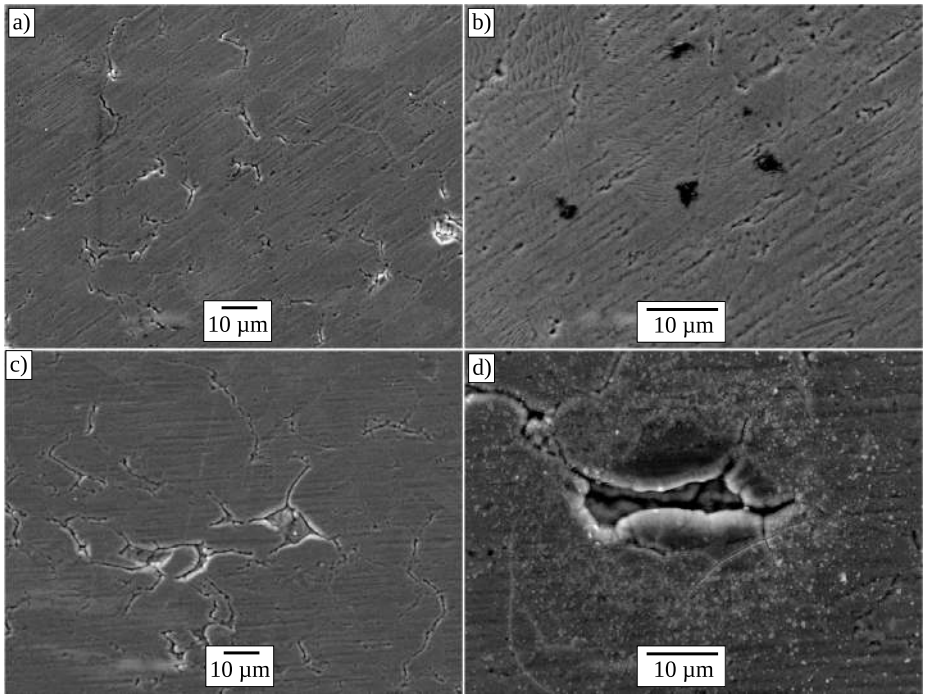

Fig. 9. SEM micrographs of 316L/13C (a, b) and 316L/43C (c, d) samples, before (a, c) and after (b, d) corrosion tests in Hanks' Balanced Salt Solution.

The polarisation curves obtained for the 13C and 43C films deposited on Si substrate (inset in Fig. 8) show a large convergence with those collected for the 316L/13C and 316L/43C systems. Thus, one can assume that, similarly to 0C and 5C coatings, the corrosion processes occur in the film only, without the involvement of the steel substrate. This is confirmed by SEM images obtained for pristine and electrolyte exposed areas of the 316L/13C and 316L/43C samples (cf. Fig. 9). The corrosion tests performed did not cause any significant changes in the surface morphology of the 316L/13C sample, understood as a loss of coating material (cf. Fig. 9b).

Similarly, no development of corrosion centres has been observed at the surface of 316L/43C system, even within shallow coating defects. However, some precipitates visible on the sample surface may be related to the presence of free carbon in the coating, which is inactive in the HBSS environment (cf. Fig. 7d).

The conclusions drawn from the potentiodynamic polarisation tests are consistent with the observations of changes in OCP during the 12-hour immersion of 316L/CoCrMo-C systems in HBSS (Fig. 10). For the 316L/0C sample, the open circuit potential increases linearly, similar to CoCrMo alloy (cf. Fig. 5a), confirming the strong ability of the 0C deposit to oxidise in an aerated solution. The 316L/5C system displays similar properties. In the initial immersion stage (2 h), the oxidation reaction of the metal components proceeds at a high rate leading to the formation of a oxide layer, which is manifested as the stabilisation of potential value.

On the other hand, 316L/13C and 316L/43C systems (with amorphous/quasi-amorphous coatings) exhibit high chemical resistance under the measurement conditions. The metallic components of the coatings, not bound to carbon, undergo rapid oxidation and OCP values remain nearly stable over the entire measuring time. Nevertheless, all 316L/CoCrMo-C systems achieved higher OCP values in the final measurement step compared to uncoated 316L steel (cf. Table 1). This proves their higher chemical resistance in the environment of a body fluid simulator.

In order to verify the resistance of 316L/CoCrMo-C systems to pitting corrosion, cyclic potentiodynamic measurements were carried out. The results obtained were compared with the cyclic polarisation curve recorded for uncoated 316L stainless steel (Fig. 11). The tests were performed after a 12-hour immersion of the samples in the electrolyte. In Fig. 11, the results obtained for the 316L/5C and 316L/43C systems are given as examples. In the case of bare 316L steel, the forward scan with

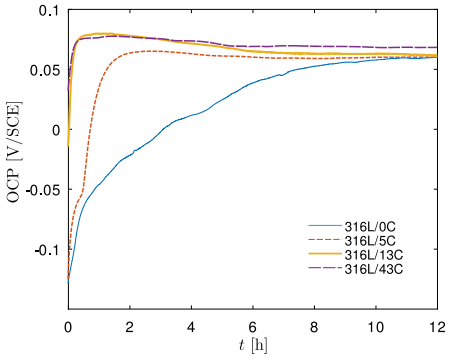

Fig. 10. Open circuit potentials (OCPs) recorded for 316L/CoCrMo-C systems during 12-hour immersion in Hanks' Balanced Salt Solution.

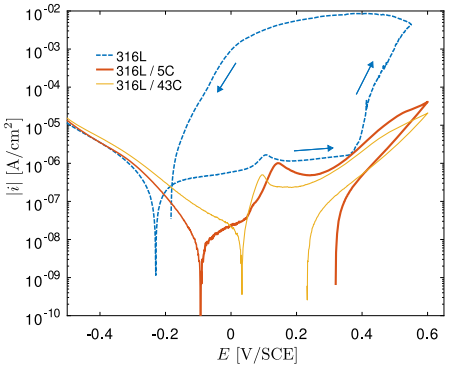

Fig. 11. Cyclic polarisation curves recorded in Hanks' Balanced Salt Solution for bare 316L steel and 316L/5C and 316L/43C systems.

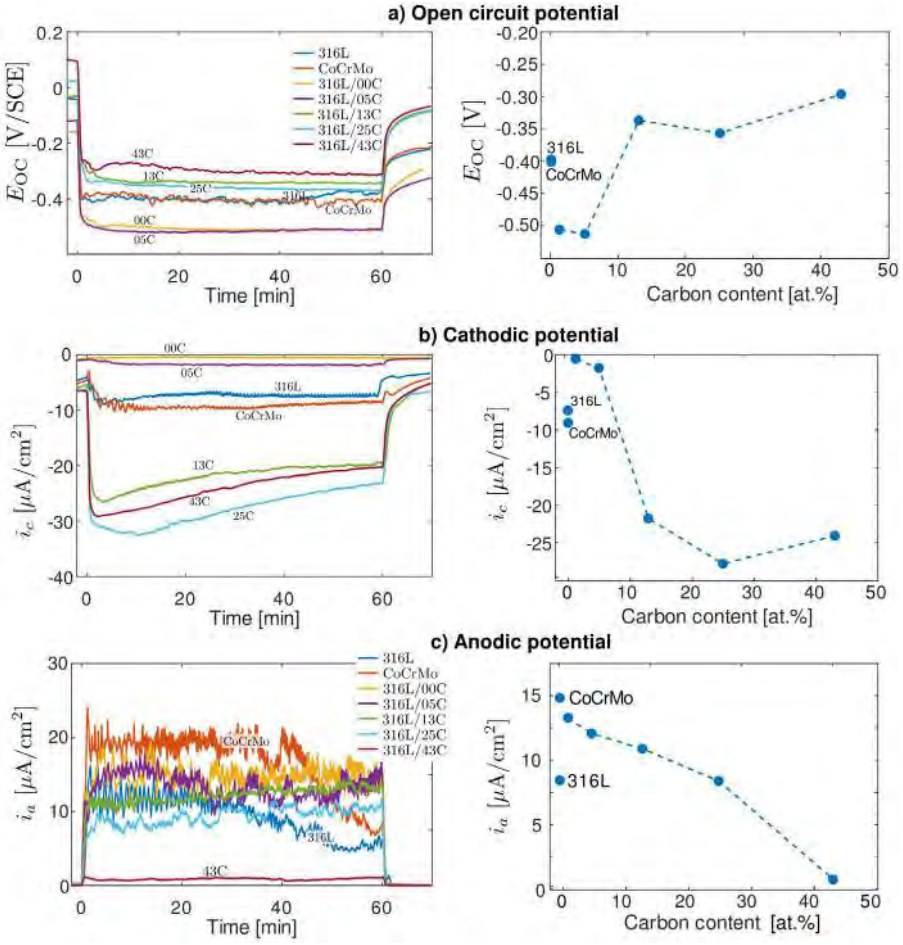

Fig. 12. Electric signal recorded during a series of tribocorrosion experiments performed on 316L and CoCrMo alloy, along with the 316L/CoCrMo-C systems. a) Time dependence of open circuit potential E_{OC} and the dependence of E_{OC} on carbon content in the coatings. b) Time dependence of the cathodic current density i_c (at −0.6 V/SCE) and the dependence of i_c on the carbon content. c) Time dependence of the anodic current density i_a (at +0.2 V/SCE) and the dependence of i_a on the carbon content.

a clearly seen breakdown potential coincides with polarisation curve presented in Fig. 5.

In the reversed scan, a hysteresis loop is observed, which is a consequence of the passive layer destruction, formation of stable pits and their further development [40]. Pits growth is stopped when the potential drops to values lower than the protection potential (E_{prot}). E_{prot}, defined as the intersection of the forward and reverse scans [41], takes the value of −0.177 V in this case.

In the contrary to 316L steel, the cyclic polarisation curves obtained for 316L/5C and 316L/43C systems show no hysteresis loops. The curves recorded during the return scan, which are likely a result of a uniform corrosion occurring in the transpassive region and/or oxygen evolution, are characteristic of alloys resistant to the initiation and propagation of pitting corrosion [42]. These results are consistent with the microscopic observations of the 316L/5C and 316L/43C samples exposed to the corrosive medium (Fig. 7d, Fig. 9d), where no distinct, deep pits were found. Thus, it leads us to the conclusion that all coatings tested, regardless of the carbon content, protect the steel against the development of localised corrosion. However, amorphous/quasi-amorphous coatings exhibiting positive corrosion potential are expected to provide more effective protection to steel components made of 316L steel against body fluids than low carbon coatings.

3.2.3. Tribocorrosion behaviour

Tribocorrosion tests were conducted by holding the sample in HBSS at three potentials: −0.6 V/SCE (cathodic potential, CP), +0.2 V/SCE (anodic potential, AP) and open circuit potential. In addition, tribocorrosion tests were also performed on the 316L/25C sample. The results obtained for 316L/CoCrMo-C systems, as in the case of polarisation tests, were compared to those received for 316L steel and CoCrMo alloy. The values of the electrical signals recorded during the tests and their mean values during movement of the pin are presented in Fig. 12. Values of the friction coefficient and wear rate, corresponding to these results are shown in Fig. 13.

In order to describe and explain the dependencies presented in Fig. 12, the system used in tribocorrosion measurements can be presented in the form of a simple model, considering the formation of thin oxide layer at the surface of coatings (as proven by previous electrochemical studies). The model can be considered as an extension of concepts presented by Diomidis et al. [43,44], Guadalupe-Maldonado [45] Espallargas [46], Namus [47,48].

The model in form of electric diagrams is presented in Fig. 14. The potentiostat voltage measuring system is represented by a voltmeter V showing measured value E_{RE} of the sample potential with respect to the reference electrode (SCE). In the case of unoxidised sample at open circuit configuration (cf. Fig. 14a) the measured value E_{RE} should be equal $-E_s$. However, potential of the sample raises by the value of E, due to formation of oxide layer. Values of the two electromotive forces E_s and E depend on the chemical composition of the material.

In OCP configuration (cf. Fig. 14a) and in the absence of wear, the resistance of active area R_a (worn part of the surface) does not exist and the measured potential E_{RE} takes a value E_1:

$$E_{RE} = E_1 = -E_s + E \ . \tag{3}$$

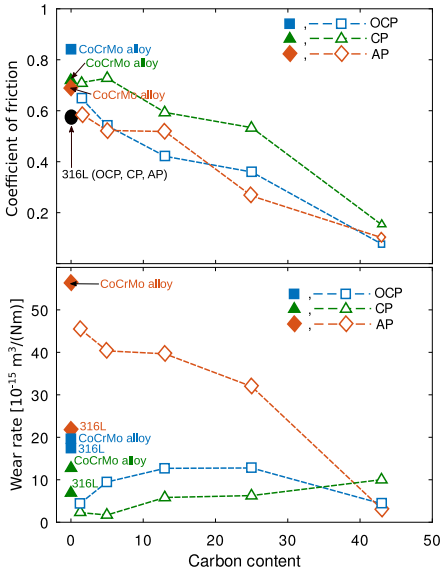

Fig. 13. Coefficient of friction and wear rate for 316L steel and CoCrMo alloy (filled markers), and for the 316L/CoCrMo-C systems (blank markers) determined in the tribocorrosion tests in HBSS at open circuit potential (blue squares), cathodic and anodic potential (green triangles and red diamonds respectively).

When the friction begins, the oxide layer is partially removed and a galvanic microcell is formed between worn and unworn areas i.e. unoxidised and oxidised areas respectively. The value of E represents also a driving force behind the repassivation process of the worn area, and resistances R_p and R_a become significant this process.

R_p is, at a first approximation, the resistance of the oxide film at the unworn sample surface, and R_a is the contact resistance of the worn sample surface with the electrolyte. The resistance values R_p and R_a depend among others on the surface area exposed to the electrolyte (the surface area of the unworn area is much larger than that of the worn area), and on the composition and structure of the oxide layer.

The potential E_{RE} measured during friction takes a value of E_2 resulting from the appearance of I_p repassivation current, and is equal to the sum of the E_s and the voltage drop across the resistance R_a:

$$E_{RE} = E_2 = -E_s + I_p R_a = -E_s + \frac{R_a}{R_a + R_p} E \ . \tag{4}$$

The equation (4) shows that the smaller the resistance R_a is, the more the measured potential is close to the sample potential E_s. On the other hand, the combination of the above equations: (3) and (4) shows that the decrease in measured potential, $\Delta E = E_1 - E_2$, after the start of friction and its increase after the end of friction should be equal to:

$$\Delta E = E_2 - E_1 = E\left(\frac{R_a}{R_a + R_p} - 1\right) \ . \tag{5}$$

Thus, the lower is R_a, the larger is voltage drop and it is closer to the potential difference between active and oxidised surface areas of the sample. The resistance is the smaller the larger the active surface is. Hence, a greater drop in potential should be observed at larger loads and higher friction speeds. Such relationship has been actually observed by J.-P. Celis and co-workers [49].

When a cathodic potential is applied (cf. Fig. 14b), the situation changes, and I_c current start flowing in the circuit, forcing the voltage drop on the R_a and R_p resistances, so as to maintain the E_{SP} set point value of the potential $(E_{RE} = E_{SP})$ In the absence of friction, the current $I_c = I_{c1}$ flows only through the R_p resistance (there is no R_a), and causes a voltage drop on that resistance. E_{SP} is then equal to

$$E_{SP} = -E_s + E - I_{c1} R_p \ , \tag{6}$$

and hence

$$I_{c1} = \frac{-E_{SP} - E_s + E}{R_p} \ . \tag{7}$$

It should be noted that the expression $-E_s + E$ in equation (3) represents the potential of the oxidised sample surface, so the smaller difference between this potential and E_{SP} the smaller the absolute value of I_{c1}. Furthermore, the higher the resistance of oxide layer, the lower the current that is needed to reach the given potential. By substituting the experimental data into the formula, it is possible to estimate the resistivity of the oxide layer at about 0.15 MΩ cm^2 for 316L/CoCrMo-C systems, which is of the same order as the initial resistivity of these layers measured in the EIS experiments (cf. Fig. 4).

During friction, the set point value of the potential is equal to the sum of the E_s and the voltage drop across the resistance R_a, whereas the current flowing through this resistance is equal to $I_c = I_{c2}$ recorded by the potentiostat but reduced by the value of the repassivation current I_p of the microcell:

$$E_{SP} = -E_s - (I_{c2} - I_p) R_a \ . \tag{8}$$

After transforming one gets:

$$I_{c2} = -\frac{E_s + E_{SP}}{R_a} + I_p \ , \tag{9}$$

$$I_{c2} = -\frac{E_s + E_{SP}}{R_a} + \frac{E}{R_a + R_p} \ . \tag{10}$$

It is characteristic that changes in absolute value of cathodic current density with carbon content (Fig. 12b) generally follow the changes in the open circuit potential (Fig. 12a). This fact is well explained by the proposed model. As can be seen from the equation (9) the current I_{c2} depends, ignoring the small passivation current I_p, on the difference between the sample potential E_s and the E_{SP} set point equal to −0.6 V in the case of these studies. The sample potential E_s is approximately equal to the value of the potential measured during friction under open circuit conditions (Fig. 12a) and therefore these two dependencies are similar.

However, one cannot expect that the current I_{c2} can be simply related to only friction or wear (cf. Fig. 13). It depends also on the E_s and E electrochemical parameters and contains two components of opposite signs; the forced cathodic current and the microcell I_p current. Further, according to the proposed model, I_{c2} is dependent on the resistance R_a, i.e. on the state of the sample surface subjected to friction.

From equation (9), by neglecting the current I_p, it is even possible to estimate the value of the resistance R_a (from 1×10^4 Ω for the 316L/13C, 316L/25C and 316L/43C samples, to 8×10^4 Ω for the 316/0C and 316L/5C samples), but it is difficult to give some specific meaning to these values. However when the friction ceases, the repassivation of the friction track should cause a increase in R_a and decrease in the current I_c, which is actually observed (cf. Fig. 12b).

When the experiment is carried out at the anodic potential (cf. Fig. 14d), equations (7), (9) and (10) take the form of:

$$I_{a1} = \frac{E_{SP} + E_s - E}{R_p} \ , \tag{11}$$

$$I_{a2} = \frac{E_s + E_{SP}}{R_a} - I_p \ , \tag{12}$$

$$I_{a2} = \frac{E_s + E_{SP}}{R_a} - \frac{E}{R_a + R_p} \ . \tag{13}$$

It follows from equation (13) that the lower the R_a resistance, for example as a result of more intensive removal of the oxidised layer, the higher the anodic current. Such an increase in current was observed by Guadalupe as a result of applying a greater normal force on stellite alloys in sulphuric acid environment [45].

Based on the results obtained at the anodic potential, using the equation (12) and omitting the current I_p, it is also possible to estimate the

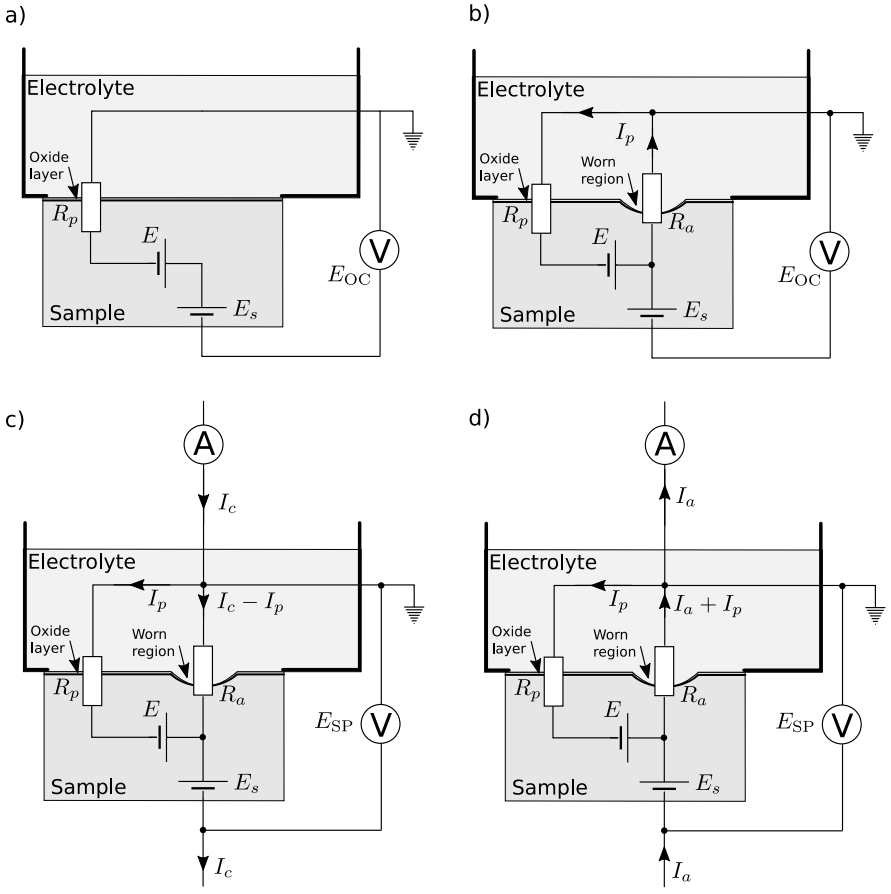

Fig. 14. Model of current flow and potentials during tribocorrosion test: (a) under open circuit conditions in absence of friction, (b) under open circuit conditions during friction, (c) at externally set cathodic potential, (d) at set anodic potential. E_s is the (negative) potential of the non-oxidized sample, which is normally increased by the value of E due to oxide layer formation. R_p represents the resistance of the oxide layer and R_a represents the resistance of the active (worn) area in the wear path. I_p is the current of the self-repassivation loop consisting of E, R_a, R_p. E_{OC} is the potential measured under open circuit conditions. E_{SP} represents the set potential value. E_{SP} is forced by cathodic current I_c (c) or by anodic current I_a (d).

resistance R_a. It has a value of approx. $4{\times}10^5$ Ω for 316L/43C sample, and approx. $4–5{\times}10^4$ Ω for the remaining samples.

Both currents (microcell I_p current and externally forced I_a oxidation current) flow through R_a in the same direction, and the measured I_a value provides some information about the kinetics of oxidation reactions in the tribo-contact area, which is confirmed by the results presented further in this article.

With regard to the coefficient of friction (cf. Fig. 13), there are clear features of the presented relationship, even when taking into account the 10–15% deviations observed between measurements under the same conditions:

1. The COF values measured at the cathodic potential for all samples are visibly higher than the values measured at OCP and the anodic potential, which are close to each other.
2. The coefficient of friction measured for CoCrMo alloy is higher than that for 316L steel samples covered with 0C coating.
3. The nature of COF changes determined for samples with different carbon contents is independent of the type of polarisation used.
4. The coefficient of friction decreases almost linearly with increasing carbon content and reaches the lowest value of 0.08 for the 316L/43C sample.

The first feature can be explained by the well-known concept of Bowden and Tabor [50]. Under cathodic potential coefficient of friction is higher since the amount of surface oxides – a third body being able to reduce shear strength of the tribo-contact, is somewhat reduced. The Bowden-Tabor concept also explains the second remark. For 316L/0C sample tested at OCP and the anodic potential, the coefficient of friction is lower than that measured on disks made of CoCrMo alloy. It may be because 0C coating is harder than a CoCrMo bulk sample [20], which ensures smaller real contact area at a similar composition of the third body (oxides). This leads to reduction of the real contact area and the shear force. In the case of cathodic potential, presence of the third body is limited. Thus, according to Bowden-Tabor, higher hardness does not affect by itself the coefficient of friction – higher hardness ensures smaller real contact area but also increases shear force.

Regardless of the applied potential, friction tests reveal a systematic decrease of the friction coefficient with increasing carbon content. It proves that even relatively low carbon content significantly influences tribological phenomena. Such a decrease of the friction coefficient with the carbon content and the progressive amorphisation of the surface was also observed by C. Liu et al. [17], who modified the CoCrMo alloy by implanting carbon ions. From the dependence presented in Fig. 13 it can also be concluded that even at the highest carbon content, surface oxidation plays a role for friction.

The relationship between wear rate and the carbon content at different potentials studied is presented in Fig. 13b. Deviations between values of the wear rate for different samples with the same carbon content, at the same test conditions, were in the range of 10–20%, and larger deviations were observed for small values.

The relationship (cf. Fig. 13b) is more complex than that for the coefficient of friction (cf. Fig. 13a). There is a very clear monotonic decrease in the wear rate at the anodic potential for samples with coatings containing from 0 to 43 at.% of carbon. At this potential, the surface of

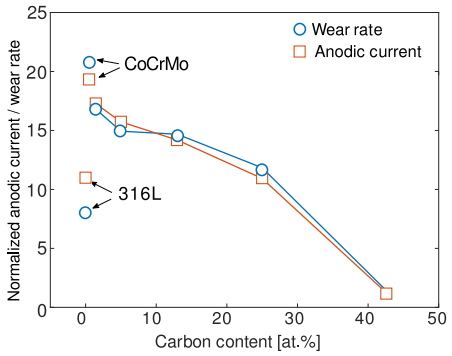

Fig. 15. Normalised values of anodic current density and wear rate depending on the carbon content. As the normalisation factor (denominator), values close to the quantities obtained for the 316L/43C sample were taken.

wear track undergoes alternating processes of oxidation and oxide removal. The mechanism seems to be dominant at the anodic potential, because changes in current density recorded under these conditions follow changes of the wear rate. It is illustrated by the plot in Fig. 15 presenting normalised values of anodic current density and the wear rate as a function of the carbon content. As the denominators, values of these quantities close to those recorded for the 316L/43C sample were taken.

The wear rate is closely related to the value of the anodic current, and thus to the surface oxidation process. The addition of carbon therefore either slows down the electrochemical oxidation process or hinders the mechanical removal of oxides. At the highest carbon content and low coefficient of friction, the mechanism of oxides removal is ineffective and the wear rate becomes even smaller than at the cathodic potential (cf. Fig. 13). This also corresponds to a higher R_a resistance and low I_{a2} anodic current (cf. Fig. 12c). It may be as well responsible for a certain qualitative change occurring in the range of 30–40% of the carbon content, where the wear rate measured at the cathodic potential becomes higher than at the open and anode potential.

There is no clear relationship between the recorded values of electrical quantities and the wear rate in the case of OCP and the cathodic potential. It can be seen, however, that the higher absolute value of the cathodic current (smaller R_a) corresponds generally to higher value of the wear rate. On the one hand, as shown in the model, the oxidation of the contact surface takes place at its own pace, which is determined by the characteristics of the microcell at the surface. Thus tribocorrosion must be considered as a subtle interplay between the chemical, electrochemical and mechanical reactivity of surfaces (J.-P. Celis et al. [49]). This can be illustrated by the characteristic appearance of the friction track cross-sectional profiles shown in the Fig. 16.

Wear tracks caused by friction at the cathodic and anodic potentials, with a relatively smooth surface, correspond to a mild type of wear. The wear track caused by friction at OCP could be interpreted as a result of abrasive wear. However, taking into account that the COF in this case is equal to the coefficient recorded at the anode potential, it should rather be interpreted as an effect of corrosion that occurs locally along the scratches caused by friction. Therefore both types of wear; chemical and mechanical are present. However, it is rather impossible to separate them and estimate their respective contributions.

Comparable wear values on similar materials in similar conditions were obtained, for example by: C. Liu et al. [17] on carbon-implanted CoCrMo alloy samples tested in a bovine serum albumina fluid, R. Chetcuti et al. [51] on CoCrMoC coatings deposited with reactive magnetron sputtering, tested in Ringer's solution, and R. Namus and W.M. Rainforth [48] on CoCrMo alloy tested a simulated body fluid at OCP and two cathodic potentials (−0.7 and −0.9 V). It is difficult however to compare our results with those gained by X. Luo et al. [52] on CoCrMo samples plasma carburized in H_2/CH_4 atmosphere, tested in Ringer's solution. The wear rate was an order of magnitude higher in that case.

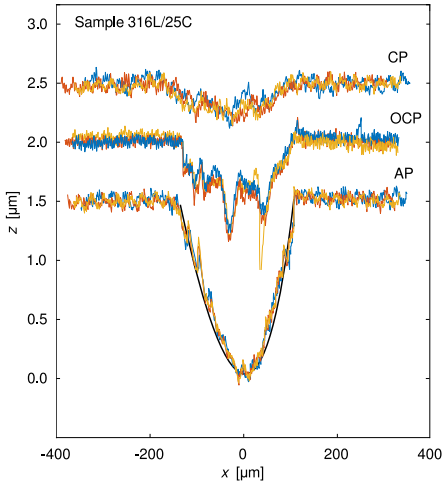

Fig. 16. Wear track profiles of the 316L/25C sample, after friction tests at cathodic potential (CP), open circuit potential (OCP), and anodic potential (AP). Each profile consists of three, measured at different positions on the track.

This may have been contributed by the application of a large load, which probably caused plastic deformation.

4. Conclusions

CoCrMo-C coatings with different carbon content deposited by reactive magnetron sputtering of CoCrMo alloy (ISO 5832-12) on 316L steel substrates were subjected to electrochemical and tribocorrosion tests in Hanks' Balanced Salt Solution.

Electrochemical impedance spectroscopy experiments revealed that the passive/blocking layer formed on the CoCrMo-C coatings is, regardless of the carbon content, more stable than that forming on the bulk CoCrMo alloy, and has an ohmic and capacitive character. The best insulating properties, understood as blocking the flow of charge carriers, were demonstrated for the amorphous coating containing 13 at.% carbon.

The potentiodynamic polarization tests showed that coating of 316L steel with CoCrMo-C films enhances its chemical stability in the corrosive environment used. The oxidation reactions observed during the tests occurred exclusively within the CoCrMo-C coatings, without the involvement of the steel substrate. The best corrosion protection in HBSS environment was provided by the amorphous coatings containing more than 13 at.% of carbon. The corrosion potentials determined for the 316L/13C and 316L/43C systems were positive.

Cyclic potentiodynamic tests proved that CoCrMo-C coatings, regardless of the carbon content, provide 316L steel with total resistance to pitting corrosion. Thus, they grant 316L stainless steel properties similar to those of the CoCrMo medical alloy used for long-term implants.

A model was developed to relate the electrical values recorded during tribocorrosion experiments with the phenomena that characterize the coating wear process. The wear rate was found to be closely related to the magnitude of anodic current – the rate of the oxidation reactions. With increasing carbon content in the coatings, electrochemical oxidation and mechanical oxide removal were successively suppressed. At the open circuit potential, some influence on the wear rate, in addition to mechanical factors, was exerted by oxidation processes occurring in the microcells formed within the wear tracks.

As the carbon content increased, the friction coefficient decreased, regardless of the applied potential, reaching a value of approx. 0.1. At the cathodic potential, the value of friction coefficient was always about 20% higher than that measured with the other polarisations.

The best properties in terms of tribology were provided by the coatings with the highest carbon content (approx. 40 at.%), for which the

lowest friction coefficient and low wear rate were recorded, independently of the applied measurement conditions.

CRediT authorship contribution statement

Ewa Dobruchowska: Conceptualization, Data curation, Investigation, Methodology, Resources, Writing – original draft, Writing – review & editing. **Tomasz Suszko:** Data curation, Investigation, Methodology, Resources, Software, Writing – original draft, Writing – review & editing. **Grzegorz Greczynski:** Investigation, Writing – review & editing. **Dorota Adamczewska:** Investigation. **Witold Gulbiński:** Writing – review & editing.

Declaration of competing interest

The authors declare that they have no known competing financial interests or personal relationships that could have appeared to influence the work reported in this paper.

Data availability

Data will be made available on request.

References

[1] N. Eliaz, Corrosion of metallic biomaterials: a review, Materials 12 (3) (2019) 407, https://doi.org/10.3390/ma12030407.

[2] R.I. Asri, W.S. Harun, M. Samykano, N.A. Lah, S.A. Ghani, F. Tarlochan, M.R. Raza, Corrosion and surface modification on biocompatible metals: a review, in: Mater. Sci. Eng. C, vol. 77, Elsevier Ltd, 2017, pp. 1261–1274.

[3] C. Aslan, J.L. Gilbert, In vitro corrosion assessment of the Essure® medical device in saline, simulated inflammatory solution and neutral buffered formalin, Acta Biomater. 147 (2022) 414–426, https://doi.org/10.1016/j.actbio.2022.05.028.

[4] I. Milošev, H.H. Strehblow, The composition of the surface passive film formed on CoCrMo alloy in simulated physiological solution, Electrochim. Acta 48 (19) (2003) 2767–2774, https://doi.org/10.1016/S0013-4686(03)00396-7.

[5] K. Rahmouni, A. Besnard, K. Oulmi, C. Nouveau, A. Hidoussi, L. Aissani, M. Zaabat, In vitro corrosion response of CoCrMo and Ti-6Al-4V orthopedic implants with Zr columnar thin films, Surf. Coat. Technol. 436 (2022) 128310, https://doi.org/10.1016/j.surfcoat.2022.128310.

[6] Y. Liu, D. Zhu, D. Pierre, J.L. Gilbert, Fretting initiated crevice corrosion of 316LVM stainless steel in physiological phosphate buffered saline: potential and cycles to initiation, Acta Biomater. 97 (2019) 565–577, https://doi.org/10.1016/j.actbio.2019.07.051.

[7] H. Mäntymäki, P. Lankinen, T. Vahlberg, A. Reito, A. Eskelinen, K. Mäkelä, Repeated cobalt and chromium ion measurements in patients with large-diameter head metal-on-metal ReCap-M2A-Magnum total hip replacement, Acta Orthop. 90 (2019) 243–248, https://doi.org/10.1080/17453674.2019.1595469.

[8] B. Stojanović, C. Bauer, C. Stotter, T. Klestil, S. Nehrer, F. Franek, M. Rodríguez Ripoll, Tribocorrosion of a CoCrMo alloy sliding against articular cartilage and the impact of metal ion release on chondrocytes, Acta Biomater. 94 (2019) 597–609, https://doi.org/10.1016/j.actbio.2019.06.015.

[9] F. Eltit, J. Noble, M. Sharma, N. Benam, A. Haegert, R.H. Bell, F. Simon, C.P. Duncan, D.S. Garbuz, N.V. Greidanus, B.A. Masri, T.L. Ng, R. Wang, M.E. Cox, Cobalt ions induce metabolic stress in synovial fibroblasts and secretion of cytokines/chemokines that may be diagnostic markers for adverse local tissue reactions to hip implants, Acta Biomater. 131 (2021) 581–594, https://doi.org/10.1016/j.actbio.2021.06.039.

[10] B.D. Gessner, T. Steck, E. Woelber, S.S. Tower, A systematic review of systemic cobaltism after wear or corrosion of chrome-cobalt hip implants, J. Patient Saf. 15 (2019) 97–104, https://doi.org/10.1097/PTS.0000000000000220.

[11] M. Umar, N. Jahangir, M. Faisal Khan, Z. Saeed, F. Sultan, A. Sultan, Cobalt cardiomyopathy in hip arthroplasty, Arthroplast. Today 5 (3) (2019) 371–375, https://doi.org/10.1016/j.artd.2019.04.010.

[12] K.H. Salem, N. Lindner, M. Tingart, A.D. Elmoghazy, Severe metallosis-related osteolysis as a cause of failure after total knee replacement, J. Clin. Orthop. Trauma 11 (1) (2020) 165–170, https://doi.org/10.1016/j.jcot.2019.04.010.

[13] C.C. Wyles, C.R. Paradise, T.L. Masters, R. Patel, A.J. van Wijnen, M.P. Abdel, R.T. Trousdale, R.J. Sierra, Cobalt and chromium ion release in metal-on-polyethylene and ceramic-on-polyethylene THA: a simulator study with cellular and microbiological correlations, J. Arthroplast. 35 (4) (2020) 1123–1129, https://doi.org/10.1016/j.arth.2019.11.031.

[14] J. Langhorn, A. Borjali, E. Hippensteel, W. Nelson, B. Raeymaekers, Microtextured CoCrMo alloy for use in metal-on-polyethylene prosthetic joint bearings: multidirectional wear and corrosion measurements, Tribol. Int. 124 (2018) 178–183, https://doi.org/10.1016/j.triboint.2018.04.007.

[15] C.V. Vidal, A.I. Muñoz, Effect of thermal treatment and applied potential on the electrochemical behaviour of CoCrMo biomedical alloy, Electrochim. Acta 54 (6) (2009) 1798–1809, https://doi.org/10.1016/j.electacta.2008.10.018.

[16] C. Liu, Z. Zhou, K.Y. Li, Improved corrosion resistance of CoCrMo alloy with self-passivation ability facilitated by carbon ion implantation, Electrochim. Acta 241 (2017) 331–340, https://doi.org/10.1016/j.electacta.2017.04.127.

[17] C. Liu, Z. Zhou, P. Shum, K.-Y. Li, Surface gradient CoCrMo alloy generated by carbon ion implantation with enhanced tribocorrosion resistance, Surf. Coat. Technol. 320 (2017) 590–594, https://doi.org/10.1016/j.surfcoat.2016.10.085.

[18] P. Wongpanya, N. Pintitraratibodee, K. Thumanu, C. Euaruksakul, Improvement of corrosion resistance and biocompatibility of 316L stainless steel for joint replacement application by Ti-doped and Ti-interlayered DLC films, Surf. Coat. Technol. 425 (2021) 127734, https://doi.org/10.1016/j.surfcoat.2021.127734.

[19] O.V. Penkov, V.E. Pukha, S.L. Starikova, M. Khadem, V.V. Starikov, M.V. Maleev, D.-E. Kim, Highly wear-resistant and biocompatible carbon nanocomposite coatings for dental implants, Biomaterials 102 (2016) 130–136, https://doi.org/10.1016/j.biomaterials.2016.06.029.

[20] T. Suszko, W. Gulbiński, E. Dobruchowska, G. Greczynski, L. Hultman, J. Morgiel, Quasi-amorphous, nanostructural CoCrMoC/a-C:H coatings deposited by reactive magnetron sputtering, Surf. Coat. Technol. 378 (2019) 124910, https://doi.org/10.1016/J.SURFCOAT.2019.124910.

[21] C. Tonna, C. Wang, D. Mei, S.V. Lamaka, M.L. Zheludkevich, J. Buhagiar, Biodegradation behaviour of Fe-based alloys in Hanks' Balanced Salt Solutions: Part I. material characterisation and corrosion testing, Bioact. Mater. 7 (2022) 426–440, https://doi.org/10.1016/j.bioactmat.2021.05.048.

[22] M.J.K. Lodhi, K.M. Deen, M.C. Greenlee-Wacker, W. Haider, Additively manufactured 316L stainless steel with improved corrosion resistance and biological response for biomedical applications, Addit. Manuf. 27 (2019) 8–19, https://doi.org/10.1016/j.addma.2019.02.005.

[23] I. Sailer, A. Philipp, A. Zembic, B.E. Pjetursson, C.H. Hämmerle, M. Zwahlen, A systematic review of the performance of ceramic and metal implant abutments supporting fixed implant reconstructions, Clin. Oral Implants Res. 20 (Suppl 4) (September 2009), https://doi.org/10.1111/j.1600-0501.2009.01787.x.

[24] G. Greczynski, D. Primetzhofer, J. Lu, L. Hultman, Core-level spectra and binding energies of transition metal nitrides by non-destructive x-ray photoelectron spectroscopy through capping layers, Appl. Surf. Sci. 396 (2017) 347–358, https://doi.org/10.1016/J.APSUSC.2016.10.152.

[25] M. Seah, Summary of ISO/TC 201 standard: VII ISO 15472:2001 - surface chemical analysis - x-ray photoelectron spectrometers - calibration of energy scales, Surf. Interface Anal. 31 (8) (2001) 721–723, https://doi.org/10.1002/sia.1076.

[26] G. Greczynski, L. Hultman, A step-by-step guide to perform x-ray photoelectron spectroscopy, J. Appl. Phys. 132 (1) (2022) 011101, https://doi.org/10.1063/5.0086359.

[27] E. McCafferty, Validation of corrosion rates measured by the Tafel extrapolation method, Corros. Sci. 47 (12) (2005) 3202–3215, https://doi.org/10.1016/j.corsci.2005.05.046.

[28] T. Suszko, W. Gulbiński, J. Morgiel, G. Greczynski, E. Dobruchowska, P. Dłużewski, J. Lu, L. Hultman, Amorphous FeCrNi/a-C:H coatings with self-organized nanotubular structure, Scr. Mater. 136 (2017) 24–28, https://doi.org/10.1016/J.SCRIPTAMAT.2017.03.040.

[29] G.K. Wertheim, S.B. DiCenzo, S.E. Youngquist, Unit charge on supported gold clusters in photoemission final state, Phys. Rev. Lett. 51 (25) (1983) 2310–2313, https://doi.org/10.1103/PhysRevLett.51.2310.

[30] A. Ramirez-Ledesma, E. Lopez-Molina, H. Lopez, J. Juarez-Islas, Athermal ϵ-martensite transformation in a Co-20Cr alloy: effect of rapid solidification on plate nucleation, Acta Mater. 111 (2016) 138–147, https://doi.org/10.1016/J.ACTAMAT.2016.03.047.

[31] I.D. Raistrick, J.R. Macdonald, D.R. Franceschetti, Theory, in: E. Barsoukov, J.R. Macdonald (Eds.), Impedance Spectroscopy Theory, Experiment, and Applications, John Wiley & Sons, Ltd, 2018, pp. 21–105, Ch. 2.

[32] Y.-S. Li, K. Wang, P. He, B.X. Huang, P. Kovacs, Surface-enhanced Raman spectroelectrochemical studies of corrosion films on implant Co–Cr–Mo alloy in biosimulating solutions, J. Raman Spectrosc. 30 (2) (1999) 97–103.

[33] I. Milošev, CoCrMo alloy for biomedical applications, in: S.S. Djokić (Ed.), Biomedical Applications, Springer US, Boston, MA, 2012, pp. 1–72.

[34] S. Kannan, A. Balamurugan, S. Rajeswari, Electrochemical characterization of hydroxyapatite coatings on HNO_3 passivated 316L SS for implant applications, Electrochim. Acta 50 (10) (2005) 2065–2072, https://doi.org/10.1016/j.electacta.2004.09.015.

[35] P. Schmuki, S. Virtanen, A.J. Davenport, C.M. Vitus, Transpassive dissolution of Cr and sputter-deposited Cr oxides studied by in situ X-ray near-edge spectroscopy, J. Electrochem. Soc. 143 (12) (1996) 3997–4005, https://doi.org/10.1149/1.1837327.

[36] K.D. Ralston, N. Birbilis, C.H.J. Davies, Revealing the relationship between grain size and corrosion rate of metals, Scr. Mater. 63 (12) (2010) 1201–1204, https://doi.org/10.1016/j.scriptamat.2010.08.035.

[37] K.D. Ralston, D. Fabijanic, N. Birbilis, Effect of grain size on corrosion of high purity aluminium, Electrochim. Acta 56 (4) (2011) 1729–1736, https://doi.org/10.1016/j.electacta.2010.09.023.

[38] M. Fenker, M. Balzer, H. Kappl, Corrosion protection with hard coatings on steel: past approaches and current research efforts, Surf. Coat. Technol. 257 (2014) 182–205, https://doi.org/10.1016/j.surfcoat.2014.08.069.
[39] A. Gilewicz, P. Chmielewska, D. Murzynski, E. Dobruchowska, B. Warcholinski, Corrosion resistance of CrN and CrCN/CrN coatings deposited using cathodic arc evaporation in Ringer's and Hank's solutions, Surf. Coat. Technol. 299 (2016) 7–14, https://doi.org/10.1016/j.surfcoat.2016.04.069.
[40] J.R. Galvele, Tafel's law in pitting corrosion and crevice corrosion susceptibility, Corros. Sci. 47 (12) (2005) 3053–3067, https://doi.org/10.1016/j.corsci.2005.05.043.
[41] M. Pourbaix, Significance of protection potential in pitting and intergranular corrosion, Corrosion 26 (10) (2013) 431–438, https://doi.org/10.5006/0010-9312-26.10.431.
[42] Standard test method for conducting cyclic potentiodynamic polarization measurements for localized corrosion susceptibility of iron-, nickel-, or cobalt-based alloys, June 2018, https://doi.org/10.1520/G0061-86R18.
[43] N. Diomidis, J.-P.P. Celis, P. Ponthiaux, F. Wenger, A methodology for the assessment of the tribocorrosion of passivating metallic materials, Lubr. Sci. 21 (2) (2009) 53–67, https://doi.org/10.1002/ls.73.
[44] N. Diomidis, J.P. Celis, P. Ponthiaux, F. Wenger, Tribocorrosion of stainless steel in sulfuric acid: identification of corrosion–wear components and effect of contact area, Wear 269 (1–2) (2010) 93–103, https://doi.org/10.1016/J.WEAR.2010.03.010.
[45] S. Guadalupe Maldonado, S. Mischler, M. Cantoni, W.J. Chitty, C. Falcand, D. Hertz, Mechanical and chemical mechanisms in the tribocorrosion of a Stellite type alloy, Wear 308 (1–2) (2013) 213–221, https://doi.org/10.1016/j.wear.2013.04.007.
[46] N. Espallargas, C. Torres, A.I. Muñoz, A metal ion release study of CoCrMo exposed to corrosion and tribocorrosion conditions in simulated body fluids, Wear 332–333 (2015) 669–678, https://doi.org/10.1016/j.wear.2014.12.030.
[47] R. Namus, J. Nutter, J. Qi, W.M. Rainforth, The influence of protein concentration, temperature and cathodic polarization on the surface status of CoCrMo biomedical grade alloys, Appl. Surf. Sci. 499 (2020) 143908, https://doi.org/10.1016/J.APSUSC.2019.143908.
[48] R. Namus, W.M. Rainforth, The influence of cathodic potentials on the surface oxide layer status and tribocorrosion behaviour of Ti6Al4V and CoCrMo alloys in simulated body fluid, Biotribology 30 (2022) 100212, https://doi.org/10.1016/J.BIOTRI.2022.100212.
[49] J.P. Celis, P. Ponthiaux, F. Wenger, Tribo-corrosion of materials: interplay between chemical, electrochemical, and mechanical reactivity of surfaces, Wear 261 (9) (2006) 939–946, https://doi.org/10.1016/j.wear.2006.03.027.
[50] F.P. Bowden, D. Tabor, Friction: An Introduction to Tribology, Anchor Press/Double Day, 1973.
[51] R. Chetcuti, P.A. Dearnley, A. Mazzonello, J. Buhagiar, B. Mallia, Tribocorrosion response of duplex layered CoCrMoC/CrN and CrN/CoCrMoC coatings on implant grade 316LVM stainless steel, Surf. Coat. Technol. 384 (2020) 125313, https://doi.org/10.1016/j.surfcoat.2019.125313.
[52] X. Luo, X. Li, Y. Sun, H. Dong, Tribocorrosion behavior of S-phase surface engineered medical grade Co–Cr alloy, Wear 302 (1) (2013) 1615–1623, https://doi.org/10.1016/j.wear.2013.01.023.

Applied Surface Science 591 (2022) 153134

Contents lists available at ScienceDirect

Applied Surface Science

journal homepage: www.elsevier.com/locate/apsusc

Full length article

Nano-columnar, self-organised NiCrC/a-C:H thin films deposited by magnetron sputtering

Tomasz Suszko [a,*], Witold Gulbiński [a], Karol Załęski [b], Grzegorz Greczynski [c], Jerzy Morgiel [d], Vasilina Lapitskaya [e]

[a] Koszalin University of Technology, ul. Śniadeckich 2, 75-453 Koszalin, Poland
[b] NanoBioMedical Centre, Adam Mickiewicz University, ul. Wszechnicy Piastowskiej 3, 61-614 Poznań, Poland
[c] Thin Film Physics Division, Department of Physics (IFM), 581 83 Linköping, Sweden
[d] Institute of Metallurgy and Materials Sciences, Polish Academy of Science, ul. Reymonta 25, 30-059 Kraków, Poland
[e] A.V. Luikov Heat and Mass Transfer Institute of NAS of Belarus, 15 P. Brovka Street, Minsk, Belarus

ARTICLE INFO

Keywords:
NiCrC
Magnetron sputtering
Thin films
Nanocomposites
Carbon self-organised structure
Magnetic properties
Magnetic anisotropy

ABSTRACT

Thin films of NiCr–C were deposited by pulse magnetron sputtering of the NiCr20 alloy cathode in an atmosphere containing a mixture of argon and acetylene. Their structure, chemical composition, and magnetic properties were studied using X-ray diffraction, X-ray photoelectron spectroscopy, high-resolution transmission electron microscopy, atomic and magnetic force microscopy, and superconducting quantum interference magnetometry methods. Film amorphisation observed upon increasing carbon content was followed by amorphous carbon segregation. As a result of the self-assembly processes during the coating growth, nanostructures were obtained consisting of metallic columns surrounded in carbon sheaths, with axes parallel to the growth direction. The resulting films exhibited weak ferromagnetism in a direction parallel to the axis of the nanocolumns, while the system's response was superparamagnetic for the direction of magnetisation perpendicular to the nanocolumns.

1. Introduction

Nanocomposite structures of thin films containing carbon are formed when metals are co-deposited with carbon [1]. Once the carbon content exceeds the stoichiometry limit specific for the metal carbide, the excess carbon segregates to grain boundaries and forms an amorphous matrix. In PVD processes, the source of carbon is an ion sputter graphite cathode or alternatively carbon originates from hydrocarbon gas decomposed in a plasma discharge. In the latter case, the carbon matrix is hydrogenated.

When the chemical affinity of metal for carbon, measured by the enthalpy of formation [2], is high, as in the case of metals from groups 4–6, the structures of nanocomposites contain nanocrystals of carbides of these metals in a matrix of amorphous carbon [1]. For metals with low affinity for carbon, as is the case of iron, cobalt or nickel, the precipitates embedded in the carbon matrix are metallic, or metastable carbides are formed [3–8].

In some cases, depending on deposition conditions, these systems tend to self-assemble, leading to nano-columnar structures. El Mel et al. [9,10] described the formation of aligned nanowires or nickel-filled nanotubes in the Ni–C coatings. Cobalt containing self-organised nano-columnar carbon-based nanocomposite thin film structures were studied by F. Wang [11,12]. They also investigated these ordered nanostructures' mechanical, electrical, and magnetic properties and proposed growth models for films based on such binary metal–carbon systems.

The transition from binary to ternary systems entailed new phenomena investigated by B. Trindade et al. [13] and G. Tome et al. [14]. They have shown that the addition of a weak carbide forming metal to thermodynamically stable transition metal carbide influences the structural order, leading finally to amorphisation of the film and carbon segregation.

Carbon segregation occurs due to the formation and subsequent decomposition of metastable carbides of the $M_{1-x}Me_xC_y$ type, where: M and Me are metals with high and low affinity for carbon, respectively. In combination with the mechanisms of carbon segregation, this phenomenon has been widely discussed by U. Jansson and E. Lewin [1] in their works on the design and deposition of thin films of ternary carbides. They concluded that the threshold of carbon segregation in ternary systems could be tuned by doping them with metal showing a low affinity for carbon. At present, knowledge of the thin film

* Corresponding author.
E-mail address: tomasz.suszko@tu.koszalin.pl (T. Suszko).

https://doi.org/10.1016/j.apsusc.2022.153134
Received 26 January 2022; Received in revised form 10 March 2022; Accepted 16 March 2022
Available online 29 March 2022

structures of carbon-based ternary systems combining metals with high and low affinity for carbon is quite limited. Recently, we reported self-organised nanotubular structures of multicomponent FeCrNi-aC:H [15] and CoCrMo-aC:H [16] thin films deposited by magnetron sputtering. The main metallic components (Fe or Co) showed a low affinity for carbon in both cases.

Properties of carbon-based nanocomposite coatings were characterised mainly in their mechanical, tribological and anti-corrosion performance. There are also few reports on their electrical [3,17–19] and magnetic properties [20–22]. Recently, nanocomposite coatings of that type attracted attention due to their piezoresistive properties for strain sensor applications [23–25].

Self-organised nano-columnar structures of composite films are characterised by a very high aspect ratio of nanocolumns. It is why an anisotropy of mechanical, magnetic or electrical film properties can be expected. For this study, we selected the NiCr–C system. The aim was to deposit films showing an quasi-amorphous, self-organised nanotubular structure already observed for other, similar Me–C systems. Furthermore, we aimed to verify whether the structure containing nanocolumns aligned along the growth direction result in anisotropy of coatings' magnetic properties.

The addition of chromium to the simple Ni–C system was chosen and found advantageous for two reasons. First, non-magnetic targets are required for effective magnetron sputtering. The NiCr20 alloy used for the target meets this condition because Ni–Cr alloys in the form of solid solutions exhibit paramagnetic properties above 15 at.% Cr. [26,27].

Secondly, due to chromium's higher affinity to carbon, the formation of metastable, mixed carbides of $Cr_{1-x}Ni_xC_y$ type should promote their decomposition and carbon segregation during growth [28].

2. Material and methods

NiCr–C thin films have been deposited from 100 mm in diameter planar cathode made of NiCr20 alloy ($Ni_{78}Cr_{22}$) of 99.95% purity by reactive magnetron sputtering in Ar/C_2H_2 atmosphere, with the C_2H_2 fraction varying from 0 to 50 vol.%. The sputtering source operated in pulsed mode, with a frequency of 100 kHz modulated by 1 kHz, and a constant average current of 1 A resulting in power of approx. 1.1 kW. The base pressure of the system was 1×10^{-5} hPa. The total pressure of the processing gas mixture was set at 0.4 Pa, whereas its composition was flow controlled i.e. a constant argon flow of 6 sccm and a variable acetylene flow from 0 to 6 sccm were used.

Austenitic stainless steel (316L) and single crystal (100) silicon substrates were placed at a distance of 60 mm from the cathode, biased at −70 V DC. The substrate was kept at a temperature of 250 °C during deposition. To control the temperature, a thermocouple inside the substrate holder was used, combined with a controller and a resistance heater. Before the actual deposition process, the target was sputtered in pure argon with the same current/power for 5 min, and the substrate was masked by a shutter. The deposition rate, dependent on process reactivity, was 0.17 to 0.26 μm/min. The thickness of all films was 3 ± 0.1 μm.

The film structure was examined by X-ray diffraction (XRD) using Malvern Panalytical Empyrean 3 diffractometer working with the Cu–Kα source in Bragg–Brentano geometry. The chemical bonding and elemental composition of coatings were determined by X-ray photoelectron spectroscopy (XPS). The analysis was performed in an Axis Ultra DLD instrument (Kratos Analytical, UK) with monochromatic Al–Kα radiation ($h\nu$ = 1486.6 eV). The base pressure during spectra acquisition was 1.5×10^{-7} Pa. The binding energy scale was calibrated by examining the sputter-cleaned Au, Ag, and Cu samples according to the recommended ISO standards for monochromatic Al Kα sources that place Au $4f_{7/2}$, Ag $3d_{5/2}$, and Cu $2p_{3/2}$ peaks at 83.96, 368.21, and 932.62 eV respectively [29]. The Fermi edge, clearly observed for all NiCr–C layers, was set as 0 eV and used as the charge Ref. [30]. Before analysis, all samples were sputter-etched to remove adsorbed contaminants, first, with 4 keV Ar^+ ions for 120 s followed by 0.5 keV Ar^+ for 600 s, both at the take-off angle of 20°. All spectra were collected from the area of 0.3×0.7 mm^2 and at a normal emission angle. The analyser pass energy was set to 20 eV, resulting in the full width at half a maximum of 0.55 eV for the Ag $3d_{5/2}$ peak. Casa XPS software (version 2.3.16) was used to quantify XPS spectra based upon peak areas. Elemental sensitivity factors were supplied by Kratos Analytical Ltd. The confidence level is typically around ±5%.

High-resolution observations of the coating's microstructure were performed using Tecnai G2 F20 TEM, operating at 200 kV accelerating voltage. Samples for TEM investigations were prepared by using FIB-Quanta 3D dual beam instrument. Chemical composition and the ratio of metallic component concentrations were verified by EDS method using Oxford Instruments INCA PentaFET × 3 EDS analyser coupled with JEOL JSM 5500-LV scanning electron microscope.

Atomic force microscopy (AFM) was used to study surface morphology, adhesion force values and phase on a Dimension FastScan atomic force microscope (Bruker, USA) in the Magnetic Force and PeakForce QNM modes. The standard silicon cantilevers of the CSG 10 SS type (Tips NANO, Russia) with a tip radius of 2.0 nm and console stiffness of 0.5 N/m for measurements in the PeakForce QNM mode. In Magnetic Force mode, standard silicon cantilevers with CoCr coating of the MESP-RC-V2 type (Bruker, USA) with a tip radius of 10 nm and console stiffness of 5.0 N/m were used.

Magnetic measurements were carried out on a SQUID magnetometer MPMS-XL (Quantum Design Inc.). The magnetisation was measured for two magnetic field configurations for each sample: parallel and perpendicular to the film's surface. Magnetisation curves (M–H) were registered at 300 K within a magnetic field of ±5 kOe. Zero-field cooling (ZFC) and field cooling (FC) curves were registered in the same temperature range: 5–325 K. For zero-field-cooled (ZFC) magnetisation measurements, the sample was initially cooled to 5 K in zero field, and subsequently, magnetisations were measured under 100 Oe fixed field upon heating. Next, the field-cooled (FC) magnetisation was recorded during cooling.

3. Results and discussion

3.1. Elemental composition and chemical binding state

A series of samples with increasing carbon content χ_C was prepared. It should be noted that the atomic proportions of nickel and chromium in the cathode material were practically preserved in the films deposited in pure argon, as confirmed by the EDS analysis. This result is expected, taking into account the similarity of atomic masses and argon sputtering yields of nickel and chromium.

The carbon content determined from XPS analyses based on the C 1s spectra shown in Fig. 1 varied from about $\chi_C = 4$ at.% for films deposited in pure argon to 63 at.% in the case of coatings deposited with the highest acetylene content in the atmosphere (50 vol.% of C_2H_2). Low carbon content detected for samples deposited in pure argon likely resulted from magnetron cathode contamination with residual carbon or metal carbide deposit formed due to target poisoning during the preceding depositions. It should be mentioned here that very long target pre-sputtering (and chamber conditioning) is required to obtain carbon-free coatings. Otherwise, even with zero acetylene flow, samples contain some carbon.

As shown in Fig. 1c, for lower carbon content, $\chi_C < 19$ at.%, the spectrum is dominated by a low binding energy component located at 283.1 eV and corresponding to the formation of carbide-type bonds [31,32]. For coatings containing approx. 19 at.% C, the new C 1s component appears at 284.4 eV, corresponding to the C–C bonds in sp^2 bonded amorphous carbon (a-C:H). It indicates that carbon starts to segregate above this concentration threshold. The intensity of the sp^2

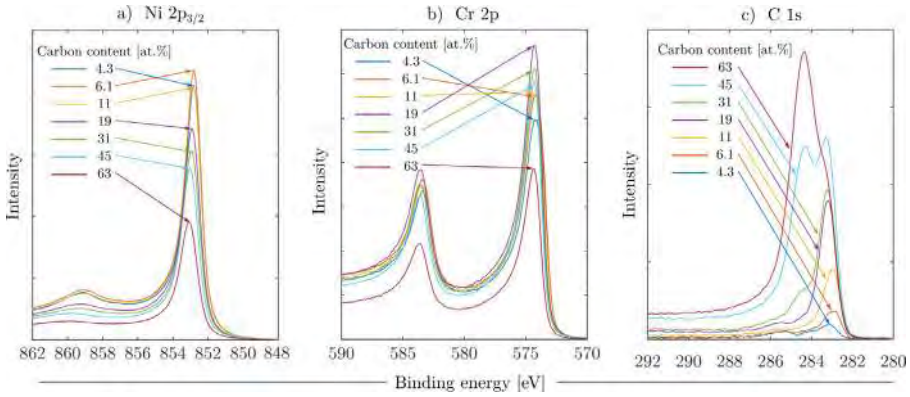

Fig. 1. XPS spectra NiCr–C films with increasing carbon content. (a) Ni $2p_{3/2}$, (b) Cr 2p, (c) C 1s core levels.

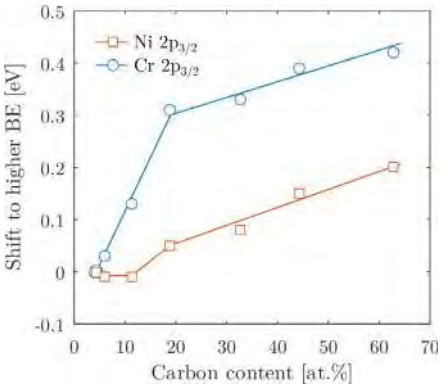

Fig. 2. The chemical shift to higher binding energy of Ni 2p and Cr 2p core levels for NiCr–C films with increasing carbon content.

C 1s peak continues to increase with further increasing carbon content and eventually for χ_C = 63 at.%, dominates the spectrum.

The process of carbon segregation is not only the result of its excess in relation to the chromium available for the reaction. As reported by U. Jannson et al. [1], under conditions where metals with high (Cr) and low (Ni) chemical affinity for carbon (standard enthalpy od formation for Cr_7C_3 is about −14 kJ/mole, and for Ni_3C is +1.2 kJ/mole [2]) coexist in the film, metastable ternary carbides of the $Cr_{1-x}Ni_xC_y$ type can form. By analysing the thermodynamics of the reaction, they have shown that the decomposition of these carbides leads to (i) nickel precipitates, which is thermodynamically favoured but slow due to low nickel diffusivity, and (ii) carbon precipitates thanks to faster C diffusion owing the lower activation energy as compared to that of Ni. Consequently, this process explains the observed segregation of free carbon. In addition, there may exist regions with uneven distribution of nickel and chromium.

Detailed analysis of Ni $2p_{3/2}$ and Cr $2p_{3/2}$ core-level spectra of metallic components (cf. Fig. 1a–b) revealed a slight chemical shifts with increasing carbon content to higher binding energy as compared to metallic positions: Ni $2p_{3/2}$ — 852.4 eV and Cr $2p_{3/2}$ — 574.4 eV. This is plotted in Fig. 2. Up to 11 at.% carbon, the shift is only observed for the chromium line, which may be interpreted as an indication of a larger charge transfer between Cr and C atoms, hence, preferential formation of Cr–C rather than Ni–C bonds. The rate of the peak shift (the slope of the lines in the graph) for carbon content higher than 19 at.% is the same for both Cr $2p_{3/2}$ and Ni $2p_{3/2}$ peaks. This suggests that, within this compositional range, shifts of metal lines are the consequence of a decreasing diameter of metallic nanotubes (cf. Fig. 4). As nanotubes become narrower with increasing C content, the screening of core holes decreases (due to worse lateral conductivity) leading to lowered kinetic energy of escaping photoelectrons, and, hence, higher binding energy of related peaks [33].

The studied NiCr–C films undoubtedly contain a certain amount of hydrogen, whose share was not investigated in this work. Therefore, the influence of hydrogen on the structural and magnetic properties was not studied. Even if the incorporation of hydrogen into the NiCr alloy is highly probable, it seems to be mainly bound to carbon [7]. As shown there, the share of hydrogen in the films, expressed as H/C atom number ratio, varies in a narrow range from 0.2 to 0.35, while the total hydrogen content in the layer depends on the amount of free, excess carbon. Assuming that the studied magnetic properties depend mainly on the metallic components of the film, at the present stage of research we treat the influence of hydrogen on these properties as slight. Due to the presence of hydrogen, NiCr–C samples with high carbon content are consistently denoted as NiCrC/a-C:H.

3.2. XRD structural analysis

The films deposited from the $Cr_{22}Ni_{78}$ cathode in a pure argon atmosphere had a fine-crystalline structure. Diffraction studies on the deposited thin NiCr–C films showed that their structure and the degree of crystallinity evolved with increasing carbon content. The XRD spectrum (c.f. Fig. 3) shows only two diffraction peaks: at 2ϑ values of 44.1 and 51.85 degrees. These peaks are assigned to the (111) and (200) crystallographic planes of the fcc-type structure of Ni–Cr solid solution (ISDD 04-19-3113), respectively. Due to tensile stresses in films containing up to several percent of carbon the diffraction peaks (especially (200)) are shifted slightly to the higher diffraction angle from their original positions. The stresses had a value about 0.6–0.8 GPa for samples containing up to 11 at.% C, as measured by the Stoney method — details not reported here.

For χ_C = 4.3 at.% the film show a strong (111) preferred growth orientation. A transformation to the distinct (200) preferred orientation occurs at a carbon content of about 11 at.%. Above this level, χ_C > 19 at.%, the XRD patterns show only peaks from the substrate and one very broad peak (36–49°), probably coming from the short-range ordering, which reveals complete amorphisation of the films. This result agrees very well with XPS analyses which show amorphous C segregation for χ_C > 19 at.%. No diffraction traces of metastable nickel carbide (Ni_3C) or chromium carbides were observed.

It is worth to emphasise the fact that the amorphisation of the NiCr–C deposit occurs already at χ_C = 19 at.%, while the Ni–C films (nickel nanowires in amorphous carbon) deposited in similar conditions retain the crystal structure with a carbon content of up to 46 at.% C [10]. The lowering of the amorphisation threshold of NiCr–C thin films deposited by sputtering is interpreted as the result of chromium addition, which, by forming highly dispersed carbides with a complex unit cell ($Cr_{23}C_6$, Cr_7C_3), promotes the amorphisation of the deposit [34].

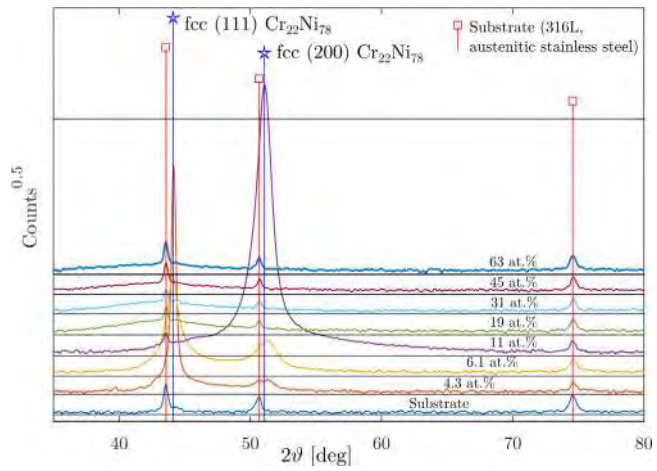

Fig. 3. X-ray diffraction patterns for the NiCr–C films deposited on 316L stainless steel substrates.

3.3. Microstructure and magnetic properties

For more detailed studies on microstructure and magnetic properties, samples with a carbon content of: (i) 19 at.% — the limit value above which carbon segregation is observed, (ii) 63 at.% — the carbon content at which the film still has sufficient cohesion and adhesion to the substrate, and (iii) 38 at.% — an intermediate value, were selected.

The sample containing 19 at.% of carbon has a completely amorphous microstructure in diffraction (cf. Figs. 3 and 4a). At higher carbon content (38 at.%) a specific nanostructure with segregated carbon is observed (cf. Figs. 4b–4d). The segregation favours the initiation of self-assembling nano-columnar growth. Such nanocolumn structure, previously observed for other systems: both two-component (Ni–C, Co–C) [10,12] and complex (FeNiCrC/a-C:H or CoCrMoC/a-C:H) [15,16], also reveals in our NiCrC/a-C:H films.

The scenario of the self-organisation process of Ni/a-C:H and Co/a-C:H coatings leading to the formation of columnar nanostructures was described in the works of F.L. Wang et al. [11,12,35] and A. A. El Mel et al. [9,10]. These authors agree that the shape of the nanostructures arises from a competition between the phase separation and the continuous material deposition on the surface of the growing film. In this structure, the metal-containing nanocolumns are separated by amorphous carbon shells with a thickness depending on the carbon content. Thus, with increasing hydrocarbon concentration in the atmosphere of the deposition process, it was possible to obtain nanocolumns of different diameters (from 3 to 7 nm) surrounded with carbon walls of different thicknesses up to 3 nm (cf. Fig. 4).

It is also very likely that the metallic elements in the nanocolumns' cores formed during the film growth are unevenly distributed, and nickel enriched regions compared to the original cathode composition may appear. The energy of particles in the plasma environment is high enough to activate the formation of chromium carbides of the type $(NiCr)_7C_3$ and Cr_3C_2 in equilibrium with the γ-NiCr–C solid solution [36].

The nanocolumns extend up to the surface of the films what was confirmed using atomic force microscopy (AFM) working also in magnetic mode (MFM) (cf. Fig. 5). By juxtaposing the surface topography image (Fig. 5a) with the magnetic contrast image (Fig. 5b), identifying the magnetic domain regions corresponding to the nanocolumn cores was possible.

The presence of metal-containing high aspect ratio nanocolumns in the tested films provoked us to study their magnetic properties. These studies aimed to determine the magnetic response of the coatings, paying particular attention to the potential anisotropy of this response, depending on the direction of the magnetic field.

Ferromagnetism is observed for nickel and nickel–chromium alloys containing less than 15 at.% chromium [27]. The existence of chromium depleted areas may have resulted in weak ferromagnetic properties. Magnetisation measurements were carried out in two directions, i.e. in the direction of magnetic field perpendicular to the film surface – out-of-plane geometry (along the nanocolumns), and for the field parallel to the film surface – in-plane geometry (perpendicular to the columns). The tests were done on films characterised by: amorphous structure without visible effects of self-organisation (19 at.% C), and well-developed nanocolumn structure (38 and 63 at.% C).

In magnetisation terms, all the samples are weakly magnetic. However, the magnetisation increased gradually from 0.022 emu/cm^3 to 0.212 emu/cm^3 with increasing carbon content (cf. Fig. 6). Furthermore, a slight difference in magnetic response measured in in-plane and out-of-plane magnetic field configuration appears for a middle carbon content sample. The first effect may be due to the increasing content of the ferromagnetic phase resulting from the depletion of the NiCr alloy in chromium, caused by its bonding with carbon. The second effect is probably related to the columnar morphology of the film.

The appearance of carbon segregation and the structure self-organisation resulting in the formation of nano-columns parallel to the film growth direction caused a change in the magnetic response. We observed a slight difference in the coercive field H_c and the remanent to saturation magnetisation ratio M_r/M_s, depending on magnetisation direction (cf. Fig. 7).

The sample containing 19 at.% of carbon was magnetically isotropic. The values of the coercive field and the magnetisation ratio were independent on the sample orientation in the magnetic field. The sample with the columnar microstructure (38 at.% C) preferred magnetisation along the nanocolumns, showing signs of easy-axis out of the film's plane. Thus, we observed anisotropy of the magnetic response related to the ordering direction of the columnar nanostructure. The anisotropy seems to vanish for the sample containing 63 at.% of carbon. The reason could be the reduction of the diameter of the nanocolumns, leading locally to a break in their continuity.

Nanocolumns' cores, with a length comparable to the film thickness (cf. Fig. 4d) are composed of an alloy with a nominal atomic composition of $Ni_{78}Cr_{22}$. However, they are locally depleted in chromium due to its reaction with carbon. As a result, they show weak ferromagnetism during magnetisation along the axis. The temperature dependence of magnetisation of NiCr/a-C:H nanocomposite films in ZFC (zero-field-cooling) and FC (field-cooling) conditions was recorded at a magnetic field of 100 Oe directed in the plane of the sample (cf. Fig. 8).

The ZFC and FC curves, recorded in in-plane configuration, diverge at low temperatures and almost coincide at high temperatures. Moreover, a maximum centred around the 115 K in the ZFC curve resembles the spin blocking temperature T_B, related to the transformation of the ferromagnetic state (below T_B) to the superparamagnetic one (above T_B). Most likely ferromagnetic NiCr–C nano-columns separated by diamagnetic carbon shells have shown superparamagnetic behaviour. The considerable width of the maximum at the ZFC curve may have indicated a significant dispersion of the magnetic nanoparticle sizes.

We analysed the nanoparticle diameter distribution by analysing $M–H$ curve. For the analysis the curve for the NiCrC/a-C:H sample containing 63 at.% C, measured in the in-plane field, at the temperature of 300 K was used. We assumed that pure Ni with saturation magnetisation M_s = 484 emu/cm^3 was the material for the nanostructure building blocks. The Langevin function was used to predict the $M–H$ curve (cf. Fig. 9a) using log-normal function of the nanoparticle diameter distribution [37,38] (Fig. 9b). The distribution median estimated for the studied sample was 8 nm, which corresponds well to the diameter of the nanocolumns.

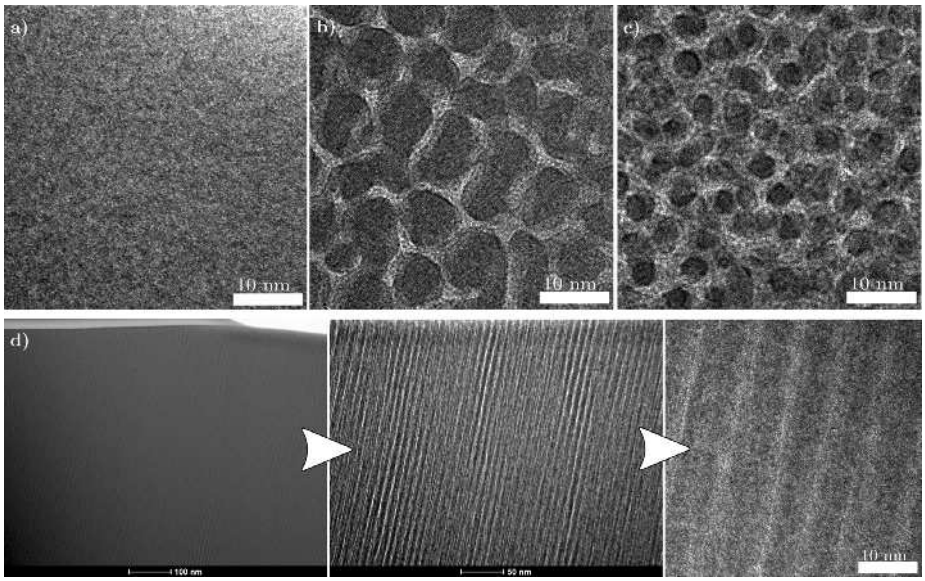

Fig. 4. TEM images of NiCr–C coatings: (a) — cross-section of the sample containing 21 at.% C, (b) — plan view of the sample with 38 at.% C, (c) — plan view of the sample containing 63 at.% C, (d) cross-section of the sample with 38 at.% C in successive higher magnifications.

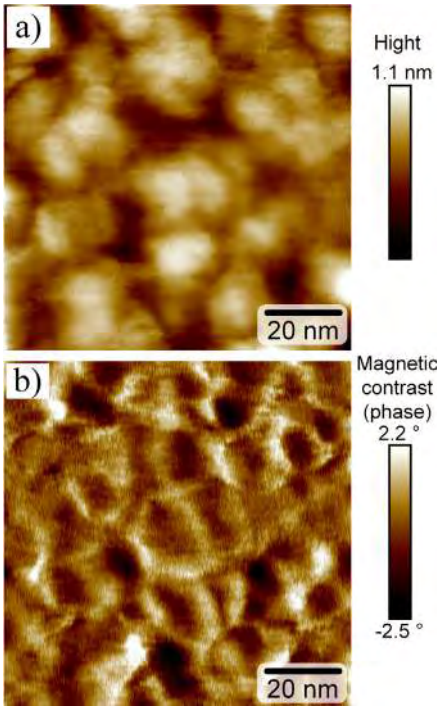

Fig. 5. SPM (scanning probe microscopy) images of NiCrC/a-C:H film containing 38 at.% C: (a) registered in topography mode (AFM), and (b) magnetic phase contrast mode (MPM).

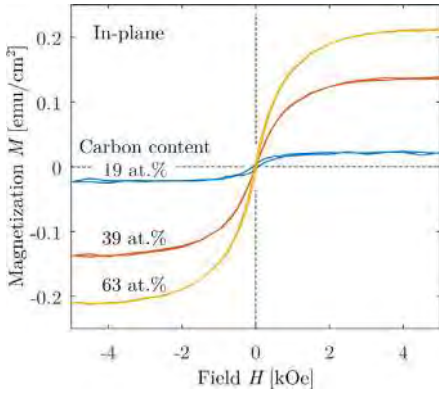

Fig. 6. In-plane magnetisation curves for NiCr–C films with various carbon content.

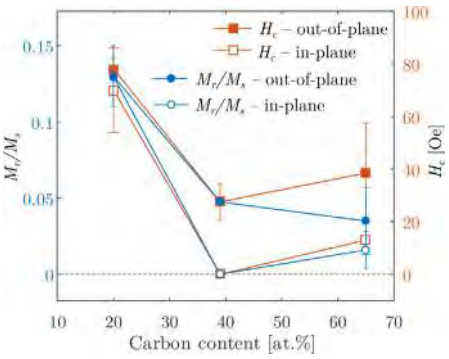

Fig. 7. Coercive field H_c and remanent and saturation magnetisation ratio M_r/M_s measured at room temperature for NiCr–C films with increasing carbon content.

4. Conclusions

Films of the NiCr–C type have been deposited by reactive magnetron sputtering from NiCr20 alloy cathode in the atmosphere containing acetylene. An abrupt amorphisation with increasing acetylene content was observed at 19 at.% carbon in the film. The amorphisation was followed by carbon segregation and forming of self-organised nanostructure, consisting of metallic columns with a diameter of 3–7 nm, separated by a thin layer of amorphous hydrogenated carbon. The study of the magnetic properties revealed an anisotropy being a derivative of the nanocolumnar structure. Magnetisation measurements conducted along the nanocolumn axis allowed observing weak ferromagnetism. The saturation magnetisation increased with the carbon content in NiCr–C coatings changing from 19 to 63 at.%, which suggests a progressive depletion of the nanocolumn cores in chromium forming carbides. For the same films, magnetised perpendicularly to the nanocolumn axis, the system's response was superparamagnetic, and the blocking

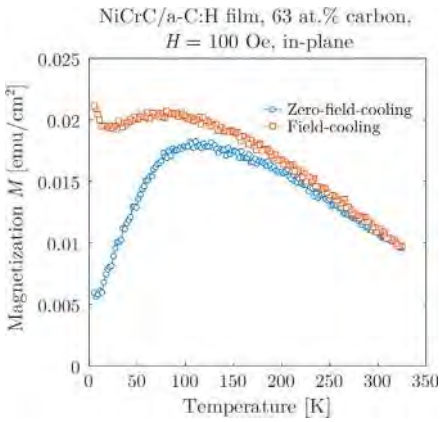

Fig. 8. Zero-field-cooling (ZFC) and field-cooling (FC) curves recorded at a magnetic field of 100 Oe directed in the sample plane.

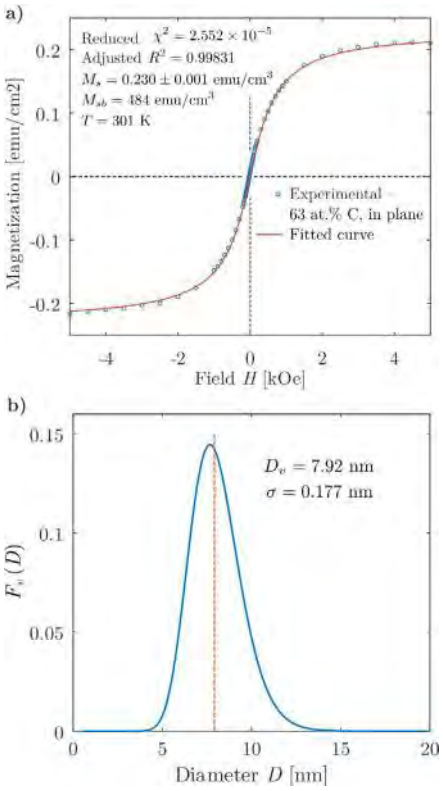

Fig. 9. The result of fitting the $M–H$ curve (a) with the calculated size distribution of nickel nanoparticles (b).

temperature T_B was determined to be approximately 115 K. Fitting the $M-H$ magnetisation curve obtained for the film containing 63 at.% of carbon with the Langevin function and the assumed log-normal distribution of nanoparticle diameters gives a nanoparticle size distribution median of nearly 8 nm, which is consistent with the observed diameter of nanocolumns.

CRediT authorship contribution statement

Tomasz Suszko: Methodology, Resources, Investigation, Data curation, Writing – original draft, Writing – review & editing. **Witold Gulbiński:** Conceptualisation, Methodology, Writing – original drafts, Writing – review & editing. **Karol Załęski:** Methodology, Investigation, Data curation, Writing – original draft. **Grzegorz Greczynski:** Investigation, Data curation, Writing – review & editing. **Jerzy Morgiel:** Investigation, Data curation. **Vasilina Lapitskaya:** Investigation, Data curation.

Declaration of competing interest

The authors declare that they have no known competing financial interests or personal relationships that could have appeared to influence the work reported in this paper.

Acknowledgement

K.Z. acknowledges the financial support from the National Science Centre of Poland by the SONATA Project No. UMO-2016/23/D/ST3/02121.

References

[1] U. Jansson, E. Lewin, Sputter deposition of transition-metal carbide films — A critical review from a chemical perspective, Thin Solid Films 536 (2013) 1–24, http://dx.doi.org/10.1016/j.tsf.2013.02.019.
[2] S.V. Meschel, O.J. Kleppa, Standard enthalpies of formation of some 3d transition metal carbides by high temperature reaction calorimetry, J. Alloys Compd. 257 (1–2) (1997) 227–233, http://dx.doi.org/10.1016/S0925-8388(97)00023-6.
[3] H. Wang, S.P. Wong, W.Q. Li, M.F. Chiah, C.Y. Poon, W.Y. Cheung, N. Ke, Structural and electrical properties of Co_xC_{1-x} nanogranular films prepared by pulsed filtered vacuum arc deposition, Thin Solid Films 405 (1–2) (2002) 304–309, http://dx.doi.org/10.1016/S0040-6090(01)01771-0.
[4] P. Vijaibharathy, Y.Y. Chang, D. Nataraj, Q. Yang, S.M. Yang, D. Mangalaraj, L. Yang, T.J. Webster, Effect of nickel incorporation on structural, nanomechanical and biocompatible properties of amorphous hydrogenated carbon thin films prepared by low energy biased target ion beam deposition, in: Thin Solid Films, Vol. 519, Elsevier, 2010, pp. 1623–1628, http://dx.doi.org/10.1016/j.tsf.2010.08.164.
[5] A. Furlan, J. Lu, L. Hultman, U. Jansson, M. Magnuson, Crystallization characteristics and chemical bonding properties of nickel carbide thin film nanocomposites, J. Phys. Condens. Matter 26 (41) (2014) 415501, http://dx.doi.org/10.1088/0953-8984/26/41/415501.
[6] R. Koppert, S. Uhlig, H. Schmid-Engel, D. Göttel, A.C. Probst, G. Schultes, U. Werner, Structural and physical properties of highly piezoresistive nickel containing hydrogenated carbon thin films, Diam. Relat. Mater. 25 (2012) 50–58, http://dx.doi.org/10.1016/j.diamond.2012.01.031.
[7] S. Kukiełka, W. Gulbiński, Y. Pauleau, S.N. Dub, J.J. Grob, Nickel/hydrogenated amorphous carbon composite films deposited in acetylene/argon microwave plasma discharge, Rev. Adv. Mater. Sci. 15 (2007) 127–133.
[8] G.J. Kovács, I. Bertóti, G. Radnóczi, X-ray photoelectron spectroscopic study of magnetron sputtered carbon-nickel composite films, Thin Solid Films 516 (21) (2008) 7942–7946, http://dx.doi.org/10.1016/j.tsf.2008.06.005.
[9] A.A. El Mel, E. Gautron, B. Angleraud, A. Granier, P.Y. Tessier, Synthesis of nickel-filled carbon nanotubes at 350 C, Carbon N. Y. 49 (2011) 4595–4607, http://dx.doi.org/10.1016/j.carbon.2011.06.001.
[10] A.A. El Mel, N. Bouts, E. Grigore, E. Gautron, A. Granier, B. Angleraud, P.Y. Tessier, Shape control of nickel nanostructures incorporated in amorphous carbon films: From globular nanoparticles toward aligned nanowires, J. Appl. Phys. 111 (11) (2012) 114309, http://dx.doi.org/10.1063/1.4728164.
[11] F. Wang, Multifunctional Nanocomposite Co- Containing Diamondlike Carbon Thin Films, (Ph.D. thesis), (December) Luisiana State University, 2004, p. 118, URL https://digitalcommons.lsu.edu/gradschool{}dissertations/2680.
[12] F.L. Wang, J.C. Jiang, E.I. Meletis, Self-assembled co nanorods in diamond-like carbon thin films synthesized by plasma-assisted magnetron sputtering, Appl. Phys. Lett. 83 (12) (2003) 2423–2425, http://dx.doi.org/10.1063/1.1610813.
[13] B. Trindade, M.T. Vieira, Modification of the structural order of transition metal–carbon systems by the addition of a group VIII element, Mater. Sci. Eng. A 352 (1–2) (2003) 195–201, http://dx.doi.org/10.1016/S0921-5093(02)00865-1.
[14] G. Tomé, B. Trindade, M.T. Vieira, Synthesis and characterisation of new sputtered metastable carbides, Vacuum 64 (3–4) (2002) 205–210, http://dx.doi.org/10.1016/S0042-207X(01)00309-8.
[15] T. Suszko, W. Gulbiński, J. Morgiel, G. Greczynski, E. Dobruchowska, P. Dłużewski, J. Lu, L. Hultman, Amorphous FeCrNi/a-c:H coatings with self-organizednanotubular structure, Scr. Mater. 136 (2017) 24–28, http://dx.doi.org/10.1016/J.SCRIPTAMAT.2017.03.040.
[16] T. Suszko, W. Gulbiński, E. Dobruchowska, G. Greczynski, L. Hultman, J. Morgiel, Quasi-amorphous, nanostructural CoCrMoC/a-C:H coatings deposited by reactive magnetron sputtering, Surf. Coatings Technol. 378 (2019) 124910, http://dx.doi.org/10.1016/J.SURFCOAT.2019.124910.

[17] K. Sedláčková, P. Lobotka, I. Vávra, G. Radnóczi, Structural, electrical and magnetic properties of carbon-nickel composite thin films, Carbon N. Y. 43 (10) (2005) 2192–2198, http://dx.doi.org/10.1016/j.carbon.2005.03.035.
[18] A.P. Ryaguzov, R.R. Nemkayeva, N.R. Guseinov, A.R. Assembayeva, S.I. Zaitsev, Percolation conductivity in amorphous carbon films modified with palladium nanoparticles, J. Non. Cryst. Solids 532 (2020) 119876, http://dx.doi.org/10.1016/j.jnoncrysol.2019.119876.
[19] J.L. Endrino, D. Horwat, R. Gago, J. Andersson, Y.S. Liu, J. Guo, A. Anders, Electronic structure and conductivity of nanocomposite metal (Au, Ag, Cu, Mo)-containing amorphous carbon films, Solid State Sci. 11 (10) (2009) 1742–1746, http://dx.doi.org/10.1016/j.solidstatesciences.2008.08.007.
[20] A. Shimamoto, Y. Ichinose, T. Ishiguro, Magnetic properties and structures of Co–C thin films prepared by sputtering, Mater. Trans. JIM 32 (1) (1991) 84–89, http://dx.doi.org/10.2320/matertrans1989.32.84.
[21] R. Paul, M.K. Sharma, R. Chatterjee, S. Hussain, R. Bhar, A.K. Pal, Ferromagnetism in nanocrystalline nickel incorporated diamond-like carbon thin films, Appl. Surf. Sci. 258 (15) (2012) 5850–5857, http://dx.doi.org/10.1016/j.apsusc.2012.02.114.
[22] D. Babonneau, J. Briatico, F. Petroff, T. Cabioc'h, A. Naudon, Structural and magnetic properties of Fe_xC_{1-x} nanocomposite thin films, J. Appl. Phys. 87 (7) (2000) 3432–3443, http://dx.doi.org/10.1063/1.372363.
[23] B. Wang, Y.C. Jiang, R. Zhao, G.Z. Liu, A.P. He, J. Gao, Piezoresistive effect observed in flexible amorphous carbon films, J. Phys. D. Appl. Phys. 51 (17) (2018) http://dx.doi.org/10.1088/1361-6463/aab75c.
[24] G. Schultes, H. Schmid-Engel, S. Schwebke, U. Werner, Granular metal–carbon nanocomposites as piezoresistive sensor films – Part 1: Experimental results and morphology, J. Sensors Sens. Syst. 7 (1) (2018) 1–11, http://dx.doi.org/10.5194/jsss-7-1-2018.
[25] S. Schwebke, U. Werner, G. Schultes, Granular metal–carbon nanocomposites as piezoresistive sensor films – Part˜2: Modeling longitudinal and transverse strain sensitivity, J. Sensors Sens. Syst. 7 (1) (2018) 69–78, http://dx.doi.org/10.5194/jsss-7-69-2018.
[26] J.R. Thompson, Ni-Cr textured substrates with reduced ferromagnetism for coated conductor applications J. R. Thompson, Physica C 370 (2002) (2008) 169–176.
[27] M.J. Besnus, Y. Gottehrer, G. Munschy, Magnetic properties of Ni-Cr alloys, Phys. Status Solidi (B) 597 (1972) 597–607.
[28] M. Rasander, E. Lewin, O. Wilhelmsson, B. Sanyal, M. Klintenberg, O. Eriksson, U. Jansson, M. Rrasander, E. Lewin, O. Wilhelmsson, B. Sanyal, M. Klintenberg, O. Eriksson, U. Jansson, Carbon release by selective alloying of transition metal carbides, J. Phys. Condens. Matter 23 (35) (2011) 355401, http://dx.doi.org/10.1088/0953-8984/23/35/355401.
[29] M.P. Seah, Summary of {ISO/TC 201} standard: {VII ISO 15472:2001} - surface chemical analysis - X-ray photoelectron spectrometers - calibration of energy scales, Surf. Interface Anal. 31 (8) (2001) 721–723, http://dx.doi.org/10.1002/sia.1076.
[30] G. Greczynski, L. Hultman, X-ray Photoelectron spectroscopy: Towards reliable binding energy referencing, Prog. Mater. Sci. 107 (2020) 100591, http://dx.doi.org/10.1016/j.pmatsci.2019.100591.
[31] NIST X-ray photoelectron spectroscopy database, 2000, http://dx.doi.org/10.18434/T4T88K.
[32] G. Greczynski, D. Primetzhofer, L. Hultman, Reference binding energies of transition metal carbides by core-level X-ray photoelectron spectroscopy free from Ar+ etching artefacts, Appl. Surf. Sci. 436 (2018) 102–110, http://dx.doi.org/10.1016/J.APSUSC.2017.11.264.
[33] G.K. Wertheim, S.B. DiCenzo, S.E. Youngquist, Unit charge on supported gold clusters in photoemission final state, Phys. Rev. Lett. 51 (25) (1983) 2310–2313, http://dx.doi.org/10.1103/PhysRevLett.51.2310.
[34] E. Bauer-Grosse, A. Aouni, Glass-forming range and glass thermal stability in binary 3d TM-C systems, J. Non Cryst. Solids 353 (32–40) (2007) 3644–3649, http://dx.doi.org/10.1016/j.jnoncrysol.2007.05.127.
[35] F.L. Wang, J.C. Jiang, E.I. Meletis, Microstructural evolution of Co nanostructures in diamond-like carbon by plasma-assisted processing, J. Appl. Phys. 95 (9) (2004) 5069–5074, http://dx.doi.org/10.1063/1.1691181.
[36] B.I. Leonovich, Thermodynamic analysis and phase equilibria in the Ni-Cr-C system, Steel Transl. 41 (5) (2011) 371–375, http://dx.doi.org/10.3103/S096709121105010X.
[37] R. Chantrell, J. Popplewell, S. Charles, Measurements of particle size distribution parameters in ferrofluids, IEEE Trans. Magn. 14 (5) (1978) 975–977, http://dx.doi.org/10.1109/TMAG.1978.1059918.
[38] M. El-Hilo, Nano-particle magnetism with a dispersion of particle sizes, J. Appl. Phys. 112 (10) (2012) http://dx.doi.org/10.1063/1.4766817.

NiMo-C coatings synthesised by reactive magnetron sputtering for application as a catalyst for the hydrogen evolution reaction in an acidic environment

Tomasz Suszko,*,† Ewa Dobruchowska,† Witold Gulbiński,† Grzegorz Greczynski,‡ Jerzy Morgiel,¶ Bartosz Kawczyński,§ Karol Załęski,§ Krzysztof Dorywalski,‖ and Stanisław Pogorzelski‖

†*Koszalin University of Technology, Ul. Śniadeckich 2, Koszalin, 75-453, Poland*

‡*Thin Film Physics Division, Department of Physics (IFM), Linköping University, 581 83 Linköping, Sweden*

¶*Institute of Metallurgy and Materials Sciences, Polish Academy of Science, Ul. Reymonta 25, Kraków, 30-059, Poland*

§*NanoBioMedical Centre, Adam Mickiewicz University, ul. Wszechnicy Piastowskiej 3, 61-614 Poznań, Poland*

‖*Institute of Experimental Physics, Faculty of Mathematics Physics and Informatics, University of Gdańsk, Wita Stwosza 57, 80-308 Gdańsk, Poland*

E-mail: tomasz.suszko@tu.koszalin.pl

Abstract

This study examines the structure and properties of NiMo-C coatings synthesized via reactive magnetron sputtering of a NiMo alloy target in an argon/acetylene at-

mosphere. The coatings structure evolves with carbon content from nanocrystalline, through amorphous to quasi-amorphous with nanocolumnar structure. The nanostructure consists of metallic columns perpendicular to the substrate surrounded by amorphous carbon shell. The coatings are evaluated for their potential use as catalytic materials in the hydrogen evolution reaction (HER) in an acidic environment. The medium carbon content coatings show optimal properties in this direction, i.e. high corrosion resistance in an acidic environment and good HER performance described by the Tafel slope and characteristic overpotentials. Even at the highest carbon content, 74 at.%, the Tafel slope does not increase substantially, what is more likely attributable to the distinctive nanocolumnar structure, which ensures presence of catalytic centres in the form of metallic islands on the surface. At the highest current densities applied, a weak but visible correlation is observed between the characteristic overpotentials and the contact angle hysteresis derived from the wettability measurements.

Introduction

In light of the necessity to reduce CO_2 emissions, the contemporary economy is undergoing a gradual transition towards alternative energy sources, with hydrogen emerging as a particularly essential component. At present, leading research on hydrogen production for energy purposes is focused on water electrolysis. A key objective is the development of electrode materials that exhibit high catalytic activity and durability when operating in both acidic and alkaline environments. In this context, the replacement of noble metals with other, more cost-effective, and readily available materials with negligible differences in catalytic properties represents a significant challenge.

The selection process for electrode materials used in the Hydrogen Evolution Reaction (HER) is based on specific descriptors of catalytic activity. In the case of transition metals, the majority of theoretical descriptions of the HER activity focuses on the d-band centre, which is defined as the mean weighted energy of the d-band.[1,2] This value provides an ac-

curate representation of the intermediate hydrogen (H*) binding strength, expressed as the Gibbs free energy of H* adsorption (ΔG_{H^*}). The ΔG_{H^*} values determined for the individual metals follow a volcano-like relationship (so-called volcano plot), with the $\Delta G_{H^*} \approx 0$ corresponding to the highest catalytic activity.[3,4]

Besides pure metals with sufficiently low ΔG_{H^*} values such as Mo, W, Nb, Co, Ni and their alloys,[5–8] a large number of related compounds were investigated.[9–11] Much work has also been done on carbon-based composites.[12] Nevertheless, the so-far laboratory-developed electrodes for HER with the best properties, primarily based on nanostructured metal oxides,[13,14] sulfides[15,16] or phosphides,[17,18] are mainly manufactured using sophisticated multi-step technological processes. The reproducibility of these processes and the feasibility of their large-scale implementation have yet to be fully demonstrated. Consequently, their application in industrial-scale electrolysers remains limited.

From an economic standpoint, emphasizing material consumption and recycling, there is a growing interest in using specialized catalytic coatings deposited by physical vapour deposition (PVD) techniques on conductive substrates that serve only as current collectors. The class of coatings that have been the subject of intensive study comprises binary and ternary metal-carbon nanocomposites. The binary systems are based on an amorphous carbon matrix and contain either metallic (such as nickel or cobalt) or carbide precipitates (such as MoC, WC, NbC) in the nanoscale range.[19–21]

The presence of the carbon matrix protects the catalytically active metallic or carbide precipitates against corrosion while simultaneously limiting electrical conductivity and, thus, the effective charge transfer. As a consequence, augmented over-potential values have been observed,[21] predominantly resulting from the intrinsic activation barriers inherent to both electrodes and additional resistances, including the specific resistance of the electrode material and the contact resistance.

The complete miscibility of carbides is often observed in the ternary systems comprising two metals with a high affinity for carbon. This is evidenced by the examples of TiC-

VC, TiC-NbC, VC-TaC and HfC-TaC.[22] Exceptions to this general rule can be observed in systems such as VC-HfC, VC-CrC, or CrC-MoC and CrC-WC, which exhibit limited mutual solubility.[23] The growth mechanism of ternary carbide thin films becomes more intricate when the second metal is a weak carbide former. U. Jansson et al.[23] postulated that the processes underlying the growth of thin films in such systems entail the formation and subsequent decomposition of metastable carbides of the $M_{1-x}Me_xC_y$ type, where M and Me represent strong (e.g., Ti, Nb, Cr, W) and weak (e.g., Co, Ni, Fe) carbide formers, respectively.

These considerations lead to the conclusion that the coexistence of metals with a high and low chemical affinity for carbon within the deposit facilitates both the amorphization of the deposit and the segregation of carbon. Concurrently, the segregation of carbon during the deposition process can facilitate the self-organization phenomenon, as previously observed for simple Me-C binary systems (where Me = Fe, Co, Ni), which results in the formation of nanocolumnar structures.[24,25] Our recent research on the FeCrNi-C,[26] CoCrMo-C,[27] and NiCr-C[28] systems have demonstrated the viability of producing amorphous thin films with ordered structures also in ternary and multicomponent composites.

These coatings comprise densely packed and separated metallic or carbide nanocolumn cores surrounded by amorphous carbon shells. The observed nanocolumns extend throughout the entire films, as confirmed by atomic force microscopy working in magnetic mode.[28] Consequently, such coatings should guarantee easy access to the metallic/catalytic centres at the film surface and high electrical conductivity along the columns. Both features are beneficial for efficient hydrogen generation by the electrolytic decomposition of water.

In addition to materials research aimed at optimizing the catalytic activity of new materials, it is essential to gain a deeper understanding of the dynamics of electrode/gas/electrolyte interfaces and the impact of gas bubble behavior on the interface. In this regard, research on wetting, hydrogen bubble nucleation, and desorption from the electrode is an important trend.[29,30]

During hydrogen evolution, gas bubbles grow on the catalyst surface. Since the grown gas bubbles hinder the space for catalytic reaction, their fast detachment is of critical importance. There is the three-phase interface of the electrolyte. A gas bubble can grow easily at a large receding contact angle Θ_R. For a small receding contact angle, a gas bubble cannot grow up and becomes detached with a small bubble size.[30] Thus, controlling surface energy, dynamic contact angles, and their hysteresis by modifying the composition and nanogeometry of the surface becomes an important tool to optimize the gas release process from the electrode.

In the current work, we present the initial investigation on the utilization of NiMo-C coatings, synthesized via reactive magnetron sputtering of the $Ni_{80}Mo_{20}$ alloy in an argon/acetylene atmosphere, as prospective catalysts for HER operating in an acidic environment. The composition of the coatings was selected at the design stage based on the criteria and characteristics of the individual components and their systems, as outlined below.

1. Ni atoms are acknowledged as effective dissociative centers for water due to their low ΔG_{H^*} value[4] and exhibit sufficiently low carbide-forming properties.[28] The latter feature is expected to facilitate the separation and release of amorphous carbon in the NiMo-C system.

2. Incorporation of Mo results in lattice expansion within the Ni elemental cell, accompanied by alterations to its cubic crystal structure. These changes result in a diminished ΔG_{H^*} value compared to that of pure nickel by tuning the electronic structure of the NiMo alloy. A synergistic catalytic effect towards HER has been demonstrated for the Ni_4Mo alloy in alkaline media.[31–33]

3. The addition of Mo in an amount of 12-14 at.% endows the NiMo alloy with paramagnetic properties, thereby ensuring an efficient magnetron sputtering process, which is of pivotal importance for producing coatings on an industrial scale.[34,35]

4. In the NiMo-C system, the carbon separation process is not impaired at 20 at.% of Mo. Conversely, it is hypothesized that Mo will have an amorphising effect, thereby

enhancing the corrosion resistance of the deposit.

5. Carbon segregation will ensure the formation of quasi-amorphous ordered structures in the NiMo-C system studied.

The chemical and phase composition of the as-designed NiMo-C coatings and the evolution of their structure, surface morphology, and stability/corrosion resistance with increasing carbon content in the deposits were investigated and discussed. The electrocatalytic properties of the coatings were evaluated by comparison with the catalytic capacity of platinum and graphite (two reference materials) under identical experimental conditions. The overpotential (η), defined as the difference between the potential applied to deliver a specific current density (e.g., 0.01 A/cm^2) and the thermodynamic potential value, as well as the Tafel slope, which is a kinetic parameter that indicates the rate of HER, were selected as the primary parameters for the assessment of electrocatalyst activity.[36]

Materials and methods

The thin films being studied were deposited using the reactive magnetron sputtering technique. A planar magnetron source equipped with a $Ni_{80}Mo_{20}$ alloy cathode, 100 mm in diameter, was operated at 1 kW in a pulse mode with a frequency of 100 kHz and 1 kHz modulation. The coatings were deposited on Si (100) wafers and AISI 316L steel substrates placed at a distance of 60 mm from the cathode and heated to 200°C by the temperature controlled resistive heater and kept at at the bias potential of -50 V DC.

Films with a thickness of 3 ± 0.1 μm and a gradual increase in carbon content were deposited in an argon/acetylene working atmosphere. Argon flow was maintained at a constant rate of 12 standard cubic centimeters per minute (sccm), while acetylene flow was stepwise varied from 0 to 6 sccm in order to obtain films with varying carbon content. The total pressure of the process atmosphere was maintained at 0.6 Pa.

Samples characterisation

The structure of the deposits was examined by X-ray diffraction (XRD) using a Malvern Panalytical Empyrean 3 diffractometer operating with a Cu-Kα source in two geometries: Bragg-Brentano, and at the constant low incidence angle ω=3°.

The chemical composition and the binding state of coatings components were studied by X-ray Photoelectron Spectroscopy (XPS) with the Axis Ultra DLD instrument (Kratos Analytical, UK) working with monochromatic Al-Kα radiation ($h\nu$ = 1486.6 eV) and at the base pressure of 1.5×10^{-7} Pa. The energy analyzer was calibrated using Au $4f_{7/2}$, Ag $3d_{5/2}$, and Cu $2p_{3/2}$ core levels at 83.96, 368.21, and 932.62 eV, respectively. All spectra were charge-referenced to the Fermi edge of NiMo-C films.[37] The analyser pass energy was set to 20 eV, resulting in the full width at a half maximum of 0.55 eV for the Ag $3d_{5/2}$ peak. The XPS spectra were quantified using Casa XPS software (version 2.3.16) and the sensitivity factors supplied by Kratos Analytical Ltd. Before spectra acquisition, the as-loaded samples were sputter-etched with 4 keV Ar^+ ions for 120 s followed by 0.5 keV Ar^+ for 600 s.

Observations of the microstructure, down to the nanometer scale, were carried out using the HAADF-STEM (High-Angle Annular Dark-Field Scanning Electron Microscopy) technique using a Tecnai G2 F20 high-resolution transmission electron microscope (HRTEM), operating at a voltage of 200 kV and coupled to the EDX analyzer. QUANTA 3D – a focused ion beam (FIB) instrument was used for sample preparation.

The studied coatings' surface topography and electrical conductivity maps were collected using an Atomic Force Microscope (AFM) Icon Dimension (Bruker, USA) equipped with a PeakForce-TUNA module. The maps were imaged in a Conductive AFM (C-AFM) mode by a Scanning Capacitance Microscopy - Platinium-Iridium coated (SCM-PIC) probe with an electrically conductive tip. The C-AFM mode allows us to simultaneously measure topography and electrical conductivity while scanning the sample's surface. To induce the current flow between a tip and a sample the 8mV voltage was applied. Since the samples are highly conductive (metallic), an additional 1 MOhm resistor was soldered between the film surface

and the sample holder to lower the current.

Electrochemical tests were performed using an Atlas 0531 potentiostat, galvanostat (Atlas Sollich, Poland). The HER measurements were conducted in a standard three-electrode cell, with the samples (NiMo-C coated steel substrates) serving as the working electrodes. The active surface area of each working electrode was 0.3 cm^2. The recorded currents were converted to current densities, considering the surface dimensions of the electrode materials. A saturated standard calomel electrode (SCE, $Hg/Hg_2Cl_2/KCl$) and a platinum plate were used as the reference and counter electrodes respectively. Potential values were subsequently recalculated according to the reversible hydrogen electrode (RHE).

All measurements were carried out at room temperature (25 ± 1°C) in an unstirred sulphuric acid solution (0.1M H2SO4) without resistance compensation (iR). The linear voltammetry (LV) curves were recorded at two different scan rates, i.e., 0.005 V/s and 0.03 V/s, within the potential range of 0 V to -1.2 V vs. RHE. In order to ascertain the stability of the examined coatings, cyclic voltammetry (CV) measurements were conducted from the free potential for each sample to -0.8 V (vs. RHE) at a scanning rate of 0.03 V/s. Subsequent to 200 cycles, a comparison was made between the LV curve recorded at this stage and that obtained on the unaltered sample.

A cathodic-anodic polarization method was employed to evaluate the corrosion resistance of NiMo-C coatings when immersed in an acidic environment. Polarization curves were obtained at a scanning rate of 1.7×10^{-4} V/s. The curves were subsequently used to estimate the corrosion potential (E_{corr} vs. SCE) and the corrosion current density (i_{corr}) by the Tafel extrapolation method.[38] The Stern-Geary equation was employed for the purpose of calculating the polarization resistance (R_p).[39]

The wetting properties of the coatings under investigation were characterized through the measurement of dynamic contact angles, with the difference between the angles defined as the contact angle hysteresis (CAH). Potential origins of the hysteresis phenomenon include porosity, chemical heterogeneity, and molecular reorientation at the solid-liquid interface.

In the case of chemically heterogeneous and non-porous flat surfaces, the advancing and receding contact angles of a polar probing liquid drop can be taken as a rough approximation of the equilibrium contact angles of the most hydrophobic and the most hydrophilic surface fractions.[40]

The CAH measurements were carried out using a sessile drop method using a laboratory-built apparatus developed at the University of Gdansk.[41] In this setup, a drop is deposited on the sample surface by a syringe controlled by a stepper motor. Deionized water (Millipore system, conductivity 0.05 [μS/cm]), pH = 5.8 ± 0.1 , surface tension $\gamma_{SV} = 71.2 \pm 0.2$ mN/m) was used as the probe liquid. The advancing Θ_A and receding Θ_B contact angles are determined from the images captured by a high-resolution camera (8Mpix Touptek U3CMOS) during gradual volume increase and volume removal, respectively, until dewetting occurs. The images were further analyzed using OpenDrop software.

Results and disscussion

Chemical composition and binding state

By gradually changing the acetylene fraction in the process atmosphere, a series of coatings with an increasing carbon content was deposited. The chemical composition of the coatings, and in particular the carbon content, which is crucial for the nanostructure evolution, was determined using the XPS and EDX techniques. The measured values of carbon content ranged from 5.6 to 75.3 at.%, as shown in Table 1 and Fig. 1. The amount of metallic components in all coatings was in the same atomic proportions Mo/Ni = 20/80 $\pm$ 0.005, corresponding to the cathode composition.

Since the use of both XPS and EDX techniques has some limitations, in the remainder of this article, approximated values will be used to characterize specific samples. The source of carbon present in coatings deposited in pure argon is most likely contamination of the technological chamber where numerous processes involving acetylene were carried out.

Table 1: Carbon content determined from XPS spectra, EDX measurements, approximate values obtained by fitting with a second-degree polynomial, and oxygen content measured by XPS.

C_2H_2 flow [sccm]	Carbon content [at.%]			Oxygen
	XPS	EDX	approx	XPS [at.%]
0.0	5.6	7.8	6.6	4.2
0.5	6.3	8.6	7.4	2.8
1.0	7.4	10.2	8.7	2.3
2.0	14.7	15.7	15.1	1.1
3.0	22.4	24.4	23.3	1.2
4.0	41.3	34.3	37.6	1.1
5.0	61.9	44.3	52.9	0.7
6.0	75.3	73.6	74.2	0.6

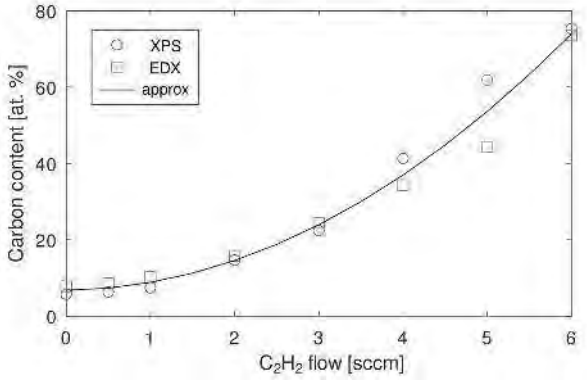

Figure 1: Dependence of carbon content on acetylene flow during deposition. Data were obtained using the XPS and EDX methods. The solid line corresponds to the approximation by a second-degree polynomial.

The coatings contained a certain amount of oxygen found as contamination in the coatings. The oxygen content measured by XPS decreases gradually from 4.2 at.%. for coatings deposited without acetylene flow to 0.6 at.% for coatings with the highest carbon content (cf. Tab. 1). Since acetylene was used as a carbon-carrying gas in the deposition process, the coatings certainly contain a certain amount of hydrogen. Its content however, has not been tested in the presented work.

Up to the C content of 23 at.% the C 1s spectra (cf. Fig. 2) are dominated by the low energy peak at 283.4 eV, which corresponds to the chemical shift characteristic of carbon bound in metal carbides.[42] Above the threshold of about 23 at.% C, a high-energy component becomes clearly visible at the binding energy of 284.4eV, characteristic of C–C bonds in sp^2-bonded amorphous carbon. This signifies the onset of carbon segregation process. Carbon segregation is favoured by the decomposition process of unstable carbides of $Mo_{(1-x)}Ni_xC_y$ type as described by U. Jansson et al.,[43] which decompose through energetically preferred carbon out-diffusion. The formation of this type of unstable ternary carbide is favored by the simultaneous presence of metals with high (Mo) and low (Ni) chemical affinity for carbon.

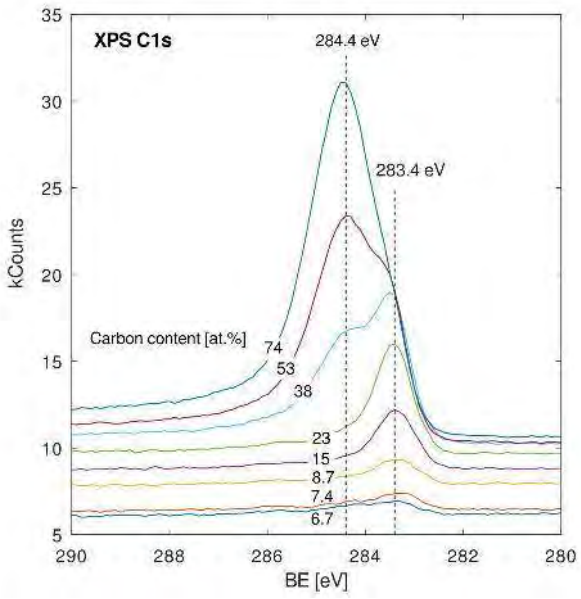

Figure 2: C 1s spectra for NiMo-C coatings with increasing carbon content.

Looking at the Mo 3d and Ni 2p XPS spectra (cf. Fig. 3), and in particular the chemical

shifts (Fig. 3 c), there are several characteristic features. The Mo $3d_{5/2}$ peak shifts from 228.0 eV for low carbon films to 228.25 eV for the film with highest C content. Two distinguishable parts of the BE shift in dependence on C content are visible.. With an increasing carbon content of about 20 at.%, the chemical shift increases rapidly, and then the increase decelerates. For nickel, this difference is considerably less pronounced, and the BE increases almost linearly from 853.0 eV to 853.20 eV with carbon content. It may be interpreted as an indication of a larger charge transfer between Mo and C atoms, hence, preferential formation of Mo–C rather than Ni–C bonds.

This observation is consistent with the fact that the molybdenum carbide Mo_2C is characterized by a relatively large negative enthalpy of formation $\Delta H_0 = -27 \pm 3$ kJ/mol,[44] while the standard enthalpy of formation of nickel carbide Ni_3C is $\Delta H_0 = 1.2$ kJ/mol.[45] Considering that the coating deposition process was carried out at a temperature of 200°C, that is, significantly below the decomposition temperature of the metastable nickel carbide Ni_3C, defined as 300°C,[46] its presence in the deposit should be expected. Although, at the same time, the ion assistance caused by the substrate bias during layer growth can promote the decomposition of these unstable nickel carbides.

The linear growth in chemical shift observed at the same rate for both spectra (cf. Fig. 3 c) is likely associated with forming carbon precipitates. When the concentration of carbon exceeds the release threshold (approximately 20 at.%), regions of reduced electrical conductivity are formed. Therefore, as suggested by G.K. Wertheim et al.,[47] This leads to a decrease in the kinetic energy of the escaping photoelectrons and thus to an apparent increase in the binding energy.

Structure, nanostructure, and self-organization of the coatings

The structure of coatings undergoes a gradual transformation with increasing carbon content, evolving from nanocrystalline to amorphous, as illustrated in Fig. 4.

The diffraction pattern for the steel substrate is dominated by two peaks (111) and

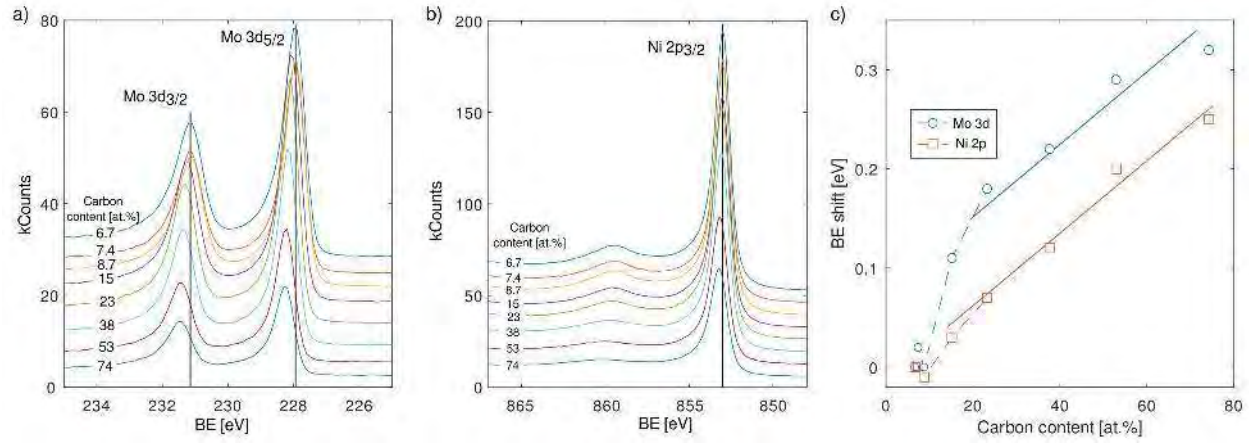

Figure 3: Mo3d (a), Ni2p (b) core level spectra for coatings with increasing carbon content along with the chemical shift of these lines vs carbon content (c).

(200) characteristic of austenite (fcc) and the accompanying reflection (110), indicating some participation of ferrite (bcc). In the diffraction pattern of the $Ni_{80}Mo_{20}$ target, peaks were mainly found corresponding to the fcc solid solution of molybdenum in nickel-like $Mo_{0.12}Ni_{0.88}$ (ICDD card 04-023-7853). It is also possible that the tetragonal phase $MoNi_4$ (ICDD card 01-071-9765) occurs there, but closely located peaks may overlap in the case of this fine-crystalline structure.

The occurrence of weak peaks, barely visible in Fig. 4, with two theta angles of 34.3, 37.8, and 39.4 degrees, indicates the presence of some inhomogeneity identified as a molybdenum-rich hexagonal phase close to the $Mo_{84}Ni_{16}$ (ICDD card 04-007-4030) with peaks shifted to lower diffraction angles. The observations are in agreement with the Ni-Mo phase diagram.[48]

The structure of coatings with a small share of carbon roughly corresponds to the structure of cathode material, with a clear broadening of the peaks and caused by a nanocrystalline structure of the coatings. There is also an additional peak observed at 40.6°, which corresponds to the (110) planes of bcc molybdenum (ICDD card 04-014-7439). It is not excluded that the strong affinity of molybdenum for carbon may result in the metal diffusing and forming precipitates containing carbon. Moreover, significant changes in the film texture appear, as can be seen in the mutual intensities between peaks (111) and (200) in the patterns recorded in both configurations for samples containing 7.4 and 8.7 at.% carbon.

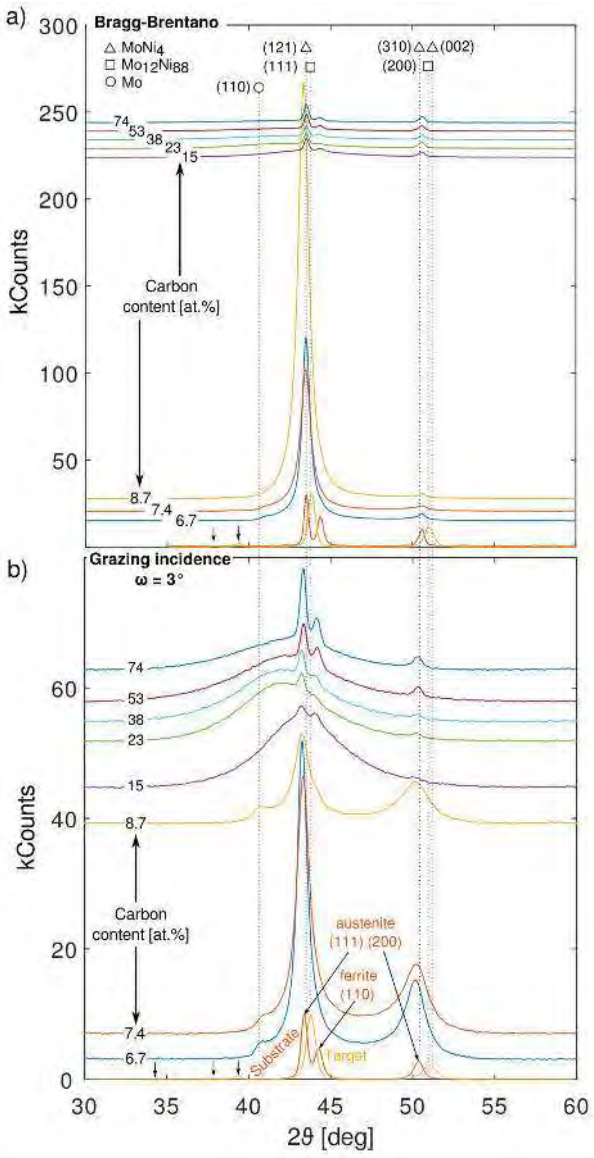

Figure 4: X-ray diffraction patterns of substrate material (316L steel), target ($Ni_{80}Mo_{20}$ alloy), and NiMo-C coatings with increasing carbon content. The patterns recorded in a) Bragg-Brentano geometry and b) low constant incidence angle.

Increasing the carbon content to more than about 8 at.% leads to an even more pronounced refinement of the deposit, which is reflected in broadening of the diffraction peaks and a decrease in their intensity. For coatings containing 15 at.% carbon, the XRD pattern indicates the amorphization of the deposit. Only one broad peak is observed at 43 degrees, indicating close-range ordering and the contribution of peaks originating from the substrate.

An increase in the carbon content first results in shifting the broad peak to 42 degrees, corresponding to the beginning of the carbon segregation. A gradual decrease in the intensity is then observed because of the increasing content of the light element, carbon. The coating's decreased X-ray reflection/absorption leads to the reappearance of peaks originating from the substrate material.

In order to reveal the nanostructure of tested coatings, observations using HRTEM were carried out. Samples for nanostructure observations were cut using the FIB technique in planes parallel (plan view) and perpendicular (cross-section) to the substrate plane. Coatings with a carbon content below the carbon segregation threshold were featureless (cf. Fig.5 a and d). The increase in the carbon share led to the formation of a columnar nanostructure composed of nanopillars several nanometres in diameter, orientated parallel to the growth direction (cf. Fig. 5 b, c, e, f). In agreement with the XRD patterns, the broad electron diffraction ring (inset in Fig. 5 b) reveals a close-range ordering.

High-resolution plan-view images revealed that these nanopillars are composed of metallic cores surrounded by a shell of amorphous carbon (cf. Fig. 5). These coatings we denote, in accordance with the scheme adopted in previous publications,[26–28] as NiMoC/a-C:H. They are formed during a self-assembly process of the nanostructure, which results from: i) material transport and its reactive deposition at the substrate, ii) nucleation of molybdenum carbides as well as unstable nickel carbides and ternary carbides of the $Mo_{(1-x)}Ni_xC_y$ type, iii) decomposition of unstable carbides and carbon segregation. Detailed observations using the HAADF-STEM technique combined with a local composition analysis using the EDX technique allowed the identification of chemical nature of the cores and shell of the nanopil-

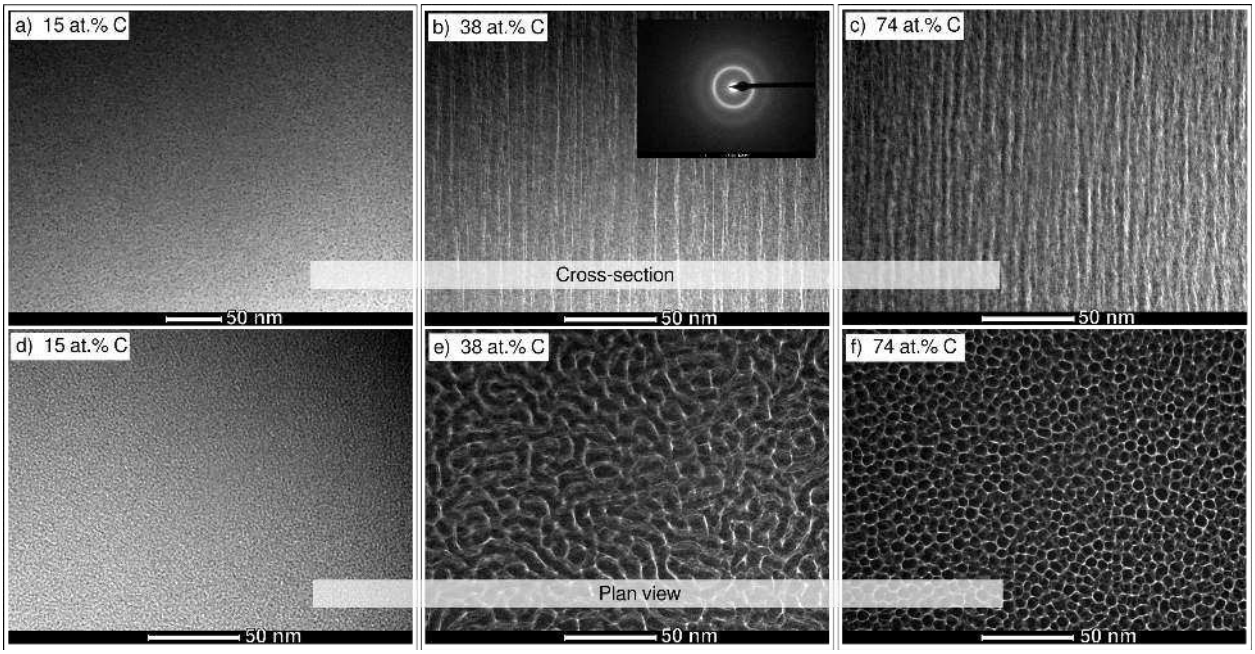

Figure 5: HRTEM image in cross-section (top row – a, b, c) and plan view (bottom row – d, e, f) of NiMo-C thin films containing increasing amounts of carbon. Inset in (b) – electron diffraction image of the sample containing 38 at.% C.

lars (cf. Fig. 6).

As confirmed by the combination of the EDX signal acquired along line indicated in the HAADF image of the film with 74 at. % C (cf. Fig. reffig-HAADF), segregation resulting from diffusion and accumulation of carbon in the form of nanopillars' shells occurs. In the cores of nanopillars, where the metals/C ratio is much higher, carbon dissolved and/or bound to metals (Ni and Mo) is also present. Note that the molybdenum content is almost the same in the core and shell of the nanopillar, regardless of the position in the nanostructure. This may be due to its immobilization resulting from its strong bonds with carbon.

Microscopic observations of the columnar nanostructure described above were made on internal parts of the coatings. To visualise the morphology of the coating surfaces, tests were carried out using techniques: AFM (cf. Fig.7 a) and C-AFM (cf. Fig. 7 b), in topography and conductivity mapping modes respectively. The results of these studies revealed that the nanocolumnar structure observed in the cross-sections is not directly reproduced at the coating surface. The observed separated high-conductivity regions have diameters of about

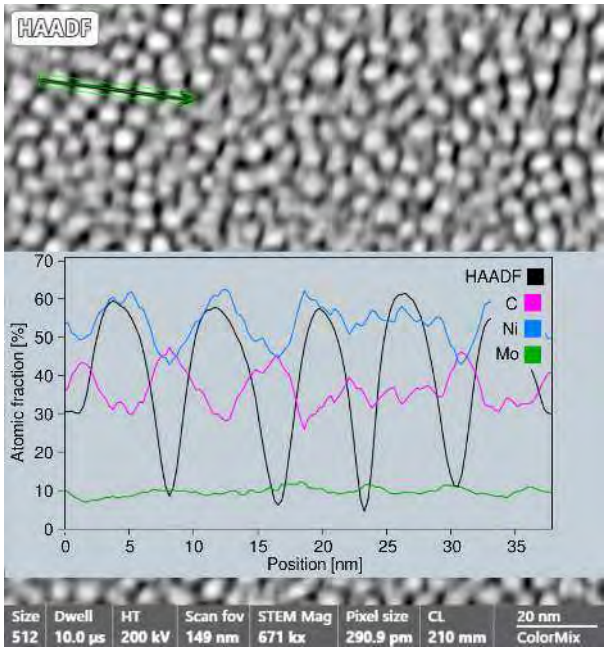

Figure 6: HAADF plan view picture of the NiMoC/a-C:H thin film containing 74 at.% carbon, combined with EDS line scan.

20 nm (cf. Fig. 7 b), which is significantly larger than the diameters of the columns from internal parts of the coatings observed by TEM. It can be postulated that these areas, formed by merging the tops of metallic columns, will act as catalytic centers for hydrogen during the electrolytic decomposition of water.

Electrochemical behaviour in acidic environment

The electrochemical properties of Ni-based alloys have been extensively investigated, with a particular emphasis on their catalytic activity and corrosion stability in alkaline environments. The main reason for this lies in the use of nickel alloys in the manufacture of cathodes for conventional alkaline electrolysers, in conjunction with the inherent lower corrosion resistance of these alloys in acidic environments.[33]

In the present study, the cathodic-anodic polarization method was used for the purpose of testing and comparing the durability and corrosion resistance in an acidic medium of individual coatings deposited on steel substrates. Subsequently, the same environment was

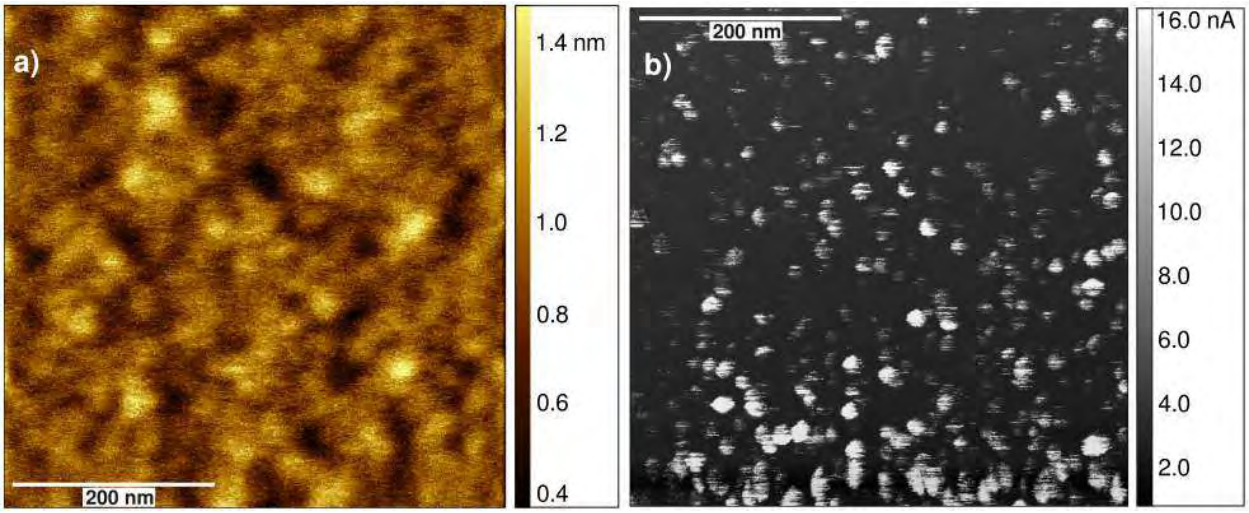

Figure 7: Surface morphology (a) and the conductivity map (b) registered for the NiMo/a-C:H sample (38 at.% C), using AFM and C-AFM techniques, respectively.

utilized to assess the HER activity of the NiMo-C coatings. Coatings synthesized without acetylene and with an acetylene flow of 0.5 sccm (6.7 and 7.4 at.% C, respectively) show very similar properties. Therefore, to improve the readability of the data and graphs, data for the latter were abandoned when describing their properties in electrochemical reactions.

The exemplary polarization curves recorded in a 0.1M H_2SO_4 solution(at a scanning rate of 1.7×10^{-4} V/s) are shown in Fig. 8 a and Fig. 8 b. The electrochemical parameters characterizing the corrosion processes are summarized in Table 2.

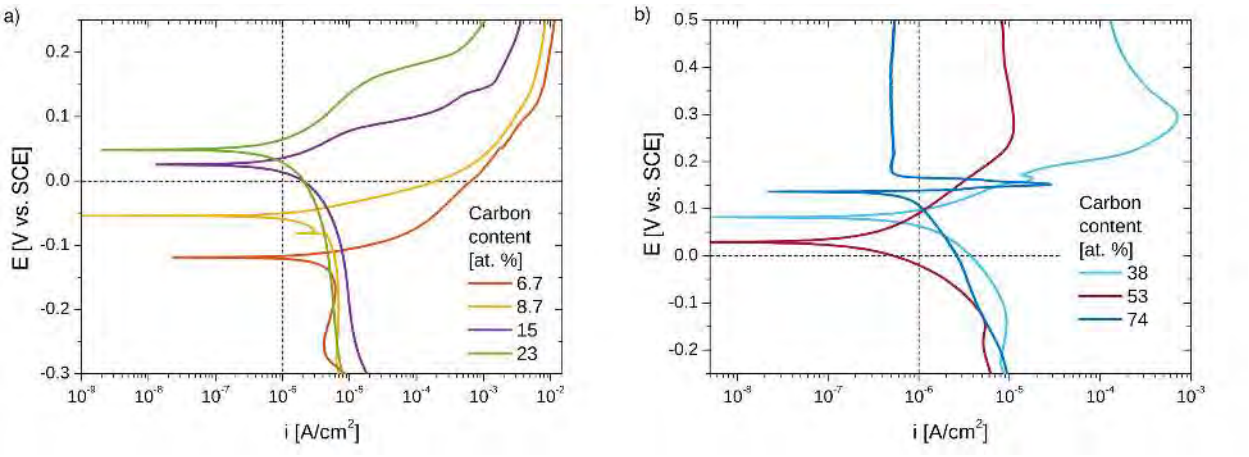

Figure 8: Polarization curves recorded in 0.1 M H_2SO_4 for NiMo-C coatings with different carbon content; 6.7–23 at.% (a) and 38–74 at.% (b).

Table 2: Corrosion parameters were determined for NiMo-C coatings (with increasing carbon content) immersed in 0.1 M H_2SO_4, where $-b_c$ and b_a correspond to the cathodic and anodic Tafel constant respectively.

Carbon content at.%	E_{corr} [V]	i_{corr} [10^{-6} A/cm^2]	$-b_c$ [V/dec]	b_a [V/dec]	R_p [Ωcm^2]
6.7	−0.119	2.4	0.062	0.025	3×10^3
8.7	−0.054	2.5	0.090	0.031	4×10^3
15	0.025	1.8	0.121	0.072	11×10^3
23	0.048	0.59	0.137	0.070	34×10^3
38	0.082	1.6	0.168	0.096	16×10^3
53	0.029	0.32	0.162	0.137	1×10^5
74	0.136	1.1	0.173	0.012	4×10^3

An analysis of the obtained data has indicated that the coating with a carbon content of 6.7 at.% exhibited the lowest corrosion resistance under the measurement conditions applied. The corrosion potential E_{corr} of this sample was found to be −0.119 V, which represents the minimum value observed. Upon exceeding the E_{corr} threshold, the oxidation reactions of the coating/substrate components proceeded rapidly, as evidenced by the relatively high corrosion current density and low polarization resistance values (cf. Table 2; i_{corr} and R_p values). Increasing the carbon content to 8.7 at.% resulted in a shift of E_{corr} towards higher values.

This behaviour can be attributed to the refinement of grains within the deposit. As evidenced by the broadening of the XRD pattern observed (cf. Fig. 4) and our previous findings,[27,49] the addition of carbon at this level has a disruptive effect on grain growth, while simultaneously leading to the formation of new nucleation centers. As posited by Ralston et al.,[50,51] the high degree of refinement in the structure of metal/metal alloys enhances their potential for surface passivation. Furthermore, the high density of grain boundaries provides an environment conducive to the diffusion of metal ions into the passive layer, thereby facilitating oxide formation and improving its stability. However, failure of this natural blocking layer at a potential value equivalent to the corrosion potential results

in the rapid and uniform dissolution of the sample material (cf. Table 2; i_{corr} and R_p values).

An increase in carbon content to about 23 at. % results in the amorphization of the coatings, as evidenced by the featureless XRD patterns depicted in Fig. 4. The structureless or quasi-amorphous nature of these deposits, coupled with a restricted number of defects in the form of micropores or microcolumns, impedes the diffusion of electrolyte deep into the coating towards the substrate. This results in the formation of a robust protective barrier. The aforementioned features are evidenced in the electrochemical tests and the resultant polarization curves (Fig. 8 a and b) through a shift in the corrosion potential towards more positive values and a reduction in the corrosion rate, as indicated by lowering the corrosion current density (cf. Table 2). The latter feature is most apparent in samples with a carbon content of 23 at.% and 53 at.%. All amorphous coatings exhibited positive corrosion potential values.

The ennoblement of E_{corr} results in a notable alteration in the profile of the anodic branches of the polarization curves, which is most pronounced in the case of the coating with a carbon content of 74 at.%. For this sample, following the exceedance of the critical passivation potential value of 0.15 V, a sharp decrease in the current density was observed, stabilizing at a value of 5×10^{-7} A/cm^2, which value can be regarded as an indicative of the passivation current density. The formation of a stable passive range, in the course of polarization curve, indicates the chemical inertness of coating in the corrosive medium used. The sample's surface remains stable despite a further increase in potential value.

The trend towards a passive state is evident for all deposits where XPS studies show the separation of amorphous carbon (cf. Fig. 3). Consequently, coatings with a carbon content of 23 at.% or higher fulfill the criterion of high corrosion resistance in acidic environments.

Electrochemistry, HER

The electrochemical activity of the samples for hydrogen generation was determined by analyzing polarization linear voltammetry (LV) curves. The curves recorded at two different

scanning rates are presented in Fig. 9. In addition, curves recorded under the same conditions for reference materials; platinum and graphite are also presented.

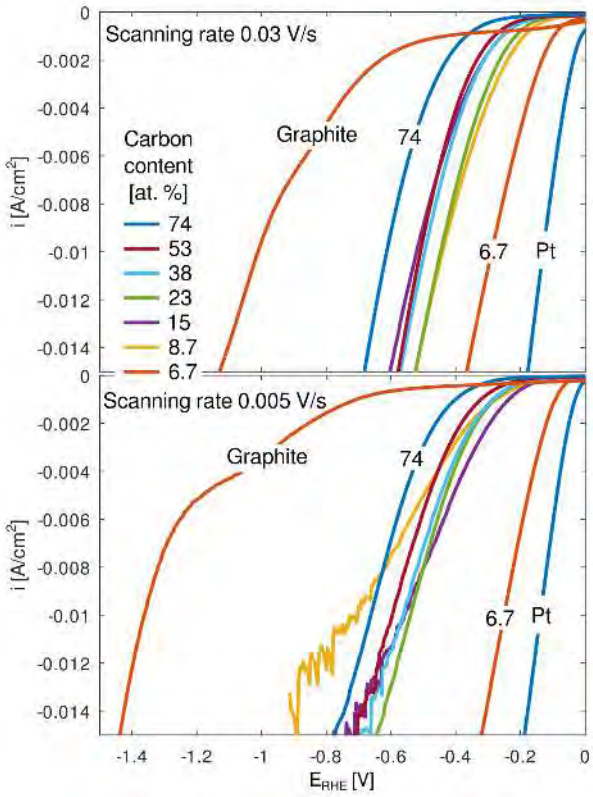

Figure 9: Linear voltammetry polarization curves for studied NiMo-C coatings measured at the two scanning rates.

Several characteristic features can be observed. The plots are exponential between approximately 10^{-4} and 10^{-3} A/cm^2. Therefore, the Tafel slopes characterizing the overall HER reaction rate can be calculated even though the exponential sections are relatively small due to instrumentation limitations, such as the lack of rotating disk electrode. Subsequently, a linear (ohmic) portion of the graph can be identified, and at even higher values of current density, distortions due to the build-up and release of hydrogen bubbles can be observed, particularly at lower scan rates.

The curves recorded for graphite differ significantly from the others, and the division into exponential and linear parts is not so obvious. Therefore, the parameters obtained from them should be treated with caution and as indicative only. It is also visible that two curves

recorded for the tested coatings presented in Fig. 9 stand out: the curve for coating with the carbon content of 6.7 at.%, which is closer to platinum, and the curve recorded for the coating with the highest carbon content (74 at.%), which is distinguished by lower current densities for a given potential than the remaining coatings.

The ohmic component of the graph enables a value of the onset overpotential η_{onset} to be determined. It can be defined as the potential at which the extrapolated linear part intersects the potential axis, that is to say, the point of intense HER. Furthermore, an additional type of overpotential can be derived directly from the graph, typically presented when describing the catalytic capability in HER, namely the overpotential that results in the current density of 0.01 A/cm2 – η_{10}.

The Tafel slope for platinum 0.048 V/dec (cf. Fig. 10) calculated from the LV curve recorded at 0.005 V/s is close to the value characteristic of the Heyrovsky reaction when the discharge of hydronium ions (Volmer reaction) is rapid and the electrochemical desorption is the limiting step.[52] The Tafel slope value for the fastest route of the HER reaction (0.029 V/dec) characteristic for chemical desorption was not obtained, most probably due to equipment limitations. Increasing the scan rate to 0.03 V/s results in a larger Tafel slope, indicating that diffusion can become a limiting factor under these conditions.

Similar values, and therefore similar reaction mechanisms, are observed for the NiMo-C coating containing 6.7 at.% C with the Tafel slope of 0.070 V/dec. The coating exhibits favorable catalytic properties; however, at the scanning rate of 0.03 V/s, diffusion represents a limiting factor in the overall reaction rate. For coatings with even higher carbon content, the Tafel slope reaches a value of 0.15 V/dec and can be attributed to the hydrogen desorption step as limiting rate of the overall hydrogen evolution reaction.[52] The observation that the Tafel slope for samples containing more than 8 at.% carbon is independent of the scan rate employed lends support to this assertion.

The Tafel slope increases gradually up to 0.2 V/dec with increasing carbon content from 15 to 74 at.%, and it is important to note that even at the highest carbon content of 74 at.%,

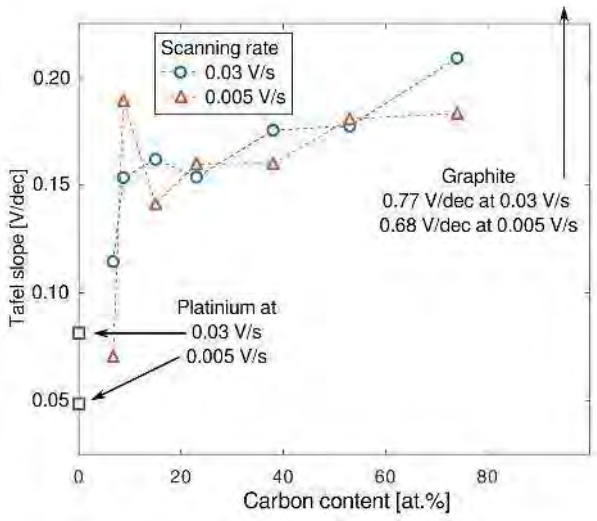

Figure 10: Tafel slopes calculated for exponential sections of linear voltammetry curves presented in Fig. 9

it remains significantly lower than that of graphite. The structural analysis demonstrates that throughout the entire range of carbon content, the electrolyte is in contact with the metal catalyst. At low carbon contents the complete surface area of the coating acts as a catalyst, while at higher carbon content the metallic islands can act as the catalytic centres (cf. Fig. 7).

The overpotentials η_{onset} and η_{10}, obtained from the curves depicted in Fig.9, are summarized in Fig. 11. The lowest overpotentials for the tested coatings were observed in samples with the lowest carbon content (6.7 at.%), exhibiting a difference of approximately 0.1 V compared to those of platinum. An increase in the carbon content to 8.7 at.% results in an abrupt rise in the overpotential values. Subsequently, a gradual increase in the values is observed. The dependence on carbon content is more noticeable for η_{onset} than for η_{10}. As with Tafel slopes, all samples exhibit overpotentials η_{onset} andη_{10} that are markedly superior to those of graphite.

Furthermore, it is evident that the results depicted in Fig.11 exhibit differences between the two scanning rates. It is important to note that different parts of the LV curves are utilized to ascertain the overpotentials than those used to calculate the Tafel slopes. In

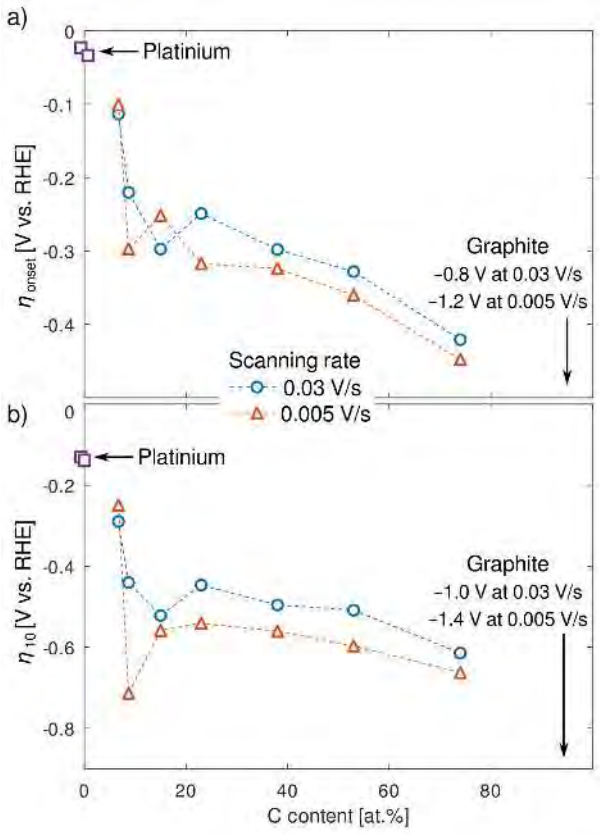

Figure 11: Onset overpotential η_{onset} and the overpotential that results in the current density of 10 mA/cm^2 – η_{10} . The values were read from the linear voltammetry curves presented in Fig. 9

the case of the overpotentials, the current densities are higher, and the amount of hydrogen accumulating on the electrodes is greater when the slower scanning rate is employed.

A notable increase in the Tafel slopes and the overpotentials η_{onset} and η_{10} are observed as the carbon content changes from 6.7 to 8.7 at. % (cf. Fig. 10 and 11), and this cannot be attributed solely to the C content. The effect can be assigned to a notable change in the texture of the coatings. The sample with a carbon content of 8.7 at.% exhibits a peak intensity from the family planes (111) aligned parallel to the sample surface that is twice that of the sample with 6.7 at.%, and it is known that catalytic activity of HER depends on the texture.[53]

In order to ascertain the long-term catalytic activity of the examined coatings, cyclic voltammetry (CV) measurements were conducted, and a comparison was made between LV curves recorded on untreated samples and after 200 cycles of CV. The results are presented in Fig. 12. The most significant observation in the comparison is that the sample containing 23 at.% carbon is the most stable and the determined parameters η_{onset} and η_{10} are shifted to smaller values, and are superior to those obtained prior to the CV.

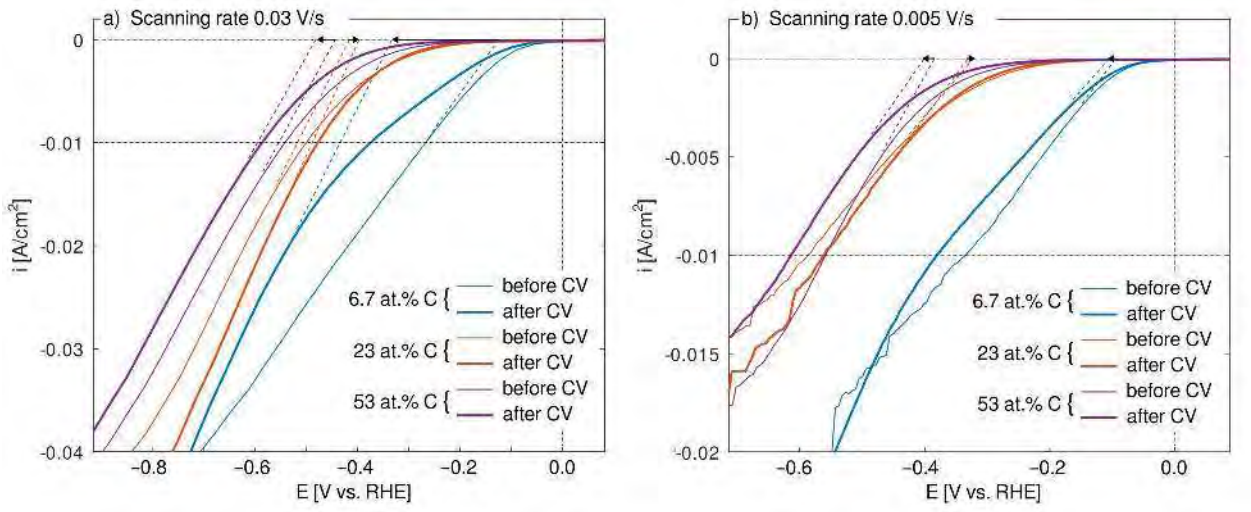

Figure 12: The linear voltammetry curves registered at two scanning rates: a) 0.03 V/s and b) 0.005 V/s. The samples contained varying amounts of carbon.

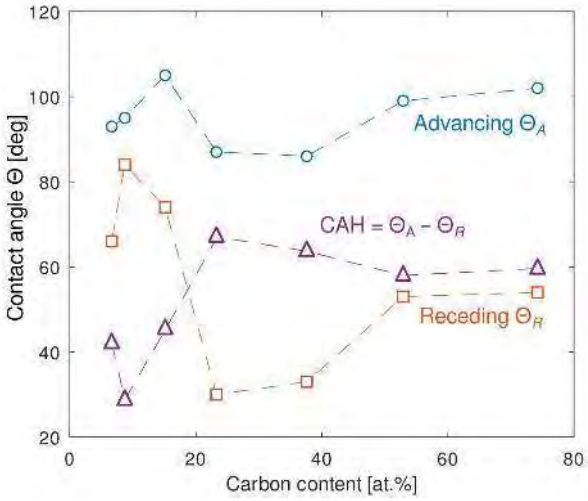

Figure 13: Relationship between the advancing and receding contact angles, Θ_A and Θ_R, respectively, and the difference between them (the contact angle hysteresis CAH) in dependence on carbon content in the studied coatings.

Wettability

Given the established influence of released gas bubbles on the course of electrochemical reactions,[29,30] an attempt was made to identify a correlation between the HER reaction parameters on the tested coatings and the surface wettability, as determined by the values of contact angles. The relationship between measured advancing and receding contact angles and the carbon content is presented in Fig. 13.

The advancing contact angle Θ_A is largely independent of the carbon content, while the receding angle Θ_R exhibits a distinct minimum at carbon content between 20 and 40 at.%, indicating the high wettability of these samples. It is evident that the contact angle hysteresis (CAH) is higher for samples with contents above 20 at.%, that is to say, for those in which the release of free carbon and the development of a columnar nanostructure is observed. The sole parameter that exhibits a correlation with contact angles or their hysteresis is the overpotential η_{10}. This observation is understandable when one considers that, at this current density, the release of gas bubbles becomes an important element of the processes occurring at the cathode.

Conclusions

The present paper reports on the structural and electrochemical properties of NiMo-C coatings synthesized by reactive magnetron sputtering of the $Ni_{80}Mo_{20}$ alloy target in an Ar/C_2H_2 atmosphere. The structure of the coatings evolves as a function of the carbon content from: i) nanocrystalline for carbon contents between 6 and 10 at.%, through ii) amorphous for carbon contents of 10 to 20 at.%, to iii) quasi-amorphous, with a gradually revealing nanocolumnar structure, for carbon contents in the range 20–74 at.%.

The formation of the nanocolumnar structure is associated with the release of excess carbon from metastable ternary carbides formed during the synthesis. Ultimately, this nanostructure consists of metallic columns perpendicular to the surface of the samples surrounded by shells of amorphous carbon.

The coatings were evaluated for their potential use as catalytic materials in the hydrogen evolution reaction (HER) in acidic environments. It has been shown that coatings with a carbon content of 23 at.% or higher exhibited a high corrosion resistance in acidic medium.

The best catalytic properties from the application point of view were observed for coatings with the lowest amount of carbon (6.7%), for which the Tafel slope was 0.07 V/dec, as compared to 0.05 V/dec obtained under the same conditions for platinum. Tafel slopes for samples with higher carbon content exhibited higher values: from 0.15 to 0.20 V/dec, and the mechanism limiting the reaction was considered to be the slow hydrogen desorption.

However, even for the highest carbon content, the Tafel slope does not differ substantially from that measured for samples with a lower carbon content. This advantageous property is likely attributable to the distinctive nanopillar structure, which comprises catalytic centres in the form of metallic islands on the surface.

A similar conclusion can be drawn if the overpotentials η_{onset} and η_{10} are taken into account. Optimal coatings are characterized by the lowest carbon amount, while coatings with higher carbon content show similar properties despite large differences in the carbon content. The impact of carbon is evident in the stability tests of the examined coatings. It

was determined that the least significant changes observed after CV tests occurred in the samples with intermediate carbon content.

A correlation between the contact angle hysteresis CAH and the overpotential η_{10} was found. Although the correlation is not strong at the current density values applied, it is possible that at higher values it could become an important factor. In order to determine a functional relationship between these quantities that is of practical importance, it is necessary to acquire a larger set of measurement data.

References

(1) D. Strmcnik, P. P. Lopes, B. Genorio, V. R. Stamenkovic, N. M. Markovic, Design principles for hydrogen evolution reaction catalyst materials, Nano Energy 29 (2016) 29–36. doi:10.1016/j.nanoen.2016.04.017.

(2) B. Wang, F. Zhang, Main Descriptors To Correlate Structures with the Performances of Electrocatalysts, Angew. Chemie - Int. Ed. 61 (4) (2022). doi:10.1002/anie.202111026.

(3) J. K. Nørskov, T. Bligaard, A. Logadottir, J. R. Kitchin, J. G. Chen, S. Pandelov, U. Stimming, Trends in the Exchange Current for Hydrogen Evolution, J. Electrochem. Soc. 152 (3) (2005) J23. doi:10.1149/1.1856988.

(4) P. Quaino, F. Juarez, E. Santos, W. Schmickler, Volcano plots in hydrogen electrocatalysis-uses and abuses, Beilstein J. Nanotechnol. 5 (1) (2014) 846–854. doi:10.3762/bjnano.5.96.

(5) J. M. Jakšić, M. V. Vojnović, N. V. Krstajić, Kinetic analysis of hydrogen evolution at Ni-Mo alloy electrodes, Electrochim. Acta 45 (25-26) (2000) 4151–4158. doi:10.1016/S0013-4686(00)00549-1.

(6) J. A. Bau, S. M. Kozlov, L. M. Azofra, S. Ould-Chikh, A. H. Emwas, H. Idriss, L. Cavallo, K. Takanabe, Role of Oxidized Mo Species on the Active Surface of Ni-Mo Elec-

trocatalysts for Hydrogen Evolution under Alkaline Conditions, ACS Catal. 10 (21) (2020) 12858–12866. doi:10.1021/acscatal.0c02743.

(7) S. Shetty, A. C. Hegde, Magnetically Induced Electrodeposition of Ni-Mo Alloy for Hydrogen Evolution Reaction, Electrocatalysis 8 (3) (2017) 179–188. doi:10.1007/s12678-017-0350-5.

(8) A. Laszczyńska, W. Tylus, I. Szczygieł, Electrocatalytic properties for the hydrogen evolution of the electrodeposited Ni–Mo/WC composites, Int. J. Hydrogen Energy 46 (44) (2021) 22813–22831. doi:10.1016/j.ijhydene.2021.04.103.

(9) Y. Zhong, X. H. Xia, F. Shi, J. Y. Zhan, J. P. Tu, H. J. Fan, Transition metal carbides and nitrides in energy storage and conversion, Adv. Sci. 3 (5) (2015). doi:10.1002/advs.201500286.

(10) X. Zou, Y. Zhang, Noble metal-free hydrogen evolution catalysts for water splitting, Chem. Soc. Rev. 44 (15) (2015) 5148–5180. doi:10.1039/c4cs00448e.

(11) S. Upadhyay, O. P. Pandey, Synthesis of Mo2C/MoC/C nanocomposite for hydrogen evolution reaction, J. Solid State Electrochem. 26 (2) (2022) 559–564. doi:10.1007/s10008-021-05096-5.

(12) W. Zhou, J. Jia, J. Lu, L. Yang, D. Hou, G. Li, S. Chen, Recent developments of carbon-based electrocatalysts for hydrogen evolution reaction, Nano Energy 28 (2016) 29–43. doi:10.1016/j.nanoen.2016.08.027.

(13) W. Liu, J. Bao, L. Xu, M. Guan, Y. Lei, Chromium-modulated multifunctional electrocatalytic activities of spinel oxide for Zn-air batteries and overall water splitting, J. Power Sources 479 (October) (2020). doi:10.1016/j.jpowsour.2020.229099.

(14) R. Liu, M. Anjass, S. Greiner, S. Liu, D. Gao, J. Biskupek, U. Kaiser, G. Zhang, C. Streb, Bottom-up Design of Bimetallic Cobalt–Molybdenum Carbides/Oxides

for Overall Water Splitting, Chem. - A Eur. J. 26 (18) (2020) 4157–4164. doi:10.1002/chem.201905265.

(15) M. S. Faber, R. Dziedzic, M. A. Lukowski, N. S. Kaiser, Q. Ding, S. Jin, High-performance electrocatalysis using metallic cobalt pyrite (CoS 2) micro- and nanostructures, J. Am. Chem. Soc. 136 (28) (2014) 10053–10061. doi:10.1021/ja504099w.

(16) Z. Lu, W. Zhu, X. Yu, H. Zhang, Y. Li, X. Sun, X. Wang, H. Wang, J. Wang, J. Luo, X. Lei, L. Jiang, Ultrahigh hydrogen evolution performance of under-water "super-aerophobic" MoS2 nanostructured electrodes, Adv. Mater. 26 (17) (2014) 2683–2687. doi:10.1002/adma.201304759.

(17) P. Xiao, M. A. Sk, L. Thia, X. Ge, R. J. Lim, J. Y. Wang, K. H. Lim, X. Wang, Molybdenum phosphide as an efficient electrocatalyst for the hydrogen evolution reaction, Energy Environ. Sci. 7 (8) (2014) 2624–2629. doi:10.1039/c4ee00957f.

(18) J. Wu, P. Li, A. Parra-Puerto, S. Wu, X. Lin, D. Kramer, S. Chen, A. Kucernak, Controllable Heteroatom Doping Effects of Cr xCo2-xP Nanoparticles: A Robust Electrocatalyst for Overall Water Splitting in Alkaline Solutions, ACS Appl. Mater. Interfaces 12 (42) (2020) 47397–47407. doi:10.1021/acsami.0c10441.

(19) S. Lee, B. Min, J. Bang, Substrate effect on hydrogen evolution reaction in two-dimensional Mo2C monolayers, Sci. Rep. 12 (1) (2022) 1–8. doi:10.1038/s41598-022-09935-x.

(20) S. Ahmad, I. Ashraf, M. A. Mansoor, S. Rizwan, M. Iqbal, An overview of recent advances in the synthesis and applications of the transition metal carbide nanomaterials, Nanomaterials 11 (3) (2021) 1–36. doi:10.3390/nano11030776.

(21) E. Coy, L. Yate, D. P. Valencia, W. Aperador, K. Siuzdak, P. Torruella, E. Azanza, S. Estrade, I. Iatsunskyi, F. Peiro, X. Zhang, J. Tejada, R. F. Ziolo, High Electrocatalytic Response of a Mechanically Enhanced NbC Nanocomposite Electrode Toward

Hydrogen Evolution Reaction, ACS Appl. Mater. Interfaces 9 (36) (2017) 30872–30879. doi:10.1021/acsami.7b10317.

(22) P. Vilars, A. Prince, H. Okamoto, Handbook of Ternary Alloy Phase Diagrams, ASM International, 1995.

(23) U. Jansson, E. Lewin, Sputter deposition of transition-metal carbide films — A critical review from a chemical perspective, Thin Solid Films 536 (2013) 1–24. doi:10.1016/j.tsf.2013.02.019.

(24) A. A. El Mel, E. Gautron, B. Angleraud, A. Granier, P. Y. Tessier, Synthesis of nickel-filled carbon nanotubes at 350 C, Carbon N. Y. 49 (2011) 4595–4607. doi:10.1016/j.carbon.2011.06.001.

(25) F. Wang, Multifunctional Nanocomposite Co- Containing Diamondlike Carbon Thin Films, Doctoral dissertation, Luisiana State University (2004).

(26) T. Suszko, W. Gulbiński, J. Morgiel, G. Greczynski, E. Dobruchowska, P. Dłużewski, J. Lu, L. Hultman, Amorphous FeCrNi/a-C:H coatings with self-organizednanotubular structure, Scr. Mater. 136 (2017) 24–28. doi:10.1016/j.scriptamat.2017.03.040.

(27) T. Suszko, W. Gulbiński, E. Dobruchowska, G. Greczynski, L. Hultman, J. Morgiel, Quasi-amorphous, nanostructural CoCrMoC/a-C:H coatings deposited by reactive magnetron sputtering, Surf. Coatings Technol. 378 (2019) 124910. doi:10.1016/j.surfcoat.2019.124910.

(28) T. Suszko, W. Gulbiński, K. Załęski, G. Greczynski, J. Morgiel, V. Lapitskaya, Nanocolumnar, self-organised NiCrC/a-C:H thin films deposited by magnetron sputtering, Appl. Surf. Sci. 591 (2022) 153134. doi:10.1016/j.apsusc.2022.153134.

(29) S. F. Jones, G. M. Evans, K. P. Galvin, Bubble nucleation from gas cavities - A review, Adv. Colloid Interface Sci. 80 (1) (1999) 27–50. doi:10.1016/S0001-8686(98)00074-8.

(30) X. Zhao, H. Ren, L. Luo, Gas Bubbles in Electrochemical Gas Evolution Reactions, Langmuir 35 (16) (2019) 5392–5408. doi:10.1021/acs.langmuir.9b00119.

(31) S. H. Park, D. T. To, N. V. Myung, A review of nickel-molybdenum based hydrogen evolution electrocatalysts from theory to experiment, Appl. Catal. A Gen. 651 (September 2022) (2023) 119013. doi:10.1016/j.apcata.2022.119013.

(32) S. Martinez, M. Metikoš-Huković, L. Valek, Electrocatalytic properties of electrodeposited Ni-15Mo cathodes for the HER in acid solutions: Synergistic electronic effect, J. Mol. Catal. A Chem. 245 (1-2) (2006) 114–121. doi:10.1016/j.molcata.2005.09.040.

(33) E. Navarro-Flores, Z. Chong, S. Omanovic, Characterization of Ni, NiMo, NiW and NiFe electroactive coatings as electrocatalysts for hydrogen evolution in an acidic medium, J. Mol. Catal. A Chem. 226 (2) (2005) 179–197. doi:10.1016/j.molcata.2004.10.029.

(34) P. Singh, R. Banerjee, M. Rahaman, A. V. Ruban, B. Sanyal, A. Mookerjee, Magnetic behaviour of AuFe and NiMo alloys, Pramana - J. Phys. 76 (4) (2011) 639–656. doi:10.1007/s12043-011-0056-9.

(35) S. Ghosh, N. Das, A. Mookerjee, Magnetic properties of Ni-Mo single-crystal alloys; theory and experiment, J. Phys. Condens. Matter 10 (50) (1998) 11773–11780. arXiv:9809137, doi:10.1088/0953-8984/10/50/016.

(36) A. Raveendran, M. Chandran, R. Dhanusuraman, A comprehensive review on the electrochemical parameters and recent material development of electrochemical water splitting electrocatalysts, RSC Adv. 13 (6) (2023) 3843–3876. doi:10.1039/d2ra07642j.

(37) G. Greczynski, L. Hultman, A step-by-step guide to perform x-ray photoelectron spectroscopy, J. Appl. Phys. 132 (1) (2022) 11101. doi:10.1063/5.0086359.

(38) E. McCafferty, Validation of corrosion rates measured by the Tafel extrapolation method, Corros. Sci. 47 (12) (2005) 3202–3215. doi:10.1016/j.corsci.2005.05.046.

(39) A. L. G. Stern, M., Electrochemical Polarization: I . A Theoretical Analysis of the Shape of Polarization Curves, J. Electrochem. Soc. 104 (1) (1957) 56.

(40) M. Strobel, C. S. Lyons, An essay on contact angle measurements, Plasma Process. Polym. 8 (1) (2011) 8–13. doi:10.1002/ppap.201000041.

(41) P. Rochowski, M. Grzegorczyk, S. Pogorzelski, A wettability-based approach for the monitoring of drug transport through biological membranes, J. Colloid Interface Sci. 555 (2019) 352–360. doi:10.1016/j.jcis.2019.07.111.

(42) G. Greczynski, D. Primetzhofer, L. Hultman, Reference binding energies of transition metal carbides by core-level x-ray photoelectron spectroscopy free from Ar+ etching artefacts, Appl. Surf. Sci. 436 (2018) 102–110. doi:10.1016/J.APSUSC.2017.11.264.

(43) U. Jansson, E. Lewin, M. Råsander, O. Eriksson, B. André, U. Wiklund, Design of carbide-based nanocomposite thin films by selective alloying, Surf. Coatings Technol. 206 (4) (2011) 583–590. doi:10.1016/j.surfcoat.2010.06.017.

(44) G. K. Johnson, W. N. Hubbard, E. K. Storms, The enthalpies of formation of Mo2C(c) and Mo3C2(c) by fluorine bomb calorimetry, J. Chem. Thermodyn. 9 (11) (1977) 1021–1026. doi:10.1016/0021-9614(77)90178-1.

(45) S. V. Meschel, O. J. Kleppa, Standard enthalpies of formation of some 3d transition metal carbides by high temperature reaction calorimetry, J. Alloys Compd. 257 (1–2) (1997) 227–233. doi:10.1016/S0925-8388(97)00023-6.

(46) B. C. Bayer, D. A. Bosworth, F. B. Michaelis, R. Blume, G. Habler, R. Abart, R. S. Weatherup, P. R. Kidambi, J. J. Baumberg, A. Knop-Gericke, R. Schloegl, C. Baehtz, Z. H. Barber, J. C. Meyer, S. Hofmann, In Situ Observations of Phase Transitions

in Metastable Nickel (Carbide)/Carbon Nanocomposites, J. Phys. Chem. C 120 (39) (2016) 22571–22584. doi:10.1021/acs.jpcc.6b01555.

(47) G. K. Wertheim, S. B. Dicenzo, S. E. Youngquist, Unit charge on supported gold clusters in photoemission final state, Phys. Rev. Lett. 51 (25) (1983) 2310–2313. doi:10.1103/PhysRevLett.51.2310.

(48) Y. Wang, C. Woodward, S. H. Zhou, Z. K. Liu, L. Q. Chen, Structural stability of Ni-Mo compounds from first-principles calculations, Scr. Mater. 52 (1) (2005) 17–20. doi:10.1016/j.scriptamat.2004.09.007.

(49) E. Dobruchowska, T. Suszko, G. Greczynski, D. Adamczewska, W. Gulbiński, Amorphous/quasi-amorphous CoCrMo-C coatings for improved electrochemical properties and tribocorrosion resistance of biomedical alloys, Surf. Coatings Technol. 460 (2023) 129398. doi:10.1016/j.surfcoat.2023.129398.

(50) K. Ralston, N. Birbilis, C. Davies, Revealing the relationship between grain size and corrosion rate of metals, Scr. Mater. 63 (12) (2010) 1201–1204. doi:10.1016/j.scriptamat.2010.08.035.

(51) K. D. Ralston, D. Fabijanic, N. Birbilis, Effect of grain size on corrosion of high purity aluminium, Electrochim. Acta 56 (4) (2011) 1729–1736. doi:10.1016/j.electacta.2010.09.023.

(52) K. Ojha, S. Saha, P. Dagar, A. K. Ganguli, Nanocatalysts for hydrogen evolution reactions, Phys. Chem. Chem. Phys. 20 (10) (2018) 6777–6799. doi:10.1039/c7cp06316d.

(53) C. Xu, P. Chen, B. Hu, Q. Xiang, Y. Cen, B. Hu, L. Liu, Y. Liu, D. Yu, C. Chen, Porous nickel electrodes with controlled texture for the hydrogen evolution reaction and sodium borohydride electrooxidation, CrystEngComm 22 (25) (2020) 4228–4237. doi:10.1039/d0ce00344a.

Dane wnioskodawcy

1 Imię i Nazwisko: **Tomasz Suszko**

2 Miejsce pracy:

Politechnika Koszalińska, ul. Śniadeckich 2, 75–453 Koszalin

3 Adres korespondencyjny:

3.a służbowy: **jw.**

3.b prywatny:

4 Nr telefonu:

:

5 Adres e-mail:

5.a służbowy: **tomasz.suszko@tu.koszalin.pl**

5.b prywatny:

6 Numer PESEL:

7 Numer i seria dokumentu tożsamości w przypadku braku nadania numeru PESEL:

—

……

(podpis wnioskodawcy)